

Alma Mater Studiorum - Università di Bologna

DOTTORATO DI RICERCA IN
CHIMICA

Ciclo 34

Settore Concorsuale: 03/A2 - MODELLI E METODOLOGIE PER LE SCIENZE CHIMICHE

Settore Scientifico Disciplinare: CHIM/02 - CHIMICA FISICA

NON-COVALENT INTERACTIONS IN WEAKLY BOUND MOLECULAR
COMPLEXES: A HIGH-RESOLUTION ROTATIONAL SPECTROSCOPY STUDY

Presentata da: Dingding Lv

Coordinatore Dottorato

Domenica Tonelli

Supervisore

Sonia Melandri

Co-supervisore

Fabrizia Negri

Luca Evangelisti

Esame finale anno 2022

Preface

My research interests during my doctoral years have been focused on high resolution rotational studies of molecules and weakly bound molecular complexes. Information on the molecular structure, internal motions and intermolecular interactions that can be obtained by applying suitable theoretical models to the analysis of these unusually complex spectra allows the determination and understanding of the driving forces involved in formation of the molecular complex. In this way, many types of non-covalent interactions have been characterized, from pure van der Waals interactions in complexes of rare gases to moderate-strength¹ and weak hydrogen bonds (HBs)² and to the most recent halogen bonds,³ pnictogen⁴ or chalcogen bonds⁵.

In this thesis, we first introduce the theory of rotational spectroscopy, including that of the asymmetrical rotor, the effects of centrifugal distortion, nuclear quadrupole coupling effects and those of internal motions. In the second part, we introduce the experimental apparatuses that were used and related theoretical knowledge.

In the third part, chloropentafluorobenzene (C_6F_5Cl) and bromopentafluorobenzene (C_6F_5Br) are chosen as case studies to investigate the effect of perfluorination on the molecular structure and electronic properties. C_6F_5Cl and C_6F_5Br are important fine chemical intermediates and have broad application prospects in the fields of medicine, pesticides, liquid crystals and olefin polymerization catalysis.⁶⁻⁸ The precise data obtained by rotational spectroscopy for the perfluorinated aryl halides have been compared to those of the non-perfluorinated compounds in trying to assess the effects of successive addition of fluorine atoms on the molecular properties in isolated conditions.

In the fourth and fifth parts, we discuss the 1:1 complexes of acrolein-methanol and acrolein-ethanol. Acrolein is one of the most important environmental pollutants and plays an important role in the formation of atmospheric aerosols. Acrolein-methanol and acrolein-ethanol are the simplest mixed aldehyde and alcohol dimers, appearing to be very promising targets for the study of HBs between unsaturated aldehydes and alcohol. The complexes of aldehydes and alcohols are particularly interesting systems in HB competition studies because they contain a combination of stronger HB and weaker hydrophobic interactions.

In chapters six to eight I report the results on the microwave detection and analysis of the 1:1 complexes of dimethyl sulfoxide (DMSO) with water, methanol and ethanol, respectively, in the gas phase. DMSO is an important substance commonly used as a polar aprotic solvent, antifreeze fluid and cryo-protectant.⁹ The DMSO complex system is well known for exhibiting a strongly non-ideal mixing behaviour. Insights into how DMSO interacts with other molecules are essential in explaining

ice-blocking mechanisms and biological toxicity. A bottom-up approach to the problem of solvation can be achieved by the study of small molecular clusters by high resolution spectroscopy in particular rotational spectroscopy performed in gas phase.

Reference

- 1 J. M. Hutson, *Annu. Rev. Phys. Chem.*, 1990, **41**, 123–154.
- 2 S. Suzuki, P. G. Green, R. E. Bumgarner, S. Dasgupta, W. A. Goddard and G. A. Blake, *Science (80-.)*, 1992, **257**, 942–945.
- 3 G. R. Desiraju, P. S. Ho, L. Kloo, A. C. Legon, R. Marquardt, P. Metrangolo, P. Politzer, G. Resnati and K. Rissanen, *Pure Appl. Chem.*, 2013, **85**, 1711–1713.
- 4 S. Zahn, R. Frank, E. Hey-Hawkins and B. Kirchner, *Chem. Eur. J.*, 2011, **17**, 6034–6038.
- 5 W. Wang, B. Ji and Y. Zhang, *J. Phys. Chem. A*, 2009, **113**, 8132–8135.
- 6 A. Cairncross, W. A. Sheppard and E. Wonchoba, *Org. Synth.*, 2003, **59**, 122.
- 7 A. Haloui and E. Haloui, *J. Mol. Struct.*, 2014, **1068**, 140–148.
- 8 A. Haloui and E. Haloui, *Magn. Reson. Chem.*, 2011, **49**, 717–724.
- 9 Ç. A. Akkök, K. Liseth, T. Hervig, A. Rynningen, Ø. Bruserud and E. Ersvær, *Cytotherapy*, 2009, **11**, 749–760.

Catalogs

Preface.....	I
Catalogs.....	III
Chapter I.....	1
Theory of rotational spectroscopy	1
1.1. Angular momentum and the Rigid-Rotor Hamiltonian.....	1
1.2. The Asymmetric rotor	4
1.3. Centrifugal Distortion	5
1.4. Nuclear quadrupole coupling	6
1.5. Internal Rotation.....	7
1.6. Evaluation of Molecular Structure	11
1.7 Theoretical calculations	13
1.8 Reference	13
Chapter II	15
Experimental techniques in rotational spectroscopy.....	15
2.1. FJ-MMWA Spectrometer.....	15
2.2. PJ-FTMW spectrometer	19
2.3. Reference	24
Chapter III	25
σ -hole activation and structural changes upon perfluorination of aryl halides: direct evidence from gas phase rotational spectroscopy	25
3.1. Introduction.....	25
3.2. Experimental	28
3.3. Results and discussion.....	28
3.4. Conclusions.....	43
3.5. References.....	44

Chapter IV	47
Intermolecular interactions and conformational Equilibria between Aldehydes and Alcohols: Rotational Spectra of Acrolein-Methanol Complex	47
4.1. Introduction	47
4.2. Methods	49
4.3. <i>Ab initio</i> results	50
4.4. Experimental results	52
4.5. Conclusion	61
4.6. Reference	62
Chapter V	65
Intermolecular interactions and conformational Equilibria between Aldehydes and Alcohols: Rotational Spectra of Acrolein-Ethanol Complex	65
5.1. Introduction	65
5.2. Methods	67
5.3. <i>Ab initio</i> results	68
5.4. Experimental results	70
5.5. Conclusion	77
5.6. Reference	78
Chapter VI	80
Characterizing the interactions of dimethyl sulfoxide with water: a rotational spectroscopy study	80
6.1. Introduction	80
6.2. Methods	81
6.3. <i>Ab initio</i> results	82
6.4. Experimental results	83
6.5. Conclusion	92
6.6. Reference	93
Chapter VII	95
Characterizing the interactions of dimethyl sulfoxide with methanol: a rotational spectroscopy study	95
7.1. Introduction	95
7.2. Methods	96
7.3. <i>Ab initio</i> results	96

7.4. Experimental results.....	98
7.5. Conclusion	104
7.6. Reference	105
Chapter VIII	107
Characterizing the interactions of dimethyl sulfoxide with ethanol: a rotational spectroscopy study..	107
8.1. Introduction.....	107
8.2. Methods.....	108
8.3. <i>Ab initio</i> results	109
8.4. Experimental results.....	111
8.5. Conclusion	117
8.6. Reference	118
Appendix III	120
Appendix IV.....	136
Appendix V	143
Appendix VI.....	150
Appendix VII	162
Appendix VIII	163
Conclusion	164
Acknowledgements.....	166

Chapter I

Theory of rotational spectroscopy

In this thesis, we revise the basic knowledge of microwave spectroscopy including the fundamental theory of the rotational spectroscopy. The slower end-to-end rotation of the molecule has a characteristic frequency in the microwave range. Molecular rotation spectroscopy is one of the most powerful sources for accurately determining the chemical structure and physical properties of molecules, and it occupies a prominent position in the field of high-resolution molecular spectroscopy. Dirac ¹ and Von Neumann ² gave the derivation of the principles of quantum mechanics. Therefore, the quantized motion that produces the rotation spectrum has nothing to do with the rotation of the macroscopic object. Mathematical descriptions are given in some classic books by Gordy and Cook ³, Townes and Schawlow⁴, and Kroto⁵. In this thesis, only the key aspects of the theory necessary to process the experimental data obtained are introduced.

1.1. Angular momentum and the Rigid-Rotor Hamiltonian

The starting point for the derivation of the molecular structure from rotating spectrum requires the knowledge of classical mechanics of a rotating rigid system. The angular momentum of a rigid system in classical mechanics is

$$\mathbf{P}=\mathbf{I}\cdot\boldsymbol{\omega} \tag{1.1}$$

where $\boldsymbol{\omega}$ is the angular velocity and \mathbf{I} is the moment of inertia tensor, which is written as

$$\begin{aligned} \mathbf{I} = & I_{xx}\mathbf{i}\mathbf{i} + I_{yy}\mathbf{j}\mathbf{j} + I_{zz}\mathbf{k}\mathbf{k} \\ & + I_{xy}\mathbf{j}\mathbf{i} + I_{yx}\mathbf{i}\mathbf{j} + I_{yz}\mathbf{j}\mathbf{k} \\ & + I_{zy}\mathbf{k}\mathbf{j} + I_{zx}\mathbf{k}\mathbf{i} + I_{xz}\mathbf{i}\mathbf{k} \end{aligned} \tag{1.2}$$

where:

$$\begin{aligned}
I_{xx} &= \sum m(y^2 + z^2) \\
I_{yy} &= \sum m(z^2 + x^2) \\
I_{zz} &= \sum m(x^2 + y^2) \\
I_{xy} &= I_{yx} = -\sum mxy \\
I_{yz} &= I_{zy} = -\sum myz \\
I_{zx} &= I_{xz} = -\sum mxz
\end{aligned} \tag{1.3}$$

where the x, y, z are the molecular fixed coordinates of the particular particle originating at the center of mass and the m is its mass. When the center of mass is determined as the origin of the coordinate system, the total kinetic energy is considered as the sum of the kinetic energy of the translational motion and the kinetic energy of the rotational motion. The elements in the moment of inertia tensor can vanish by the diagonalization of the tensor, leaving only the diagonal elements, called the principal moments of inertia. They correspond the three roots I of the equation:

$$\begin{vmatrix} I_{xx} - I & I_{xy} & I_{xz} \\ I_{yx} & I_{yy} - I & I_{yz} \\ I_{zx} & I_{zy} & I_{zz} - I \end{vmatrix} = 0 \tag{1.4}$$

we can obtain three roots which are the eigenvalues, notated as I_x, I_y, I_z , respectively. The rotational kinetic energy is

$$E_r = \frac{P_x^2}{2I_x} + \frac{P_y^2}{2I_y} + \frac{P_z^2}{2I_z} \tag{1.5}$$

For convenience, the moments of inertia will be substituted by rotational constants in the rotational energy calculation.

$$A = \frac{\hbar}{4\pi I_x}; B = \frac{\hbar}{4\pi I_y}; C = \frac{\hbar}{4\pi I_z} \tag{1.6}$$

Rotational constants are generally expressed in MHz; moments of inertia are in amu A^2 . In the general convention, the increasing orders are normally defined as:

$$I_x \leq I_y \leq I_z; A \geq B \geq C \tag{1.7}$$

Based on the symmetry of the molecular structures, they can be classified into four classes as shown in Figure 1:

- 1) Spherical tops ($I_x = I_y = I_z$).
- 2) Linear molecules ($I_x \ll I_y = I_z$).

- 3) Symmetric tops: prolate-tops ($I_x \geq I_y = I_z$), oblate-tops ($I_x = I_y \geq I_z$).
 4) Asymmetric tops ($I_x \leq I_y \leq I_z$).

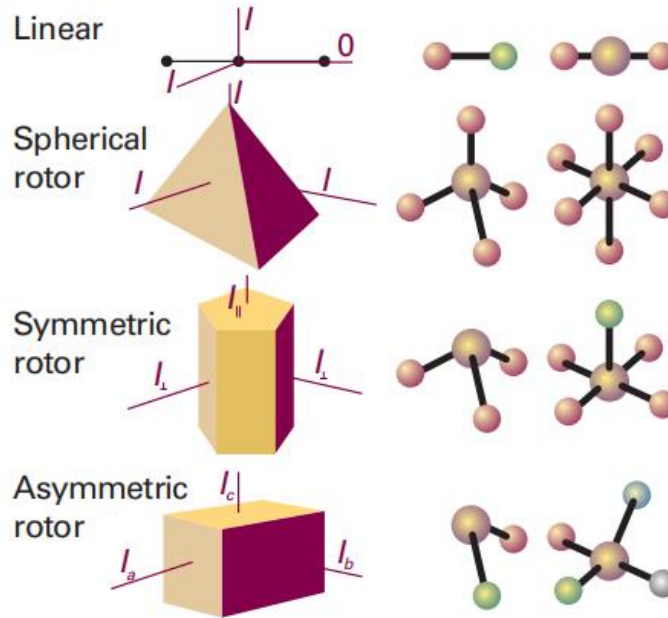


Figure 1.1 A schematic illustration of the classification of rigid rotors.

The transformation from the classical rotational energy to the quantum mechanical rigid rotor Hamiltonian is straightforward by introducing the angular momentum operator \hat{J} :

$$\hat{H}_r = A\hat{J}_a^2 + B\hat{J}_b^2 + C\hat{J}_c^2 \quad (1.8)$$

According to Heisenberg's uncertainty principle, only the operators \hat{J}^2 , \hat{J}_z , and \hat{J}_z , can be measured simultaneously. z is from the body fixed principal axes system xyz and Z is from XYZ axes system in terms of the space fixed reference. The quantum numbers J , K , and M are used to describe the wave functions for the operators \hat{J}^2 , \hat{J}_z , and \hat{J}_z , as shown below^{6,7}:

$$\langle J, K, M | \hat{J}^2 | J, K, M \rangle = J(J + 1)\hbar^2 \quad (1.9)$$

$$\langle J, K, M | \hat{J}_z^2 | J, K, M \rangle = K^2 \hbar^2 \quad (1.10)$$

$$\langle J, K, M | \hat{J}_z^2 | J, K, M \rangle = M^2 \hbar^2 \quad (1.11)$$

where:

$$\begin{aligned} J &= 0, 1, 2, \dots \\ K &= -J, -J + 1, \dots, 0, J - 1, J \\ M &= -J, -J + 1, \dots, 0, J - 1, J \end{aligned} \quad (1.12)$$

The selection rules for allowed transitions between rotational energy levels depend on the type of rotor. For linear and symmetric tops, rotational transitions are only allowed for:

$$\Delta J = \pm 1, \Delta K = 0, \Delta M = 0, \pm 1 \quad (1.13)$$

1.2. The Asymmetric rotor

The asymmetry of a molecule is given by the value of Ray's asymmetry parameter κ :

$$\kappa = \frac{2B - A - C}{A - C} \quad (1.14)$$

It can be easily seen that κ varies from -1 (prolate symmetric-top) to +1 (oblate symmetric-top).

The most asymmetric top has $\kappa = 0$. The energy levels of asymmetric rotors differ from the limiting symmetric-top ones essentially in that the levels corresponding to $-K$ and $+K$, which are always degenerate in the symmetric rotor, are separated in the asymmetric rotor. Thus, an asymmetric rotor has $(2J + 1)$ distinct rotational sublevels for each value of J . A qualitative indication of the levels of the asymmetric rotor is given in the Figure 1.2 as below:

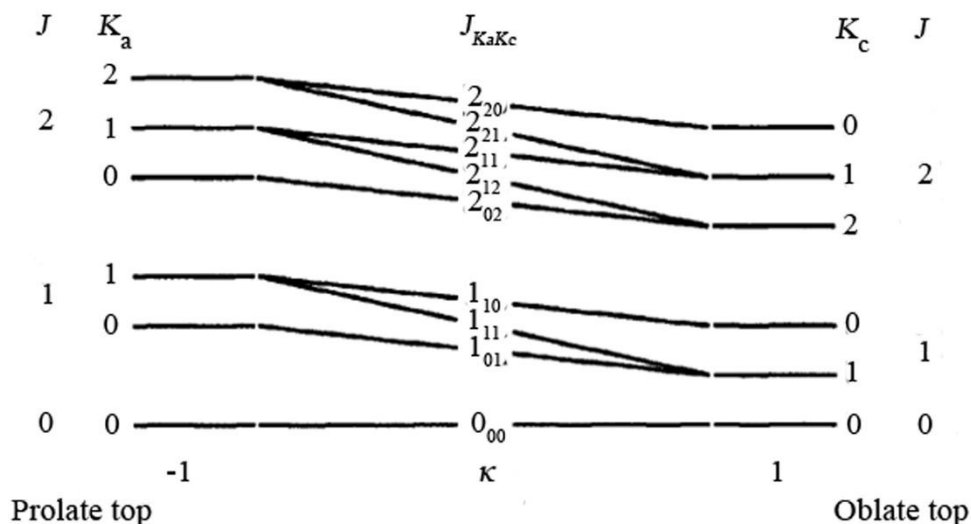


Figure 1.2. energy levels diagram as a function of the asymmetry parameter κ . the limit values of κ are shown for prolate-top (-1) and oblate-top (1).

Selection rules for asymmetric rotor transitions with respect to J are $\Delta J = 0, \pm 1$. In the absence of external fields each rotational level is M -fold degenerate, where $M = 2J + 1$.

The condition $\Delta J = 0$ gives rise to Q -branch, $\Delta J = -1$ to P -branch and $\Delta J = +1$ to R -branch transitions. The selection rules for rotational transition in the asymmetric molecules can be expressed in terms of K_a and K_c . Asymmetric rotors can have three nonzero components of the dipole moment μ_a, μ_b, μ_c giving rise to three types of transitions, called a -, b -, c -type respectively, governed by different ΔK_a and ΔK_c rules, as indicated in the table below.

Table 1.1. Selection rules for the pseudo-quantum numbers (K_a, K_c) of the asymmetric rotor.

Note that larger variations in the indices (in parentheses) produce weak transitions.

Transition type	ΔK_a	ΔK_c
a	$0 (\pm 2, \pm 4, \dots)$	$\pm 1 (\pm 3, \pm 5, \dots)$
b	$\pm 1 (\pm 3, \pm 5, \dots)$	$\pm 1 (\pm 3, \pm 5, \dots)$
c	$\pm 1 (\pm 3, \pm 5, \dots)$	$0 (\pm 2, \pm 4, \dots)$

1.3. Centrifugal Distortion

In the preceding paragraph, molecules were assumed as rigid rotors for simplicity. However, the atomic structure cannot be absolutely rigid. Molecular vibrations, internal rotations, and centrifugal forces can distort the geometry of a molecule from its equilibrium. In order to correct for centrifugal stretching of the molecule due to its rotation, higher order terms of the angular momenta need to be included into the Hamiltonian. In many cases this effect can be treated as a perturbation to the rigid rotor Hamiltonian (H_r).

The theory of the centrifugal distortion was initiated by Wilson,⁸ introducing a series of centrifugal distortion coefficients ($\tau_{\alpha\beta\gamma\delta}$) relating the molecular distortions and force constants. Kivelson and Wilson applied first-order perturbation theory, expressing the Hamiltonian for the semi-rigid rotor as:

$$\hat{H}_{rot} = \hat{H}_r + \hat{H}_d \quad (1.15)$$

$$\hat{H}_d = \frac{\hbar^4}{4} \sum_{\alpha\beta\gamma\delta} \tau_{\alpha\beta\gamma\delta} \hat{J}_\alpha \hat{J}_\beta \hat{J}_\gamma \hat{J}_\delta \quad (1.16)$$

where \hat{H}_d is the contribution of the centrifugal distortion part to the total Hamiltonian. α, β, γ and δ can take any value of x, y or z . The quartic centrifugal distortion coefficients

parameters $\tau_{\alpha\beta\gamma\delta}$ are related to the force constants which have components. Based on symmetry properties and commutation relations, Watson demonstrated^{9,10} that their number can be reduced to five determinable linear combinations of fourth-order corrections. Two different reduction schemes have been established in rotational spectroscopy: the A- and the S-reduction. The Watson asymmetric (A) reduction, is best suited for most asymmetric top molecules.¹¹

$$\hat{H}_d^{(A)} = -\Delta_J \hat{J}^4 - \Delta_{JK} \hat{J}^2 \hat{J}_z^2 - \Delta_K \hat{J}_z^4 - 2\delta_J \hat{J}^2 \hat{J}_{xy}^2 - \delta_K (\hat{J}_z^2 \hat{J}_{xy}^2 + \hat{J}_{xy}^2 \hat{J}_z^2) \quad (1.17)$$

where $J^2 = J \cdot J$, $J_{xy}^2 = J_x^2 - J_y^2$.

The A-reduction includes the following five centrifugal distortion constants: Δ_J , Δ_K , Δ_{JK} , δ_J and δ_K . The problem with this reduction is that for asymmetric rotors that are close to the prolate or oblate limit, the rotation constant and the centrifugal distortion constant are highly correlated. In addition, it should be noted that the centrifugal distortion constant δ_K blows up for near prolate rotor because it contains the rotation constant (B-C) in the denominator. For this reason, it is convenient to use the alternative symmetric (S) reduction, which is expressed as

$$\hat{H}_d^{(S)} = -D_J \hat{J}^4 - D_{JK} \hat{J}^2 \hat{J}_z^2 - D_K \hat{J}_z^4 - d_1 \hat{J}^2 (\hat{J}_+^2 + \hat{J}_-^2) - d_2 (\hat{J}_+^4 + \hat{J}_-^4) \quad (1.18)$$

where $\hat{J}_\pm = (\hat{J}_x \pm i\hat{J}_y)$ and the centrifugal distortion constants are D_J , D_K , D_{JK} , d_1 , d_2 .

1.4. Nuclear quadrupole coupling

Nuclear quadrupole coupling effect is originated from the coupling between the nuclear spin angular momentum I and the molecular rotational angular momentum J , through the interaction between the quadrupole moment Q of the nuclei and the electric field gradient. The coupling of spin angular momentum I and the rotational angular momentum J can produce a total angular momentum F :

$$F = J + I \quad (1.19)$$

which takes values according to the Clebsch-Gordan series:

$$F = J + I, J + I - 1, \dots, |J - I| \quad (1.20)$$

The selection rule of the transitions between different energy level are:¹²

$$\Delta J = 0, \pm 1; \Delta F = 0, \pm 1 \quad (1.21)$$

A quantum mechanical Hamiltonian can be derived:

$$\hat{H}_Q = \frac{eQq_J}{2(2J-1)I(2I-1)} \left[3(\hat{I} \cdot \hat{J})^2 + \frac{3}{2}\hat{I} \cdot \hat{J} - \hat{I}^2 \cdot \hat{J}^2 \right] \quad (1.22)$$

and by convention, the coupling constants are designated as:

$$\chi_{gg'} = eQq_{gg'} \quad (1.23)$$

where $g = a, b, c$ are the principal inertia axes, where

$$q_{gg'} = \frac{\partial^2 V}{\partial g g'} \quad (1.24)$$

Due to Laplace's equation, the quadrupole coupling tensor is traceless, that is:

$$\chi_{aa} + \chi_{bb} + \chi_{cc} = 0 \quad (1.25)$$

1.5. Internal Rotation

Internal rotation is a large amplitude motion observed in molecules containing an internal group which rotates independently from the rest of the molecule. Large-amplitude motion refers to the internal movement with amplitudes on the order of the molecular bond length, which may significantly change the molecular structure or convert the molecule from one equivalent structure to another one through tunneling. The effect of internal rotation on the rotation spectrum is that every rotational transition will exhibit a fine structure caused by the interaction of internal rotation and overall rotation. Using high-resolution and accurate measurements of microwave spectroscopy to analysis this fine structure, potential barriers hindering the motion can be evaluated.

A good starting point for the description of the utilized methods is the model Hamiltonian for an asymmetric rotor with a single methyl internal rotor, which is given in the principal axes system by:

$$\hat{H} = \hat{H}_R + \hat{H}_T + \hat{H}_{TR} \quad (1.26)$$

where \hat{H}_R , \hat{H}_T and \hat{H}_{TR} depend on the reduced angular momentum (P), the internal angular momentum (p), the adimensional moment of inertial rotor (F) and the barrier to internal rotation (V_n), they are described as follows:

$$\hat{H}_R = \hat{H}_r + F\hat{P}^2 \quad (1.27)$$

$$\hat{H}_T = F\hat{p}^2 + \frac{1}{2}V_n(1 - \cos 3\alpha) \quad (1.28)$$

$$\hat{H}_{TR} = -2F\hat{P}\hat{p} \quad (1.29)$$

where α is the torsional angle with respect to the two rotating groups of the molecule. Apparently, the potential energy is a periodic function of α with the period $2\pi/N$, where N represents the degree of the symmetry of the rotor. With the setting potential $V=0$ at $\alpha=0$, the potential function can be expressed as a Fourier expansion as:

$$V(\alpha) = \frac{V_N}{2}(1 - \cos N\alpha) + \frac{V_{2N}}{2}(1 - \cos 2N\alpha) + \dots \quad (1.30)$$

As an example, shown in Figure 1.3, we consider here only the threefold barrier such as the internal rotation of the CH₃ group in many organic molecules. In this case the potential function (omitting the higher orders V_6 term which is generally less than 3% of V_3) can be expressed as:

$$V(\alpha) = \frac{V_3}{2}(1 - \cos 3\alpha) \quad (1.31)$$

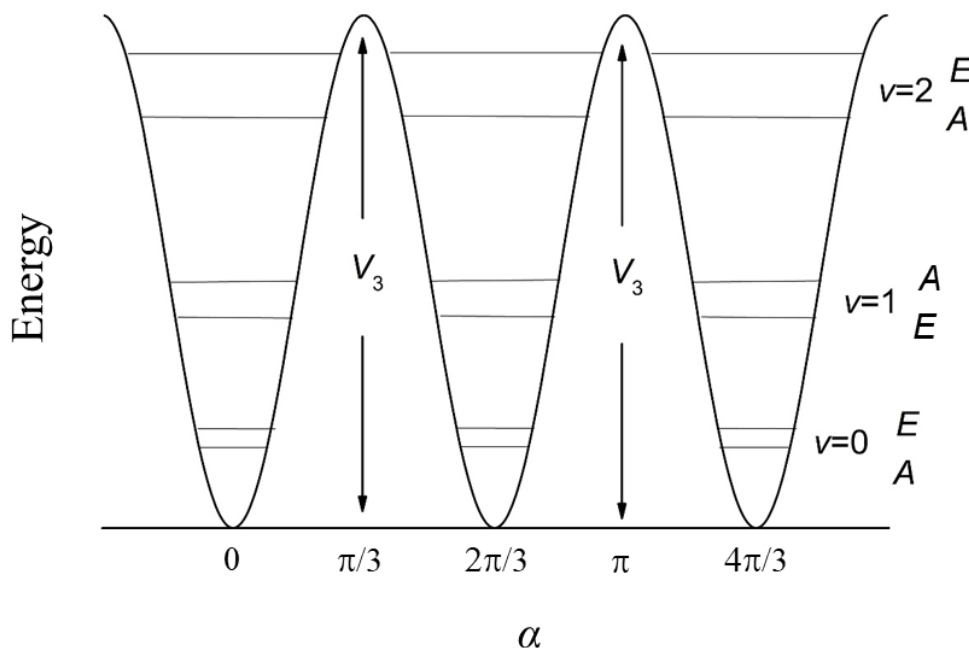


Figure 1.3. The potential curve and the torsional energy levels as the function of α . v is the torsional quantum number and A and E are their symbols related to their symmetry.

Substituting the potential function into the wave equation for internal rotation, it is:

$$-F \frac{d^2 U(\alpha)}{d\alpha^2} + \left[\frac{V_3}{2}(1 - \cos 3\alpha) - E \right] U(\alpha) = 0 \quad (1.32)$$

where:

$$F = \frac{\hbar^2}{2I_r} \quad (1.33)$$

I_r is the reduced moment of inertia of the two parts (α, β) rotated with respect to each other in the molecule, calculated as:

$$I_r = \frac{I_\alpha I_\beta}{I_\alpha + I_\beta} \quad (1.34)$$

Two extreme cases, which are the free rotor limit ($V_3 \rightarrow 0$) and the three-fold harmonic oscillator limit ($V_3 \rightarrow \infty$) are helpful to understand the spacing between the energy levels in the case of a finite barrier. For a general case with a finite barrier, the torsional energy level can be represented as the schematic diagram as below

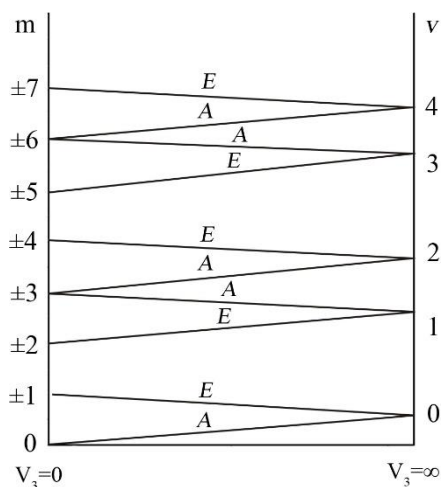


Figure 1.4. The torsional energy level between the energy levels of free internal rotation labeled by quantum number m , and three-fold harmonic torsional oscillation labeled by quantum number v . The levels labeled by A are nondegenerate while the E levels are doubly degenerate.

The eigenfunctions and eigenvalues of two extremes can be obtained easily from equation (1.32). Considering the free rotor limit, they are

$$U_{v\sigma}(\alpha) = \frac{1}{\sqrt{2\pi}} e^{i(3k+\sigma)\alpha} \quad (1.35)$$

$$E_{v\sigma} = F(3k + \sigma)^2 \quad (1.36)$$

where $k = 0, \pm 1, \pm 2, \dots$, and the indexes $\sigma = 0, \pm 1$ represent A and E states, respectively. For the infinite barrier limit, they are

$$\begin{aligned}
U_{v0}(\boldsymbol{\alpha}) &= \frac{1}{\sqrt{3}}[H_v^{(1)} + H_v^{(2)} + H_v^{(3)}] \\
U_{vI}(\boldsymbol{\alpha}) &= \frac{1}{\sqrt{3}}[H_v^{(1)} + \boldsymbol{\varepsilon}H_v^{(2)} + \boldsymbol{\varepsilon}^2H_v^{(3)}] \\
U_{v,-I}(\boldsymbol{\alpha}) &= \frac{1}{\sqrt{3}}[H_v^{(1)} + \boldsymbol{\varepsilon}^2H_v^{(2)} + \boldsymbol{\varepsilon}H_v^{(3)}]
\end{aligned} \tag{1.37}$$

$$E_v = 3(V_3F)^{1/2}(v+1/2) \tag{1.38}$$

where $\boldsymbol{\varepsilon} = \exp(i2\pi/3)$, and $H_v^{(1)}$, $H_v^{(2)}$, $H_v^{(3)}$ are the harmonic oscillator functions with the centers at 0, $2\pi/3$, and $4\pi/3$, respectively.

The splitting of the rotational spectra can be interpreted by the interaction between the overall and internal rotations. In the classical theory, the kinetic energy of a molecule with an internal rotation top can be written as:

$$\begin{aligned}
T &= \frac{1}{2} \sum_g I_g \boldsymbol{\omega}_g^2 + \frac{1}{2} I_\alpha \dot{\boldsymbol{\alpha}}^2 + I_\alpha \dot{\boldsymbol{\alpha}} \sum_g \lambda_g \boldsymbol{\omega}_g \\
&g = x, y, z
\end{aligned} \tag{1.39}$$

I_g are the principal moments of inertia of the whole molecule, I_α is the moment of inertia of the rotating top around its symmetry axis, $\boldsymbol{\omega}_g$ are the angular velocity components of the molecule, $\boldsymbol{\alpha}'$ is the angular velocity of the top relative to the framework, and λ_g are the cosines between the rotating top and the principal axes of the molecule. After substituting the following equations

$$\begin{aligned}
P_g &= \frac{\partial T}{\partial \boldsymbol{\omega}_g} = I_g \boldsymbol{\omega}_g + \lambda_g I_\alpha \dot{\boldsymbol{\alpha}} \\
p &= \frac{\partial T}{\partial \dot{\boldsymbol{\alpha}}} = I_\alpha \dot{\boldsymbol{\alpha}} + I_\alpha \sum_g \lambda_g \boldsymbol{\omega}_g
\end{aligned} \tag{1.40}$$

into (1.39), then it can be written as

$$T = \frac{1}{2} \sum_g \frac{P_g^2}{I_g} + \frac{1}{2} r I_\alpha \dot{\boldsymbol{\alpha}}^2 \tag{1.41}$$

and

$$r = 1 - \sum_g \frac{\lambda_g^2 I_\alpha}{I_g} \tag{1.42}$$

1.6. Evaluation of Molecular Structure

The rotational spectrum is dominated by the molecular structure. The characteristic of molecular structure is that the position of each atom is determined by the nature of the chemical bond that connects it with neighboring atoms.

Once the rotation spectrum is obtained and assigned, it generates rotation constants and obtains the moment of inertia from these rotation constants, thereby obtaining a relatively conformational structure.

The r_s substitution structure is derived from isotope substitution. Kraitchman's¹³ method is used to calculate the position of an atom in a molecule, using the change in the moment of inertia caused by the substitution of a single isotope of the atom. Given enough spectral information from different isotopes, the complete structure of the molecule can be determined.

The non-planar asymmetric top was discussed as a general case here. It is convenient to use the plane moment of inertia \mathbf{P} to obtain r_s . From the experimental rotational constants, the principal moments of the parent body and the substituted species can be obtained. The relationship between them and the principal moment of inertia are:

$$\begin{aligned}P_x &= \frac{1}{2}(-I_x + I_y + I_z) \\P_y &= \frac{1}{2}(-I_y + I_z + I_x) \\P_z &= \frac{1}{2}(-I_z + I_x + I_y)\end{aligned}\tag{1.47}$$

The matrix of the plane moment of inertia \mathbf{P} of the parent molecule in its principal axis system is shown below:

$$\mathbf{P} = \begin{vmatrix} \sum m_i x_i^2 & 0 & 0 \\ 0 & \sum m_i y_i^2 & 0 \\ 0 & 0 & \sum m_i z_i^2 \end{vmatrix}\tag{1.48}$$

With respect to the same axes system for the isotopically substituted molecule, the elements of \mathbf{P}' written as:

$$\begin{aligned}
P'_{xx} &= P_x + \mu x^2 \\
P'_{yy} &= P_y + \mu y^2 \\
P'_{zz} &= P_z + \mu z^2 \\
P'_{xy} &= \mu xy \\
P'_{xz} &= \mu xz \\
P'_{yz} &= \mu yz
\end{aligned} \tag{1.49}$$

The reduced mass for the substituted species is defined as

$$\mu = \frac{M\Delta m}{M + \Delta m} \tag{1.50}$$

with M is the total mass of the parent molecule, Δm is the mass difference of the isotopically substituted atoms.

Hence, the secular equation for the substituted molecule is:

$$\begin{vmatrix}
P_x + \mu x^2 - P' & \mu xy & \mu xz \\
\mu xy & P_y + \mu y^2 - P' & \mu yz \\
\mu xz & \mu yz & P_z + \mu z^2 - P'
\end{vmatrix} = 0 \tag{1.51}$$

after resolving the equation, the coordinates of the substituted atom are obtained:

$$\begin{aligned}
|x| &= \left[\frac{\Delta P_x}{\mu} \left(1 + \frac{\Delta P_y}{P_y - P_x} \right) \left(1 + \frac{\Delta P_z}{P_z - P_x} \right) \right]^{1/2} \\
|y| &= \left[\frac{\Delta P_y}{\mu} \left(1 + \frac{\Delta P_z}{P_z - P_y} \right) \left(1 + \frac{\Delta P_x}{P_x - P_y} \right) \right]^{1/2} \\
|z| &= \left[\frac{\Delta P_z}{\mu} \left(1 + \frac{\Delta P_x}{P_x - P_z} \right) \left(1 + \frac{\Delta P_y}{P_y - P_z} \right) \right]^{1/2}
\end{aligned} \tag{1.52}$$

where

$$\begin{aligned}
\Delta P_x &= \frac{1}{2} (-\Delta I_x + \Delta I_y + \Delta I_z) \\
\Delta P_y &= \frac{1}{2} (-\Delta I_y + \Delta I_z + \Delta I_x) \\
\Delta P_z &= \frac{1}{2} (-\Delta I_z + \Delta I_x + \Delta I_y)
\end{aligned} \tag{1.53}$$

1.7 Theoretical calculations

Quantum chemistry calculations have developed to be a powerful tool for searching for rotational spectra and conformational assignment based on the calculated resulting information on rotational constants, dipole moment components, relative stabilized energies and quadrupole coupling constants. *Ab initio* and density functional theory (DFT) are used to assist the assignment of the rotational spectra. Geometry optimizations are used to predict the molecular equilibrium structure and conformational preferences from the potential energy surface (PES). In this present work, *ab initio*, using the second order Møller-Plesset (MP2)¹⁴ method which gives a good balance between accuracy and computational cost for spectroscopic purposes, have been running at the correlation consistent basis set of aug-cc-pVDZ level. The method and most common basis set employed based in DFT is Becke, three parameter, Lee-Yang-Parr (B3LYP)¹⁵ functional with def2tzvp basis set due to the good efficiency-computational cost ratio. In some cases, the calculated results were compared with the other basis sets, such as 6-311++G**. Frequency calculations are used to calculate the zero point energy and force constants, and to evaluate if the geometry optimized is a real minimum. As to the case of molecular adducts, the basis set superposition error (BSSE)¹⁶ corrections have been also taken into the account to evaluate the dissociation energies of different isomers. All theoretical calculations in this dissertation are performed with Gaussian 16 program¹⁷.

1.8 Reference

- 1 P. A. M. Dirac, *The principle of quantum mechanics*, Addison-Wesley, Mass, 1961.
- 2 J. Von Neumann, *Mathematical foundations of quantum mechanics*, Princeton university press, 1955.
- 3 W. Gordy, R. L. Cook and A. Weissberger, *Microwave molecular spectra*, Wiley New York, 1984, vol. 18.
- 4 C. H. Townes and A. L. Schawlow, *Microwave spectroscopy*, Dover, New York, 1975.
- 5 H. W. Kroto, *Molecular Rotation Spectra*, John Wiley & Sons, Ltd, London-New York-Sydney-Toronto, 1975.

- 6 A. Bauder, in *High-resolution Spectroscopy*, eds. M. Quack and J. B. Howard, John Wiley & Sons, Ltd, 2011, pp. 57–116.
- 7 R. N. Zare and W. G. Harter, *Angular momentum: understanding spatial aspects in chemistry and physics*, John Wiley & Sons, Ltd, New York, 1988.
- 8 E. B. Wilson Jr and J. B. Howard, *The Journal of Chemical Physics*, 1936, **4**, 260–268.
- 9 J. K. G. Watson, *Indeterminacies of fitting parameters in molecular spectroscopy*, John Wiley & Sons, Ltd, New York, 2011, vol. 46.
- 10 J. K. G. Watson, *The Journal of Chemical Physics*, 1967, **46**, 1935–1949.
- 11 J. K. G. Watson, *Vibrational spectra and structure*, Oxford&New York, 1977, vol. 6.
- 12 R. Chang, *Basic principles of spectroscopy*, McGraw-Hill., New York, 1971.
- 13 J. Kraitchman, *American Journal of Physics*, 1953, **21**, 17–24.
- 14 Chr. Møller and M. S. Plesset, *Physical Review*, 1934, **46**, 618–622.
- 15 C. Lee, W. Yang and R. G. Parr, *Physical Review B*, 1988, **37**, 785–789.
- 16 S. F. Boys and F. Bernardi, *Molecular Physics*, 1970, **19**, 553–566.
- 17 M. J. Frisch, G. W. Trucks, H. B. Schlegel, G. E. Scuseria, M. A. Robb, J. R. Cheeseman, G. Scalmani, V. Barone, G. A. Petersson, H. Nakatsuji and others, *Gaussian Inc. Wallingford CT*.

Chapter II

Experimental techniques in rotational spectroscopy

Since the first study of molecular (NH_3) rotational spectroscopy in 1934,¹ this technology has been used and developed for more than 80 years. As a powerful tool of molecular science, rotational spectroscopy has made remarkable progress.^{2,3} This chapter introduces the current configuration of two spectrometers, a Free-Jet Absorption MilliMeter Wave spectrometer (FJAMMW) and a Pulsed-Jet Fourier Transform MicroWave spectrometer (PJ-FTMW) operating at the University of Bologna.

2.1. FJ-MMWA Spectrometer

The FJAMMW was built by Professor P. Favero, Professor W. Caminati and Professor S. Melandri at the University of Bologna (UNIBO) in 1993,⁴ and updated during the years.⁵ The instrument covers a frequency range of 60-78 GHz (extendable to 118 GHz), with excellent frequency measurement accuracy around 50 kHz. A scheme of the instrument is shown in Figure 2.1, and it is to the one developed at Monash University,⁶ but introduces some new functions. Briefly, a monochromatic radiation passes through a teflon lens system and it is fed into a cylindrical vacuum chamber intersecting the molecular beam perpendicularly. The molecular absorption of radiation can change its intensity and the transmission recorded as a function of radiation frequency forms the spectrum.

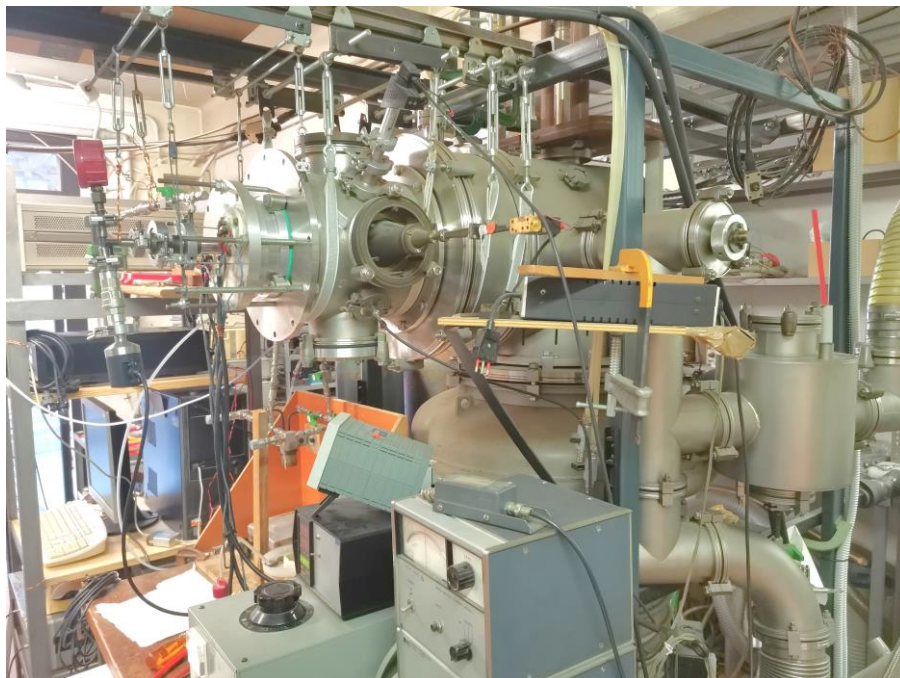


Figure 2.1. Free-Jet Absorption MilliMeter Wave spectrometer built at UNIBO.

The sketch of the absorption cell and is shown in Figure 2.2. The supersonic beam expands along the x -axis of a cylindrical vacuum chamber with a diameter of 25 cm and a length of 25 cm. The vacuum chamber is evacuated with an effective vacuum yield of approximately 4000 ls^{-1} , and the background pressure is maintained in the range of 10^{-5} Pa . A chevron baffle cooled with liquid nitrogen can be placed at the end of the chamber to prevent the vacuum system from the contamination of the non-volatile components of the jet. The nozzle diameter can range from 0.02 to 0.05 cm. Generally, argon is used as the carrier gas, and the stagnation pressure is 10-100 kPa. The molecular beam can reach an estimated rotation temperature of approximately 10 K. Along the y -axis, the lens system (Montech-Clayton, Australia) concentrates the radiation into the plume area. Along the z axis, S and S' are two plates spaced by 5 cm, providing Stark modulation. The unearthed plates are guarded and a voltage of up to 3 kV can be applied to the plates at a frequency of 33 kHz. The scheme of the nozzle (which can also be pulsed) is shown in Figure 2.2(C). (a) part is the nozzle saturation chamber, which is electrically heated, and the temperature is controlled up to $200 \text{ }^\circ\text{C}$ to observe the rotational spectra of non-volatile or solid substances; part (b) is the drive Gas preheating chamber; part (c) includes the driving gas inlet and the system for filling the saturation chamber with liquid substances under vacuum operation.

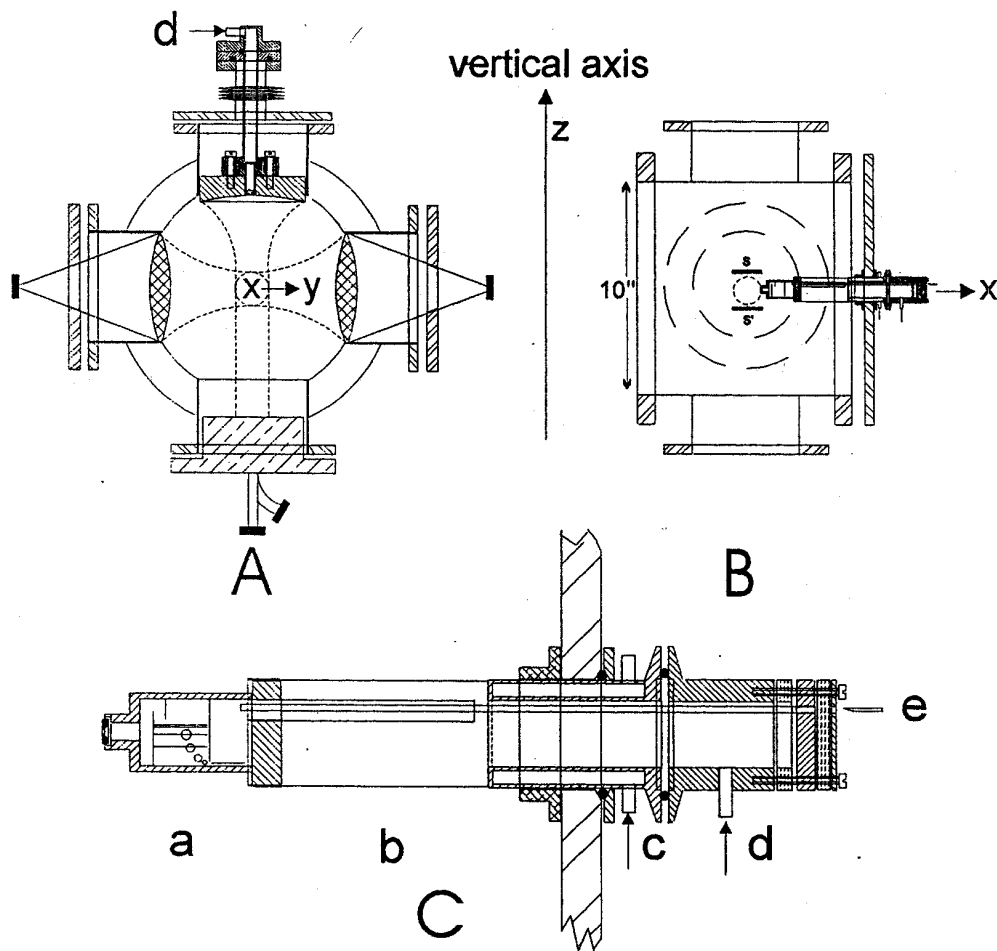


Figure 2.2. Schematic absorption cell (A and B) and the molecular beam system (C) of the FJAMMW spectrometer.

A synthesizer working in the frequency range 2MHz-40GHz (HP 83640B) is used as the radiation source, and multiplied by four through a custom-built amplifier-multiplier chain, the transmitted power is detected by Schottky diodes (Millitech DXW10, Millitech 47324H-1211) and a lock-in amplifier multiplier chain (Stanford SR820). Nominally the system works in the 60–78 GHz region, but it can be expanded to 118 GHz using a x6 multiplier without any apparent degradation (only a diminished transmitted power) of the factory specifications, and the accuracy of the frequency measurements is better than 50 kHz.

The following describes the setup of the system (see Figure 2.2), and the FJ-AMMW laboratory at UNIBO is shown in Figure 2.3.

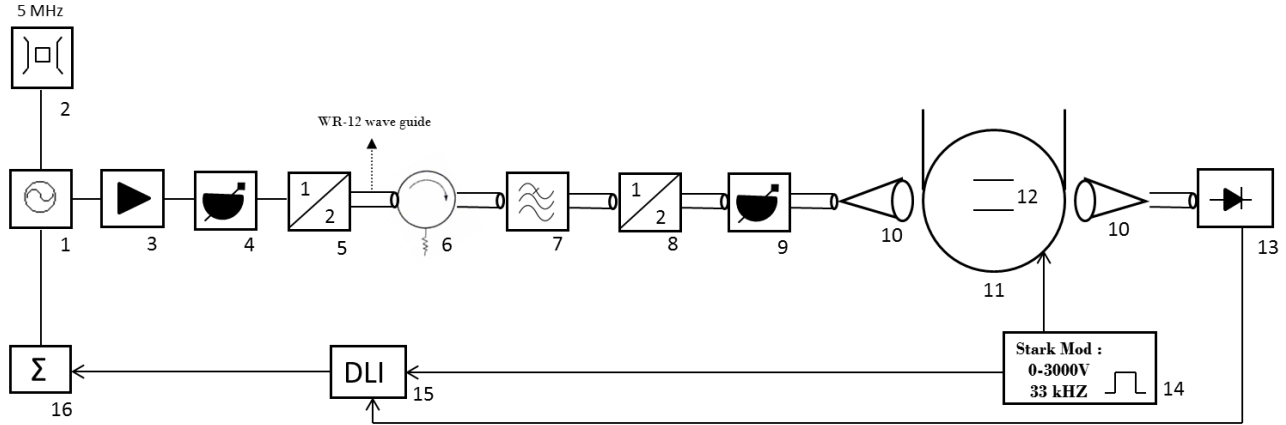


Figure 2.3. Block diagram of the Free-jet absorption millimeter wave spectrometer (FJAMMW): 1. Microwave synthesizer HP 83640B (2–40 GHz). 2. Reference signal, Rb oscillator (5 MHz), Ball-Efraton FRK-LLN. 3. Hittite Amplifier MW (5–20 GHz) Gain: +20 dB. 4. Variable attenuator, NARDA (10 dB). 5. Frequency doubler Spacek-laboratories (26.5–40 GHz). Output power: +17 dBm Waveguide WR28. 6. Dorado Isolator (26.5–40 GHz, 41 GHz). 7. Low pass filter Spacek-laboratories, $f_{\max} = 41$ GHz. 8. Frequency doubler Spacek-laboratories (53–80 GHz). Output power: –3 dBm to 0 dBm, Waveguide WR12. 9. Variable attenuator (0–35 dB). 10. Horn-dielectric lens system (Montech-Clayton, Australia). 11. Supersonic-jet expansion chamber. 12. Stark plates. 13. Schottky-diode detector: Millitech DXW10 for frequencies above 60 GHz or a Millitech 4731 4H-1111 for frequencies below 60 GHz. 14. High-voltage square-wave modulation: electric field up to $750 \text{ V}\cdot\text{cm}^{-1}$ at a frequency of 33 kHz. 15. Digital lock-in amplifier. 16. Experimental control and data acquisition.

2.2. PJ-FTMW spectrometer

The technique of PJ-FTMW has been developed in 1979 by Flygare and colleagues,⁷ which allows pulsed Fourier transformation (FT) microwave spectroscopy to be performed on a supersonic jet of an appropriate gas mixture pulsed from a supersonic nozzle into an evacuated Fabry-Pérot cavity. The first Fabry-Pérot cavity PJ-FTMW spectrometer of the Balle-Flygare type at the university of Bologna, as shown in Figure 2.4, was built in 2004 by Professor W. Caminati and his colleagues at UNIBO,⁸⁻¹⁰ covering the frequency range of 6.5-18 GHz, and proposed the Coaxial Directional Beam Resonator Arrangement (COBRA).¹¹ The design of the spectrometer follows the guidelines given by Andresen et al.¹² and Grabow et al.,¹³ and most of the details come from the spectrometer of Professor Alonso's group in Valladolid.¹⁴ The block diagram including the vacuum chamber and electrical parts is shown in Figure 2.5.



Figure 2.4. The PJ-FTMW spectrometer at UNIBO.

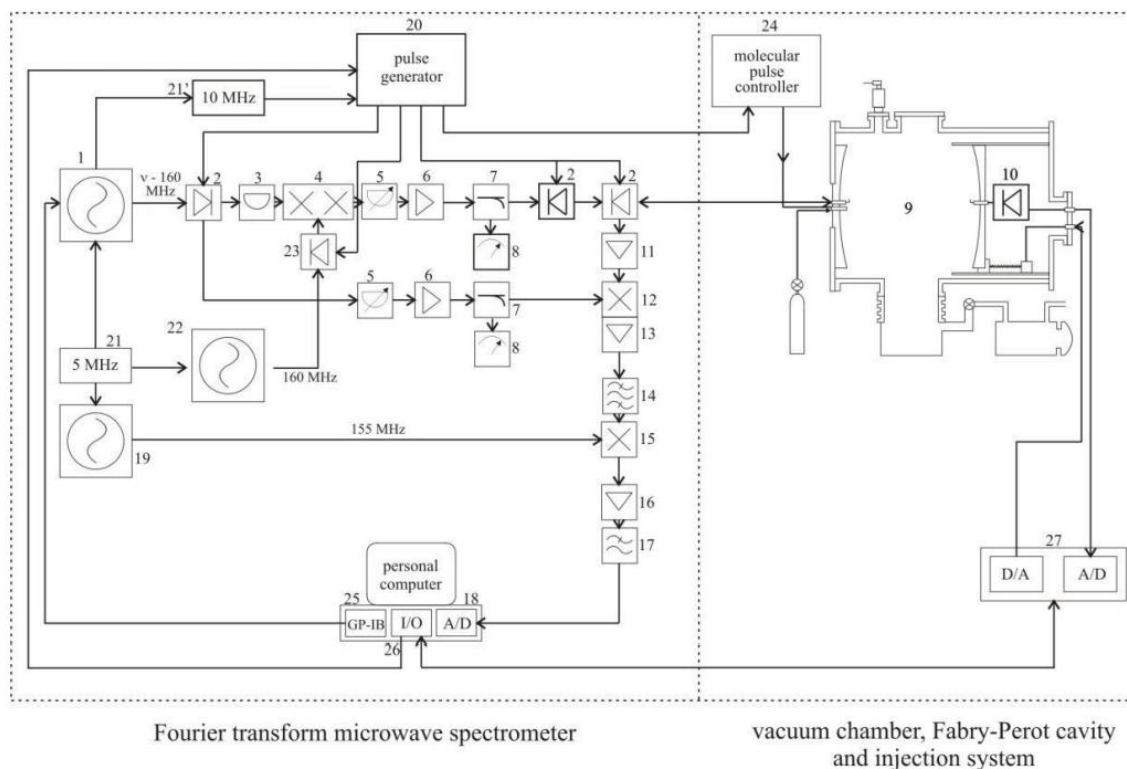


Figure 2.5. Block diagram of the PJ-FTMW spectrometer. MW = Microwave; RF = Radio Frequency; P = output power, IF = intermediate frequency, IL = insertion losses, G = gain, NF = noise figure, IS = isolation, IR = image rejection: 1. MW synthesizer, HP 8672 A. 2. MW switch SPDT, SMT SFD0526-001S. 3. Fixed attenuator MCL BW-S3W2. 4. Single side band modulator, MITEQ MN0226LC1C. 5. Variable attenuator, NARDA 4798. 6. MW amplifier ALC Microwave ALS0618-30-20. 7. Directional coupler NARDA 4203-16. 8. Power meter, HP 435 B + Power sensor 8485A. 9. Fabry-Pérot resonator, see text. 10. MW crystal detector HP8470B. 11. MW low noise amplifier, MITEQ JSD4-0600-1800-16-8P. 12. Image rejection mixer, MITEQ IR0226LC1C. 13. 160 MHz RF amplifier, MITEQ AU-1466-140. 14. Bandpass filter, TTE KC6-160M-20M. 17. RF mixer, HP 10514A. 16. RF amplifier, MCL MAN 1LN. 17. Lowpass Filter, TTE LC5-25M-50-7135. 18. Transient recorder, SPECTRUM PAD 82A, modified following the design of the Kiel University. 19. RF synthesizer, PTS 160-M7020. 20. Pulse Sequencer TTL, made at the University of Valladolid, based on a PCB card from the University of Kiel. 21. Reference signal, Rb oscillator 5 MHz, Ball-Efraton FRK-LLN. 22. RF synthesizer, MARCONI 2019A. 23. RF switch MCL 7MSW-1111. 24. Pulse controller General Valve IOTA ONE. 25.

IEEE 488 interface, NI GP-IB-488 PCII. 26. I/O card, NI PC-DIO-96. 27. A/D and D/A converter for Stepper motor control made in Valladolid.

2.2.1. Time domain technique

The MW spectrometers passing the radiation for a short period of time, through a molecular beam to induce the radiative response in the presence of a sample. The response signal is recorded as a function of time and subjected to FT to obtain the spectrum. A significant improvement in sensitivity with respect to absorption measurements is achieved since the detection of the response signal is performed without any power from the microwave oscillator and modulation.

Although the relaxation time in the gas phase rotational system is very short, the time-dependent behaviour of absorption and emission of a two-level quantum mechanical systems makes it possible to measure rotational transitions in the time domain. The interaction of the MW radiation and the molecular beam results in rotational coherence. The molecular signal power is related to the ratio of the total energy stored in the field within the volume of the resonator. Since the jet expansion and the MW radiation are coaxial, the amplitude of the molecular signal is approximated by:

$$S_{ab}(t) \propto s' \exp(i(\omega_{ab} - kv_{\infty})t + \theta'_{ab}) + s'' \exp(i(\omega_{ab} + kv_{\infty})t + \theta''_{ab}) \quad (2.1)$$

where $\omega = 2\pi\nu$ is the angular resonance frequency and $k = \omega/c$ is the wavenumber of the radiation. The Doppler doublet composed of frequency components at $\nu_{ab} (1-\nu_{\infty}/c)$ and $\nu_{ab} (1+\nu_{\infty}/c)$ is observed in the frequency domain. Then, the molecular resonance frequency is recovered as the arithmetic mean of the components separated by $\Delta\nu_{ab} = 2\nu_{ab}\nu_{\infty}/c$. The line width of each component is about 1.5 kHz; an unblended line can achieve a frequency accuracy of 150 Hz under an obvious S/N ratio.

2.2.2. Pulsed supersonic-jet expansion

The gas pulse emerging from the nozzle has many characteristics, which have an important influence on the molecular rotation spectrum detected by this method. The properties are the effective translational, rotational and vibrational temperature of the molecule, the spatial distribution of the molecule in the pulse and its time dependence, and the nature of the molecular species present. In our PJ-FTMW spectrometer, the solenoid valve (General Valve, Series 9) is used to generate the supersonic expansion (nozzle diameter 0.5 mm), which is located above the

antenna in the fixed mirror and arranged coaxially with the MW radiation. Compared with the molecular beam perpendicular to the direction of MW pulse excitation, COBRA can significantly improve the resolution and sensitivity. The pulse jet valve can be ideally combined with pulse excitation radiation to reduce the load on the vacuum system. Under the total pressure in the range of 0.1~0.6 MPa, ~1% of the sample seeded in the rare gas is expanded into the high vacuum cavity. The schematic diagram is shown in Figure 2.6.

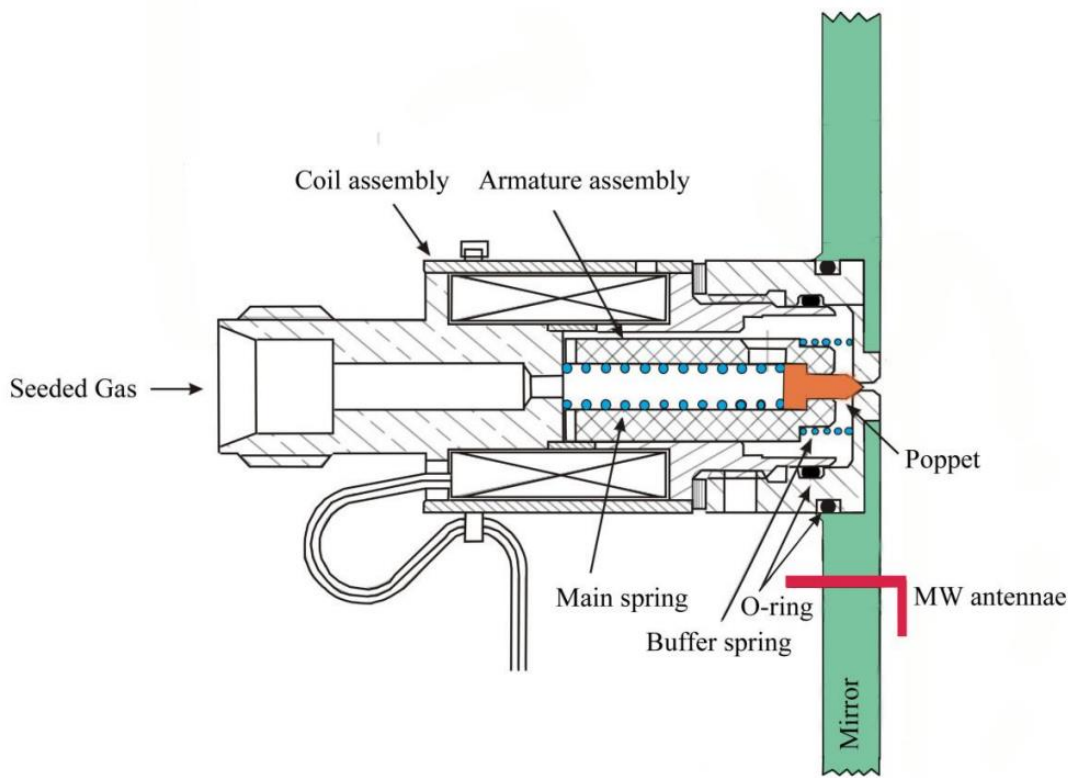


Figure 2.6. Supersonic-jet expansion source.

The gas can be described as having a Maxwell distribution of molecular velocities before expansion. However, after adiabatic expansion, there is a highly directional mass flow. The binary collision in the nozzle during expansion effectively causes the random translational energy of all materials to be converted into the directional kinetic energy of the flowing gas. The internal energy of molecular species is also transformed into kinetic energy. In this case, the rotation and vibration temperature of the seed molecule drops rapidly, while the Maxwell velocity distribution narrows. The properties of expansion are determined by the rare gas because it exists in a predominant excess. The temperature of the rare gas that expands at supersonic speed can be calculated. Under

the described conditions (high efficiency of rotation to translation energy transfer), the expected rotational temperature value is ~ 1 K.

2.2.3. Resonator cavity

A short molecular jet of gas mixture is expanded into an evacuated chamber through the pulse nozzle and the microwave radiation propagates into the resonator cavity. The Balle-Flygare resonator is made of two aluminum mirrors with a radius of curvature of 60 cm and a diameter of 35 cm. They are placed in a cylindrical stainless steel high vacuum chamber (manufactured by HVP of Parma, Italy). The diameter of the chamber is 40 cm while the length is 85 cm. The chamber was evacuated using an 8000 s^{-1} diffusion pump driven by two Leybold mechanical pumps (D65B and Ruvac WAU 251, rotary pump and booster pump, respectively). These mirrors are arranged in a nearly confocal manner, one of which is fixed on a flange of the vacuum chamber, and the other is mounted on a motorized sliding frame. A computer program that can control a stepper motor allows the resonator to be tuned to the correct polarization frequency. The schematic diagram of the mechanical part is shown in Figure 2.7.

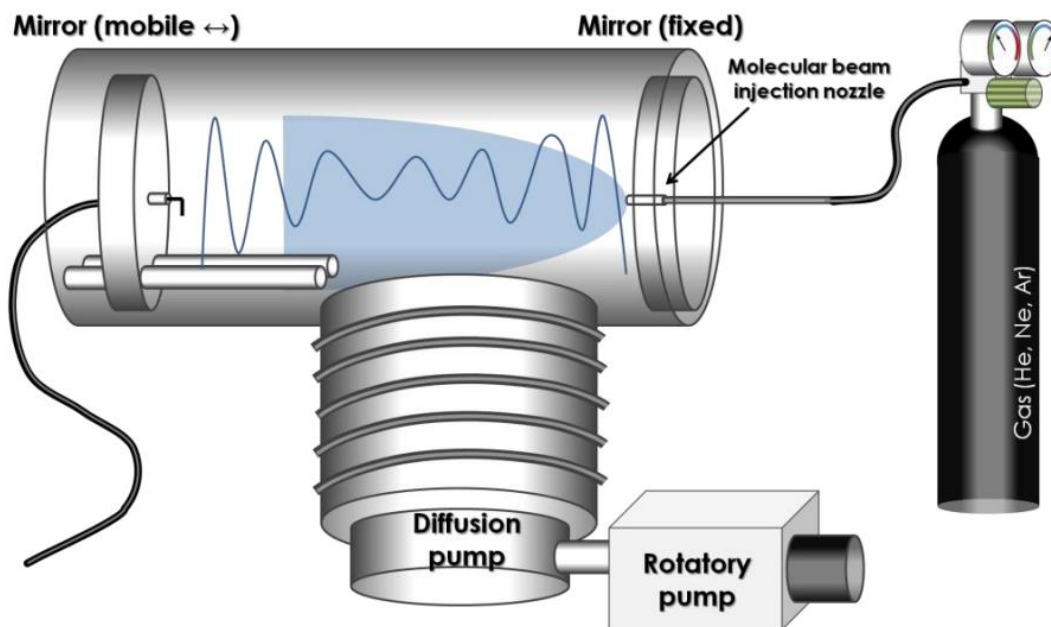


Figure 2.7. Illustration of the mechanic part of the PJ-FTMW.

2.3. Reference

- 1 C. E. Cleeton and N. H. Williams, *Phys. Rev.*, 1934, **45**, 234.
- 2 W. Caminati and J.-U. Grabow, in *Frontiers of molecular spectroscopy*, Elsevier, 2009, pp. 455–552.
- 3 W. Caminati and J.-U. Grabow, in *Frontiers and Advances in Molecular Spectroscopy*, Elsevier, 2018, pp. 569–598.
- 4 S. Melandri, W. Caminati, L. B. Favero, A. Millemaggi and P. G. Favero, *J. Mol. Struct.*, 1995, **352**, 253–258.
- 5 C. Calabrese, A. Vigorito, A. Maris, S. Mariotti, P. Fathi, W. D. Geppert and S. Melandri, *J. Phys. Chem. A*, 2015, **119**, 11674–11682.
- 6 R. D. Brown, J. G. Crofts, P. D. Godfrey, D. McNaughton and A. P. Pierlot, *J. Mol. Struct.*, 1988, **190**, 185–193.
- 7 T. J. Balle and W. H. Flygare, *Rev. Sci. Instrum.*, 1981, **52**, 33–45.
- 8 J.-U. Grabow, W. Stahl and H. Dreizler, *Rev. Sci. Instrum.*, 1996, **67**, 4072–4084.
- 9 B. Velino, S. Melandri and W. Caminati, *J. Phys. Chem. A*, 2004, **108**, 4224–4227.
- 10 W. Caminati, L. Evangelisti, G. Feng, B. M. Giuliano, Q. Gou, S. Melandri and J.-U. Grabow, *Phys. Chem. Chem. Phys.*, 2016, **18**, 17851–17855.
- 11 P. Felder and H. H. Günthard, *Chem. Phys.*, 1982, **71**, 9–25.
- 12 R. S. Ruoff, T. D. Klots, T. Emilsson and H. S. Gutowsky, *J. Chem. Phys.*, 1990, **93**, 3142–3150.
- 13 G. M. Florio, R. A. Christie, K. D. Jordan and T. S. Zwier, *J. Am. Chem. Soc.*, 2002, **124**, 10236–10247.
- 14 P. D. Godfrey and R. D. Brown, *J. Am. Chem. Soc.*, 1998, **120**, 10724–10732.

Chapter III

σ -hole activation and structural changes upon perfluorination of aryl halides: direct evidence from gas phase rotational spectroscopy

3.1. Introduction

Covalently bound halogen atoms show unique properties both nucleophilic and electrophilic. It is well known that they can act as electron donors in the formation of HBs¹ and also as electron acceptors in halogen bonds.^{2,3}

While the behavior of halogen atoms as HB acceptors, is easily attributable to their rich electron cloud, their behavior as electrophilic ligands is related to a particular feature of the halogen atom (in particular Cl, Br or I) which shows a region of positive electrostatic potential on its outermost portion (called the σ -hole)⁴ which can interact with another entity showing a negative electrostatic potential in the so-called σ -hole interaction. Actually, the electron density at the halogen atom shows an anisotropy which leads to the electrophilic σ -hole collinear with the C–X bond and the nucleophilic belt around the equator of X.^{5–7}

Besides their intrinsic properties, when halogen atoms, in particular fluorine, act as substituents their electron withdrawing effect can dramatically change the electronic distribution in the molecules compared to the unsubstituted species. In hexafluorobenzene, for example, perfluorination causes the formation of a positive electrostatic potential region in the center of the ring. This region, differently from the one formed on the tip of the halogen atoms, is called a π -hole, because it is formed perpendicularly to the molecular frame.⁸ The existence of such a hole has been demonstrated by quantum chemical

calculations^{9,10} but also by the direct experimental observation of a lone pair... π -hole interaction in the 1:1 complex of water with hexafluorobenzene¹¹ or pentafluoropyridine¹² by rotational spectroscopy. The rotational study on the complex pentafluoropyridine-water also indicates that the presence of the fluorine substituents not only creates a different binding site (the π -hole) but also weakens the capacity of the heterocyclic nitrogen to act as a HB acceptor. The concepts of σ - and π -hole can be extended to other classes of atoms and molecular frames and their importance in biological systems and the design of new materials has been described.¹³

On these premises, studying the effects of perfluorination on the structural and electronic properties of aryl halides seems particularly interesting since the electronic charge distributions shown by the halogen atom in halobenzenes can be altered by substitution of fluorine atoms on the aromatic ring.

The effects of perfluorination can also be important in relation to the reactivity of aryl halides. These molecules are used as synthetic intermediates that can undergo nucleophilic aromatic substitution reactions (S_NAr) when strong electron-withdrawing groups are present on the aromatic ring. These processes have been studied in condensed phase¹⁴ and in the gas phase.¹⁵ Another effect of the addition of strong electron-withdrawing groups to an arene is that the aryl moiety is converted into a good leaving group and this favours the occurrence of S_N2 reactions on a halogen substituent (generally bromine or iodine).¹⁶

Based on these considerations chloropentafluorobenzene (C_6F_5Cl) and bromopentafluorobenzene (C_6F_5Br) are chosen as case studies to investigate the effect of perfluorination on the molecular structure and electronic properties. Rotational spectroscopy is chosen as the technique of investigation since its high resolution and sensitivity allows the accurate determination of structural parameters both in molecules^{17,18} and non-covalently bound complexes.^{19,20} Moreover, rotational transitions can show hyperfine splittings due to the coupling of the nuclear spin via its quadrupole moment (if the nucleus has spin greater than $\frac{1}{2}$) to the overall rotation. Analysis of the nuclear hyperfine structure of the rotational spectra allows the accurate determination of the nuclear coupling tensor or its main components.

Regarding the latter, the Townes–Dailey (TD)²¹ model has been used for decades to interpret the nuclear coupling constants in terms of p valence orbital's populations and

recently its three dimensional formulation, the Extended Townes-Dailey (ETD) method, has been proposed.²² The results provide insight into the electronic properties of the bonds involving the quadrupole bearing atom: orbital hybridization, degree of covalence in a chemical bond (or ionic bond character), molecular geometry and recently to discuss the potential of molecules in forming a halogen bond.^{23,24} In a recent theoretical paper it has been proposed to use a modified ETD model to calculate the Valence *p*-orbital Population Anisotropy (VPPA) directly related to the quadrupole coupling tensor to quantify and visualize those properties.²⁵ The VPPA, being related to charge imbalance, also allows the quantification of other properties such as the extent of the σ -hole on the halogen atoms.

The interest in the structure and electronic properties of halobenzenes and poly and perfluorinated arenes is proven by the rotational spectroscopy studies performed on several species: fluorobenzene,^{26,27} 1,2- and 1,3-difluorobenzene,²⁸ 1,2,3-trifluorobenzene,²⁹ 1,2,4-trifluorobenzene,³⁰ 1,2,3,4-tetrafluorobenzene,³¹ pentafluorobenzene,³² chlorobenzene,³³ bromobenzene,^{34,35} iodobenzene,^{36,37} 1-chloro-2-fluorobenzene,³⁸ 1-chloro-3-fluorobenzene,³⁹ 1-chloro-4-fluorobenzene.⁴⁰ C₆F₅Cl and C₆F₅Br are important fine chemical intermediates and have broad application prospects in the fields of medicine, pesticides, liquid crystals and olefin polymerization catalysis.⁴¹ The r_α structure of C₆F₅Cl and C₆F₅Br was investigated by Haloui A. and Haloui E.^{42,43} utilizing NMR spectroscopy. As stated by the authors, the accuracy of that technique is significantly less than that of microwave spectroscopy and solvent effect cannot be neglected.

On the contrary, the precise data obtained by rotational spectroscopy for the perfluorinated aryl halides can be compared to those of the non-perfluorinated compounds in trying to assess the effects of successive addition of fluorine atoms on the molecular properties in isolated conditions. They can also be used to benchmark quantum chemical results from widely used computational methods to assess their performance in modelling structural and electronic properties.

In the previously cited work by Rinald and Wu²⁵ the VPPA method is applied to theoretically calculated values of the quadrupole tensors and orbital populations but we propose to use it here to derive those electronic properties directly from the experimentally determined quadrupole coupling tensor in order to gain insight into the electronic properties of the C-X (X=Cl, Br) bond and their changes upon perfluorination.

3.2. Experimental

C_6F_5Cl was purchased from Sigma-Aldrich and used without further purification. A sample containing about 0.1% C_6F_5Cl in neon, at a backing pressure of around 1 atmosphere was expanded through three pulsed valves of the spectrometer, which were oriented perpendicular to the axis of microwave propagation. The spectrum was recorded using a chirped pulse (CP)-FTMW spectrometer at the University of Virginia.⁵⁷ A survey scan was recorded over the 6.0 – 18.0 GHz range, with ten free induction decays (FID) recorded per gas pulse. A total of 320,000 FIDs were averaged to give the final spectrum. A second spectrum was obtained over the 6.8 – 9.0 GHz range. The reduced bandwidth combined with a lower digitization rate allowed fifty FIDs to be averaged per gas pulse, and 8.4 million FIDs were averaged to give the final spectrum. This reduced-bandwidth, high S/N spectrum was used for observation of ^{13}C isotopologue transitions in natural abundance.

C_6F_5Br was purchased from Alpha Aesar (purity >99%) and used without further purification. The COBRA-type pulsed supersonic-jet Fourier-transform microwave (FTMW) spectrometer⁵⁸⁻⁶¹ was used to measure the spectra. Helium at a stagnation pressure of about 2 bar, was flowed over the samples resulting in about 1% mixture of C_6F_5Br . The molecular gas was then expanded through a solenoid valve (General Valve, Series 9, nozzle diameter of 0.5 mm) into a Fabry–Perot cavity. During the expansion, the molecule can reach quite low rotational temperatures (a few K) obtaining a simplification of the spectrum with respect to room temperature spectra by depopulation of high-J and enhanced intensity for low-J transitions.

3.3. Results and discussion

3.3.1. Theoretical

The *ab initio* full optimizations of the structures of the perfluorinated compounds C_6F_5Cl and C_6F_5Br and their hydrogenated counterparts C_6H_5Cl and C_6H_5Br were carried out with the GAUSSIAN 16 suite of programs⁴⁴ using second-order Møller–Plesset (MP2) theory at the aug-cc-pVTZ level under the constraint of C_{2v} symmetry. This method has proved its

reliability in calculating rotational constants with good accuracy.⁴⁵ The principal axes system's coordinates of the optimized structures are available in the Appendix (Tables A3.1-A3.4). The quadrupole coupling constants were estimated from the MP2/aug-cc-pVTZ optimized structures using the Douglas-Kroll-Hess 2nd order scalar relativistic core Hamiltonian⁴⁶, in the point nuclear approximation, with the recontracted aug-cc-pVTZ-DK basis set^{47,48} freely available at Basis Set Exchange Database.⁴⁹

The rotational spectra were predicted based on the theoretical values of the spectroscopic constants for the most abundant isotopologue which are reported in Table 3.1.

Due to the C_{2v} molecular symmetry only μ_a type transition lines can be observed. Also, considering the natural relative abundance of the two most abundant isotopes of chlorine (³⁵Cl 76% and ³⁷Cl 24%), the intensity of the rotational spectra belonging to ³⁷Cl isotopes is expected to be 1/3 of that for the ³⁵Cl species. Bromine has two almost equally abundant isotopes (⁷⁹Br 50.7% and ⁸¹Br 49.3%), thus the rotational spectra of the two isotopologues should have very similar intensity. Regarding ¹³C, considering the natural abundance and the C_{2v} symmetry of the molecules, four mono-substituted species are expected (see Figure 3.1 for numbering of the atoms), two with 1.1% abundance (¹³C1, ¹³C4) and two with 2.2% (¹³C2, ¹³C3) abundance with respect to the parent species. Due to the nuclear quadrupole coupling of both isotopes of chlorine and bromine and their nuclear spin quantum number I=3/2, the rotational spectrum of C₆F₅Cl and C₆F₅Br is expected to be split into a multiplet of hyperfine components.

Table 3.1. *Ab initio* (MP2/aug-cc-pVTZ) rotational constants (A , B , C), quadrupole coupling constants (χ_{aa} , χ_{bb} , χ_{cc}), asymmetry parameter (η), planar moments of inertia (M_{aa} , M_{bb}) and electric dipole moment (μ_a) of parent species.

	C ₆ F ₅ Cl	C ₆ F ₅ Br	C ₆ H ₅ Cl	C ₆ H ₅ Br
A / MHz	1027.83	1027.69	5693.27	5691.00
B / MHz	751.91	496.97	1578.01	1000.35
C / MHz	434.24	334.98	1235.55	850.80
χ_{aa} / MHz	-80.85	653.80	-71.62	562.16
χ_{bb} / MHz	43.64	-353.16	37.57	-292.37
χ_{cc} / MHz	37.20	-300.65	34.05	-269.80
η / MHz ^[a]	-0.0870	-0.0928	-0.0597	-0.0505
M_{aa} / u Å ² [b]	672.13	1016.93	320.26	505.20
M_{bb} / u Å ²	491.69	491.76	88.77	88.80
μ_a / D	-0.37	-0.56	1.70	1.72

[a] η is the asymmetry parameter defined as $\eta = (\chi_{bb} - \chi_{cc}) / \chi_{aa}$. [b] The planar moments of inertia $M_{aa} = \sum_i m_i a_i^2$, $M_{bb} = \sum_i m_i b_i^2$, M_{cc} is zero by symmetry.

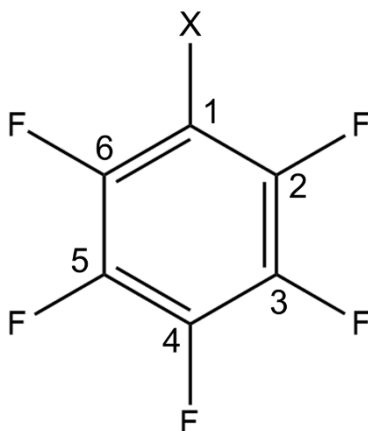


Figure 3.1. The atom numbering scheme used to describe the structural parameters ($X=\text{Cl}, \text{Br}$).

3.3.2. Microwave spectra

For $\text{C}_6\text{F}_5\text{Cl}$, initial predictions at the MP2/aug-cc-pVTZ level were accurate enough to quickly identify a -type $K_a = 0$ and 1 transitions close to predicted frequencies, and with hyperfine patterns in agreement to the *ab initio* ones. Unresolved and partially overlapping hyperfine components meant some strong transitions had to be excluded from the fit; however, 217 hyperfine components were fitted for ^{35}Cl , and 87 were fitted for ^{37}Cl . Using the SPFIT package⁵⁰ the spectra were fitted by a reduced semirigid Hamiltonian in the I^R representation which includes an additional term to fit the nuclear hyperfine structure.⁵¹ Only D_J and d_I centrifugal distortion constants were determined, and these were fixed to the values from the ^{35}Cl isotopologue for analyses of all other isotopic species.

Initial assignments of ^{13}C spectra for the ^{35}Cl isotopologue were made using a reduced bandwidth spectrum with a high number of experimental averages, to enhance the signal-to-noise ratio (see Experimental section). Spectra of all four unique ^{13}C species were assigned, with 45 and 36 transitions fitted for the 2% abundance species ($^{13}\text{C}2$ and $^{13}\text{C}3$, respectively), and 31 and 33 transitions fitted for the 1% abundance species ($^{13}\text{C}1$ and $^{13}\text{C}4$, respectively). Nuclear quadrupole coupling constants for ^{35}Cl were adjusted for all ^{13}C species, giving values identical to the parent to within experimental uncertainties. Note that only the diagonal terms of the nuclear quadrupole coupling tensor are different from zero due to the symmetry of the molecules. Full lists of assigned transitions for all isotopic species can be found in Supplementary Table A3.5, while Figure 3.2 shows resolved and

unresolved hyperfine components for several transitions of the parent and ^{13}C isotopologues.

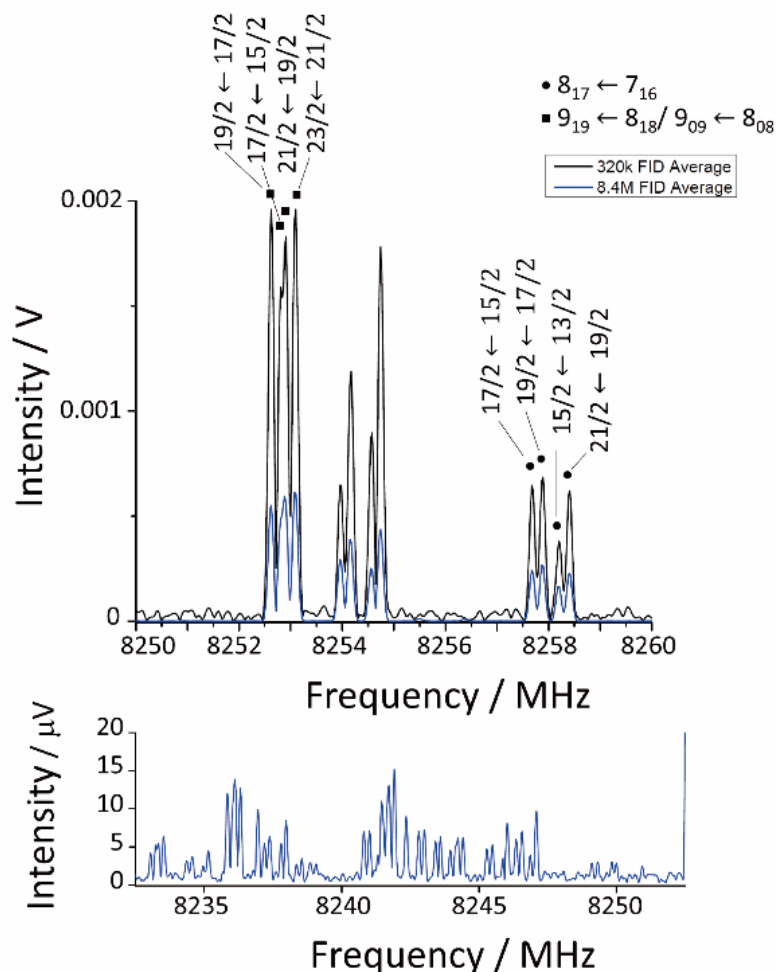


Figure 3.2. Top: Hyperfine components $F' \leftarrow F''$ for the $8_{1,7} \leftarrow 7_{1,6}$, $8_{2,7} \leftarrow 7_{2,6}$ (unlabeled in the figure), $9_{1,9} \leftarrow 8_{1,8}$ and $9_{0,9} \leftarrow 8_{0,8}$ transitions of $\text{C}_6\text{F}_5\text{Cl}$ parent species. Bottom: 1000x vertical magnification showing detail of the same transitions (overlapping) for all four ^{13}C species.

For $\text{C}_6\text{F}_5\text{Br}$ a total of 224 lines were included in the fit for ^{79}Br and 243 lines for ^{81}Br , and as for the previous system, all transitions were fitted with the SPFIT program⁵⁰ to a semirigid Hamiltonian in the I^R representation including nuclear quadrupole coupling terms.⁵¹

The rotational spectra of the two ^{13}C most abundant species were also measured, corresponding to the ^{13}C substitution at C2 and C3 in the isotopologue bearing ^{79}Br . The observation of these isotopologues' spectra was close to the limit of detection thus the spectra originating from substitution of atoms C1 and C4 could not be observed. In total, 18 lines were observed for the $^{13}\text{C}_2$ and 11 lines for the $^{13}\text{C}_3$ species. Due to the small number of observable lines, the values of the quadrupole coupling constants were fixed to those of the parent species in the fit.

Full lists of the transition frequencies for the parent and isotopologues species (^{81}Br , $^{13}\text{C}_2$ and $^{13}\text{C}_3$) are available from the Supplementary Table A3.6. The hyperfine structures of the $12_{0,12} \leftarrow 11_{0,11}$ and $12_{1,12} \leftarrow 11_{1,11}$ transitions of $\text{C}_6\text{F}_5\text{Br}$ are depicted in Figure 3.3. The rotational constants and nuclear quadrupole coupling constants of all the observed species are summarized in Tables 3.2 and 3.3 for $\text{C}_6\text{F}_5\text{Cl}$ and $\text{C}_6\text{F}_5\text{Br}$, respectively.

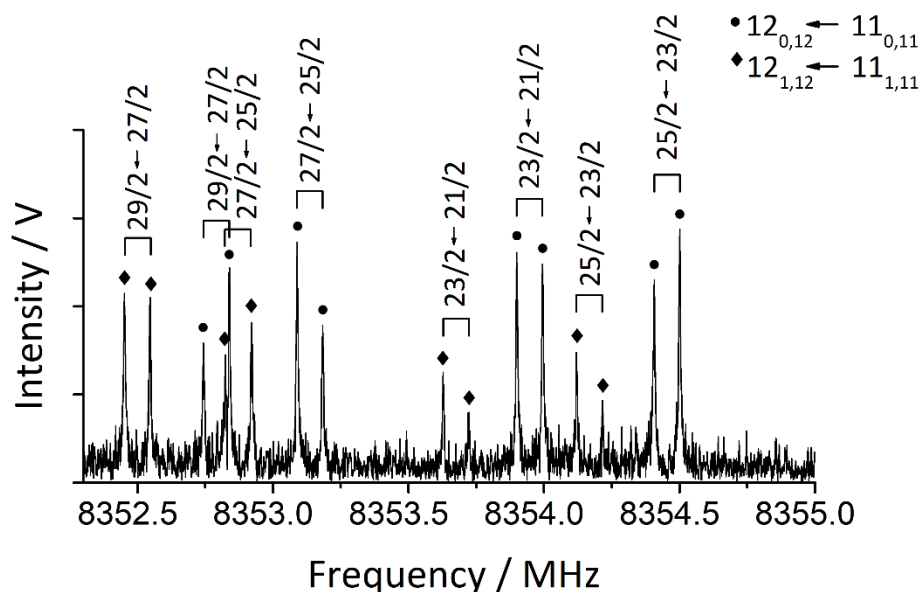


Figure 3.3. The $12_{0,12} \leftarrow 11_{0,11}$ and $12_{1,12} \leftarrow 11_{1,11}$ transitions of the $\text{C}_6\text{F}_5\text{Br}$ parent species showing the main $F' \leftarrow F''$ hyperfine components.

In agreement with the prediction of a planarity, the planar moments of inertia along the c axis ($M_{cc} = \sum_i m_i c_i^2$) are very close to zero. The slightly positive values are consistent

with low-frequency, small amplitude out-of-plane vibrations, which would be expected for rigid ring molecule.³⁴

3.3.3. Structural considerations

For the determination of the structures, we relied on the information carried by the rotational spectra of the isotopologues combined with that obtained by the theoretical calculations. From the isotopologues' experimental rotational constants, it is possible to determine the principal axis coordinates of the substituted atoms (substitution coordinates, r_s) using Kraitchman's single isotopic substitution analysis.⁵² The obtained values are reported in the Appendix (Table A3.1-A3.4) for the two perfluorinated systems (C_6F_5Cl and C_6F_5Br) and their hydrogenated counterparts (the rotational constants for C_6H_5Cl and C_6H_5Br were taken from references 33 and 34 respectively) where they are also compared to the r_e values determined by the theoretical calculations. Since the atom coordinates in Kraitchman's equations appear as their squares, their signs cannot be unambiguously determined but must be compared to the calculate ones. Costain's rule was used to calculate the uncertainties.⁵³

As a second method we utilized the *ab initio* structure as a starting point and adjusted the ring structural parameters and the position of the Cl or Br atom to obtain the best fit to the set of planar moments of inertia measured for the isotopologues of each molecular species. The fit was obtained using the STRFIT program⁵⁴ and the resulting structure adjusted to reproduce the vibrational ground state rotational parameters is known as the r_0 structure.

Table 3.2. Experimental spectroscopic parameters of parent and five observed isotopologues of C₆F₅Cl.

	Parent	³⁷ Cl	¹³ C1	¹³ C2	¹³ C3	¹³ C4
<i>A</i> / MHz	1028.5412(2) ^[a]	1028.5439(7)	1028.568(2)	1025.572(2)	1025.563(2)	1028.578(2)
<i>B</i> / MHz	751.8207(2)	734.4795(2)	750.4372(4)	751.6505(4)	750.7696(4)	748.7217(4)
<i>C</i> / MHz ^[b]	434.3531(3)	428.5081(2)	433.898(5)	433.7654(4)	433.4701(4)	433.3233(4)
χ_{aa} / MHz	-79.52(2)	-62.67(2)	-79.7(5)	-79.45(5)	-79.43(5)	-79.51(7)
χ_{bb} / MHz	43.6(1)	34.39(1)	43.7(2)	43.56(3)	43.60(3)	43.59(3)
χ_{cc} / MHz	35.92(2)	28.27(4)	36.0(3)	35.89(9)	35.84(9)	35.91(9)
η / MHz ^[c]	-0.0965(4)	-0.098(2)	-0.096(9)	-0.0967(9)	-0.098(2)	-0.097(2)
<i>N</i> ^[d]	217	87	31	45	36	33
M_{aa} / u Å ² ^[e]	672.1865(5)	688.0580(5)	673.4227(7)	672.340(1)	673.129(1)	674.970(1)
M_{bb} / u Å ²	491.3348(5)	491.3341(5)	491.3189(7)	492.758(1)	492.763(1)	491.317(1)
M_{cc} / u Å ²	0.0204(5)	0.0198(5)	0.0235(7)	0.020(1)	0.019(1)	0.020(1)
Δv_{rms} / kHz ^[f]	6.1	4.8	5.5	4.9	4.1	5.0

[a] Error in parentheses in units of the last digit. [b] Centrifugal distortion constants were adjusted for the parent species and fixed at those values for all other species: $D_J = 3.8(1.0)$ Hz, $d_1 = 3.4(9)$ Hz. [c] η is the asymmetry parameter, defined as $\eta = (\chi_{bb} - \chi_{cc}) / \chi_{aa}$. [d] N = Number of transitions fitted. [e] The planar moments of inertia $M_{gg} = \sum_i m_i g_i^2$ ($g = a, b, c$). [f] $\Delta v_{rms} = [\sum (v_{obs} - v_{calc})^2 / N]^{1/2}$.

Table 3.3. Experimental spectroscopic parameters of parent and three observed isotopologues of C₆F₅Br.

	Parent	⁸¹ Br	¹³ C2= ¹³ C6	¹³ C3= ¹³ C5
<i>A</i> / MHz	1027.7040(2) ^[a]	1027.7040(2)	1024.743(6)	1024.725(8)
<i>B</i> / MHz	495.05251(4)	489.42319(4)	495.056(2)	493.925(3)
<i>C</i> / MHz ^[b]	334.11342(2)	331.53944(2)	333.8016(1)	333.2851(1)
χ_{aa} / MHz	637.68(3)	532.83(3)	[637.68] ^[b]	[637.68]
χ_{bb} / MHz	-346.12(4)	-289.2(2)	[-346.12]	[-346.12]
χ_{cc} / MHz	-291.56(4)	-243.6(2)	[-291.56]	[-291.56]
η / MHz ^[c]	-0.0856(1)	-0.086(1)	-	-
<i>N</i> ^[d]	224	243	18	11
<i>M</i> _{aa} / u Å ² ^[e]	1020.8507(1)	1032.5933(1)	1020.843(4)	1023.181(5)
<i>M</i> _{bb} / u Å ²	491.7466(1)	491.7474(1)	493.167(4)	493.176(5)
<i>M</i> _{cc} / u Å ²	0.0088(1)	0.0081(1)	0.009(4)	0.009(5)
Δv_{rms} / kHz ^[f]	13.9	5.9	2.7	2.4

[a] Error in parentheses in units of the last digit. [b] Fixed at the ⁷⁹Br monomer value. [c] η is the asymmetry parameter, defined as $\eta = (\chi_{bb} - \chi_{cc}) / \chi_{aa}$. [d] *N* = Number of transitions fitted. [e] The planar moments of inertia $M_{gg} = \sum_i m_i g_i^2$ ($g = a, b, c$). [f] $\Delta v_{\text{rms}} = [\sum (v_{\text{obs}} - v_{\text{calc}})^2 / N]^{1/2}$.

In the fitting procedure we imposed the C_{2v} symmetry by adjusting the C-C bonds and angles in matching couples and pinning the halogen atom (X), C1 and C4 atoms onto the symmetry axis. A suitable fitting was possible adjusting the C1-X, C1-C2 and C2-C3 (and their corresponding C1-C6 and C5-C6) bond lengths, the C2C1X and C3C2C1 (and their corresponding C6C1X and C5C6C1) angles and the C4-C1 distance. Only in the case of C₆F₅Br this last value was fixed to a corrected *ab initio* value. The correction was obtained accounting for the difference between the fitted distance and the theoretical one in C₆H₅Br. The results of the fitting procedures are reported in the Appendix (Table A6.7) while the theoretical and experimental structures are depicted in Figure 3.4.

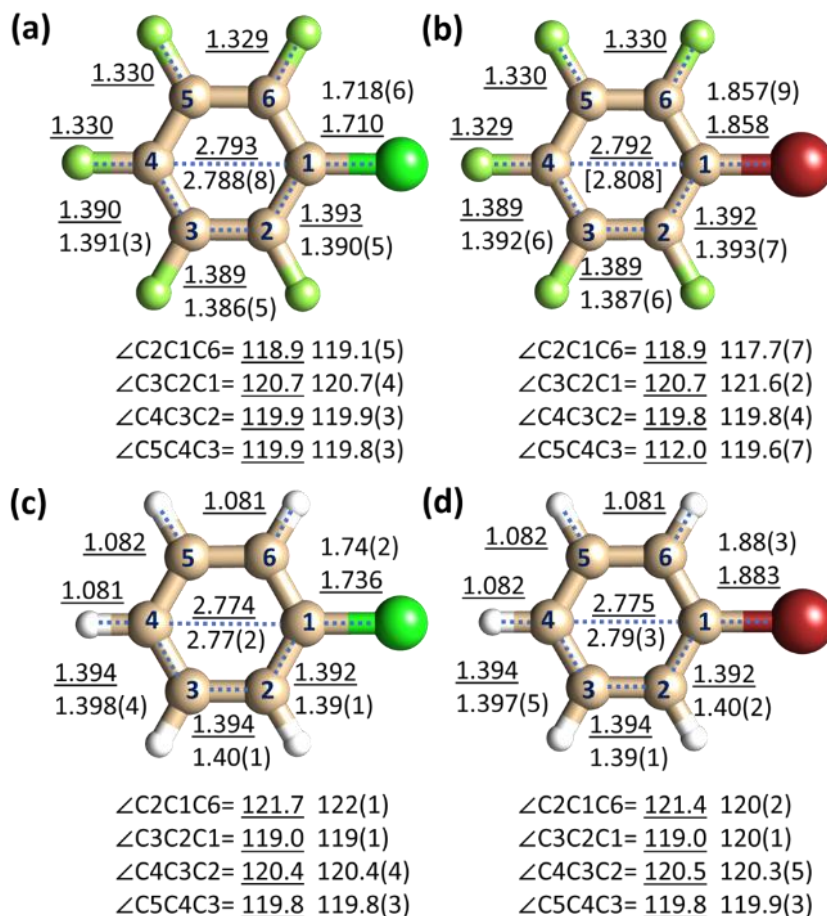


Figure 3.4. Geometries of (a) C_6F_5Cl , (b) C_6F_5Br , (c) C_6H_5Cl and (d) C_6H_5Br MP2/aug-cc-pVTZ parameters (underlined values) and experimental values (normal font). Distances in Å, angles in degrees. The $R(C1C4)$ parameter in C_6F_5Br (in square brackets) is fixed to 2.808 Å (see text for details). Error in parentheses in units of the last digit. Rotational constants of C_6H_5Cl and C_6H_5Br taken from reference 33 and 34 respectively.

This allows us to make some considerations and comparisons between chlorine and bromine substituted molecules as well as hydrogenated and perfluorinated species. Let us first consider the structural changes occurring when chlorine is substituted by bromine. We observe an increase of 0.14(1) Å in the C-X bond length both in the hydrogenated and perfluorinated species in agreement with difference in their covalent radii ($R_{Br}-R_{Cl}=0.15$ Å) while the C-C bond lengths do not change significantly. As regards the ring angles, the biggest changes are seen in the *ipso* and *ortho* angles with an average change of -1.4° and 0.8° respectively while the other angles show smaller differences. These effects in the

angles are not very large and fall close to the uncertainties with which they are determined thus they should be considered an indication of a trend more than accurate values. Focusing alternatively on the chlorine or the bromine substituted molecules we can infer the effects of perfluorination on the structural properties. In this case the bond lengths are not affected very much but we can see larger changes on the angles. Upon perfluorination of the ring, the *ipso* angles show an average decrease of 2.6° and the *ortho* angles an average increase of 1.9° while the *meta* and *para* angles decrease by less than 1°.

A more direct evaluation of structural changes can be done directly using the coordinates of the substituted atoms (r_s). In this way we calculated the C2–C6 distance and C3–C5 distance in C₆F₅X (X=H, F, Cl, Br) which are compared to the same parameters of C₆H₅X (X=H, F, Cl, Br) in Table 3.4. In the same table the *ab initio* values (r_e) are also reported.

Table 3.4. *Ab initio* (r_e , MP2/aug-cc-pVTZ) and structural parameters derived from substitution structure (r_s) for the C₆F₅X and C₆H₅X (X=H, F, Cl, Br).

	C2C6 / Å		C3C5 / Å	
	r_s	r_e	r_s	r_e
C ₆ H ₆	-	2.4151	-	2.4151
C ₆ H ₅ F ²⁷	2.434(4) ^[a]	2.4307	2.416(4)	2.4131
C ₆ H ₅ Cl ³³	2.430(6)	2.4274	2.422(6)	2.4069
C ₆ H ₅ Br ³⁴	2.426(6)	2.4281	2.412(8)	2.4110
C ₆ F ₅ H ³²	2.373(3)	2.3831	2.404(3)	2.4140
C ₆ F ₆	-	2.4077	-	2.4077
C ₆ F ₅ Cl	2.3884(8)	2.3998	2.3972(8)	2.4069
C ₆ F ₅ Br	2.384(4)	2.3974	2.398(4)	2.4065

[a] Error in parentheses in units of the last digit.

The observed geometric changes of the C2–C6 distance and C3–C5 distance in C₆F₅X relative to C₆H₅X are significant and consistent. The C2–C6 and C3–C5 distances are shorter in the perfluorinated molecules than those in the hydrogenated ones. In addition, the changes in the C2–C6 distances are greater than those of the C3–C5 distances. In C₆F₅Cl (or C₆F₅Br), the C2–C6 distance is 0.01 Å (or 0.032 Å) shorter than in C₆H₅Cl (or C₆H₅Br), while the C3–C5 distance is slightly shorter, but not outside the error limits. These results, which have been calculated independently of the structural fit, are in agreement with the latter and in particular with the reduction of the *ipso* and *para* angles upon fluorination as they are in agreement also with the theoretical distances reported in the table. These observed geometric changes also agree with the trends found in C₆F₅H³² relative to C₆H₆ and in C₆F₆ relative to C₆H₅F²⁷.

3.3.4. Electronic effects

According to the ETD model, only the valence electron population in the *p*-orbitals contribute to the quadrupole coupling tensor. If the atomic quadrupole tensor axes system and the *p*-orbitals are coincident, the populations (*P*) and the nuclear quadrupole coupling constants (χ) are related by three simple equations which contain the population of each orbital and the one-electron contribution to the coupling tensor, χ_0 :²²

$$\chi_{xx} = \chi_0 \left(P_{xx} - \frac{1}{2}P_{yy} - \frac{1}{2}P_{zz} \right) \quad (1)$$

$$\chi_{yy} = \chi_0 \left(-\frac{1}{2}P_{xx} + P_{yy} - \frac{1}{2}P_{zz} \right) \quad (2)$$

$$\chi_{zz} = \chi_0 \left(-\frac{1}{2}P_{xx} - \frac{1}{2}P_{yy} + P_{zz} \right) \quad (3)$$

The experimentally derived χ_0 value for ⁷⁹Br is –769.756 MHz while for ³⁵Cl this value is 109.746 MHz.⁵⁵

From the rotational transitions the components of the nuclear quadrupolar tensor in the principal system of inertia of the molecule (*a*, *b* and *c*) are derived and according to the symmetry of the molecules examined in this thesis, the principal inertial axes are coincident with the orientation of the *p*-orbitals of the halogen atom. In fact, the *a* axis (*z* axis) lies along the C–X bond, *b* is in the plane of the molecule (*y* axis) and *c* axis (*x* axis) is perpendicular to the molecular plane. Since the inertia principal axes orientation coincide with the principal axes of the quadrupolar nucleus, the determination of the population

along the natural axes (P_{xx} , P_{yy} , P_{zz}) is straightforward through the previously introduced equations (eq. 1-3) where $\chi_{zz}=\chi_{aa}$, $\chi_{yy}=\chi_{bb}$ and $\chi_{xx}=\chi_{cc}$.

One complication which arises from the three equations not being linearly independent and some physical assumptions must be put in place to solve the system. The assumption used in the original TD model is that the electronic population of the p -orbital in the plane of the molecule and perpendicular to the C-X bond (P_{yy}) is equal to 2 and the populations of the other p -orbitals (P_{xx} and P_{zz}) are also expected to be very close to 2. With these assumptions the populations of the p -orbitals of the chlorine and bromine atoms were estimated from the experimental quadrupole coupling constants for the hydrogenated and perfluorinated benzene halides (Appendix Table A3.8). In the modified ETD model presented in ref.²⁵ the suggestion is to use the p -population anisotropies (calculated as differences in orbital's population along the axes with respect to the average population, ΔP_{xx} , ΔP_{yy} and ΔP_{zz}) in order to quantify the electronic properties. Those values are also reported in the Appendix (Table A3.8) and in Figure 3.5.

For comparison and to gain a more complete picture of the valence orbitals, a Natural Atomic Orbital (NAO) analysis was performed with the Natural Bond Orbital (NBO)⁵⁶ package within the Gaussian 16 suite of programs to calculate the populations in the halogen's valence p -orbitals. The NAO populations are also reported in the Appendix (Table A3.8) for comparison with the ones determined using the ETD model.

The NAO populations are used to characterize the lone pair halogen's orbitals (indicated as LP in Figure 3.5). In all four molecular systems the three lone pairs of the halogen atom are very similar. The C-X bond is formed by a sp hybrid orbital with essentially s character. In Figure 3.5 this is indicated by the exponent to the sp label which reports the ratio between p and s fraction of population in the orbital. The other lone pairs are in two p orbitals perpendicular to the C-X bond. Looking at the VPPA values and the orbital's labels we can see that the orbital directed along the z axis shows a decrease in population with respect to the average (ΔP_{zz} negative) while the other two show an excess (ΔP_{xx} and ΔP_{yy} positive). As discussed in ref.²⁵ the negative value of ΔP_{zz} is a direct measure of the strong electron density deficiency along the C-X bond which is also known as the σ -hole but we can also add that the p populations in the other two orbitals is related to the extent of the belt around the halogen atom.

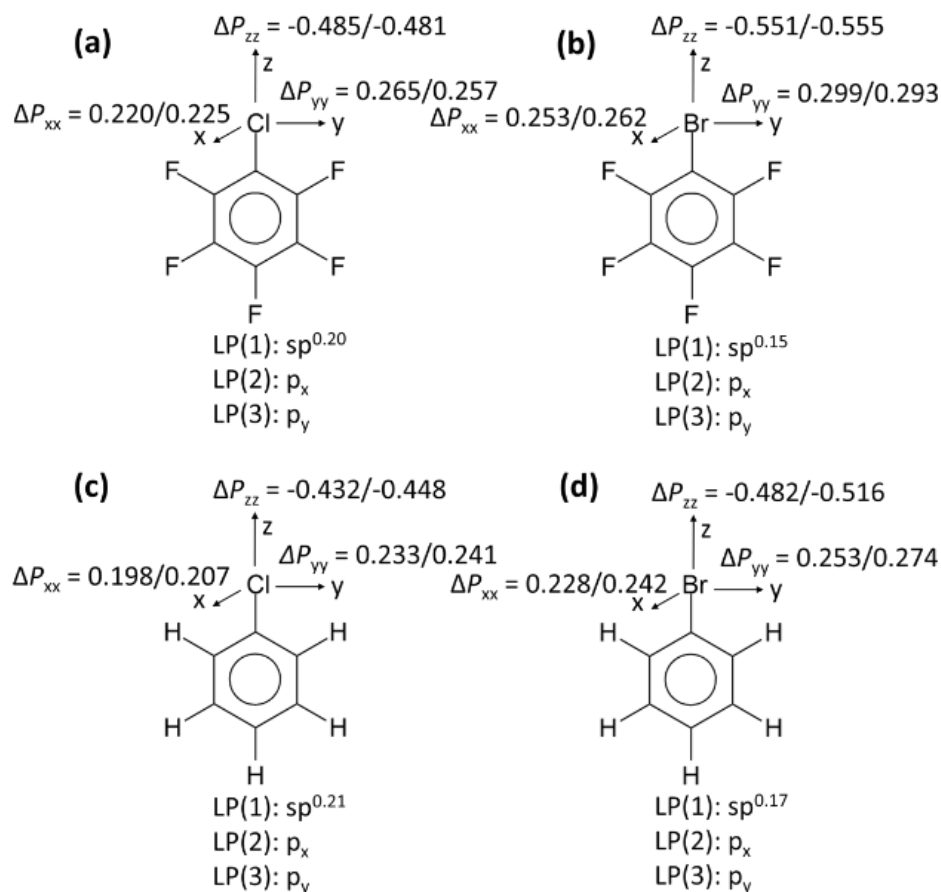


Figure 3.5. VPPA values (first value from EDT, second value from NAO) and electron lone pairs (from NAO) in (a) C_6F_5Cl , (b) C_6F_5Br , (c) C_6H_5Cl and (d) C_6H_5Br .

Looking at the ΔP_{zz} values for the four molecules we can see that this deficiency not only increases in going from chlorine to bromine, as it has been extensively pointed out in the literature, but it also increases upon ring perfluorination. In general, the effect of perfluorination is to diminish the overall p population on the halogen atom and increasing that of the nucleophilic equatorial belt.

A visualization of these effects can be obtained from the depiction of the molecular electrostatic potentials (ESP) shown in Figure 3.6. In this picture we can see the molecules along an axis perpendicular to the molecular plane while the smaller pictures are the side views along the direction of the C-X bond.

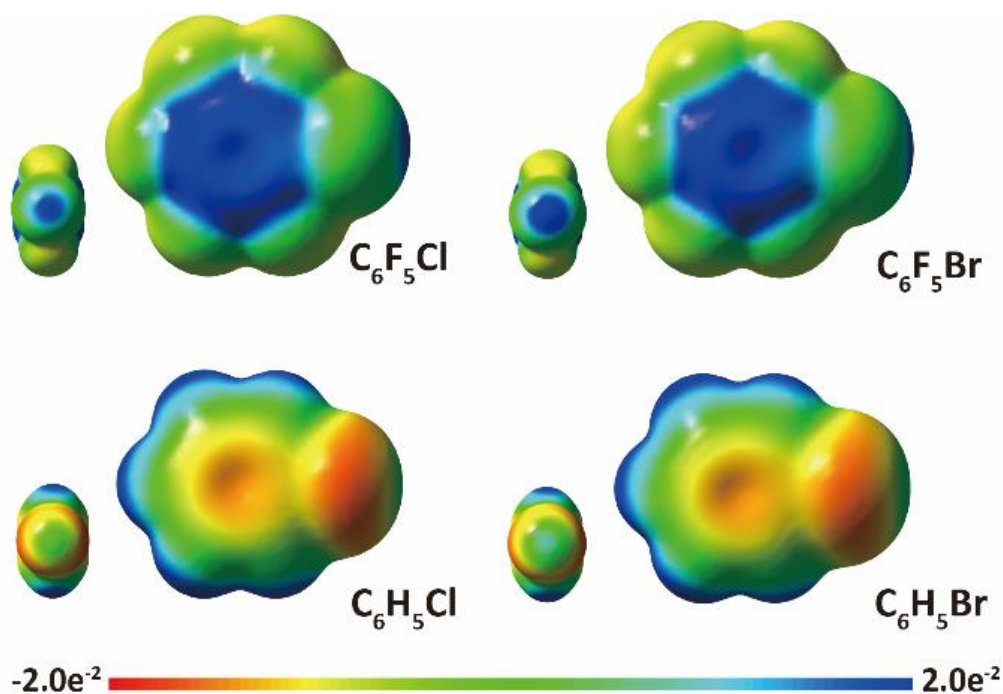


Figure 3.6. Electrostatic potential maps of C_6F_5Cl , C_6F_5Br , C_6H_5Cl , and C_6H_5Br , estimated at 0.0004 a.u. electron density by MP2/aug-cc-pVTZ calculations. The blue shading is the maximum (positive) potential, and red shading is the minimum (negative) potential. Molecules are shown along an axis perpendicular to the molecular plane; smaller pictures are the side views along the direction of the C-X bond.

The regions of the σ -system and Br or Cl atom that become positively charged and create the σ - or π -hole are seen as blue regions at the center of the ring and at the tip of Cl or Br, respectively. As discussed in the introduction, the σ -hole can generate the halogen bond located along the direction of the C-Br bond,^{5,6} while the π -hole can form the lone pair $\cdots\pi$ -hole interaction located perpendicularly to the plane of aromatic ring.^{11,13} In Figure 3.6 we can observe that the π -hole is formed only in the perfluorinated systems and it is slightly more positive in C_6F_5Cl than in C_6F_5Br . However, the σ -hole it is present in all systems, greater in Br than in Cl while it is definitely more positive in the perfluorinated systems. A nucleophilic belt is clearly visible as an electron rich region (red) along the equator of the halogen atom in the hydrogenated systems while it becomes less negative (green) in the perfluorinated ones.

3.4. Conclusions

In this work we discuss the effects of perfluorination on the structural and the electronic properties of C_6F_5Cl and C_6F_5Br . From the rotational constants determined for several isotopologues, partial structures have been determined for the two molecules and their hydrogenated counterparts. The isotopic substitution results suggest a shortening of the distances of equivalent carbon atoms for both pairs (C2-C6 and C3-C5) of about 40 mÅ which, with the C1-C4 distant not being affected, indicates an elongation of the ring along its symmetry axis, in agreement with what has been reported in the NMR study by Haloui and Haloui,^{42,43} although in that case the evidence is merely a quantum theoretical prediction.

An insight into the electronic properties of the chlorine and bromine atoms has been gained from the experimental nuclear quadrupole coupling constants determined from the rotational spectra. By applying the ETD model, the populations of the *p*-orbitals of the Cl and Br atoms have been derived and from those the valence *p*-population anisotropies (VPPA). The experimentally determined values are in agreement with those obtained using the NAO analysis and the electrostatic potential calculated at the MP2/aug-cc-pVTZ theory level. The values of the population anisotropies along the C-Cl and C-Br bonds can indicate the extent of the σ -hole present at the tip of the halogen atom while the decrease of population along the other two directions can be interpreted as a decrease of the extent of the nucleophilic belt along the equator of the halogen atom.

The results confirm that in general the σ -hole found in Br is greater than that in Cl. The results also show that the σ -hole increases upon fluorination and the chlorine atom in the perfluorinated moiety acquires a similar value to that of bromine in the hydrogenated system.

These results should be helpful in the rational design and understanding of molecular systems which exploit σ -hole and π -hole interactions.

3.5. References

- 1 K. Brendel, H. Mäder, Y. Xu and W. Jäger, *J. Mol. Spectrosc.*, 2011, **268**, 47–52.
- 2 K. A. Mason, A. C. Pearcy, I. K. Attah, S. P. Platt, S. G. Aziz and M. S. El-Shall, *Phys. Chem. Chem. Phys.*, 2017, **19**, 18603–18611.
- 3 A. C. Legon, *Phys. Chem. Chem. Phys.*, 2010, **12**, 7736–7747.
- 4 P. Politzer, P. Lane, M. C. Concha, Y. Ma and J. S. Murray, *J. Mol. Model.*, 2007, **13**, 305–311.
- 5 P. Politzer, J. S. Murray and T. Clark, *Phys. Chem. Chem. Phys.*, 2010, **12**, 7748–7757.
- 6 J. S. Murray, P. Lane, T. Clark, K. E. Riley and P. Politzer, *J. Mol. Model.*, 2012, **18**, 541–548.
- 7 T. Clark, M. Hennemann, J. S. Murray and P. Politzer, *J. Mol. Model.*, 2007, **13**, 291–296.
- 8 H. Wang, W. Wang and W. J. Jin, *Chem. Rev.*, 2016, **116**, 5072–5104.
- 9 D. Quiñonero, C. Garau, C. Rotger, A. Frontera, P. Ballester, A. Costa and P. M. Deyà, *Angew. Chemie*, 2002, **114**, 3539–3542.
- 10 I. Alkorta, I. Rozas and J. Elguero, *J. Am. Chem. Soc.*, 2002, **124**, 8593–8598.
- 11 L. Evangelisti, K. Brendel, H. Mäder, W. Caminati and S. Melandri, *Angew. Chemie*, 2017, **129**, 13887–13891.
- 12 C. Calabrese, Q. Gou, A. Maris, W. Caminati and S. Melandri, *J. Phys. Chem. Lett.*, 2016, **7**, 1513–1517.
- 13 A. Bauzá, T. J. Mooibroek and A. Frontera, *ChemPhysChem*, 2015, **16**, 2496–2517.
- 14 E. Buncel, J. M. Dust and F. Terrier, *Chem. Rev.*, 1995, **95**, 2261–2280.
- 15 S. Gronert, *Chem. Rev.*, 2001, **101**, 329–360.
- 16 L. L. Soukup and S. Gronert, *Int. J. Mass Spectrom.*, 2015, **378**, 31–37.
- 17 R. Sanchez, B. M. Giuliano, S. Melandri, L. B. Favero and W. Caminati, *J. Am. Chem. Soc.*, 2007, **129**, 6287–6290.
- 18 W. Li, A. Vigorito, C. Calabrese, L. Evangelisti, L. B. Favero, A. Maris and S. Melandri, *J. Mol. Spectrosc.*, 2017, **337**, 3–8.
- 19 C. Calabrese, W. Li, G. Prampolini, L. Evangelisti, I. Uriarte, I. Cacelli, S. Melandri and E. J. Cocinero, *Angew. Chemie Int. Ed.*, 2019, **58**, 8437–8442.
- 20 B. Velino, S. Melandri and W. Caminati, *J. Phys. Chem. A*, 2004, **108**, 4224–4227.

- 21 C. H. Townes and B. P. Dailey, *J. Chem. Phys.*, 1949, **17**, 782–796.
- 22 S. E. Novick, *J. Mol. Spectrosc.*, 2011, **267**, 13–18.
- 23 G. A. Cooper, C. J. Anderson, C. Medcraft and N. R. Walker, *J. Mol. Spectrosc.*, 2018, **354**, 15–23.
- 24 G. A. Cooper, C. Medcraft, J. D. Littlefair, T. J. Penfold and N. R. Walker, *J. Chem. Phys.*, 2017, **147**, 214303.
- 25 A. Rinald and G. Wu, *J. Phys. Chem. A*, 2020, **124**, 1176–1186.
- 26 Z. Kisiel, E. Białkowska-Jaworska and L. Pszczółkowski, *J. Mol. Spectrosc.*, 2005, **232**, 47–54.
- 27 L. Nygaard, I. Bojesen, T. Pedersen and J. Rastrup-Andersen, *J. Mol. Struct.*, 1968, **2**, 209–215.
- 28 L. Nygaard, E. R. Hansen, R. L. Hansen, J. Rastrup-Andersen and G. O. Sørensen, *Spectrochim. Acta Part A Mol. Spectrosc.*, 1967, **23**, 2813–2819.
- 29 U. Wolschendorf, U. Kretschmer and D. H. Sutter, *Zeitschrift für Naturforsch. A*, 1996, **51**, 46–52.
- 30 E. Jochims, H. Mäder and W. Stahl, *J. Mol. Spectrosc.*, 1996, **180**, 116–120.
- 31 A. Kraśnicki, M. Kręglewski and H. Mäder, *J. Mol. Struct.*, 2008, **882**, 123–127.
- 32 B. J. Bills, D. M. Carroll, A. A. Elliott, D. A. Obenchain, S. A. Peebles and R. A. Peebles, *J. Mol. Struct.*, 2012, **1023**, 149–153.
- 33 S. Cradock, J. M. Muir and D. W. H. Rankin, *J. Mol. Struct.*, 1990, **220**, 205–215.
- 34 S. A. Peebles and R. A. Peebles, *J. Mol. Struct.*, 2003, **657**, 107–116.
- 35 W. Caminati and A. M. Mirri, *Chem. Phys. Lett.*, 1971, **12**, 127–130.
- 36 O. Dorosh, E. Białkowska-Jaworska, Z. Kisiel and L. Pszczółkowski, *J. Mol. Spectrosc.*, 2007, **246**, 228–232.
- 37 A. M. Mirri and W. Caminati, *Chem. Phys. Lett.*, 1971, **8**, 409–412.
- 38 M. Onda, T. Odaka, H. Miyazaki, M. Mori, I. Yamaguchi and Y. Niide, *J. Mol. Spectrosc.*, 1996, **176**, 17–22.
- 39 M. Onda, T. Odaka, H. Miyazaki, M. Mori, I. Yamaguchi and Y. Niide, *J. Mol. Spectrosc.*, 1994, **165**, 426–432.
- 40 S. A. Peebles and R. A. Peebles, *J. Mol. Struct.*, 2002, **607**, 19–29.
- 41 A. Cairncross, W. A. Sheppard and E. Wonchoba, *Org. Synth.*, 2003, **59**, 122.

- 42 A. Haloui and E. Haloui, *J. Mol. Struct.*, 2014, **1068**, 140–148.
- 43 A. Haloui and E. Haloui, *Magn. Reson. Chem.*, 2011, **49**, 717–724.
- 44 M. J. Frisch, G. W. Trucks, H. B. Schlegel, G. E. Scuseria, M. A. Robb, J. R. Cheeseman, G. Scalmani, V. Barone, G. A. Petersson, H. Nakatsuji and others, *Gaussian Inc. Wallingford CT*.
- 45 C. Calabrese, A. Maris, I. Uriarte, E. J. Cocinero and S. Melandri, *Chem. Eur. J.*, 2017, **23**, 3595–3604.
- 46 M. Reiher, *Wiley Interdiscip. Rev. Comput. Mol. Sci.*, 2012, **2**, 139–149.
- 47 T. H. Dunning Jr, *J. Chem. Phys.*, 1989, **90**, 1007–1023.
- 48 A. K. Wilson, D. E. Woon, K. A. Peterson and T. H. Dunning Jr, *J. Chem. Phys.*, 1999, **110**, 7667–7676.
- 49 B. P. Pritchard, D. Altarawy, B. Didier, T. D. Gibson and T. L. Windus, *J. Chem. Inf. Model.*, 2019, **59**, 4814–4820.
- 50 H. M. Pickett, *J. Mol. Spectrosc.*, 1991, **148**, 371–377.
- 51 J. K. G. Watson, Elsevier Science Publishers B.V., Oxford, New York, 1977.
- 52 J. Kraitchman, *Am. J. Phys.*, 1953, **21**, 17–24.
- 53 C. C. Costain, *Trans. Am. Crystallogr. Assoc.*, 1966, **2**, 157–164.
- 54 Z. Kisiel, *J. Mol. Spectrosc.*, 2003, **218**, 58–67.
- 55 E. A. C. Lucken and E. Schempp, *Phys. Today*, 1969, **23**, 56–57.
- 56 E. D. Glendening, A. E. Reed, J. E. Carpenter and F. Weinhold, *NBO Version 3.1*, 2003.
- 57 G. G. Brown, B. C. Dian, K. O. Douglass, S. M. Geyer, S. T. Shipman and B. H. Pate, *Rev. Sci. Instrum.*, 2008, **79**, 53103.
- 58 J.-U. Grabow, W. Stahl and H. Dreizler, *Rev. Sci. Instrum.*, 1996, **67**, 4072–4084.
- 59 T. J. Balle and W. H. Flygare, *Rev. Sci. Instrum.*, 1981, **52**, 33–45.
- 60 W. Caminati, A. Millemaggi, J. L. Alonso, A. Lesarri, J. C. López and S. Mata, *Chem. Phys. Lett.*, 2004, **392**, 1–6.
- 61 W. Caminati, L. Evangelisti, G. Feng, B. M. Giuliano, Q. Gou, S. Melandri and J.-U. Grabow, *Phys. Chem. Chem. Phys.*, 2016, **18**, 17851–17855.

Chapter IV

Intermolecular interactions and conformational Equilibria between Aldehydes and Alcohols: Rotational Spectra of Acrolein-Methanol Complex

4.1. Introduction

In the past few decades, the scientific community has made great progress in the understanding of the nature and properties of the HB, which was defined by the IUPAC in 2011.¹ This definition specifies:

“The hydrogen bond is an attractive interaction between a hydrogen atom from a molecule or a molecular fragment X–H in which X is more electronegative than H, and an atom or a group of atoms in the same or a different molecule, in which there is evidence of bond formation.”

Some types of molecules (for example, alcohols,² acids,³ amides⁴) are very prone to form HBs, acting as a proton donor or acceptor. The conformational preference in forming HB affects the energetics of chemical reactions and the structure of biological macromolecules.^{5,6} Complexes involving aldehydes and alcohols are particularly interesting systems in HB studies because they contain a combination of stronger HBs and weaker secondary interactions. The study of clusters of aldehydes and alcohols aims to determine the interaction sites and relative arrangement of monomers, and determine the intermolecular forces at play, and it lays the foundation for the study of macroscopic systems.

Rotational spectroscopy is highly sensitive to atomic mass distribution, so it can be used to study conformational equilibria and isotopic species. The combination of rotational spectroscopy analysis and theoretical methods provides a synergistic method for studying the structure and internal dynamics of isolated molecules and weakly bound complexes.

In this thesis, we report the microwave detection and analysis of the 1:1 complex of acrolein (ACR) with methanol (MeOH), one of the simplest mixed aldehyde and alcohol dimers, ACR is also one of the most important environmental pollutant and plays an important role in the formation of atmospheric aerosols.⁷⁻⁹ It is also a very important synthetic intermediate in the chemical industry and is widely used in resin production and organic synthesis.¹⁰

Two conformations of ACR, *s-trans* and *s-cis*, have been characterized by microwave spectroscopy,¹¹⁻¹⁷ pointing out that the *s-trans* form is more stable than the *s-cis* one by 9.2(5) kJ mol⁻¹.¹⁸ The presence of two different conformers of the ACR monomer can make the investigation of the complex formation more interesting since the energy scale of the conformations can change upon complexation. The rotational spectra of ACR involved in binary and ternary water complexes and some of their isotopologues have been analysed.¹⁹ All the complexes show a planar heavy atom skeleton and are stabilized by ring-like structures. In the binary complexes ACR-water, the conformation where the aldehyde oxygen forms a HB with the water hydrogen and water oxygen forms a HB with the methylenic group are most stable and the ACR adopts the *s-trans* form. The electron pairs located at the aldehyde oxygen are quite efficient proton acceptors that can easily form a HB with proton donors like water, alcohols or other protonated compounds. At the same time, the hydroxyl oxygen of MeOH can easily form another interaction with the methylenic hydrogen or aldehydic hydrogen atoms of ACR. In this case, it is possible that the 1:1 complex of ACR and MeOH will also show a ring-like structure where aldehyde oxygen interacts with hydroxyl hydrogen and hydroxyl oxygen interacts with methylenic hydrogen or aldehydic hydrogen.

The rotational spectrum of the MeOH monomer and its cluster with other molecules has been studied and the splitting of the spectra caused by the internal rotation of methyl group were observed.^{9,20-28} All barriers of the methyl group internal rotation in complexes are lower than those observed in the monomer. MeOH exhibits a A-E spectral splitting pattern due to the hindered internal rotation of its methyl rotor,⁹ and the barrier was determined with a value of 4.463(4) kJ mol⁻¹.²⁹ In the studies of 1:1 complexes of MeOH with other molecules in gas phase,³⁰⁻³⁴ all the

barriers that hinder the internal rotation of the methyl group in the complex are lower than that in the MeOH monomer. For example, in the 1:1 complex of MeOH-SO₂²⁶, the observed methyl top internal rotation barrier is $V_3=1.54(1)$ kJ mol⁻¹ based on the assumption that the methyl group rotates against a heavy frame. In the more loosely bound MeOH-Ar complex²⁸, an even more striking drop in the methyl torsional barrier height to about 0.82(2) kJ mol⁻¹ was observed in the experiment, confirming that these reductions are not a result of complexation effects, but rather are related to another large amplitude internal motion. In the note by Fraser *et al.*³⁵, the decrease of the MeOH internal rotation barrier is attributed to a liberational motion of the whole MeOH moiety or the methyl group. In more recently study of the 1:1 complex of acrylonitrile–MeOH³⁶ in gas phase using rotational spectroscopy, the consistent change was not observed in the determined internal rotation parameters upon deuteration of the whole methyl group, which led them to exclude that the decrease of the MeOH internal rotation barrier after complexation is related to a liberational motion of the whole MeOH moiety or the methyl group.

4.2. Methods

The experiment was carried out in our COBRA-type pulsed supersonic-jet FTMW spectrometer.^{37–40} ACR and MeOH were acquired from Sigma-Aldrich (purity >99%), which all were used without further purification while D₂O was acquired from Cambridge Isotope Laboratories, Inc. (purity 99.9%) For the preparation of the complexes, samples of ACR (cooled to 273K) and MeOH (at 298K) were prepared in two separate containers and Helium at a stagnation pressure of about 0.6 MPa, was flowed over them creating a 1% mixture of both ACR and MeOH in the carrier gas. The molecular beam was then expanded through a solenoid valve (General Valve, Series 9, nozzle diameter of 0.5 mm) into a Fabry–Pérot cavity. During the expansion, the molecules and their complexes can reach quite low rotational temperatures and the most stable forms can be trapped at their energy minimum when certain conditions are satisfied. To determine the position of the spectral lines, Fourier transformation of the time-domain signal perform 8 k data points, recorded at a sampling interval of 100 ns. The hydroxyl enriched deuterated isotope of methanol was prepared by directly mixing methanol with the D₂O sample in 1:2 ratio.

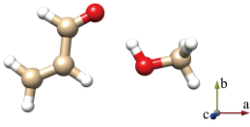
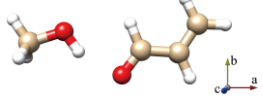
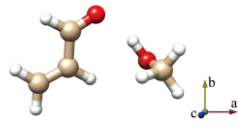
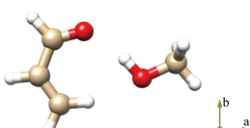
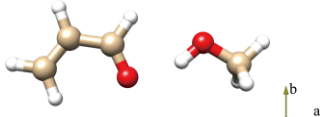
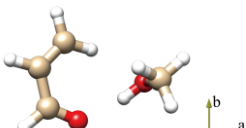
Geometry optimizations were performed using the GAUSSIAN 16 program⁴¹ and the B3LYP/6-311++G** and MP2/6-311++G** methods to determine the ground state rotational

constants. After the analysis of the results the lowest energy structures were again optimized using the method MP2/aug-cc-pVTZ. The analysis of the spectral data was performed with the program of XIAM,⁴² which is based on the combined axis method.⁴³ The non-covalent interactions between ACR and MeOH were analyzed with Johnson's NCI method,⁴⁴ which can visualize and quantify the non-covalent interactions based on RDG.

4.3. *Ab initio* results

For simplicity, the complex of ACR and MeOH are abbreviated as ACR-MeOH, and the *s-trans* and *s-cis* conformations of acrolein are labeled as *t* and *c*. Distinct conformers of the MeOH complex which originate from the same conformer of ACR have been further distinguished with a progressive number (1, 2 or 3). The choice of the initial geometries was informed by the previous study ACR-water.¹⁹ In that case four planar conformers, in which the water forms a HB with the ACR oxygen atom and a secondary interaction involving the water oxygen with either the methylenic or the aldehydic ACR hydrogen, were identified. In the ACR-MeOH case, two additional non-planar conformers (one from each of ACR's conformation and indicated by the number 3) were found. In both cases the MeOH's methyl group is located almost perpendicularly to the ACR's plane. The theoretical (MP2/aug-cc-pVTZ) spectroscopic parameters and relative energies (ΔE) of all conformers are reported in Table 4.1. These results can be also compared with those obtained with other methods and basis sets (B3LYP/6-311++G**, MP2/6-311++G**) reported in the Appendix.

Table 4.1. *Ab initio* (MP2/aug-cc-pVTZ) spectroscopic parameters, relative energies.

	<i>t</i> -ACR-MeOH-1	<i>t</i> -ACR-MeOH-2	<i>t</i> -ACR-MeOH-3
			
<i>A, B, C</i> / MHz	6233, 1390, 1145	11158, 1036, 954	4905, 1692, 1373
μ_a, μ_b, μ_c / D	-2.4, -0.5, 0.0	2.7, 0.6, 0.0	-3.2, -1.4, 1.6
ΔE / kJ mol ⁻¹	0	3.7	1.4
	<i>c</i> -ACR-MeOH-1	<i>c</i> -ACR-MeOH-2	<i>c</i> -ACR-MeOH-3
			
<i>A, B, C</i> / MHz	5974, 1505, 1211	16485, 1007, 955	4958, 1824, 1481
μ_a, μ_b, μ_c / D	-2.4, 0.0, 0.0	-2.5, 0.2, 0.0	-3.0, -1.2, -1.8
ΔE / kJ mol ⁻¹	10.5	13.5	11.0

The complexes of MeOH with *t*-ACR show in general lower energies than those with *c*-ACR. In fact, the three lowest energy structures are the complexes of MeOH with *t*-ACR span about 3.7 kJ mol⁻¹ and the lowest energy structure formed by *c*-ACR (*c*-ACR-MeOH-1) is located 10.5 kJ mol⁻¹ higher. This energy difference is very close to the energy difference (9.2(5) kJ mol⁻¹) determined for the two forms of the ACR monomer¹⁸ and the energy difference (9.9 kJ mol⁻¹) for the *t*- and *c*-ACR complexes with water.¹⁹

The six lowest energy structures (three originating from *t*-ACR and three from *c*-ACR) all exhibit a stronger OH \cdots O HB and a weaker C-H \cdots O interaction. The hydroxyl group of MeOH acts as a proton donor for the OH \cdots O interaction and as a proton acceptor for the C-H \cdots O interaction. The conformations 1 and 3, in which the MeOH oxygen forms a weak interaction with the methylenic hydrogen, are more stable than the conformations labelled 2 where the oxygen is bound to the aldehydic hydrogen. For example, conformer *t*-ACR-MeOH-2 is 3.7 kJ mol⁻¹ higher

in energy than *t*-ACR-MeOH-1 and conformer *c*-ACR-MeOH-2 is 3.0 kJ mol⁻¹ higher in energy than *c*-ACR-MeOH-1.

Considering conformations 1 and 3, where the MeOH oxygen is bound to the methylenic hydrogen, the planar conformers show lower energy than the non-planar ones although in general those differences are smaller than the ones between 1 and 2. The energy difference between *t*-ACR-MeOH-3 and *t*-ACR-MeOH-1 is 1.4 kJ mol⁻¹ and the energy difference between *c*-ACR-MeOH-3 and *c*-ACR-MeOH-1 is 0.5 kJ mol⁻¹.

4.4. Experimental results

We started our experiment with the search of the $J' \leftarrow J''$: $3 \leftarrow 2$ μ_a -R rotational transition for *t*-ACR-MeOH-1. According to the computational results, *t*-ACR-MeOH-1 is the global minimum and shows the most intense spectrum originating from the μ_a dipole moment component which is much higher with respect to μ_b and μ_c with dipole moment components. After the detection and fit of one group of rotational transitions, the measurements were extended following new predictions to 42 rotational transitions with rotational quantum number J ranging from 2 to 6 and K_a ranging from 0 to 2.

After finding all detectable *rotational* transition of conformer *t*-ACR-MeOH-1, the measurements were extended to find those of conformer *t*-ACR-MeOH-2. From its relative energy and considering the temperature prior to the expansion (273K) the population of *t*-ACR-MeOH-2 was predicted to be 19.6% of the global minimum and taking into account the values of the dipole moment components the most intense μ_a lines of *t*-ACR-MeOH-2 were predicted to be 22.0% of the most intense ones of *t*-ACR-MeOH-1. Indeed, 42 rotational transitions with the rotational quantum number J ranging from 2 to 6 and K_a ranging from 0 to 2 were observed for *t*-ACR-MeOH-2.

The list of the frequencies for both conformers is reported in the Appendix. The spectral parameters of measured conformations *t*-ACR-MeOH-1 and *t*-ACR-MeOH-2 obtained through the XIAM program⁴² have been summarized in Table 4.2. The fitted rotational constants are reproduced by those theoretical methods for the two conformers within 3%. The detected μ_a -type and μ_b -type rotational transitions without μ_c -type line confirm the assignment to the planar

conformers, in agreement with the null value of the μ_c dipole moment components for both two conformers.

As an example, the $3_{03} \leftarrow 2_{02}$ transition for *t*-ACR-MeOH-1 conformer is shown in Figure 4.1. The A-E splitting in the rotational spectra is due to the internal rotation of the methyl group of MeOH where A and E are methyl torsional state symmetry labels. The equation of the Hamiltonian used in the analysis of the spectra in its simple form is shown as follows^{45,46}:

$$H = H_{\text{rr}} + H_{\text{cd}} + H_1 \quad (1)$$

H_{rr} is the Hamiltonian of the standard rigid rotor. H_{cd} contains a set of centrifugal distortion terms, H_1 represents the part of the internal rotation Hamiltonian.

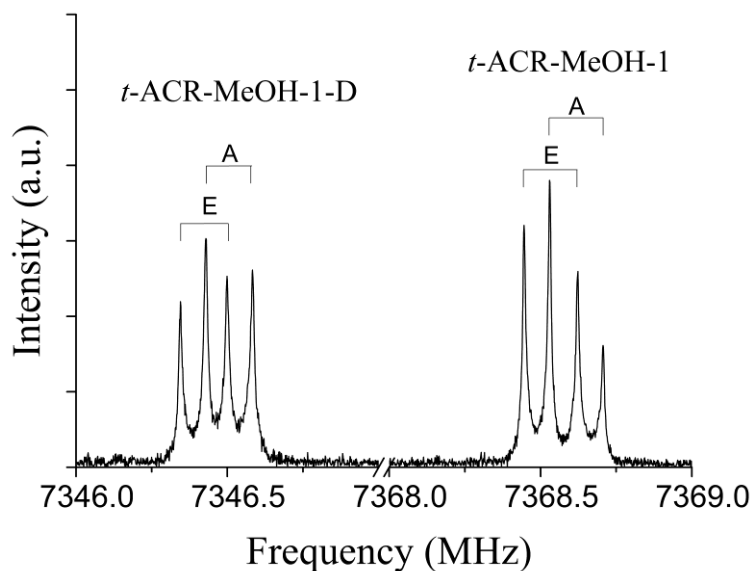


Figure 4.1. $3_{03} \leftarrow 2_{02}$ transitions of *t*-ACR-MeOH-1 and *t*-ACR-MeOH-1-D enriched isotopologue showing the methyl internal rotation A-E doublets. Each line appears as a doublet (indicated by square bracket) due to the instrumental Doppler effect.

Table 4.2. Experimental spectroscopic parameters of the parent and deuterated species of *t*-ACR-MeOH-1 and *t*-ACR-MeOH-2.

	<i>t</i> -ACR-MeOH-1	<i>t</i> -ACR-MeOH-1-D	<i>t</i> -ACR-MeOH-2	<i>t</i> -ACR-MeOH-2-D
<i>A</i> / MHz	6180.152(3) ^[a]	6193.285(9)	11263.02(4)	11312(12)
<i>B</i> / MHz	1350.2493(7)	1345.401(2)	1009.515(3)	1004.652(2)
<i>C</i> / MHz	1116.9532(7)	1114.199(1)	933.289(3)	929.742(2)
<i>D</i> _J / kHz	0.905(6)	0.905(6)	0.724(9)	0.71(1)
<i>D</i> _{JK} / kHz	-4.30(9)	-4.7(1)	-37.1(1)	-38(1)
<i>d</i> ₁ / kHz	-0.219(6)	-0.217(9)	-0.09(1)	-0.082(9)
<i>V</i> ₃ / kJ mol ⁻¹	2.686(3)	2.825(3)	2.723(6)	2.856(1)
δ / deg	0.089(7)	[0.089] ^[b]	2.896(5)	2.881(4)
<i>F</i> ₀ / GHz	155.6(1)	159.3(2)	156.1(3)	[156.1]
σ ^[c] / kHz	5.8	11.9	15.9	8.9
<i>N</i> ^[d]	42	46	42	24

[a] Error in parentheses in units of the last digit. [b] The data in brackets were fixed at the corresponding normal species values because they were not determined in the fit. [c] RMS error of the fit. [d] Number of lines in the fit.

From the fitting procedure of the experimental transition frequencies, in addition to the rotational constants and centrifugal distortion constants, internal rotation parameters are also obtained, as reported in Table 4.2. The three-fold barrier to internal rotation of the methyl group, *V*₃, is smaller in *t*-ACR-MeOH-1 (2.686(3) kJ mol⁻¹) than in *t*-ACR-MeOH-2 (2.723(6) kJ mol⁻¹). Both of them have a low internal rotational barrier compared to the MeOH monomer with a value of 4.463(4) kJ mol⁻¹.²⁹

In order to understand the decreased barrier of *V*₃ after complexation, the potential energy surface of the MeOH methyl torsion, shown in Figure 4.2, is calculated by changing the dihedral angle of $\tau = \text{HC-OH}$ on the regular grid with $\Delta\tau=10^\circ$. The calculation data expressed in red bullets are well reproduced by the threefold function: $V(\tau)=\frac{1}{2}V_3[1+\cos(3\tau)]$, which is shown with a green

line for *t*-ACR-MeOH-1 and blue line for *t*-ACR-MeOH-2 in Figure 4.2. The maximum value of *t*-ACR-MeOH-1 in (3.32 kJ mol⁻¹) represents the theoretical barrier hindering the methyl group internal rotation in the complex and it can be noticed that it is larger (about 26%) than the experimental values obtained for the normal species, $V_3=2.686(3)$ kJ mol⁻¹ for *t*-ACR-MeOH-1 (see Table 4.2). The different values of V_3 between the theoretical (3.45kJ mol⁻¹) and experimental (2.723(6) kJ mol⁻¹) were also observed in *t*-ACR-MeOH-2. It is possible to attribute these differences to the accuracy of the theoretical method and this can be tested by calculating the barrier to internal rotation for free MeOH (4.16 kJ mol⁻¹) and comparing it to the experimental barrier (4.50 kJ mol⁻¹).⁴⁷ The calculated barrier for free MeOH is indeed lower than the experimental one but only by about 7% which is quite smaller than the 26% difference found for *t*-ACR-MeOH-1 and 27% for *t*-ACR-MeOH-2. This difference could be due to a lower accuracy of the method in calculating methyl torsional barriers in molecular complexes or to a possible large amplitude motion coupled to the torsion but of which we don't have evidence in the rotational spectrum. Other reported MeOH clusters^{9,20-28} also show a decreased in the internal rotation barrier compared to the isolated MeOH monomer and this has been attributed to a libational motion of the whole MeOH moiety or the methyl group. As described by Fraser *et al.*³⁵ in a note, the apparent barrier reductions are largely an artifact of the large-amplitude libational motion of the MeOH unit about its *a* inertial axis.

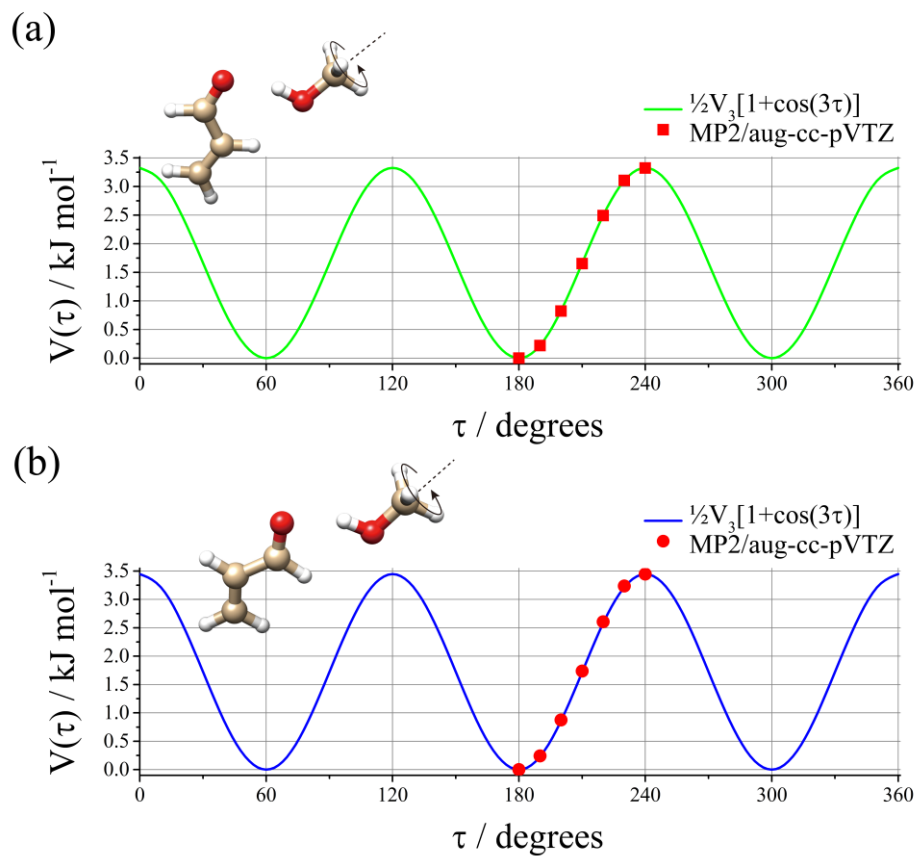


Figure 4.2. *Ab initio* methyl internal rotational potential energy surface for (a) *t*-ACR-MeOH-1 and (b) *t*-ACR-MeOH-2.

After empirical scaling of the rotation constant of the parent species, the rotation spectrum of the deuterated isotope MeOH, abbreviated as *t*-ACR-MeOH-1-D and *t*-ACR-MeOH-2-D, was measured and obtained. Consistently with the expected values, due to very small mass changes, the μ_a -R-type spectral frequencies of the isotopes corresponding lines are slightly lower than the parent species. The spectral parameters obtained through the XIAM program⁴² have been summarized in Table 4.2 and the observed transition frequencies of all measured isotopes are provided in the Appendix. As same as the spectra of parent species, the peaks in the experimental spectra of deuterated isotope are also split in a doublet pattern. As shown in Table 4.2, the deuterated species *t*-ACR-MeOH-1-D ($V_3=2.825(3)$ kJ mol^{-1}) and *t*-ACR-MeOH-2-D ($V_3=2.856(1)$ kJ mol^{-1}) show a higher barrier of V_3 than their parent species *t*-ACR-MeOH-1 ($V_3=2.686(3)$ kJ mol^{-1}) and *t*-ACR-MeOH-2 ($V_3=2.723(6)$ kJ mol^{-1}). We would expect to find a larger A–E splitting of the spectrum of deuterated specie *t*-ACR-MeOH-1-D due to the higher barrier of V_3 . Conversely,

in the $3_{03} \leftarrow 2_{02}$ transition (Figure 4.1), the deuterium bonded dimer *t*-ACR-MeOH-1-D has a splitting of ~ 0.16 MHz, while the hydrogen-bonded dimer *t*-ACR-MeOH-1 is split by ~ 0.18 MHz. The smaller splitting of A-E for deuterated species *t*-ACR-MeOH-1-D and *t*-ACR-MeOH-2-D were summarized in the Table A6.7. This differences in the splittings is due to the Ubbelohde effect that is the shortening of the HBs upon deuteration.⁴² This effect that increasing the rigidity of the deuterium bond dimer reduces the splitting of A-E was also reported in ethanol–MeOH dimer.³⁴

The most intense μ_a lines of *t*-ACR-MeOH-3 (considering its relative energy, temperature prior and the dipole moment) was predicted to be 72.0% of the most intense ones of *t*-ACR-MeOH-1, which is higher than that of *t*-ACR-MeOH-2. However, the conformer *t*-ACR-MeOH-3 was not found in the experimental spectrum. This could be attributed to a relaxation of the population of this conformation onto that of the global minimum during adiabatic expansion. In order to confirm this, the potential energy surface for the interconversion was calculated by changing the dihedral angle $\tau = \text{CO-HO}$ on a regular grid with a step of 5 degrees. As shown in Figure 4.3a, in conformations in which the MeOH oxygen is bound to the methylenic hydrogen atoms (conformers *t*-ACR-MeOH-1 and *t*-ACR-MeOH-3) the global minima correspond to conformation *t*-ACR-MeOH-1, while conformer *t*-ACR-MeOH-3 gives rise to two relative equivalent minima which are mirror-symmetrical with respect to the ACR plane. The relaxation of the population of conformation 3 during adiabatic expansion is demonstrated by the conversion between the two conformations. This is depicted in Figure 4.3a that the low barrier (around 0.1 kJ mol^{-1}) to interconversion between the two conformations. In conformations where the MeOH oxygen is bound to the aldehydic hydrogen (conformer 2), the non-planar conformer was not obtained from the calculations, as shown in Figure 4.3b. In addition to global minima corresponding to conformation 2, there is no other relative equivalent minima. This may be due to two reasons: non-planar conformer exists but was not found due to the accuracy of calculation method; non-planar conformer is not stable considering the weak intermolecular interaction between MeOH oxygen and aldehydic hydrogen.

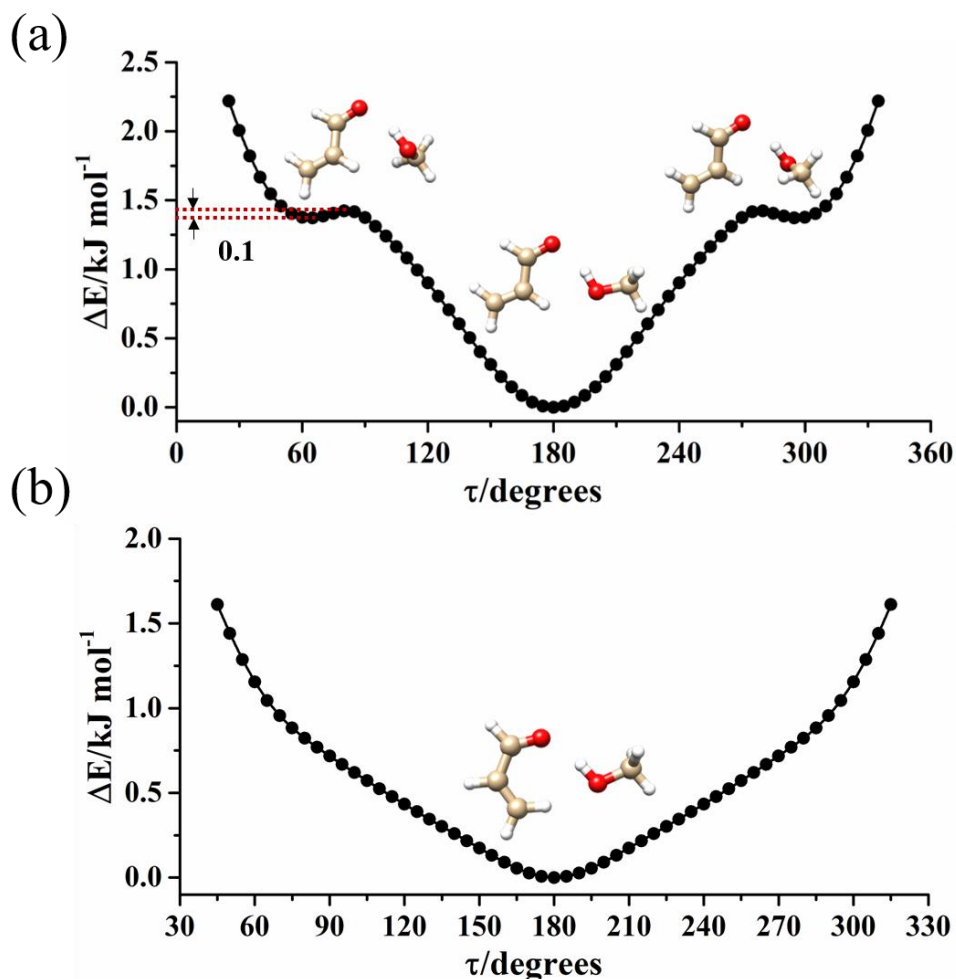
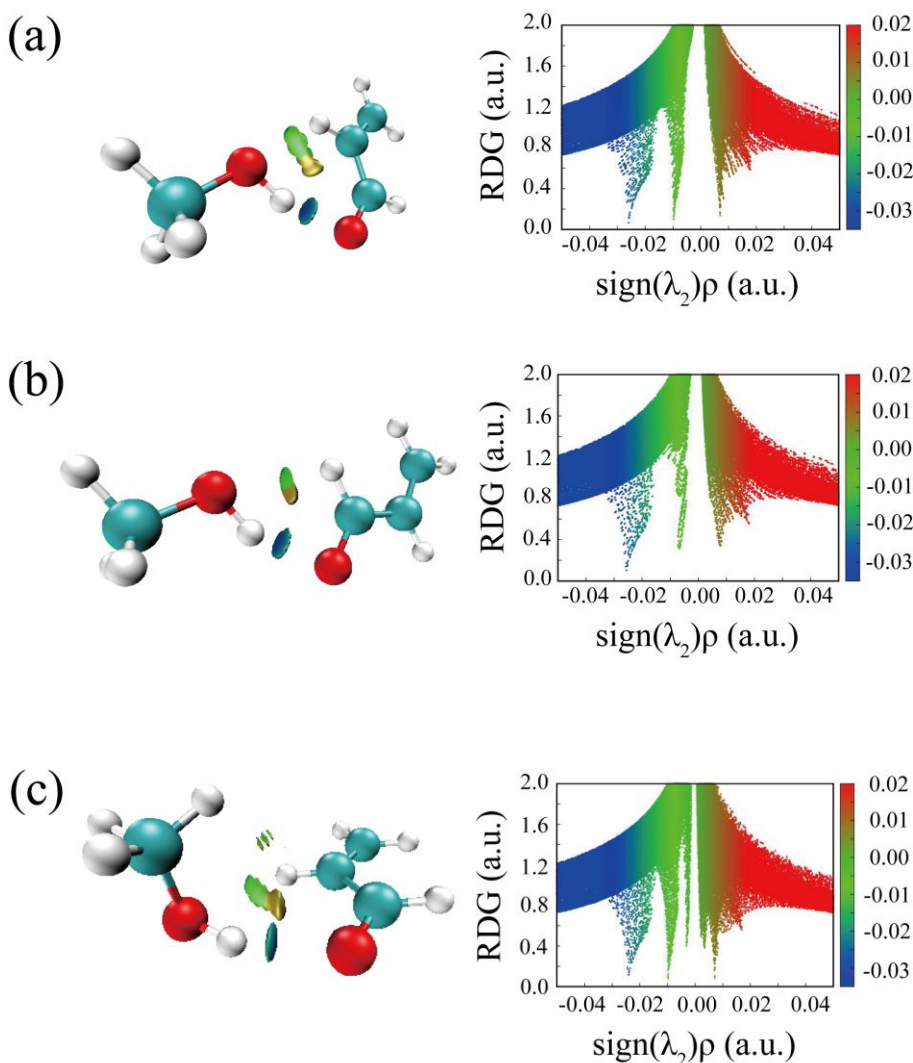


Figure 4.3. *Ab initio* potential energy surface for the torsion of the MeOH's methyl group around the OH bond for the (a) *t*-ACR-MeOH-1 and (b) *t*-ACR-MeOH-2. This motion interconverts the in-plane conformer (absolute minimum) with the out of-plane ones (relative equivalent minima).

In order to get a better visualization of the non-covalent interaction between molecules, the analysis of the HBs in the six optimized conformers was performed by Johnson's NCI method.⁴⁴ Figure 4.4 displays the NCI Plots revealing the pattern of intermolecular interactions. The gradient isosurfaces are colored according to the corresponding values of $\text{sign}(\lambda_2)\rho$. In the negative values of the $\text{sign}(\lambda_2)\rho$ and small values of the RGD (<0.5 a.u.), the blue regions suggest a stronger OH \cdots O HB and the green regions suggest a weaker C–H \cdots O interaction. In the positive values of the $\text{sign}(\lambda_2)\rho$ and small values of the RGD (<0.5 a.u.), the orange regions suggest a weak repulsive interaction.

Considering the complexes of MeOH with *t*-ACR and *c*-ACR, the relatively large orange regions between oxygen and hydrogen inside *c*-ACR, as shown in Figure 4.4(d-f), suggest a weak repulsive intramolecular interaction, responding to the less stable of *c*-ACR compared with *t*-ACR. The comparison between conformations 1 and 2, as shown in Figure 4.4(a-b), indicates that the OH...O HB in two conformations is of similar strength, while the C-H...O interaction in conformations 1 is stronger than that in conformations 2. This is in agreement with the results of the theoretical calculation (using the method MP2/aug-cc-pVTZ) that conformations 1 have lower energy than conformations 2.



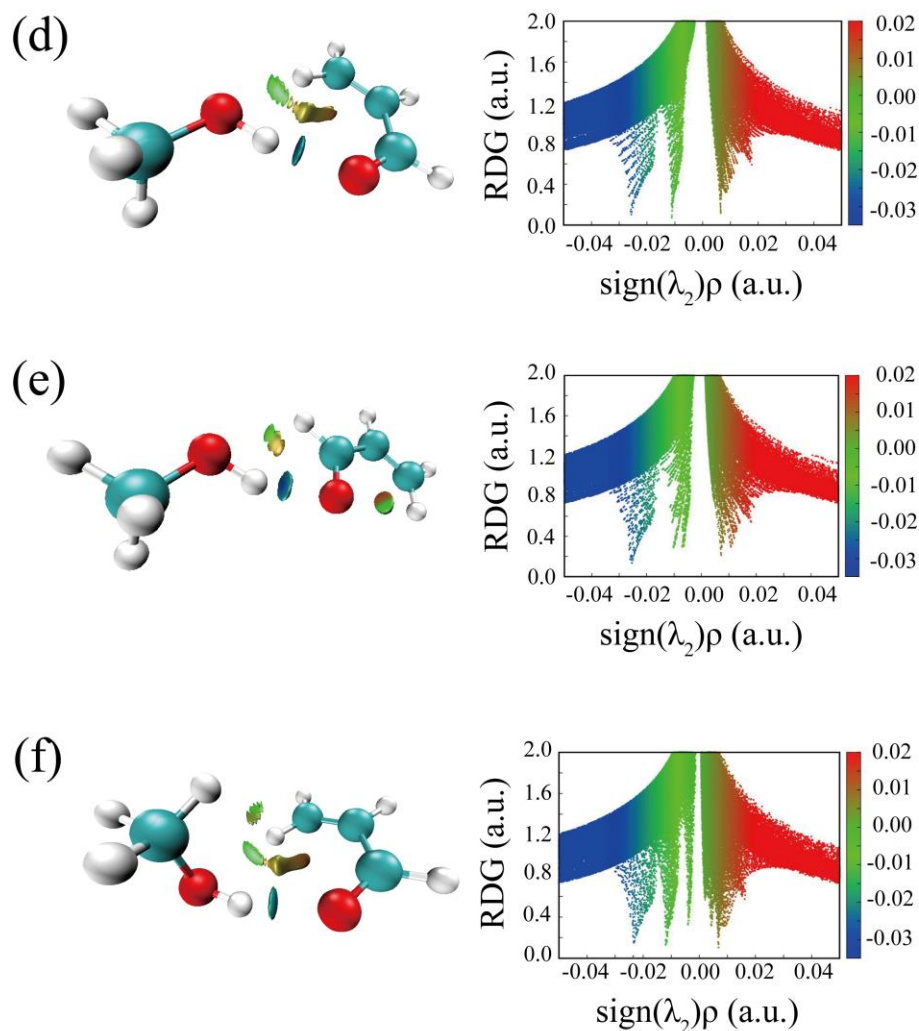


Figure 4.4. The NCI plots from the *ab initio* (MP2/aug-cc-pVTZ) outputs for three conformers: (a) *t*-ACR-MeOH-1, (b) *t*-ACR-MeOH-2, (c) *t*-ACR-MeOH-3, (d) *c*-ACR-MeOH-1, (e) *c*-ACR-MeOH-2 and (f) *c*-ACR-MeOH-3. Left panel: gradient isosurfaces according to the values of the $\text{sign}(\lambda_2)\rho$ (-0.04~0.04 a.u.). Color coding is blue (stronger attractive interactions), green (weaker attractive interactions) and orange-red (repulsive interaction). Right panel: The RDG versus $\text{sign}(\lambda_2)\rho$. Positive values of the $\text{sign}(\lambda_2)\rho$ indicate repulsive interactions, and negative values of the $\text{sign}(\lambda_2)\rho$ indicate attractive interactions.

4.5. Conclusion

In this research, we have studied the HBs between the 1:1 complex of ACR and MeOH and the barrier hindering the methyl group internal rotation in the complex. Two stable conformations of ACR- MeOH and their deuterated isotopologues have been characterized. The determined rotational constants are coherent with a theoretical determined cyclic structure (MP2/aug-cc-pVTZ) stabilized by a primary OH...O HB between MeOH and the aldehyde group and a secondary one between the terminal CH group and the MeOH oxygen which were also characterized and visualized using NCI plots. Splitting of the rotational lines due to the hindered internal rotation of the methyl group were observed and the global analysis of the spectrum leads to the determination of a V_3 value of 2.686(3) kJ mol⁻¹ and 2.723(6) kJ mol⁻¹ for two conformations, respectively. These values are about 40% lower than that experimentally determined for free MeOH. The correspondence of the reduced mass of the internal rotation motion to the one calculated from the structure, led us to exclude that the lowering of the barrier could be ascribed to a librational motion of the methyl group.

4.6. Reference

- 1 E. Arunan, G. R. Desiraju, R. A. Klein, J. Sadlej, S. Scheiner, I. Alkorta, D. C. Clary, R. H. Crabtree, J. J. Dannenberg, P. Hobza and others, *Pure Appl. Chem.*, 2011, **83**, 1637–1641.
- 2 L. J. Bellamy and R. J. Pace, *Spectrochim. Acta*, 1966, **22**, 525–533.
- 3 W. Li, L. Evangelisti, Q. Gou, W. Caminati and R. Meyer, *Angew. Chemie Int. Ed.*, 2019, **58**, 859–865.
- 4 D. A. Dixon, K. D. Dobbs and J. J. Valentini, *J. Phys. Chem.*, 1994, **98**, 13435–13439.
- 5 G. D. Rose and R. Wolfenden, *Annu. Rev. Biophys. Biomol. Struct.*, 1993, **22**, 381–415.
- 6 G. R. Desiraju and T. Steiner, *The weak hydrogen bond: in structural chemistry and biology*, International Union of Crystal, 2001, vol. 9.
- 7 Z. Li, S. A. Nizkorodov, H. Chen, X. Lu, X. Yang and J. Chen, *Atmos. Chem. Phys.*, 2019, **19**, 1343–1356.
- 8 M. T. Borchers, S. Wesselkamper, S. E. Wert, S. D. Shapiro and G. D. Leikauf, *Am. J. Physiol. Cell. Mol. Physiol.*, 1999, **277**, L489–L497.
- 9 H. E. Ayer and D. W. Yeager, *Am. J. Public Health*, 1982, **72**, 1283–1285.
- 10 A. R. Pradipta and K. Tanaka, *Chem. Rec.*, 2021, **21**, 646–662.
- 11 L. Evangelisti, A. Maris, F. Grieco, C. Calabrese and S. Melandri, *Can. J. Phys.*, 2020, **98**, 555–559.
- 12 E. A. Cherniak and C. C. Costain, *J. Chem. Phys.*, 1966, **45**, 104–110.
- 13 R. Wagner, J. Fine, J. W. Simmons and J. H. Goldstein, *J. Chem. Phys.*, 1957, **26**, 634–637.
- 14 M. Winnewisser, G. Winnewisser, T. Honda and E. Hirota, *Zeitschrift für Naturforsch. A*, 1975, **30**, 1001–1014.
- 15 A. I. Jaman and R. Bhattacharya, *J. At. Mol. Phys.*
- 16 C. E. Blom and A. Bauder, *Chem. Phys. Lett.*, 1982, **88**, 55–58.
- 17 C. E. Blom, G. Grassi and A. Bauder, *J. Am. Chem. Soc.*, 1984, **106**, 7427–7431.
- 18 A. C. P. Alves, J. Christoffersen and J. M. Hollas, *Mol. Phys.*, 1971, **20**, 625–644.
- 19 W. Li, A. Maris, C. Calabrese, I. Usabiaga, W. D. Geppert, L. Evangelisti and S. Melandri, *Phys. Chem. Chem. Phys.*, 2019, **21**, 23559–23566.

- 20 E. Fliege, H. Dreizler and V. Typke, *Zeitschrift für Naturforsch. A*, 1983, **38**, 668–675.
- 21 P. A. Stockman, G. A. Blake, F. J. Lovas and R. D. Suenram, *J. Chem. Phys.*, 1997, **107**, 3782–3790.
- 22 M. Haeckel and W. Stahl, *J. Mol. Spectrosc.*, 1999, **198**, 263–277.
- 23 F. J. Lovas and H. Hartwig, *J. Mol. Spectrosc.*, 1997, **185**, 98–109.
- 24 V. V Ilyushin, F. J. Lovas and D. F. Plusquellic, *J. Mol. Spectrosc.*, 2006, **239**, 94–100.
- 25 A. Westphal, C. Jacoby, C. Ratzer, A. Reichelt and M. Schmitt, *Phys. Chem. Chem. Phys.*, 2003, **5**, 4114–4122.
- 26 L. Sun, X. Tan, J. J. Oh and R. L. Kuczkowski, *J. Chem. Phys.*, 1995, **103**, 6440–6449.
- 27 X.-Q. Tan, I. I. Ioannou and R. L. Kuczkowski, *J. Mol. Struct.*, 1995, **356**, 105–115.
- 28 X. Q. Tan, L. H. Sun and R. L. Kuczkowski, *J. Mol. Spectrosc.*, 1995, **171**, 248–264.
- 29 R. M. Lees, F. J. Lovas, W. H. Kirchhoff and Dr. Johnson, *J. Phys. Chem. Ref. Data*, 1973, **2**, 205–214.
- 30 P. A. Stockman, G. A. Blake, F. J. Lovas and R. D. Suenram, *J. Chem. Phys.*, 1997, **107**, 3782–3790.
- 31 M. Schmitt, J. Küpper, D. Spangenberg and A. Westphal, *Chem. Phys.*, 2000, **254**, 349–361.
- 32 F. J. Lovas, R. D. Suenram, G. T. Fraser, C. W. Gillies and J. Zozom, *J. Chem. Phys.*, 1988, **88**, 722–729.
- 33 F. J. Lovas, S. P. Belov, M. Y. Tretyakov, J. Ortigoso and R. D. Suenram, *J. Mol. Spectrosc.*, 1994, **167**, 191–204.
- 34 I. A. Finneran, P. B. Carroll, G. J. Mead and G. A. Blake, *Phys. Chem. Chem. Phys.*, 2016, **18**, 22565–22572.
- 35 G. T. Fraser, F. J. Lovas and R. D. Suenram, *J. Mol. Spectrosc.*, 1994, **167**, 231–235.
- 36 C. Calabrese, A. Maris, A. Vigorito, S. Mariotti, P. Fathi, W. D. Geppert and S. Melandri, *J. Phys. Chem. A*, 2020, **124**, 3601–3608.
- 37 J.-U. Grabow, W. Stahl and H. Dreizler, *Rev. Sci. Instrum.*, 1996, **67**, 4072–4084.
- 38 T. J. Balle and W. H. Flygare, *Rev. Sci. Instrum.*, 1981, **52**, 33–45.
- 39 W. Caminati, A. Millemaggi, J. L. Alonso, A. Lesarri, J. C. López and S. Mata, *Chem. Phys. Lett.*, 2004, **392**, 1–6.

- 40 W. Caminati, L. Evangelisti, G. Feng, B. M. Giuliano, Q. Gou, S. Melandri and J.-U. Grabow, *Phys. Chem. Chem. Phys.*, 2016, **18**, 17851–17855.
- 41 M. J. Frisch, G. W. Trucks, H. B. Schlegel, G. E. Scuseria, M. A. Robb, J. R. Cheeseman, G. Scalmani, V. Barone, G. A. Petersson, H. Nakatsuji and others, *Gaussian Inc. Wallingford CT*.
- 42 A. R. Ubbelohde and K. J. Gallagher, *Acta Crystallogr.*, 1955, **8**, 71–83.
- 43 R. C. Woods, *J. Mol. Spectrosc.*, 1966, **21**, 4–24.
- 44 E. R. Johnson, S. Keinan, P. Mori-Sánchez, J. Contreras-García, A. J. Cohen and W. Yang, *J. Am. Chem. Soc.*, 2010, **132**, 6498–6506.
- 45 H. Hartwig and H. Dreizler, *Zeitschrift für Naturforsch. A*, 1996, **51**, 923–932.
- 46 N. Hansen, H. Mäder and T. Bruhn, *Mol. Phys.*, 1999, **97**, 587–595.
- 47 L.-H. Xu and F. J. Lovas, *J. Phys. Chem. Ref. Data*, 1997, **26**, 17–156.

Chapter V

Intermolecular interactions and conformational Equilibria between Aldehydes and Alcohols: Rotational Spectra of Acrolein-Ethanol Complex

5.1. Introduction

Intermolecular interactions and conformational equilibria between aldehydes and alcohols have not been extensively studied. In this chapter, we focus on the study of the dimer formed by ACR and ethanol (EtOH) by the means of rotational spectroscopy combined with quantum chemical calculations. In the previous chapter, we introduced our work about the 1:1 adduct of ACR with methanol, where a combination of stronger HB and a weaker HB was determined by rotational spectroscopy. The comparison between different systems is helpful to further understand the intermolecular forces at play, the interaction sites and relative arrangement of monomers between aldehydes and alcohols.

Rotational spectroscopy with its high degree of accuracy is suitable for studying the conformational equilibria of weakly bound complexes. Applying appropriate theoretical models to analyze these rotational spectra, information about molecular structure, intermolecular interactions and internal motions can be obtained, so that the driving forces involved in the formation of molecular complexes can be determined and understood.

In our previous works on the rotational spectrum of ACR in binary and ternary water complexes¹ and ACR with methanol, a planar heavy atom skeleton and ring-like structures were found. The electron pair located at the aldehyde oxygen acts like a quite efficient proton acceptors

that can easily form HBs with proton donors like water, alcohols or any protonated compounds. At the same time, the hydroxyl oxygen of water and alcohols can easily interact to form another HBs with the aliphatic hydrogen atoms of ACR.

We thought it would be interesting to study the structural changes occurring in the complexes of ACR when the interacting molecule is heavier and more complex for example comparing the already studied 1:1 complex of ACR with methanol to the one formed with EtOH.

The EtOH monomer can be found in three stable structures (depicted in Figure 5.1): *gauche* (dihedral angle $\tau_{\text{CCOH}} = 60^\circ$), *trans* (dihedral angle $\tau_{\text{CCOH}} = 180^\circ$) and *gauche'* (dihedral angle $\tau_{\text{CCOH}} = -60^\circ$). The two equivalent *gauche* conformations are considered to be transient chiral structures due to the interconversion through quantum tunnelling between two equivalent forms.² Kakar and Quade reported that the energy difference between two *gauche* torsional substates to $\sim 97\text{GHz}$ and the energy difference between the *gauche-trans* EtOH is measured to be $41.2 \pm 5.0 \text{ cm}^{-1}$ using H-P 8460A MRR spectrometer.³

A few microwave spectroscopy investigations on the EtOH cluster are reported concerning EtOH dimers,^{4,5} EtOH-argon,⁶ EtOH-methanol,⁷ EtOH-water,⁸ EtOH-dimethylether,⁹ EtOH-acetone¹⁰ and EtOH-(1,4-dioxane)¹¹. All of them take into account both *trans* and *gauche* forms of the EtOH monomer in the calculations, while only the *gauche* isomer is involved in the formation of most of the complexes. Only in the rotational spectroscopy study on EtOH-dimethylether and EtOH dimers, both *trans* and *gauche* forms of the EtOH monomer were observed. When the EtOH molecule interacts with water⁸ and methanol⁷ through non-covalent bonds, it generally acts as proton acceptor while when it interacts with other molecules, such as dimethylether,⁹ acetone¹⁰ or 1,4-dioxane¹¹, EtOH generally acts as proton donor.

In the studies on the EtOH dimers, a total of six conformers of the induced chiral dimers of EtOH, involving *trans* and *gauche* forms of the monomer, have been observed using microwave spectroscopy.^{4,5} With the same experimental technique the van der Waals forces in the global minimum configuration of *trans*-EtOH ... argon have been investigated.⁶ The preferred HB donor/acceptor configurations between EtOH and methanol determined by the analysis of the rotational spectra have been assigned to a *trans*-EtOH-acceptor/methanol-donor structure, a *gauche*-EtOH-acceptor/methanol-donor structure while no EtOH-donor/methanol-acceptor dimers have been found.⁷ Regarding the complexes between EtOH and water, Finneran *et al.* identify the observed conformer as a water-donor/EtOH-acceptor structure and EtOH is found to

be in the *gauche* conformation.⁸ Evangelisti *et al.* found both *trans* and *gauche* conformations of EtOH in the complex of EtOH-dimethylether, originating two conformations where dimethylether acts as the proton accepting unit. An interesting feature is that the structure involving the *gauche* EtOH is found to be the global minimum thus switching the conformational stability of EtOH after complexation with dimethylether. In the works of the 1:1 complexes of EtOH with acetone¹⁰ and the 1:1 complexes of EtOH with 1,4-dioxane¹¹, by using rotational spectroscopy, they observed the conformation of *gauche* EtOH working as the proton donor. The *trans* conformer, which is 100–200 cm⁻¹ higher in energy than the *gauche* form, was not detected in the supersonic jet due to the relaxation phenomena upon supersonic expansion.

5.2. Methods

The COBRA-type pulsed supersonic-jet FTMW spectrometer^{12–15} was used to measure the rotational spectrum of the complexes. The samples ACR, EtOH and D₂O were acquired from Sigma-Aldrich (purity >99%) and used without further purification. Enriched hydroxylic deuterated isotopologue EtOH was prepared by mixing D₂O with EtOH in the 1:1 ratio. Samples of ACR (cooled to 273K) and EtOH (at 298K) were prepared in two different containers. Helium at a stagnation pressure of about 0.6 MPa, was flowed over the samples resulting in about 1% mixture of both ACR and EtOH. The molecular beam was then expanded through a solenoid valve (General Valve, Series 9, nozzle diameter of 0.5 mm) into a Fabry Perot cavity to exploit already described features of the coaxial supersonic expansion.

The search for the stable geometries of the 1:1 complexes between ACR and EtOH were performed with CREST(conformer-rotamer ensemble sampling tool) software.^{16,17} Geometry optimizations were performed using the GAUSSIAN 16 program¹⁸ and the B3LYP/ def2tzvp and MP2/ def2tzvp methods to determine the ground state rotational constants. After the analysis of the results the six lowest energy structures were again optimized using the method MP2/aug-cc-pVTZ. The analysis of the spectral data was performed with the SPFIT program by Pickett¹⁹. The non-covalent interactions between ACR and EtOH were analyzed with Johnson's NCI method²⁰, which can visualize and quantify the non-covalent interactions based on RDG.

5.3. *Ab initio* results

For simplicity, the *s-trans* and *s-cis* conformations of ACR are labeled as *t* and *c*, and the *trans*, *gauche* and *gauch'* conformations of EtOH are labeled as *t*, *g* and *g'*. The complexes of ACR and EtOH were predicted using program of CREST¹⁷. Two conformations of ACR, *t*- and *c*-ACR, have been characterized in a previous work, pointing out that the *t*-ACR form is more stable than *c*-ACR by 9.2(5) kJ mol⁻¹.²¹ As step before three conformations of EtOH, *t*- (Figure 5.1a), *g* (Figure 5.1b) and *g'*-EtOH (Figure 5.1c) must be taken into account. The choice of the initial geometries was informed by our previous study of ACR-water¹ and ACR-methanol (Chapter VI). In the ACR-water case, four planar conformers, in which the water forms a HB with the ACR oxygen atom and a secondary interaction involving the water oxygen with either the methylenic or the aldehydic hydrogen, were identified. The conformation of *t*-ACR with water where the water oxygen interacts with the methylenic hydrogen has the lowest energy. In the ACR-methanol case, two additional conformers were identified in which the methanol's methyl group is located almost perpendicularly to ACR's plane.

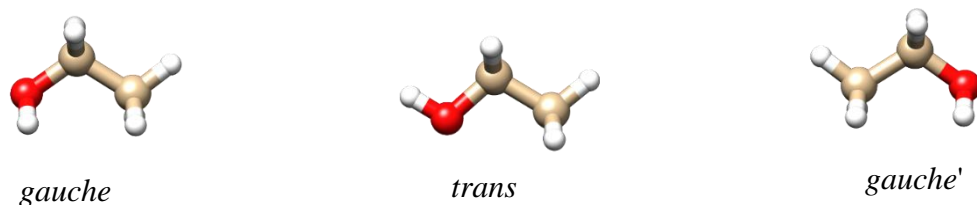


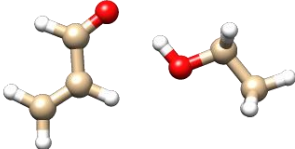
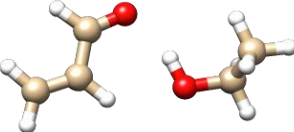
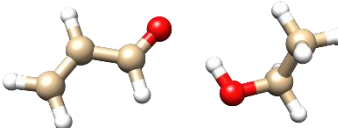
Figure 5.1. The three stable conformations of EtOH (*g*- and *g'*-EtOH are equivalent).

The choice of the initial structures for the configurational search with CREST was the conformation of *t*-ACR···*t*-EtOH where the EtOH molecule lies in the ACR plane, EtOH hydrogen interacts with the aldehydic hydrogen and the EtOH oxygen interacts with the methylenic hydrogen. All 71 resulting conformers were optimized at B3LYP levels of theory with the def2tzvp basis set giving a final set of 13 stable conformers. The 13 stable conformers were optimized subsequently at the MP2/ aug-cc-pVTZ level, as presented in Table A5.1. All the conformers were confirmed to be local minima by performing harmonic vibrational calculations. Concise symbol have been devised for each structure of the dimer. It is of the form ABx where the letters A can be

“*t*” or “*c*” and specify the *t*- or *c*-ACR. The letter B can be “*g*”, “*t*”, or “*g*” and specifies the EtOH monomer units exhibit *g*-, *t*-, or *g*'-EtOH configurations. The letter x specifies the lone pair of hydroxyl oxygen and takes values “1” or “2” depending on the methylenic hydrogen or aldehydic hydrogen involved in HBs.

The theoretical spectroscopic parameters and relative energies of 3 most stable conformers are reported in Table 5.1, while the Cartesian coordinates of the optimized structures are available in the Appendix. These results can be also compared with those obtained with other methods and basis sets (B3LYP/def2tzvp, MP2/6-311++G**) also reported in the Appendix.

Table 5.1. *Ab initio* (MP2/aug-cc-pVTZ) spectroscopic parameters, relative energies of ACR-EtOH.

	<i>tt1</i>	<i>tg1</i>	<i>tg2</i>
			
<i>A</i> / MHz	4841.3	5024.1	7473.6
<i>B</i> / MHz	890.4	937.4	737.1
<i>C</i> / MHz	759.2	834.7	700.0
μ_a / D	-2.2	2.4	-2.6
μ_b / D	1.0	-0.3	-0.7
μ_c / D	0.0	-0.4	0.3
P_{aa} / u Å ²	564.4	522.0	670.0
P_{bb} / u Å ²	101.2	83.5	52.0
P_{cc} / u Å ²	3.1	17.1	15.6
ΔE / kJ mol ⁻¹	0.0	0.2	31.3

The complexes of EtOH with *t*-ACR show in general lower energy than those with *c*-ACR. The lowest energy structure formed by *c*-ACR (TC1) is located 10.5 kJ mol⁻¹ higher. This energy difference is similar to the energy difference 9.2(5) kJ mol⁻¹ for the two forms of the ACR

monomers,²¹ the energy difference 9.9 kJ mol⁻¹ for the complexes with water¹ and the energy difference 10.5 kJ mol⁻¹ for the complexes with methanol.

The complexes of ACR with *trans*-EtOH (*tt1*) show in general lower energy than those with *g*-EtOH. The lowest energy structure formed by *g*-EtOH (*tg1*) is located 0.2 kJ mol⁻¹ higher. This energy difference is similar to the energy difference 0.5 kJ mol⁻¹ for the *g-trans* forms of the EtOH monomer.² The conformational stability of two *gauche* form of EtOH, which are equivalent in EtOH monomer, are also with similar relative energy after bounding to ACR. For example, conformer TG'1 is only 0.1 kJ mol⁻¹ higher in energy than *tg1*. Conformers *cg1* and *cg'1* is equivalent in energy and 10.1 kJ mol⁻¹ higher than global minimum.

The 13 lowest energy structures all exhibit a stronger HB and a weaker interaction. Because of the high acidity of the hydroxyl hydrogen atom, in all cases the hydroxyl group of EtOH is acting as a proton donor for the OH...O interaction and ACR as the proton acceptor. The conformations AB1, in which the EtOH oxygen forms a weak interaction with the methylenic hydrogen, are more stable than AB2 where the oxygen is bound to the aldehydic hydrogen. For example, conformer *tt2* is 3.7 kJ mol⁻¹ higher in energy than *tt1* and conformer *ct2* is 3.1 kJ mol⁻¹ higher in energy than *ct1*.

5.4. Experimental results

Our experiment started with the search of spectroscopic of rotational transition for *tt1* and *tg1* together considering that they have similar theoretical values of the rotational constants, of the calculated dipole moment components and of the relative intensities of the predicted rotational transitions in the spectrometer frequency range. As an example of the observations, the $5_{15} \leftarrow 4_{14}$ transition for *tg1* conformer is shown in Figure 5.2. After one group of rotational transitions were detected, the measurement extended to 45 rotational transitions with the rotational quantum number *J* ranging from 2 to 9 and *K_a* ranging from 0 to 2. The detected μ_a -type and μ_b -type rotational transitions and the missing μ_c -type line are in agreement with $\mu_c=0.0$ for *tt1* and the relatively low value of μ_c dipole moment components for *tg1*. The transition's frequencies are reported in the Appendix. The rotational constants of the observed conformers obtained through the SPFIT program are summarized in the Table 5.2.

The determined values of rotational constants of the observed conformer points to the assignment of *tt1* or *tg1* reproduced by the theoretical calculations with an accuracy of 4.2 % and 2.5%, respectively. The observed conformer was assigned to *tg1* (with the predicted value of planar inertia moment P_{cc} 17.12 u Å²) confirmed by the value of the planar inertia moment P_{cc} (17.91 u Å²) which is far away from the predicted value of P_{cc} (3.15 u Å²) for *tt1*.

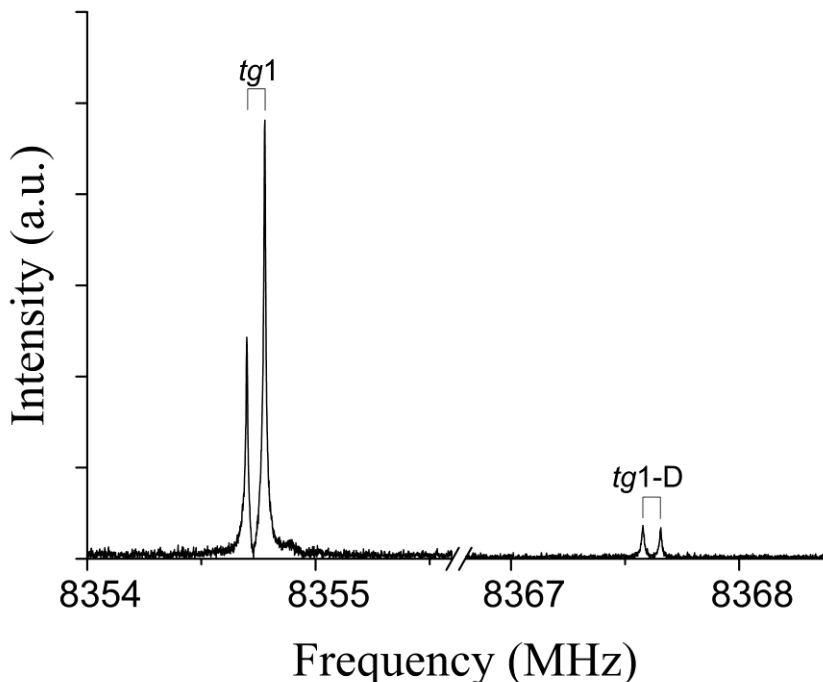


Figure 5.2. $5_{15} \leftarrow 4_{14}$ transitions of *tg1* and isotopologues. The picture denotes the enhancement with respect to the natural abundance mixing of EtOH with the D₂O sample. Each line appears as a doublet (indicated by square bracket) due to the instrumental Doppler effect.

After finding all rotational transitions of conformer *tg1*, the measurement was extended to find transitions of conformer *tg2*. Both in the complexes of ACR-water and ACR-methanol, two conformations involving that hydroxyl hydrogen forms a HB with the *s-trans*-ACR oxygen atom and a secondary interaction involving the hydroxyl oxygen with either the methylenic or the aldehydic hydrogen, were identified. From its relative energy and the temperature prior to the expansion the population of *tg2* was predicted to be 21.2% of the *tg1* and taking into account the values of the dipole moment components the most intense μ_a line of *tg2* was predicted to be 23.5% of the most intense ones of *tg1*. The detection of μ_a -type and μ_b -type rotational transitions and the

missing μ_c -type line are in agreement with the values of the dipole moment components including the relatively low value of μ_c for *tg2*. The determined values of the rotational constants of the observed conformer assignment to *tg2* are reproduced by the theoretical calculations with an accuracy of 1.8 %. The rotational constants of the observed conformers *tg2* were summarized in the Table 5.2, with a total number of 30 transitions and an RMS of 1.9 kHz. The observed transition frequencies of measured conformer are provided in the Appendix.

Table 5.2. Experimental spectroscopic parameters of the observed conformers of ACR-EtOH.

	<i>tg1</i>	<i>tg1-D</i>	<i>tg2</i>
<i>A</i> / MHz	4978.335(2) ^[a]	4977.67(9)	7272(1)
<i>B</i> / MHz	908.1839(2)	909.1131(6)	722.82(1)
<i>C</i> / MHz	812.2777 (2)	813.6817(5)	694.574(1)
<i>D_J</i> / kHz	1.262(1)	1.335(1)	-3.551(5)
<i>D_{JK}</i> / kHz	-16.97(3)	-18.92(6)	141.6(3)
<i>d₁</i> / kHz	0.0809(9)	0.100(2)	0.717(6)
<i>d₂</i> / kHz	-	-	-0.051(1)
<i>H_J</i> / Hz	-	-	0.67(2)
<i>H_{JK}</i> / kHz	-	-	0.020(1)
<i>H_{KJ}</i> / kHz	-	-	0.15(5)
<i>h₁</i> / Hz	-	-	0.21(2)
<i>P_{aa}</i> / u Å ²	538.5688(2)	537.738(1)	678.658(6)
<i>P_{bb}</i> / u Å ²	83.6123(2)	83.364(1)	48.953(6)
<i>P_{cc}</i> / u Å ²	17.9034(2)	18.166(1)	20.537(6)
σ ^[c] / kHz	2.0	2.9	1.9
<i>N</i> ^[d]	45	32	30

[a] Error in parentheses in units of the last digit. [b] The data in brackets were fixed at the corresponding normal species values because they were not determined in the fit. [c] RMS error of the fit. [d] Number of lines in the fit.

After empirical scaling of the rotational constants with those of the parent species, the rotational spectra was extended to find the rotational transitions of their hydroxyl deuterated

species. Since the spectral intensity of conformation *tg2* is low (around 2.5 a.u.), only the deuterated species of *tg1*, abbreviated as *tg1-D*, was measured and analyzed. The rotational spectrum of the hydroxyl deuterated isotopologue with enhanced intensity was observed by mixing EtOH with D₂O in 1:2 ratio and using the solution in place of the EtOH sample. The peaks in this subtracted spectrum were assigned with a total number of 32 transitions and an RMS of 0.6 kHz for deuterated isotopologues *tg1-D*. The rotational constants of the observed conformers *tg1* and isotopologue *tg1-D* were summarized in the Table 5.2. The observed transition frequencies of measured isotopologue species are provided in the Appendix. Due to the transition intensity of ¹³C isotopologues observed in natural abundance (1%) being very low, ¹³C isotopologue was not observed.

The rotational transitions belonging to the conformation of *tt1* was not observed in the experiment spectrum. In order to understand this, the potential energy surface of the methyl torsion around the OH bond in EtOH and *tt1* was calculated by changing the dihedral angle of $\tau = \text{CC-OH}$ on the regular grid with $\Delta\tau=10^\circ$, as shown in Figure 5.3. The global minima correspond to *tt1*, and the two relative equivalent minima correspond to *tg1*. The *tg1* conformation has two equivalent forms with the EtOH moiety above or below the ACR plane so it has a double degeneracy with respect to the population distribution based on the Boltzmann equation. In this case, considering its relative energy and the temperature prior to the expansion the population of *tt1* was predicted to be 53.6% of the *tg1* and considering the values of the dipole moment components the most intense μ_a line of *tt1* was predicted to be 50.2% of the most intense ones of *tg1*. Despite this, the rotational transitions of *tt1* were not observed in the spectrum although this conformation is the theoretical minimum conformation and should have been observable given the overall intensity of the spectrum. The missing *t*-EtOH form is in consistent with the result in the complexes of EtOH–water,⁸ -methanol,⁷ and -(1,4-dioxane),¹¹ where the *t*-EtOH isomer was always not observed due to the relaxation phenomena upon supersonic expansion.

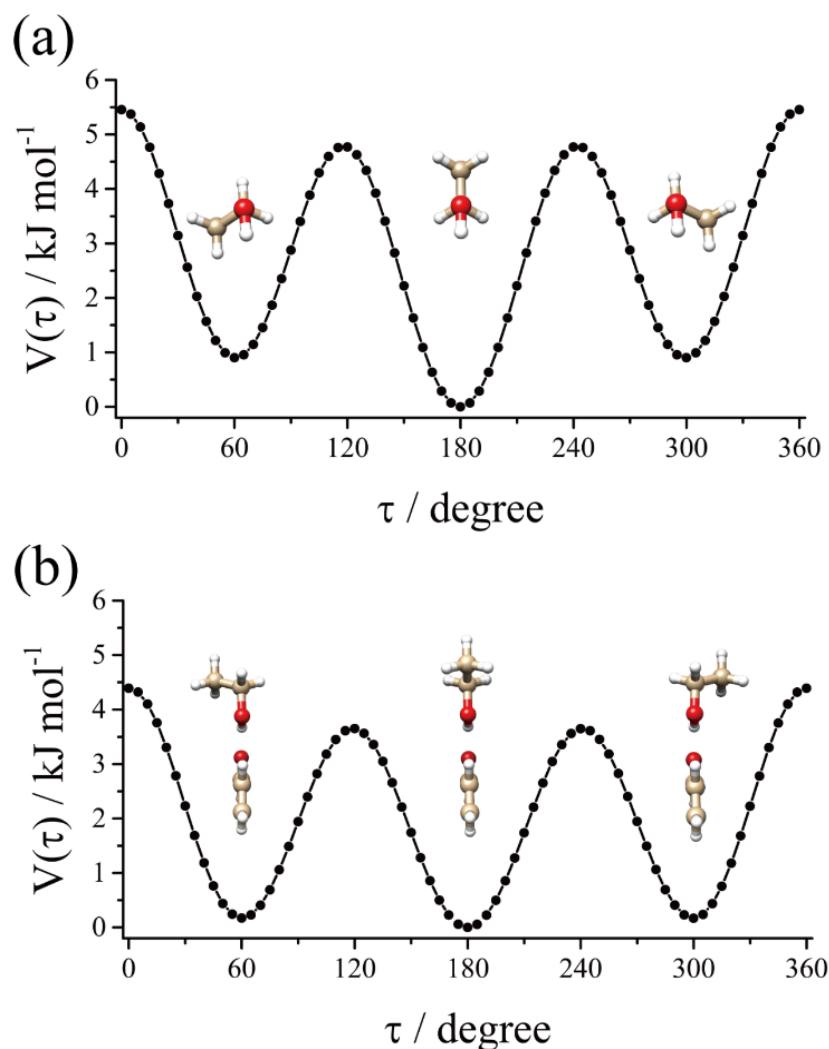


Figure 5.3. *Ab initio* (MP2/aug-cc-pVTZ) potential energy surface for the torsion of the EtOH's methyl group around the OC bond for the *tt1*. This motion interconverts *tt1* conformer (absolute minimum) with *tg1* (first relative equivalent minima), and TG'1 (second relative equivalent minima). It was also compared with the potential energy surface of EtOH.

In order to get a better visualization of non-covalent interaction between molecules, the analysis of the HBs in three conformers was performed by Johnson's NCI method²⁰. The gradient isosurfaces, see in Figure 5.4, are colored according to the corresponding values of $\text{sign}(\lambda_2)\rho$. Figure 5.4 also displays the NCI Plots revealing the pattern of intermolecular interactions. In all three conformers, the blue regions and green regions (where negative values of the $\text{sign}(\lambda_2)\rho$, small values of the RGD) suggest a strong $\text{OH}\cdots\text{O}$ HB compatible a weak $\text{C-H}\cdots\text{O}$ hydrophobic interaction, and the values orange regions (where positive of the $\text{sign}(\lambda_2)\rho$, small values of the

RGD) suggest a weak repulsive interaction. In conformations *tt1*, *tg1* and *tg2*, as shown in Figure 5.4, all three conformation show two interactions, a strong OH...O HB and a weak C-H...O interaction. Considering the complexes of EtOH with *t*-ACR and *c*-ACR, the relatively large orange regions between oxygen and hydrogen inside *c*-ACR, as shown in Figure 5.4(a,b), suggest a weak repulsive intramolecular interaction, corresponding to the less stable of *c*-ACR compared with *t*-ACR. Comparing the two conformations *tg1* and *tg2*, as shown in Figure 5.4(a,c), the OH...O HB in two conformations *tg1* and *tg2* is similar, while the C-H...O hydrophobic interaction in conformations *tg1* is stronger than conformations *tg2*. This is in agreement with the calculation result that *tg1* have lower energy than *tg2* using the method MP2/aug-cc-pVTZ.

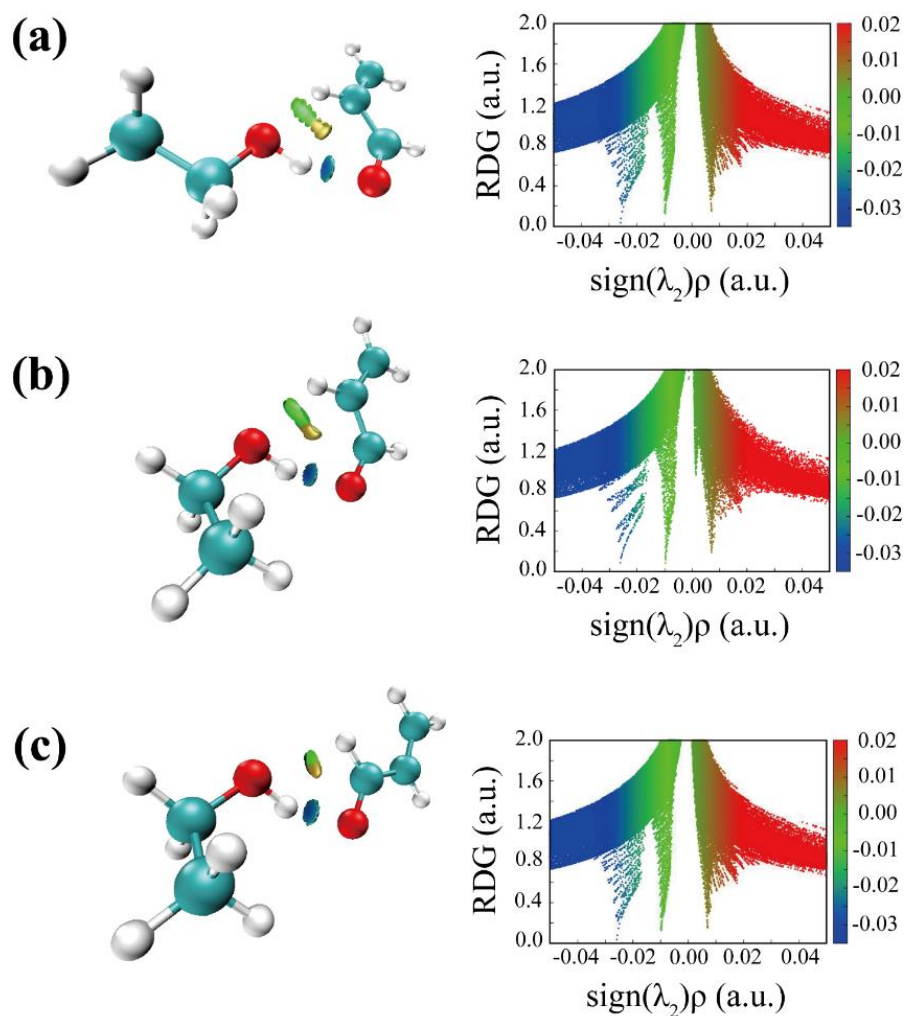


Figure 5.4. The NCI plots from the *ab initio* (MP2/aug-cc-pVTZ) outputs for three conformers: (a) *tt1*, (b) *tg1* and (c) *tg2*. Left panel: gradient isosurfaces according to the values of the $\text{sign}(\lambda_2)\rho$ (-0.04~0.04 a.u.). Color coding is blue (strong attractive interactions), green (weak attractive interactions) and orange-red (repulsive interaction). Right panel: The RDG versus $\text{sign}(\lambda_2)\rho$. Positive values of the $\text{sign}(\lambda_2)\rho$ indicate repulsive interactions, and negative values of the $\text{sign}(\lambda_2)\rho$ indicate attractive interactions.

5.5. Conclusion

The rotational spectrum of two stable conformations of ACR-EtOH and two isotopologues have been identified and characterized by Fourier-transform microwave spectroscopy. In the two observed conformations, the acrolein adopts the *t*-form and ethanol adopts the *gauche* form. The conformation belongs to *trans* ethanol isomer was not observed, which is might due to the relaxation phenomena upon supersonic expansion although we have no experimental evidence for that. The determined rotational constants are coherent with a theoretically determined cyclic structure (MP2/aug-cc-pVTZ) stabilized by a primary OH \cdots O HB between hydroxyl hydrogen and the aldehyde oxygen, where the ethanol works as the proton donor and the acrolein as proton acceptor. A secondary weak interaction between the hydroxyl oxygen and the carbonyl hydrogen or aldehyde hydrogen was characterized and visualized using NCI plots in two observed conformations, *tg1* and *tg2*, respectively. The six-membered ring structure concentrated by the two interactions is in agreement with the result of acrolein-methanol complex in Chapter VI.

5.6. Reference

- 1 W. Li, A. Maris, C. Calabrese, I. Usabiaga, W. D. Geppert, L. Evangelisti and S. Melandri, *Phys. Chem. Chem. Phys.*, 2019, **21**, 23559–23566.
- 2 J. C. Pearson, K. Sastry, E. Herbst and F. C. De Lucia, *J. Mol. Spectrosc.*, 1996, **175**, 246–261.
- 3 R. K. Kakar and C. R. Quade, *J. Chem. Phys.*, 1980, **72**, 4300–4307.
- 4 J. P. I. Hearn, R. V Cobley and B. J. Howard, *J. Chem. Phys.*, 2005, **123**, 134324.
- 5 D. Loru, I. Peña and M. E. Sanz, *J. Mol. Spectrosc.*, 2017, **335**, 93–101.
- 6 A. Maris, W. Caminati, B. Velino, C. M. Andrews and B. J. Howard, *Chem. Phys. Lett.*, 2004, **399**, 39–46.
- 7 I. A. Finneran, P. B. Carroll, G. J. Mead and G. A. Blake, *Phys. Chem. Chem. Phys.*, 2016, **18**, 22565–22572.
- 8 I. A. Finneran, P. B. Carroll, M. A. Allodi and G. A. Blake, *Phys. Chem. Chem. Phys.*, 2015, **17**, 24210–24214.
- 9 L. Evangelisti, G. Feng, R. Rizzato and W. Caminati, *ChemPhysChem*, 2011, **12**, 1916–1920.
- 10 Q. Gou, L. B. Favero, G. Feng, L. Evangelisti, C. Pérez and W. Caminati, *Chem. - A Eur. J.*, 2017, **23**, 11119–11125.
- 11 L. Evangelisti, G. Feng and W. Caminati, *Spectrochim. Acta Part A Mol. Biomol. Spectrosc.*, 2021, **261**, 120086.
- 12 J. U. Grabow, W. Stahl and H. Dreizler, *Rev. Sci. Instrum.*, 1996, **67**, 4072–4084.
- 13 T. J. Balle and W. H. Flygare, *Rev. Sci. Instrum.*, 1981, **52**, 33.
- 14 W. Caminati, A. Millemaggi, J. L. Alonso, A. Lesarri, J. C. López and S. Mata, *Chem. Phys. Lett.*, 2004, **392**, 1–6.
- 15 W. Caminati, L. Evangelisti, G. Feng, B. M. Giuliano, Q. Gou, S. Melandri and J.-U. Grabow, *Phys. Chem. Chem. Phys.*, 2016, **18**, 17851–17855.
- 16 S. Grimme, *J. Chem. Theory Comput.*, 2019, **15**, 2847–2862.
- 17 P. Pracht, F. Bohle and S. Grimme, *Phys. Chem. Chem. Phys.*, 2020, **22**, 7169–7192.

- 18 M. J. Frisch, G. W. Trucks, H. B. Schlegel, G. E. Scuseria, M. A. Robb, J. R. Cheeseman, G. Scalmani, V. Barone, G. A. Petersson, H. Nakatsuji and others, *Gaussian Inc. Wallingford CT*.
- 19 H. M. Pickett, *J. Mol. Spectrosc.*, 1991, **148**, 371–377.
- 20 E. R. Johnson, S. Keinan, P. Mori-Sánchez, J. Contreras-García, A. J. Cohen and W. Yang, *J. Am. Chem. Soc.*, 2010, **132**, 6498–6506.
- 21 A. C. P. Alves, J. Christoffersen and J. M. Hollas, *Mol. Phys.*, 1971, **20**, 625–644.

Chapter VI

Characterizing the interactions of dimethyl sulfoxide with water: a rotational spectroscopy study

6.1. Introduction

Dimethyl sulfoxide ((CH₃)₂SO, DMSO) is an important substance commonly used as a polar aprotic solvent, antifreeze fluid and cryo-protectant owing to its beneficial properties including low toxicity and environmental compatibility.¹ The DMSO/water system is well known for exhibiting a strongly non-ideal mixing behaviour. The non-ideal behaviour of DMSO/water system, reflected in a number of physical properties, such as the density,² excess mixing volume,³ viscosity,⁴ translational and rotational diffusion constants⁵, has been a very active field of research for many decades. Insights into how DMSO interacts with water are essential in explaining ice-blocking mechanisms and biological toxicity.⁶

Unique attributes of DMSO/water system has previously been investigated using various methods, such as MD (molecular dynamics) simulations,⁷⁻⁹ neutron diffraction,^{10,11} Rydberg electron-transfer spectroscopy,¹² High-pressure Spectroscopic probe,¹³ FTIR spectroscopy^{14,15} and Raman spectroscopy.¹⁶ Kirchner *et al.* described the stable conformations of DMSO/(water)_n (n=1,2,3 and 4) complexes by MD simulations and calculated the interaction energies of HB in the stable conformations with different methods.⁸ Mrázková and Hobza studied the conformations of DMSO/(water)_n (n=1, 3, 6, 16 and 32) using MD simulations and reoptimized DMSO/(water)_n (n=1, 2 and 3) at the *ab initio* levels. They found that the hydration of DMSO leads to an elongation of the S=O bond and a contraction of methyl C–H bonds.⁹ Li *et al.* studied the cooperativity between O–H···O=S HB and C–H···O_w HB in the DMSO aqueous solutions by FTIR spectroscopy and conformations DMSO/(water)_n (n=1, 2 and 3) by theoretical calculation.¹⁵ Oh *et al.* proved singly hydrogen-bonded conformations (DMSO-water and (DMSO)₂-water) and doubly hydrogen-bonded

conformation (DMSO-(water)₂) in DMSO/water binary mixtures solution using FTIR spectroscopy combined with theoretical calculations.¹⁷ They reported that DMSO disrupts the donor/acceptor balance in water by accepting up to two HBs through its oxygen lone pairs. However, despite this extensive research, HB formation mechanisms in the complex of DMSO with water are not completely understood.

A bottom-up approach to the problem of solvation can be achieved by the study of small molecular clusters by high resolution spectroscopy in particular rotational spectroscopy performed in gas phase.¹⁸ Rotational spectroscopy is highly sensitive to atomic mass distribution, so it can be used to study conformational equilibria and isotopic species. The combination of rotational spectroscopy analysis and theoretical methods provide a synergistic method for studying the structure and internal dynamics of isolated molecules¹⁹ and weakly bound complexes²⁰.

Herein we investigated the rotational spectrum of the 1:1 complex of DMSO with water (DMSO-W) and its isotopologues by rotational spectroscopy in the 6-18 GHz region and quantum chemical calculations with the aim of determining its structure and the driving forces of the interaction between DMSO and water.

6.2. Methods

The measurement of the rotational spectrum was carried out in the COBRA-type pulsed supersonic-jet FTMW spectrometer²¹⁻²⁴. The samples C₂H₆OS, H₂¹⁸O and D₂O were acquired from Sigma-Aldrich (purity >99%) and used without further purification. Samples of C₂H₆OS and water were prepared in two separate containers and cooled to 273K. Helium at a stagnation pressure of about 3 bar, was flowed over the samples resulting in about 1% mixture of both C₂H₆OS and H₂O. The molecular beam was then expanded through a solenoid valve (General Valve, Series 9, nozzle diameter of 0.5 mm) into a Fabry-Pérot cavity. During the expansion, the molecules and their complexes can reach quite low rotational temperatures (a few K) and the most stable forms can be trapped at their energy minimum when certain conditions are satisfied. To determine the position of the spectral lines, Fourier transformation of the time-domain signal perform 8 k data points, recorded at a sampling interval of 100 ns. The analysis of the spectral data was performed with the SPFIT program of Pickett²⁵. The search for the stable geometries were performed with CREST software,^{26,27} an efficient scheme by the meta-dynamics algorithm combined with semiempirical tight-binding methods. The resulting conformers were optimized using B3LYP and MP2 levels of theory at the

GAUSSIAN 16 program²⁸. The non-covalent interactions between acrolein and methanol were analyzed with Johnson's NCI method,²⁹ which can visualize and quantify the non-covalent interactions based on RDG.

6.3. *Ab initio* results

As regards the DMSO molecule, extensive research has already been done using rotational spectroscopy performed in gas phase.^{30–34} The dipole moment and r_0 structure,³⁴ r_s structure,³¹ centrifugal distortion constants^{30,33} and the internal rotation barrier V_3 of DMSO³² were determined. In terms of chemical structure, the molecule has idealized C_s symmetry and a trigonal pyramidal molecular geometry.

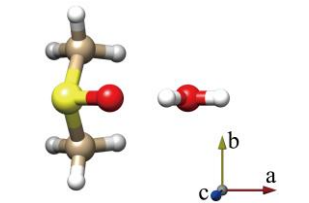
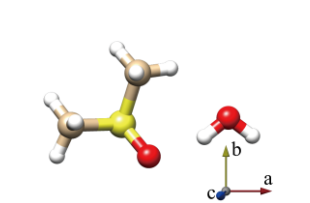
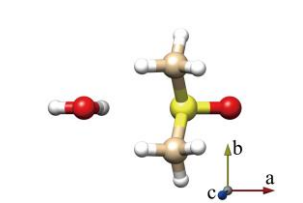
The complexes of DMSO with one water were predicted using the CREST software.^{26,27} As initial structures for the configurational search the conformation where the water molecule lies in the symmetry plane of DMSO and one hydrogen atom of water interacts with the oxygen atom of DMSO has been chosen. All ten resulting conformers were optimized at B3LYP levels of theory with the def2tzvp basis set while only three conformers were stable, as shown in Table A6.1. The three stable conformers were optimized at MP2 levels of theory with the aug-cc-pVTZ, as presented in Table 6.1. All three conformers were confirmed to be local minima by performing harmonic vibrational calculations. Distinct conformers of DMSO-W have been labelled 1, 2 or 3 based on their relative energy. The theoretical spectroscopic parameters and relative energies of all conformers are reported in Table 6.1 while the Cartesian coordinates of the optimized structures are available in the Appendix.

In the most stable conformer 1 (Conf 1), the hydrogen of water forms a $\text{OH}\cdots\text{O}$ HB with the DMSO oxygen atom. The structure has a C_s symmetry and the oxygen lone pairs participates in two $\text{C-H}\cdots\text{O}$ HBs, involving the water oxygen with two methylenic DMSO hydrogens. The value of the dipole moment of μ_b is 0.0, confirming that Conf 1 has a plane of symmetry (the symmetry plane of DMSO) with the water located on it and the complex has thus a C_s symmetry. The value of the planar inertia moment P_{bb} of Conf 1 is 60.11 u \AA^2 , which is consistent with the value of the planar inertia moment P_{aa} of DMSO is $60.5498(1) \text{ u \AA}^2$,³⁰ confirming again that the water lies in the symmetry plane of DMSO (the a , c plane).

Conformer 2 (Conf 2) is located about 6.9 kJ mol^{-1} higher than Conf 1. In this case the water molecule lies in the heavy atom plane of DMSO forming a six-membered ring structure where the water hydrogen forms a HB with the DMSO oxygen and the oxygen atom of water is involved in a HB with the methylenic DMSO hydrogen. The two lowest energy structures

all exhibit a stronger OH \cdots O HB and one (Conf 2) or two (Conf 1) weak C–H \cdots O HB(s). The hydroxyl group of water is acting as a proton donor for the OH \cdots O interaction and as a proton acceptor for the C–H \cdots O interaction.

Table 6.1. *Ab initio* (MP2/aug-cc-pVTZ) spectroscopic parameters, relative energies of the stable conformations of DMSO-W.

	Conf 1	Conf 2	Conf 3
			
$A, B, C/\text{MHz}$	4261, 2479, 2459	6785, 2072, 1739	5172, 2075, 1904
$\mu_a, \mu_b, \mu_c/\text{D}$	1.5, 0.0, 2.3	-3.2, 1.6, -0.2	4.1, 0.0, 0.9
$\Delta E/\text{kJ mol}^{-1}$	0	6.9	25.1

In conformer 3 (Conf 3) the water lies again in the DMSO symmetry plane, exhibits a OH \cdots S HB and two weak C–H \cdots O HBs with the methylenic hydrogens and is located about 25.1 kJ mol $^{-1}$ higher than Conf 1.

6.4. Experimental results

We started our experiment with the search of the rotational transition for Conf 1 of DMSO-W. The detected μ_a -type and μ_c -type rotational transitions and the missing μ_b -type line confirm the assignment to Conf 1 with plane symmetric structure coinciding with the a, c plane. As an example of the observations, the $2_{02}\leftarrow 1_{01}$ transition for Conf 1 parent species and isotopologues is shown in Figure 6.1.

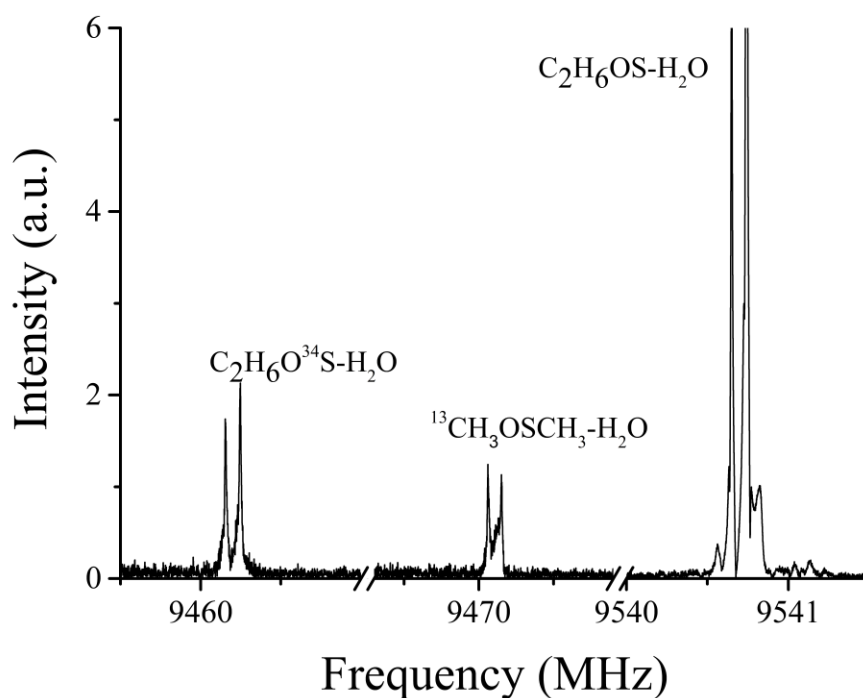


Figure 6.1. $2_{02} \leftarrow 1_{01}$ transitions of $\text{C}_2\text{H}_6\text{OS-H}_2\text{O}$ and isotopologues $\text{C}_2\text{H}_6\text{O}^{34}\text{S-H}_2\text{O}$ and $^{13}\text{CH}_3\text{OSCH}_3\text{-H}_2\text{O}$ observed in natural abundance. The transition intensity of parent species is 50 a.u. Each line appears as a doublet due to the instrumental Doppler effect.

As an isolated monomers, DMSO exhibits a spectral splitting due to hindered internal rotation of its methyl rotors that leads to a triplets AA, AE (or EA) and EE splitting pattern, where A and E are the methyl torsional state symmetry labels.³⁰ Nevertheless, in the case of the observed transitions of Conf 1 in our frequency range ($(J \leq 4; 6\text{-}18 \text{ GHz})$), the triplets splitting pattern was not observed. In any case, the potential energy surface of the methyl torsion around the OC bond in DMSO and Conf 1 was calculated by changing the dihedral angle of $\tau = \text{HC-SC}$ on the regular grid with $\Delta\tau = 10^\circ$ and is shown in Figure 6.2. The calculated data reproduced in red bullets are well reproduced with the threefold function: $V(\tau) = \frac{1}{2} V_3 [1 + \cos(3\tau)]$, which is shown as a green line for DMSO and blue line for Conf 1 of DMSO-W. The maximum value (11.6 kJ mol^{-1} for DMSO and 12.5 kJ mol^{-1} for Conf 1) represent the theoretical barrier hindering the methyl group internal rotation. It can be noticed that the value of Conf 1 is larger (about 8.4%) than the values obtained for DMSO. The increased barrier of methyl rotation is surely related to the interactions between the water oxygen and methylenic DMSO hydrogens.

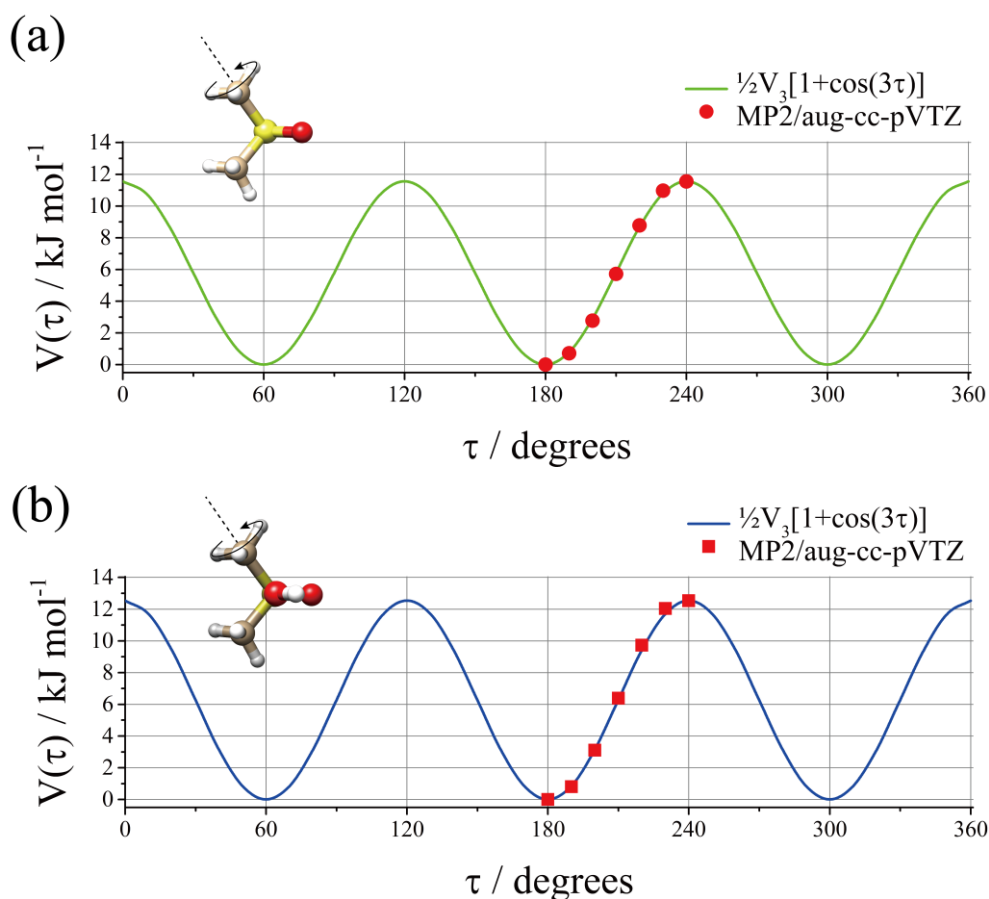


Figure 6.2. *Ab initio* methyl internal rotational potential energy surface for (a) DMSO and (b) DMSO-W (Conf 1).

After measuring all possible transition of Conf 1, the recorded spectrum was extended to find the rotational transitions of Conf 2. From its relative energy and the temperature prior to the expansion the population of Conf 2 was predicted to be 6.2% of the global minimum and taking into account the values of the dipole moment components the most intense μ_a lines of Conf 2 were predicted to be 12.9% of the most intense ones of Conf 1. The rotational transitions of Conf 2 were not observed in the spectrum although it should have been observable given the overall intensity of the spectrum. This can be attributed to a possible relaxation of the population of this conformation onto that of the global minimum during adiabatic expansion. In order to confirm this, the potential energy surface was calculated for the torsion of the water around the S=O axis on a regular grid with a step of 5 degrees, as shown in Figure 6.3. The global minima correspond to Conf 1, and the two relative equivalent minima correspond to Conf 2. The relaxation during adiabatic expansion is demonstrated by the low barrier (about 0.07 kJ mol^{-1}) of inter-conversion between the two conformations.

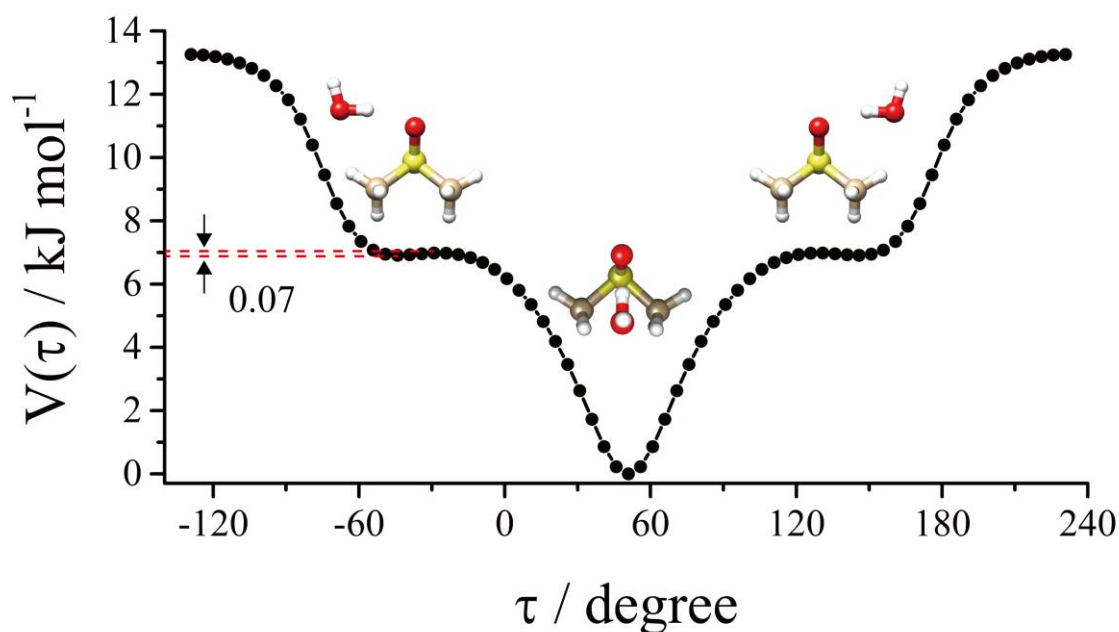


Figure 6.3. *Ab initio* potential energy surface for the torsion of the water around the S=O axis under partial relaxation. This motion interconverts Conf 1 (absolute minimum) with the Conf 2 (relative equivalent minima).

After empirical scaling of the theoretical rotational constants of the parent species, the rotational spectrum of the isotopologues ^{34}S and ^{13}C were measured and analysed in natural abundance (see Figure S1 for numbering of the atoms). The rotational spectra of the parent species, ^{34}S and ^{13}C were shown in Figure 6.1. The transition intensity of ^{34}S isotopologues (the abundance of 4.21%) was about 1/25 of those of the parent species. The transition intensity of ^{13}C isotopologues (the abundance of 1.1%) was about 1/100 of those of the parent species. The transition intensity of ^{18}O isotopologues (the abundance of 0.20%) and deuterated isotopologues (the abundance of 0.01%) is so low that it was not observed in natural abundance. In this case, the enriched H_2^{18}O and D_2O sample were used in the experiment and the spectra of $\text{C}_2\text{H}_6\text{OS-H}_2^{18}\text{O}$ and three deuterated isotopologues with increased transition intensity were observed, as shown in Figure 6.4.

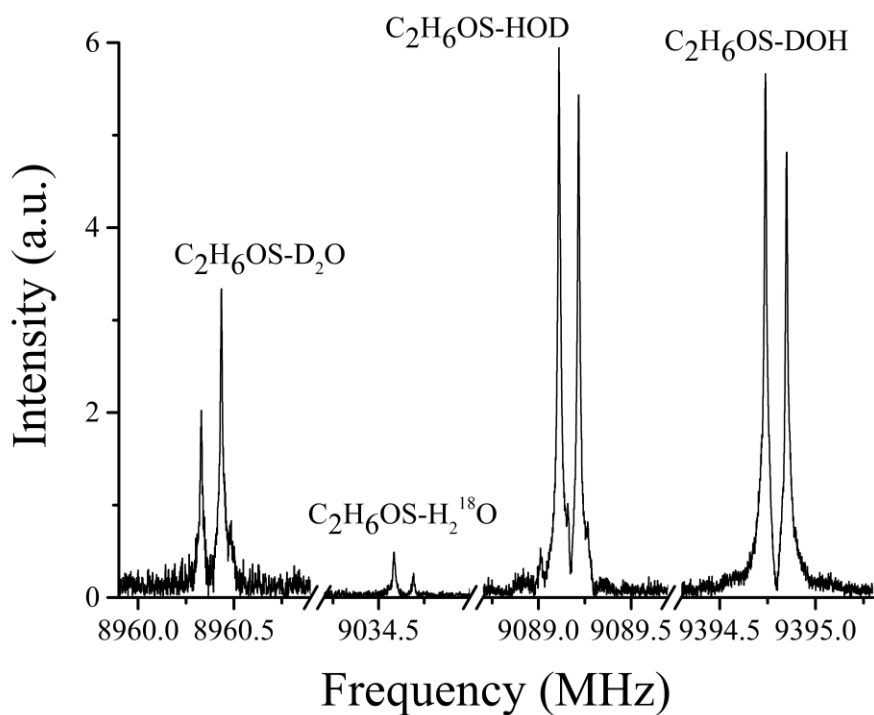


Figure 6.4. $2_{02} \leftarrow 1_{01}$ transitions of enriched $\text{C}_2\text{H}_6\text{OS-H}_2^{18}\text{O}$ and three enriched deuterated species of DMSO-W.

The rotational constants of the parent species and those of the isotopologues of DMSO (^{34}S and ^{13}C) are summarized in Table 6.2 while the experimental spectroscopic parameters of the water isotopologues of DMSO-W (H_2^{18}O and deuterated species) are shown in Table 6.3. The observed transition frequencies of all measured isotopes are provided in the Appendix. More lines belonging to deuterated species were observed due to the hyperfine structure related to the coupling of the deuterium nuclear quadrupole moment to the overall rotation. The splitting pattern caused by quadrupole coupling is very small, as shown in Figure 6.2. In this case, some values of the quadrupole coupling constants for the deuterated species (DOH and D_2O) were fixed to the predicted values.

Table 6.2. Experimental and theoretical spectroscopic parameters of DMSO-W (Conf 1) and its isotopologues

	C ₂ H ₆ OS-H ₂ O	C ₂ H ₆ O ³⁴ S-H ₂ O	¹³ CH ₃ OSCH ₃ -H ₂ O	MP2/aug-cc-pVTZ C ₂ H ₆ OS-H ₂ O
<i>A</i> / MHz	4282.940(4) ^[a]	4276.711(5)	4194.447(5)	4260.59
<i>B</i> / MHz	2405.027(1)	2383.597(2)	2396.269(2)	2478.88
<i>C</i> / MHz	2365.748(1)	2346.902(1)	2339.577(1)	2459.49
<i>D_J</i> / kHz	2.79(4)	2.7(5)	2.68(5)	2.22
<i>D_{JK}</i> / kHz	8.4(5)	7.8(8)	8.8(8)	6.36
<i>D_K</i> / kHz	-10.3(7)	9(1)	-10(1)	-6.95
<i>P_{aa}</i> / u Å ²	152.8798(2)	154.5962(2)	153.2139(2)	145.37
<i>P_{bb}</i> / u Å ²	60.7435(2)	60.7426(2)	62.7991(2)	60.11
<i>P_{cc}</i> / u Å ²	57.2546(2)	57.4275(2)	57.6886(2)	58.50
<i>Δ_c</i> / u Å ²	114.5093(3)	114.8549(4)	115.3771(4)	117.01
<i>Δv_{rms}</i> ^[b] / kHz	1.60	1.54	3.64	-
<i>N</i> ^[c]	15	11	11	-

[a] Error in parentheses in units of the last digit. [b] $\Delta v_{\text{rms}} = [\sum(v_{\text{obs}} - v_{\text{calc}})^2 / N]^{1/2}$. [c] Number of lines in the fit.

Table 6.3. Experimental spectroscopic parameters of the observed isotopologues conformers C₂H₆OS-H₂¹⁸O and deuterated species.

	C ₂ H ₆ OS-H ₂ ¹⁸ O	C ₂ H ₆ OS-DOH	C ₂ H ₆ OS-HOD	C ₂ H ₆ OS-D ₂ O
<i>A</i> / MHz	4277.763(4) ^[a]	4275.680(3)	4280.108(3)	4272.831(2)
<i>B</i> / MHz	2275.665(9)	2366.873(1)	2290.2280(7)	2256.6065(6)
<i>C</i> / MHz	2241.907(1)	2330.8164(9)	2254.6350(6)	2223.8259(5)
<i>D_J</i> / kHz	2.59(4)	2.65(4)	2.51(2)	2.40(2)
<i>D_{JK}</i> / kHz	8.1(2)	5.7(4)	6.9(3)	7.8(2)
<i>D_K</i> / kHz	-9.9(8)	-5.4(7)	-7.4(6)	-9.8(5)
<i>P_{aa}</i> / u Å ²	164.6813(2)	156.0741(1)	163.3712(1)	166.4673(1)
<i>P_{bb}</i> / u Å ²	60.7425(2)	60.7508(1)	60.7799(1)	60.7893(1)
<i>P_{cc}</i> / u Å ²	57.3985(2)	57.4477(1)	57.2963(1)	57.4880(1)
<i>Δ_c</i> / u Å ²	114.7970(4)	114.8955(3)	114.5927(2)	114.9761(2)
<i>χ_{aa}</i> / MHz	-	[0.0552] ^[b]	0.245(9)	[0.0543]/0.274(6) ^[d]
<i>χ_{bb}</i> / MHz	-	[-0.1580]	-0.163(9)	[-0.158]/-0.187(8)
<i>χ_{cc}</i> / MHz	-	[0.1028]	-0.082(9)	[0.1037]/-0.088(8)
<i>η</i> / MHz ^[c]	-	[-4.725]	-0.33(9)	[-4.821]/-0.36(7)
<i>Δv_{rms}</i> ^[e] / kHz	2.14	5.29	8.25	4.78
<i>N</i> ^[f]	16	40	48	232

[a] Error in parentheses in units of the last digit. [b] The data in brackets were fixed at the predicted values. [c] *η* is the asymmetry parameter defined as $\eta = (\chi_{bb} - \chi_{cc})/\chi_{aa}$. [d] The two values correspond to the quadrupole coupling constants for two deuterium atoms. [e] $\Delta v_{rms} = [\sum(v_{obs} - v_{calc})^2/N]^{1/2}$. [f] Number of lines in the fit.

From the rotational constants of the observed isotopologues, it is possible to determine the *r_s* substitution principal axis coordinates of the S, C, O and H atoms using Kraitchman's equations for monosubstituted isotopologues.³⁵ A summary of fitted values of the *r_s* structural parameters and the *ab initio* atom coordinates (*r_e*) is given in Table 6.4. Since the atom coordinates in Kraitchman's equations appear as their squares, their signs cannot be

unambiguously determined but must be compared to the calculate ones. The results indicate that the MP2/aug-cc-pVTZ calculation for the structure of complex is consistent with the Kraitchman fits. Actually, the determined values of the rotational constants are reproduced by this theoretical within 4 %.

Table 6.4. Principal axis coordinates (Å) for Conf 1 of DMSO-W from different structural determinations: experimental atom substitution coordinates (r_s) and equilibrium atom positions (r_e) optimized at the MP2/aug-cc-pVTZ level of theory.

		r_s	r_e
C (1)	<i>a</i>	0.5722 (1) ^[a]	0.5523
	<i>b</i>	-1.34878 (6)	-1.3425
	<i>c</i>	0.8348(1)	0.8471
S (2)	<i>a</i>	0.93612(4)	0.9337
	<i>b</i>	0.022*i(2) ^[b]	0
	<i>c</i>	-0.2999(1)	-0.2922
O (5)	<i>a</i>	-2.44993(1)	-2.3888
	<i>b</i>	0.024*i(1)	0
	<i>c</i>	0.2869(1)	0.2848
H (12)	<i>a</i>	-3.24446(2)	-3.2643
	<i>b</i>	-0.2005(3)	-0.0004
	<i>c</i>	-0.2167(3)	-0.1106
H (13)	<i>a</i>	-1.78910(3)	-1.7625
	<i>b</i>	0.0845(7)	0
	<i>c</i>	-0.4481(1)	-0.4690

[a] Error in parentheses in units of the last digit. [b] In a few cases the square of the coordinate has been determined to be small and negative leading to an imaginary value of the coordinate.

In order to get better visualization of non-covalent interaction between the molecules, the analysis of the HBs in the three conformers was performed by Johnson's NCI method.²⁹ The NCI method considers the distribution of the electron density (ρ), its gradient (s) and its second derivatives matrix ($\lambda_1, \lambda_2, \lambda_3$). A comprehensive picture can be drawn using different plots of these quantities. According to the color code reported on the graphics, the gradient isosurfaces ($s=0.5$ a.u.) visible in the NCI plots, see Figure 6.5, represent the area for attractive and repulsive interactions. The comparison between Conf 1, 2 and 3 is shown in Figure 6.5(a-c). In all three conformers, the blue regions and green regions (where negative values of

$\text{sign}(\lambda_2)\rho$ are present, small values of the RGD) suggest a stronger OH \cdots O HB and a weaker C–H \cdots O or O–H \cdots S HB while the orange regions (where positive values of the $\text{sign}(\lambda_2)\rho$ are present, small values of the RGD) suggest a weak repulsive interaction. A strong OH \cdots O HB and two weak C–H \cdots O HBs were observed in Conf 1. Only one C–H \cdots O HBs in Conf 2 was observed and the O–H \cdots O HB in Conf 3 is weaker than that in Conf 1. This result is in consistent with the calculation results that Conf 1 has lower energy than Conf 2 and 3 and constitutes the global minimum.

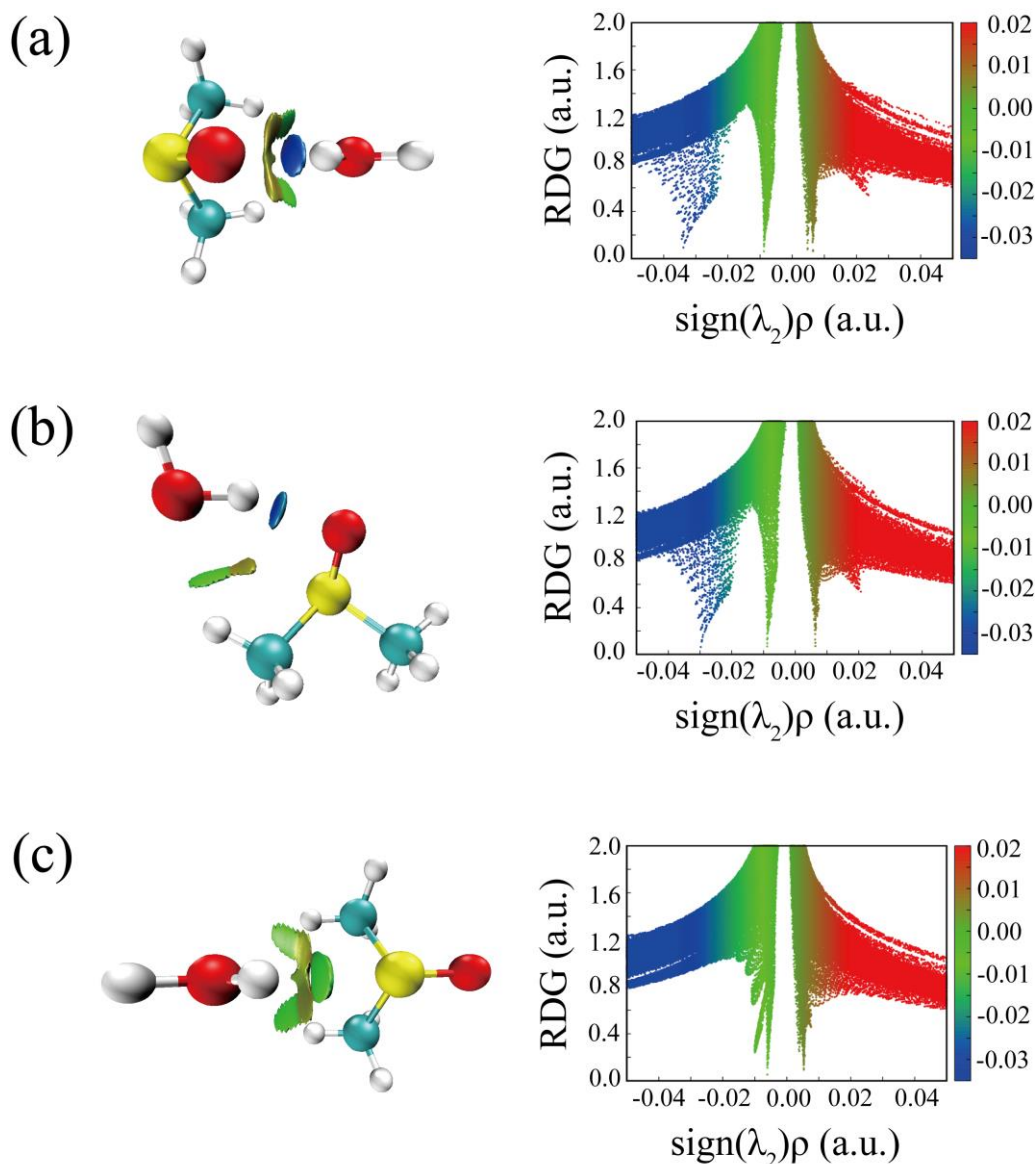


Figure 6.5. The NCI plots from the *ab initio* (MP2/aug-cc-pVTZ) outputs for three conformers: (a) Conf 1, (b) Conf 2 and (c) Conf 3. Left panel: gradient isosurfaces according to the values of the $\text{sign}(\lambda_2)\rho$ (-0.04~0.04 a.u.). Color coding is blue (strong attractive interactions), green (weak attractive interactions) and orange-red (repulsive interaction). Right panel: The RDG versus $\text{sign}(\lambda_2)\rho$. Positive values of the $\text{sign}(\lambda_2)\rho$ indicate repulsive interactions, and negative values of the $\text{sign}(\lambda_2)\rho$ indicate attractive interactions.

6.5. Conclusion

The rotational spectrum of the 1:1 DMSO-W has been assigned in the frequency ranges (6-18GHz) with the PJ-FTMW spectrometer. The observed conformation was determined as a symmetry structure where the water located on the symmetry plane of DMSO (the a,b plane of the complex). It is proved by the absence of the transitions involving μ_b (0.0) and the planar inertia moment P_{bb} ($60.7435(2) \text{ u } \text{Å}^2$), which is in consist with the P_{bb} of DMSO monomer ($60.5498(1) \text{ u } \text{Å}^2$). The observations of the isotopologues of DMSO (^{34}S and ^{13}C) in natural abundance and the enriched water isotopologues (H_2^{18}O and deuterated species) of DMSO-W allow the determination of the experimental r_s coordinates for the S and C atoms in DMSO and the O and H atoms in water. A primary $\text{OH}\cdots\text{O}$ HB between water hydrogen and the DMSO oxygen where the water works as the proton donor and the DMSO as proton acceptor, and two weak interactions between the terminal CH groups and the water oxygen where the DMSO works as the proton donors and the water as proton accepters, were characterized and visualized in observed conformation using NCI plots.

6.6. Reference

- 1 Ç. A. Akkök, K. Liseth, T. Hervig, A. Rynningen, Ø. Bruserud and E. Ersvær, *Cytotherapy*, 2009, **11**, 749–760.
- 2 R. G. LeBel and D. A. I. Goring, *J. Chem. Eng. Data*, 1962, **7**, 100–101.
- 3 J. Catalán, C. Diaz and F. Garcia-Blanco, *J. Org. Chem.*, 2001, **66**, 5846–5852.
- 4 J. M. G. Cowie and P. M. Toporowski, *Can. J. Chem.*, 1961, **39**, 2240–2243.
- 5 K. J. Packer and D. J. Tomlinson, *Trans. Faraday Soc.*, 1971, **67**, 1302–1314.
- 6 G. M. Fahy, *Cryobiology*, 2010, **60**, S45–S53.
- 7 Y. Lei, H. Li and S. Han, *Chem. Phys. Lett.*, 2003, **380**, 542–548.
- 8 B. Kirchner and M. Reiher, *J. Am. Chem. Soc.*, 2002, **124**, 6206–6215.
- 9 E. Mrázková and P. Hobza, *J. Phys. Chem. A*, 2003, **107**, 1032–1039.
- 10 A. K. Soper and A. Luzar, *J. Chem. Phys.*, 1992, **97**, 1320–1331.
- 11 A. K. Soper and A. Luzar, *J. Phys. Chem.*, 1996, **100**, 1357–1367.
- 12 S. Carles, C. Desfrancois, J. P. Schermann, J. Bergès and C. Houée-Levin, *Int. J. Mass Spectrom.*, 2001, **205**, 227–232.
- 13 H.-C. Chang, J.-C. Jiang, C.-M. Feng, Y.-C. Yang, C.-C. Su, P.-J. Chang and S. H. Lin, *J. Chem. Phys.*, 2003, **118**, 1802–1807.
- 14 K.-I. Oh, K. Rajesh, J. F. Stanton and C. R. Baiz, *Angew. Chemie*, 2017, **129**, 11533–11537.
- 15 Q. Li, X. An, B. Gong and J. Cheng, *Spectrochim. Acta Part A Mol. Biomol. Spectrosc.*, 2008, **69**, 211–215.
- 16 B. Yang, X. Cao, C. Wang, S. Wang and C. Sun, *Spectrochim. Acta Part A Mol. Biomol. Spectrosc.*, 2020, **228**, 117704.
- 17 K.-I. Oh, K. Rajesh, J. F. Stanton and C. R. Baiz, *Angew. Chemie*, 2017, **56**, 11533–11537.
- 18 M. Becucci and S. Melandri, *Chem. Rev.*, 2016, **116**, 5014–5037.

- 19 S. Melandri, L. Evangelisti, A. Maris, W. Caminati, B. M. Giuliano, V. Feyer, K. C. Prince and M. Coreno, *J. Am. Chem. Soc.*, 2010, **132**, 10269–71.
- 20 L. B. Favero, B. M. Giuliano, A. Maris, S. Melandri, P. Ottaviani, B. Velino and W. Caminati, *Chemistry*, 2010, **16**, 1761–4.
- 21 J. U. Grabow, W. Stahl and H. Dreizler, *Rev. Sci. Instrum.*, 1996, **67**, 4072–4084.
- 22 T. J. Balle and W. H. Flygare, *Rev. Sci. Instrum.*, 1981, **52**, 33.
- 23 W. Caminati, A. Millemaggi, J. L. Alonso, A. Lesarri, J. C. López and S. Mata, *Chem. Phys. Lett.*, 2004, **392**, 1–6.
- 24 W. Caminati, L. Evangelisti, G. Feng, B. M. Giuliano, Q. Gou, S. Melandri and J.-U. Grabow, *Phys. Chem. Chem. Phys.*, 2016, **18**, 17851–17855.
- 25 H. M. Pickett, *J. Mol. Spectrosc.*, 1991, **148**, 371–377.
- 26 S. Grimme, *J. Chem. Theory Comput.*, 2019, **15**, 2847–2862.
- 27 P. Pracht, F. Bohle and S. Grimme, *Phys. Chem. Chem. Phys.*, 2020, **22**, 7169–7192.
- 28 M. J. Frisch, G. W. Trucks, H. B. Schlegel, G. E. Scuseria, M. A. Robb, J. R. Cheeseman, G. Scalmani, V. Barone, G. A. Petersson, H. Nakatsuji and others, *Gaussian Inc. Wallingford CT*.
- 29 E. R. Johnson, S. Keinan, P. Mori-Sánchez, J. Contreras-García, A. J. Cohen and W. Yang, *J. Am. Chem. Soc.*, 2010, **132**, 6498–6506.
- 30 E. Fliege, H. Dreizler and V. Typke, *Zeitschrift für Naturforsch. A*, 1983, **38**, 668–675.
- 31 W. Feder, H. Dreizler, H. D. Rudolph and V. Typke, *Zeitschrift für Naturforsch. A*, 1969, **24**, 266–278.
- 32 H. Dreizler and G. Dendl, *Zeitschrift für Naturforsch. A*, 1965, **20**, 1431–1440.
- 33 H. Dreizler and G. Dendl, *Zeitschrift für Naturforsch. A*, 1965, **20**, 30–37.
- 34 H. Dreizler and G. Dendl, *Zeitschrift für Naturforsch. A*, 1964, **19**, 512–514.
- 35 J. Kraitchman, *Am. J. Phys.*, 1953, **21**, 17–24.

Chapter VII

Characterizing the interactions of dimethyl sulfoxide with methanol: a rotational spectroscopy study

7.1. Introduction

When discussing the intermolecular interactions and conformational equilibria of HB complexes, the focus is on the nature and properties of HBs, such as the number of HBs, bond lengths, and atoms or groups involved. Taking the binary system of DMSO with MeOH as an example, we have studied intermolecular interactions between them through rotational spectroscopy.

As regards the DMSO molecule, which has been well introduced in Chapter VI, it plays a key role in the fields of polar aprotic solvent, antifreeze fluid and cryo-protectant.¹ The molecular structure and internal dynamics of DMSO were determined by rotational spectrum.²⁻⁶

Extensive researches⁷⁻²³, on the rotational spectrum involving MeOH monomer and complex have been discussed in Chapter IV. MeOH exhibits a A-E spectral splitting pattern due to the hindered internal rotation of its methyl rotor and all barriers of the methyl group internal rotation in complexes are lower than those observed in the monomer. In the analysis by Fraser *et al.*¹⁴, the decrease of the MeOH internal rotation barrier is attributed to a liberational motion of the whole MeOH moiety or the methyl group.

The unique properties of the DMSO-MeOH system have been previously studied using various methods. Li *et al.*²⁴ studied the role of methyl groups in the formation of the HB in DMSO–MeOH mixtures by employing FTIR and NMR techniques and quantum chemical calculations. They found that the methyl groups of DMSO are electron-donating, whereas that of MeOH is electron-withdrawing, both making positive contributions, without focus on the atoms directly involved in the formation of a HB complex. Molecular electron density (MED) topology and natural bond orbital (NBO) analysis has been investigated to explain the strength of the interactions in 1:1 complex of DMSO and MeOH.²⁵ Singh *et al.*²⁶ analyzed the structural features and the formation of the HBs of

DMSO in water and MeOH by Raman scattering and DFT calculations. Leipertz *et al.*²⁷ studied the effects of hydrogen bonding between DMSO and MeOH on the symmetric and antisymmetric CSC stretching vibrations of DMSO by means of Raman spectroscopy. Skaf and Vechi present molecular-dynamics computer simulation results for the local structures, the HB distribution, and dynamical properties of MeOH and DMSO binary mixtures at ambient conditions over the entire composition range. Hydrogen bonding statistics show that aggregates of the type 1:1 DMSO: MeOH are formed and represent the predominant form of molecular association in these mixtures.²⁸ However, despite this extensive research, the nature and properties of HBs and the internal dynamics in the complex of DMSO with MeOH at the molecular level are not completely understood.

In this chapter, we presented our study about the 1:1 adduct of DMSO and MeOH to explore the intermolecular interactions and internal molecular dynamics of DMSO and MeOH by rotational spectroscopy in the 6-18 GHz region combining with quantum chemical calculations.

7.2. Methods

The measurement of the rotational spectrum was carried out in the COBRA-type pulsed supersonic-jet FTMW spectrometer^{29–32} present in the laboratory. The samples DMSO and MeOH were acquired from Sigma-Aldrich (purity >99%) and used without further purification. They were prepared in two separate containers and MeOH was cooled to 273K. Helium at a stagnation pressure of about 3 bar, was flowed over the samples resulting in about 1% mixture of both DMSO and MeOH in the carrier gas. The molecular beam was then expanded through a solenoid valve (General Valve, Series 9, nozzle diameter of 0.5 mm) into a Fabry–Pérot cavity to exploit already described features of the coaxial supersonic expansion. The search for the stable geometries of the complexes between DMSO-MeOH were performed with CREST software,^{33,34} an efficient scheme by the meta-dynamics algorithm combined with semiempirical tight-binding methods. The resulting conformers were optimized using B3LYP and MP2 levels of theory at the GAUSSIAN 16 program³⁵. The analysis of the spectral data was performed with the program of XIAM,³⁶ which is based on the Combined Axis Method.³⁷ The non-covalent interactions between acrolein and MeOH were analyzed with Johnson's NCI method³⁸, which can visualize and quantify the non-covalent interactions based on RDG.

7.3. *Ab initio* results

The conformations of 1:1 complexes of DMSO with MeOH were predicted using program of CREST,^{33,34} starting with the conformation where the MeOH molecule lies in the symmetry plane of

DMSO and hydroxyl hydrogen atom of MeOH interacts with the oxygen atom of DMSO as initial structures for the configurational search. The resulting 8 conformers, with relative energies ΔE less than 50 kJ mol⁻¹, were optimized at B3LYP levels of theory with the def2tzvp basis set and only three conformers were found stable. The three stable conformers were then optimized at MP2/ aug-cc-pVTZ level and are depicted in Table 7.1. All three conformers were confirmed to be local minima by performing harmonic vibrational calculations. Distinct conformers of DMSO-MeOH have been labelled 1, 2 or 3 based on their relative energy. The theoretical spectroscopic parameters and relative energies (ΔE) of all conformers are reported in Table 7.1.

Table 7.1. Spectroscopic parameters and relative energies for the DMSO-MeOH calculated at the B3LYP/def2tzvp and MP2/aug-cc-pVTZ levels of theory.

	Conf 1		Conf 2		Conf 3	
	B3LYP/def 2tzvp	MP2/aug- cc-pVTZ	B3LYP/def 2tzvp	MP2/aug- cc-pVTZ	B3LYP/def 2tzvp	MP2/aug- cc-pVTZ
A / MHz	4102.7	4139.8	5916.5	6234.7	3570.0	3604.8
B / MHz	1309.0	1323.4	1175.9	1143.4	1420.1	1413.5
C / MHz	1299.0	1319.0	1061.6	1026.6	1358.7	1347.1
μ_a / D	1.7	1.7	3.6	3.4	1.4	1.4
μ_b / D	0.0	0.0	-1.3	-1.4	-3.3	-3.4
μ_c / D	-2.2	-2.3	-1.3	-0.4	0.0	0.0
P_{aa} / u Å ²	326.0	321.5	410.2	426.6	293.1	296.3
P_{bb} / u Å ²	63.1	61.7	65.9	65.7	78.8	78.9
P_{cc} / u Å ²	60.1	60.4	19.6	15.4	62.7	61.3
ΔE / kJ mol ⁻¹	0.0	0.0	7.6	7.3	20.3	19.8

In the most stable conformer 1 (Conf 1), the hydroxyl hydrogen of MeOH forms a OH \cdots O HB with the DMSO oxygen atom. The structure has a C_s symmetry and the MeOH oxygen lone pairs participate in two C–H \cdots O interactions, each with a methylenic DMSO hydrogen. For this conformer the calculated value of the dipole moment component along *bis* is 0.0, confirming that it has a plane of symmetry (the symmetry plane of DMSO) with the MeOH located on it. The value of the planar inertia moment P_{bb} of Conf 1 is 61.7 u Å², which is slightly higher compared to the value of the planar inertia moment P_{aa} of DMSO (60.5498(1) u Å²)⁴ or P_{bb} of DMSO-W (60.7435(2) u Å² in Chapter

VI). The slightly increased value of the planar inertia moment in Conf 1 is due to the two out-of-plane carbonyl hydrogens of MeOH

Conformer 2 (Conf 2) is located about 7.3 kJ mol^{-1} higher than Conf 1. In this case the MeOH molecule lies in the heavy atom plane of DMSO forming a six-membered ring structure where the hydroxyl hydrogen forms a HB with the DMSO oxygen and the oxygen atom of MeOH is involved in a HB with the methylenic DMSO hydrogen. The two lowest energy structures all exhibit a stronger $\text{OH}\cdots\text{O}$ HB and one (Conf 2) or two (Conf 1) weaker $\text{C-H}\cdots\text{O}$ interaction(s). The hydroxyl group of MeOH is acting as a proton donor for the $\text{OH}\cdots\text{O}$ interaction and as a proton acceptor for the $\text{C-H}\cdots\text{O}$ interaction.

In conformer 3 (Conf 3), the structure is held together only by weak HBs and it is located about 25.1 kJ mol^{-1} higher than Conf 1. The methylenic hydrogen of MeOH forms a $\text{C-H}\cdots\text{O}$ interaction with the DMSO oxygen atom, the MeOH lies again in the DMSO symmetry plane and the oxygen lone pairs participates in two $\text{C-H}\cdots\text{O}$ interactions, involving the MeOH oxygen with two methylenic DMSO hydrogens. The value of the dipole moment of μ_b is 0.0, confirming that Conf 3 also has a plane of symmetry (the symmetry plane of DMSO). The value of the planar inertia moment P_{cc} of Conf 3 is 61.29 u \AA^2 is consistent with the P_{bb} of Conf 1 (61.67 u \AA^2), confirming again that the MeOH lies in the symmetry plane of DMSO (the a, b plane).

7.4. Experimental results

We started our experiment with the search of the μ_a -R rotational transitions for Conf 1. The doublet A-E splitting pattern arising from the methyl group internal rotation was observed in the spectral transitions. After the detection and fit, the measurements were extended following μ_b and μ_c -type rotational transitions. The detected μ_a -type and μ_c -type rotational transitions and the missing μ_b -type line confirm the assignment to Conf 1 to a structure which contains a plane of symmetry coinciding with the a, c plane. The observed transition frequencies of Conf 1 are provided in the Appendix. The rotational constants of the observed conformation Conf 1 obtained through the XIAM program³⁶ are summarized in Table 7.2. The fitted rotational constants are reproduced by those theoretical methods for two conformers within 3%.

Table 7.2. Experimental spectroscopic parameters of the observed Conf 1 of the DMSO-MeOH complexes.

	Conf 1
A/MHz	4153.402(2)
B/MHz	1290.3084(6)
C/MHz	1278.6844(8)
D_J/kHz	0.641(8)
D_{JK}/kHz	5.86(9)
$V_3/\text{kJ mol}^{-1}$	2.722(3)
δ°	2.863(2)
F_0/GHz	159.1(1)
$P_{aa} / \text{u } \text{\AA}^2$	332.6142(2)
$P_{bb} / \text{u } \text{\AA}^2$	62.6194(2)
$P_{cc} / \text{u } \text{\AA}^2$	59.0589(2)
σ/kHz	8.8
N	54

As an example of the observations, the $4_{04} \leftarrow 3_{03}$ transition for Conf 1 is shown in Figure 7.1. As an isolated monomers, DMSO exhibits a spectral splitting due to hindered internal rotation of its methyl rotors that leads to a triplet AA, AE (or EA) and EE splitting pattern, where A and E are the methyl torsional state symmetry labels.⁶ MeOH exhibits a doublet A-E splitting pattern spectral splitting due to its methyl rotor.²⁰ In this case, the equation of the Hamiltonian used in the analysis of the spectrum of complex of DMSO-MeOH in its simple form is shown as follows^{39,40}:

$$H = H_{\text{tr}} + H_{\text{cd}} + H_{\text{MeOH}} \quad (1)$$

H_{tr} is the Hamiltonian of the standard rigid rotor. H_{cd} contains a set of centrifugal distortion terms. H_{MeOH} represents the part of the internal rotation Hamiltonian from MeOH methyl rotor.

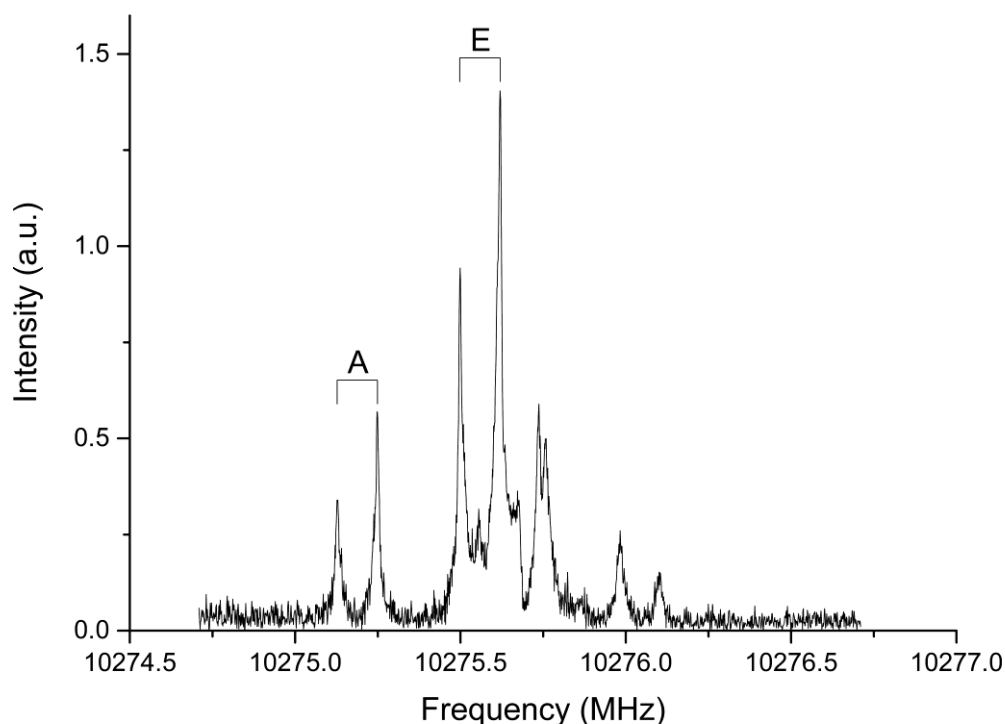


Figure 7.1. $4_{04} \leftarrow 3_{03}$ transitions of Conf 1. The other lines belong to the $4_{23} \leftarrow 3_{22}$ and $4_{22} \leftarrow 3_{21}$ transitions which are unlabeled in the figure. The peaks are split in a doublet pattern (A-E) due to the internal rotation of the methyl group of MeOH. Each line appears as a doublet (indicated by square bracket) due to the instrumental Doppler effect.

As the result, only the doublet A-E splitting pattern from MeOH methyl rotor was observed in the spectra transitions of Conf 1 in our frequency range ($J \leq 4$; 6-18 GHz). The experimental value of V_3 in Conf 1 ($2.722(3) \text{ kJ mol}^{-1}$) is smaller than that in the MeOH monomer ($4.463(4) \text{ kJ mol}^{-1}$)²¹. The decrease of the MeOH internal rotation barrier in Conf 1 compared to the isolated monomer is consistent with that in the complex of acrolein-MeOH (Chapter IV). The potential energy surfaces of the methyl torsion around the OC bond in MeOH were calculated by changing the dihedral angle of $\tau = \text{HC-OH}$ on the regular grid with $\Delta\tau = 10^\circ$ and is shown in Figure 7.2a. The calculated data reproduced in red bullets are well reproduced with the threefold function: $V(\tau) = \frac{1}{2} V_3 [1 + \cos(3\tau)]$, which is shown as green line for MeOH methyl rotor of DMSO-MeOH. The maximum value (3.29 kJ mol^{-1} for MeOH methyl rotor) represents the theoretical barrier hindering the methyl group internal rotation, which is larger (about 21%) than the experimental values ($2.722(3) \text{ kJ mol}^{-1}$). This difference could be due to a lower accuracy of the method in calculating methyl torsional barriers in molecular complexes or to a possible large amplitude motion coupled to the torsion but of which we don't have evidence in the rotational spectrum.

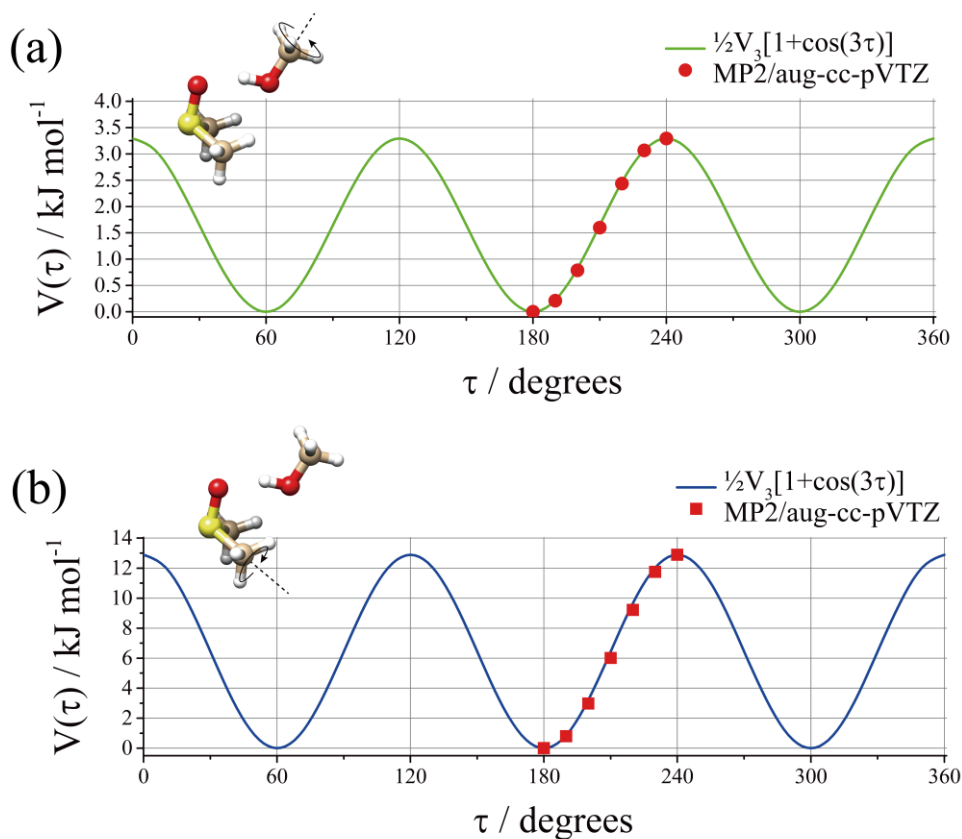


Figure 7.2. *Ab initio* methyl internal rotational potential energy surface for the methyl group of (a) MeOH and (b) DMSO in Conf 1.

The triplet splitting pattern from DMSO methyl rotors were not observed in the observed spectra of DMSO-MeOH. In order to confirm this result, the potential energy surfaces of the methyl torsion around the OC bond of DMSO in Conf 1 were also calculated by changing the dihedral angle of $\tau=HC-SC$ on the regular grid with $\Delta\tau=10^\circ$ and is shown in Figure 7.2b. The calculated data reproduced in red bullets are well reproduced with the threefold function: $V(\tau)=\frac{1}{2}V_3[1+\cos(3\tau)]$, which is shown as a blue line for DMSO methyl rotors of Conf 1. The maximum value (12.9 kJ mol^{-1}) represents the theoretical barrier hindering the methyl group internal rotation for DMSO methyl rotors. It can be noted that barrier value for DMSO methyl rotors of Conf 1 is larger (about 5%) than the value obtained for DMSO monomer ($12.0\sim 12.3 \text{ kJ mol}^{-1}$).⁶ The increased barrier is in consistent with the result of observed DMSO-W conformer and the increased barrier of methyl rotation of DMSO methyl rotors is related to the interactions between the hydroxyl oxygen and methylenic hydrogens of DMSO. Also, the experimental observations are consistent with the results in the experiment of DMSO-W where no triplet splitting pattern was observed in the rotational spectra.

After measuring all possible transition of Conf 1, the recorded spectrum was extended to find the those of Conf 2. From its relative energy and the temperature prior to the expansion the population of Conf 2 was predicted to be 5.3% of the global minimum and taking into account the values of the

dipole moment components the most intense μ_a lines of Conf 2 were predicted to be 10.7% of the most intense ones of Conf 1. The rotational transitions of Conf 2 were not observed in the spectrum although it should have been observable given the overall intensity of the spectrum. This can be attributed to a possible relaxation of the population of this conformation onto that of the global minimum during adiabatic expansion. In order to confirm this, the potential energy surface was calculated for the torsion of the MeOH around the S=O axis on a regular grid with a step of 5 degrees, as shown in Figure 7.3. The global minima correspond to Conf 1, and the two relative equivalent minima correspond to Conf 2. The relaxation during adiabatic expansion is demonstrated by the low barrier (about 0.17 kJ mol⁻¹) of inter-conversion between the two conformations.

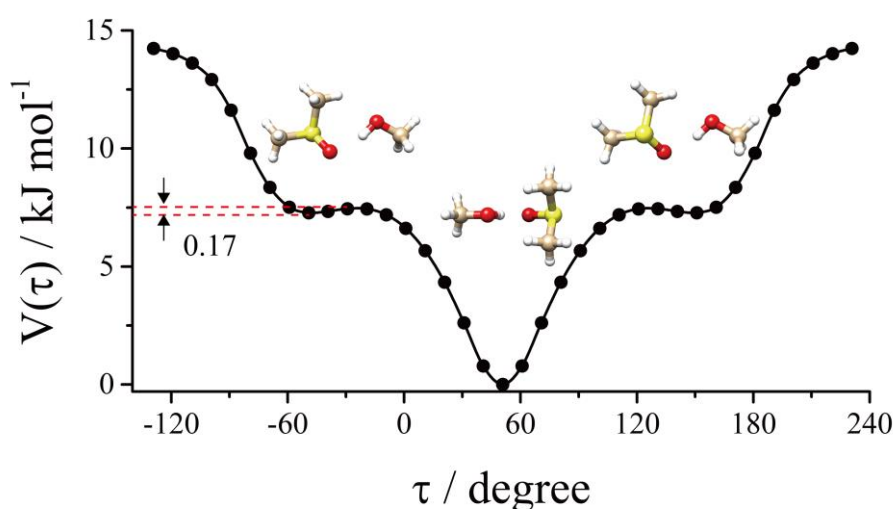


Figure 7.3. *Ab initio* (MP2/aug-cc-pVTZ) potential energy surface for the torsion of MeOH around the S=O axis under partial relaxation. This motion interconverts Conf 1 (absolute minimum) with the Conf 2 (relative equivalent minima).

In order to get a better visualization of the non-covalent interaction between the molecules, the analysis of the HBs in the three conformers was performed by Johnson's NCI method,³⁸ as shown in Figure 7.4 (a-c) for Conf 1, 2 and 3 respectively. The NCI method considers the distribution of the electron density (ρ), its gradient (s) and its second derivatives matrix ($\lambda_1, \lambda_2, \lambda_3$). A comprehensive picture can be drawn using different plots of these quantities. According to the color code reported on the graphics, the gradient isosurfaces ($s=0.5$ a.u.) visible in the NCI plots represent the area for attractive and repulsive interactions. The negative values of the $\text{sign}(\lambda_2)\rho$ and small values of the RGD (<0.5 a.u.) (blue regions) suggest a stronger OH \cdots O HB, the green regions suggest a weaker C–H \cdots O interaction while the positive values of the $\text{sign}(\lambda_2)\rho$ and small values of the RGD (<0.5 a.u.), (orange regions) suggest a weak repulsive interaction. The analysis of Figure 7.4 shows that

a stronger OH...O HB and two weaker C-H...O interactions are observed in Conf 1. Compared with Conf 1, only one C-H...O interaction in Conf 2 is present; No strong OH...O HB but another weaker C-H...O interaction was observed in Conf 3. This result is in consistent with the calculation (using the method MP2/aug-cc-pVTZ) results that Conf 1 has lower energy than Conf 2 and 3, which constitutes the global minimum.

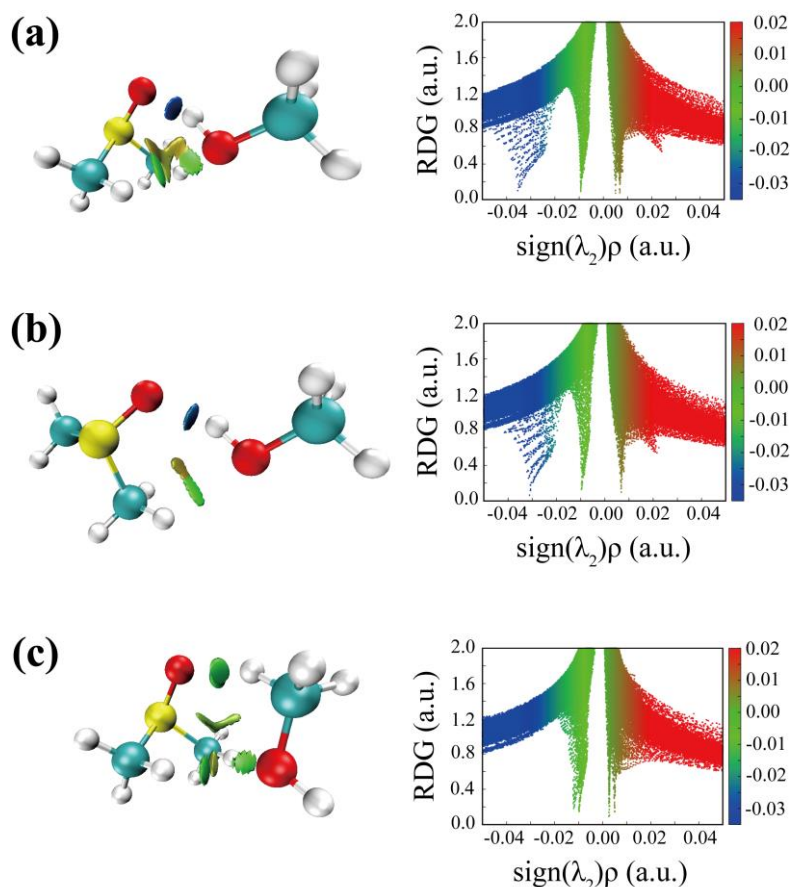


Figure 7.4. The NCI plots from the *ab initio* (MP2/aug-cc-pVTZ) outputs for three conformers: (a) Conf 1, (b) Conf 2, (c) Conf 3. Gradient isosurfaces according to the values of electronic density $\text{sign}(\lambda_2)\rho$ (-0.02~0.02 a.u.) were colored with blue (stronger attractive interactions), green (weaker attractive interactions), orange-red (repulsive interaction).

7.5. Conclusion

In this research, we have studied the HBs between the 1:1 complex of DMSO-MeOH and the barrier hindering internal rotation of the methyl group using the rotational spectroscopy. The determined rotational constants are coherent with a theoretical determined symmetry structure (MP2/aug-cc-pVTZ) stabilized by a primary OH...O HB between MeOH hydrogen and the DMSO oxygen where the MeOH works as the proton donor and the DMSO as proton acceptor. Two weak interactions between the terminal CH groups and the MeOH oxygen which were also characterized and visualized using NCI plots. The observed conformation DMSO-MeOH shown a similar structure pattern as the conformation observed in DMSO-water in Chapter VI. The dipole moment of μ_b (0.0) and the planar inertia moment P_{bb} of DMSO-MeOH ($62.61943(5) \text{ u } \text{\AA}^2$) confirm that DMSO- MeOH has a plane of symmetry (the a, c plane) with the MeOH located on it. The slightly increased value of planar inertia moment P_{bb} of DMSO- MeOH compared with the P_{bb} of DMSO-W ($60.5498(1) \text{ u } \text{\AA}^2$) is due to the two out-of-plane carbonyl hydrogens of MeOH. Splitting of the rotational lines due to the hindered internal rotation of MeOH methyl rotor were observed and the global analysis of the spectrum leads to the determination of a V_3 value of $2.722(3) \text{ kJ mol}^{-1}$. The decreased value of V_3 of MeOH methyl rotor, compared with the free MeOH monomer, is in agreement with the result in the complex of acrolein-methanol (in Chapter IV) and is partly justified by calculations although the higher apparent lowering of the barrier could be related to a coupling of the internal rotation to other intermolecular motions of MeOH.

7.6. Reference

- 1 Ç. A. Akkök, K. Liseth, T. Hervig, A. Rynningen, Ø. Bruserud and E. Ersvær, *Cytotherapy*, 2009, **11**, 749–760.
- 2 H. Dreizler and G. Dendl, *Zeitschrift für Naturforsch. A*, 1964, **19**, 512–514.
- 3 W. Feder, H. Dreizler, H. D. Rudolph and V. Typke, *Zeitschrift für Naturforsch. A*, 1969, **24**, 266–278.
- 4 E. Fliege, H. Dreizler and V. Typke, *Zeitschrift für Naturforsch. A*, 1983, **38**, 668–675.
- 5 H. Dreizler and G. Dendl, *Zeitschrift für Naturforsch. A*, 1965, **20**, 30–37.
- 6 H. Dreizler and G. Dendl, *Zeitschrift für Naturforsch. A*, 1965, **20**, 1431–1440.
- 7 P. A. Stockman, G. A. Blake, F. J. Lovas and R. D. Suenram, *J. Chem. Phys.*, 1997, **107**, 3782–3790.
- 8 V. V. Ilyushin, F. J. Lovas and D. F. Plusquellic, *J. Mol. Spectrosc.*, 2006, **239**, 94–100.
- 9 F. J. Lovas, R. D. Suenram, G. T. Fraser, C. W. Gillies and J. Zozom, *J. Chem. Phys.*, 1988, **88**, 722–729.
- 10 F. J. Lovas, S. P. Belov, M. Y. Tretyakov, J. Ortigoso and R. D. Suenram, *J. Mol. Spectrosc.*, 1994, **167**, 191–204.
- 11 I. A. Finneran, P. B. Carroll, G. J. Mead and G. A. Blake, *Phys. Chem. Chem. Phys.*, 2016, **18**, 22565–22572.
- 12 L. Sun, X. Tan, J. J. Oh and R. L. Kuczkowski, *J. Chem. Phys.*, 1995, **103**, 6440–6449.
- 13 X. Q. Tan, L. H. Sun and R. L. Kuczkowski, *J. Mol. Spectrosc.*, 1995, **171**, 248–264.
- 14 G. T. Fraser, F. J. Lovas and R. D. Suenram, *J. Mol. Spectrosc.*, 1994, **167**, 231–235.
- 15 C. Calabrese, A. Maris, A. Vigorito, S. Mariotti, P. Fathi, W. D. Geppert and S. Melandri, *J. Phys. Chem. A*, 2020, **124**, 3601–3608.
- 16 A. Westphal, C. Jacoby, C. Ratzner, A. Reichelt and M. Schmitt, *Phys. Chem. Chem. Phys.*, 2003, **5**, 4114–4122.
- 17 F. J. Lovas and H. Hartwig, *J. Mol. Spectrosc.*, 1997, **185**, 98–109.
- 18 M. Haeckel and W. Stahl, *J. Mol. Spectrosc.*, 1999, **198**, 263–277.
- 19 X.-Q. Tan, I. I. Ioannou and R. L. Kuczkowski, *J. Mol. Struct.*, 1995, **356**, 105–115.
- 20 H. E. Ayer and D. W. Yeager, *Am. J. Public Health*, 1982, **72**, 1283–1285.
- 21 R. M. Lees, F. J. Lovas, W. H. Kirchhoff and Dr. Johnson, *J. Phys. Chem. Ref. Data*, 1973, **2**, 205–214.
- 22 P. A. Stockman, G. A. Blake, F. J. Lovas and R. D. Suenram, *J. Chem. Phys.*, 1997, **107**, 3782–3790.

- 23 M. Schmitt, J. Küpper, D. Spangenberg and A. Westphal, *Chem. Phys.*, 2000, **254**, 349–361.
- 24 Q. Li, G. Wu and Z. Yu, *J. Am. Chem. Soc.*, 2006, **128**, 1438–1439.
- 25 N. R. Dhumal, *Spectrochim. Acta Part A Mol. Biomol. Spectrosc.*, 2011, **79**, 654–660.
- 26 S. Singh, S. K. Srivastava and D. K. Singh, *RSC Adv.*, 2013, **3**, 4381–4390.
- 27 K. Noack, J. Kiefer and A. Leipertz, *ChemPhysChem*, 2010, **11**, 630–637.
- 28 S. M. Vechi and M. S. Skaf, *J. Chem. Phys.*, , DOI:10.1063/1.2085052.
- 29 J. U. Grabow, W. Stahl and H. Dreizler, *Rev. Sci. Instrum.*, 1996, **67**, 4072–4084.
- 30 T. J. Balle and W. H. Flygare, *Rev. Sci. Instrum.*, 1981, **52**, 33.
- 31 W. Caminati, A. Millemaggi, J. L. Alonso, A. Lesarri, J. C. López and S. Mata, *Chem. Phys. Lett.*, 2004, **392**, 1–6.
- 32 W. Caminati, L. Evangelisti, G. Feng, B. M. Giuliano, Q. Gou, S. Melandri and J.-U. Grabow, *Phys. Chem. Chem. Phys.*, 2016, **18**, 17851–17855.
- 33 S. Grimme, *J. Chem. Theory Comput.*, 2019, **15**, 2847–2862.
- 34 P. Pracht, F. Bohle and S. Grimme, *Phys. Chem. Chem. Phys.*, 2020, **22**, 7169–7192.
- 35 M. J. Frisch, G. W. Trucks, H. B. Schlegel, G. E. Scuseria, M. A. Robb, J. R. Cheeseman, G. Scalmani, V. Barone, G. A. Petersson, H. Nakatsuji and others, *Gaussian Inc. Wallingford CT*.
- 36 A. R. Ubbelohde and K. J. Gallagher, *Acta Crystallogr.*, 1955, **8**, 71–83.
- 37 R. C. Woods, *J. Mol. Spectrosc.*, 1966, **21**, 4–24.
- 38 E. R. Johnson, S. Keinan, P. Mori-Sánchez, J. Contreras-García, A. J. Cohen and W. Yang, *J. Am. Chem. Soc.*, 2010, **132**, 6498–6506.
- 39 H. Hartwig and H. Dreizler, *Zeitschrift für Naturforsch. A*, 1996, **51**, 923–932.
- 40 N. Hansen, H. Mäder and T. Bruhn, *Mol. Phys.*, 1999, **97**, 587–595.

Chapter VIII

Characterizing the interactions of dimethyl sulfoxide with ethanol: a rotational spectroscopy study

8.1. Introduction

The dimer formed by two widely used solvents, DMSO and EtOH was chosen as the system to study the weak inter-molecules interaction by means of rotational spectroscopy combined with quantum chemical calculations. DMSO is an important substance commonly used as a polar aprotic solvent, antifreeze fluid and cryo-protectant owing to its beneficial properties including low toxicity and environmental compatibility.¹ As regards the DMSO molecule, as mentioned in Chapter VI, extensive research has already been done using rotational spectroscopy performed in gas phase. The dipole moment and r_0 structure,² r_s structure,³ centrifugal distortion constants^{4,5} and the internal rotation barrier V_3 of DMSO⁶ were determined.

As regards ethanol, there are three stable structures: the *trans* (with dihedral angle $\tau_{\text{CCOH}} = 180^\circ$) and two equivalent *gauche* structures (*gauche* with $\tau_{\text{CCOH}} = 60^\circ$ and *gauche'* with $\tau_{\text{CCOH}} = -60^\circ$). The *gauche*–*trans* energy difference has been determined to be 0.49(6) kJ mol⁻¹ using the rotational spectroscopy.⁷ The two equivalent *gauche* conformations can interconvert through quantum tunneling and for this reason they are considered to be transient chiral structures.⁸

A few microwave investigations on the EtOH clusters are reported. They concern: EtOH dimer,^{9,10} EtOH-argon,¹¹ EtOH-methanol,¹² EtOH–water,¹³ EtOH-dimethylether¹⁴ and EtOH-(1,4-dioxane)¹⁵, and they were all discussed in Chapter V. All of these studies take into account both the *trans* and *gauche* forms of the EtOH monomer in calculating the resulting complexes' structures, while only the forms involving the *gauche* isomer were observed in most of the complexes. In general EtOH can act as both proton acceptor^{12,13} and donor^{14,15} when interacting with other molecules.

Only few of researches about DMSO/EtOH system have been reported. Leipertz et al.¹⁶ studied the effects of hydrogen bonding between DMSO and EtOH on the symmetric and antisymmetric CSC

stretching vibrations of DMSO by means of Raman spectroscopy. Molecular electron density (MED) topology and natural bond orbital (NBO) analysis has been investigated to explain the strength of interactions in 1:1 adduct of DMSO and EtOH.¹⁷

A bottom-up approach to the problem of solvation can be achieved by the study of small molecular clusters by high resolution spectroscopy in particular rotational spectroscopy performed in gas phase.¹⁸ Rotational spectroscopy is highly sensitive to atomic mass distribution, so it can be used to study intermolecular interactions and isotopic species. The combination of rotational spectroscopy analysis and theoretical methods provide a synergistic method for studying the structure and internal dynamics of isolated molecules¹⁹ and weakly bound complexes²⁰.

We have investigated the rotational spectrum of the 1:1 complex of DMSO with EtOH by rotational spectroscopy in the 6-18 GHz region combined with quantum chemical calculations with the aim of determining its structure and the driving forces involved in the interaction between DMSO and EtOH.

8.2. Methods

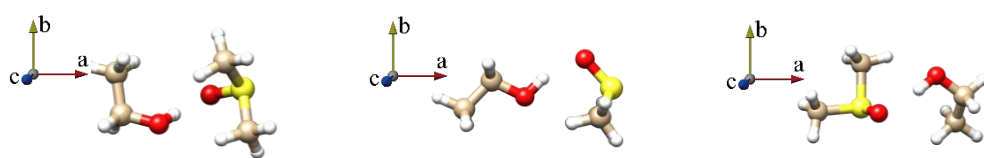
The measurement of the rotational spectrum was carried out in our COBRA-type pulsed supersonic-jet FTMW spectrometer^{21–24}. The samples of DMSO and EtOH were acquired from Sigma-Aldrich (purity>99%) and used without further purification. Samples of DMSO and EtOH were prepared in two separate containers and EtOH cooled to 273K. Helium at a stagnation pressure of about 3 bar, was flowed over the samples resulting in about 1% mixture of both DMSO and EtOH. The molecular beam was then expanded through a solenoid valve (General Valve, Series 9, nozzle diameter of 0.5 mm) into a Fabry–Pérot cavity to exploit already described features of the coaxial supersonic expansion. The analysis of the spectral data was performed with the SPFIT program of Pickett²⁵. The search for the stable geometries of the 1:1 complexes between DMSO and EtOH were performed with CREST software,^{26,27} an efficient scheme by the meta-dynamics algorithm combined with semiempirical tight-binding methods. The resulting conformers were optimized using B3LYP and MP2 levels of theory at the GAUSSIAN 16 program²⁸. The non-covalent interactions between acrolein and EtOH were analyzed with Johnson's NCI method²⁹, which can visualize and quantify the non-covalent interactions based on RDG.

8.3. *Ab initio* results

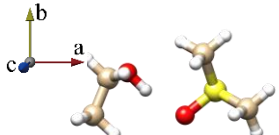
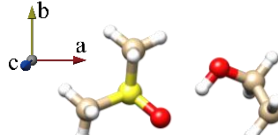
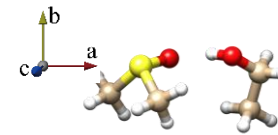
The conformational space and identification of the stable structures of the 1:1 complexes of DMSO with one EtOH were predicted using the CREST software,^{26,27} starting with the conformation where the hydroxyl hydrogen atom of *gauche*-EtOH interacts with the oxygen atom of DMSO and the hydroxyl group of *gauche*-EtOH molecule lies in the symmetry plane of DMSO as initial structures for the configurational search. The resulting conformers, with relative energies ΔE less than 50 kJ mol⁻¹, were optimized at the B3LYP/ def2tzvp level of theory and eight stable conformers were identified. The eight stable conformers were then re-optimized at MP2 levels of theory with the aug-cc-pVTZ, and the results are presented in Table 8.1. All eight conformers were confirmed to be local minima by performing harmonic vibrational calculations. Concise symbol has been devised for each structure of the dimer. It is of the form A-x where the letters A can be “g”, “t”, or “g'” and specifies the EtOH monomer units exhibit *gauche*, *trans*, or *gauche'* configurations. The letter x specifies the two DMSO carbonyl hydrogens (taking values “1”) or one DMSO carbonyl hydrogen (taking values “2”) and two different lone pairs of hydroxyl oxygen (taking values “2” or “2'”) involved in the HBs.

Table 8.1. Spectroscopic parameters and relative energies for the DMSO-EtOH calculated at the B3LYP/def2tzvp and MP2/aug-cc-pVTZ levels of theory. .

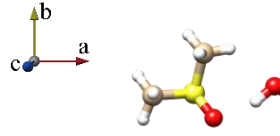
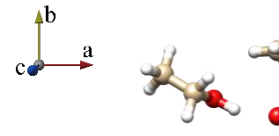
	<i>g</i> -1 (<i>g'</i> -1)		<i>t</i> -1		<i>g</i> -2	
	B3LYP/def 2tzvp	MP2/aug- cc-pVTZ	B3LYP/def 2tzvp	MP2/aug- cc-pVTZ	B3LYP/def 2tzvp	MP2/aug- cc-pVTZ
<i>A</i> / MHz	3308.3	3290.0	3707.0	3751.7	3979.1	3954.2
<i>B</i> / MHz	977.6	1017.6	812.2	823.6	914.5	947.1
<i>C</i> / MHz	924.5	958.4	803.1	812.6	862.0	881.6
μ_a / D	1.8	1.7	-1.4	-1.4	-3.5	-3.5
μ_b / D	0.5	0.7	-2.4	-2.5	0.1	0.0
μ_c / D	2.3	2.5	0.0	0.0	-2.1	-2.2
P_{aa} / u Å ²	455.4	435.2	557.6	550.4	506.0	489.6
P_{bb} / u Å ²	91.2	92.2	71.7	71.5	80.3	83.7
P_{cc} / u Å ²	61.5	61.5	64.6	63.2	46.7	44.1
ΔE / kJ mol ⁻¹	0.0	0.0	0.7	0.7	6.9	6.8



	<i>g</i> -2'		<i>g</i> '-2		<i>g</i> '-2'	
	B3LYP/def 2tzvp	MP2/aug- cc-pVTZ	B3LYP/def 2tzvp	MP2/aug- cc-pVTZ	B3LYP/def 2tzvp	MP2/aug- cc-pVTZ
<i>A</i> / MHz	3838.1	3910.6	4519.9	4630.8	3664.4	3771.0
<i>B</i> / MHz	861.9	888.9	819.0	787.5	896.2	898.8
<i>C</i> / MHz	808.0	831.0	741.2	722.9	877.4	881.3
μ_a / D	-3.8	3.9	-4.0	-3.7	-3.3	-3.3
μ_b / D	-0.9	1.0	-0.8	0.9	-3.0	-3.1
μ_c / D	2.9	2.9	1.3	0.3	0.8	0.6
P_{aa} / u Å ²	540.1	523.7	593.6	615.9	501.0	500.8
P_{bb} / u Å ²	85.4	84.4	88.3	83.2	75.0	72.6
P_{cc} / u Å ²	46.3	44.8	23.5	25.9	62.9	61.4
ΔE / kJ mol ⁻¹	8.2	8.8	7.8	7.8	7.4	8.3

	<i>t</i> -2		<i>t</i> -2'	
	B3LYP/def2tzvp	MP2/aug-cc- pVTZ	B3LYP/def2tzvp	MP2/aug-cc- pVTZ
<i>A</i> / MHz	5280.6	5650.7	4688.9	4866.9
<i>B</i> / MHz	731.3	711.2	761.3	776.5
<i>C</i> / MHz	684.2	661.2	722.6	731.4
μ_a / D	-3.4	-3.3	3.3	-3.3
μ_b / D	1.7	1.7	-3.0	3.3
μ_c / D	-1.3	-0.4	-1.5	-1.4
P_{aa} / u Å ²	667.0	692.8	627.7	619.0
P_{bb} / u Å ²	71.6	71.6	71.7	72.0
P_{cc} / u Å ²	24.1	17.8	36.1	31.9
ΔE / kJ mol ⁻¹	8.5	8.0	9.1	9.7

The theoretical spectroscopic parameters and relative energies (ΔE) of all conformers are reported in Table 8.1 while the Cartesian coordinates of the optimized structures are available in the Appendix.

In the most stable conformer of DMSO with *gauche*-EtOH (*g*-1), the hydroxyl hydrogen of *gauche*-EtOH forms a OH \cdots O HB with the DMSO oxygen atom. The EtOH oxygen lone pairs participate in two C–H \cdots O interactions, with two methylenic DMSO hydrogens. Conformer of

DMSO with *trans*-EtOH (*t*-1) is located about 0.7 kJ mol⁻¹ higher than *g*-1. The hydroxyl hydrogen of *trans*-EtOH forms a OH···O HB with the DMSO oxygen atom. The structure has a C_s symmetry and the oxygen lone pairs participates in two C–H···O interactions, involving the *trans*-EtOH oxygen with two methylenic DMSO hydrogens. The calculated value of the dipole moment of μ_b is 0.0, confirming that Conf 2 has a plane of symmetry (the symmetry plane of DMSO) with the EtOH located on it and the complex has thus a C_s symmetry.

Conformers of DMSO with EtOH (*g*-2, *g*-2', *g*'-2, *g*'-2', *t*-2 and *t*-2'), where *gauche*-EtOH, *gauche*'-EtOH or *trans*-EtOH lie in the heavy atom plane of DMSO forming a six-membered ring structure where the hydroxyl hydrogen forms a HB with the DMSO oxygen and the methylenic DMSO hydrogen is involved in a weak HB with one of the oxygen lone pairs of EtOH, as located about 6.8 kJ mol⁻¹, 8.8 kJ mol⁻¹, 7.8 kJ mol⁻¹, 8.3 kJ mol⁻¹, 8.0 kJ mol⁻¹ and 9.7 kJ mol⁻¹ respectively higher than *g*-1. The six structures all exhibit a stronger OH···O HB and one weak C–H···O interaction. The hydroxyl group of EtOH acts as a proton donor for the OH···O HB.

8.4. Experimental results

We started our experiment with the search of the rotational transition for the two most stable conformers *g*-1 and *t*-1. The detected μ_a -type and μ_b -type rotational transitions and the missing μ_c -type line confirm the assignment to *t*-1 with a structure containing a plane of symmetry coinciding with the *a*, *b* plane.

As an example of the observations, the 6₀₆←5₀₅ transition for the *t*-1 parent species is shown in Figure 8.1. As an isolated monomers, DMSO exhibits a spectral fine splitting of the rotational transitions due to hindered internal rotation of its methyl rotors that leads to a triplet AA, AE (or EA) and EE splitting pattern, where A and E are the methyl torsional state symmetry labels.⁵

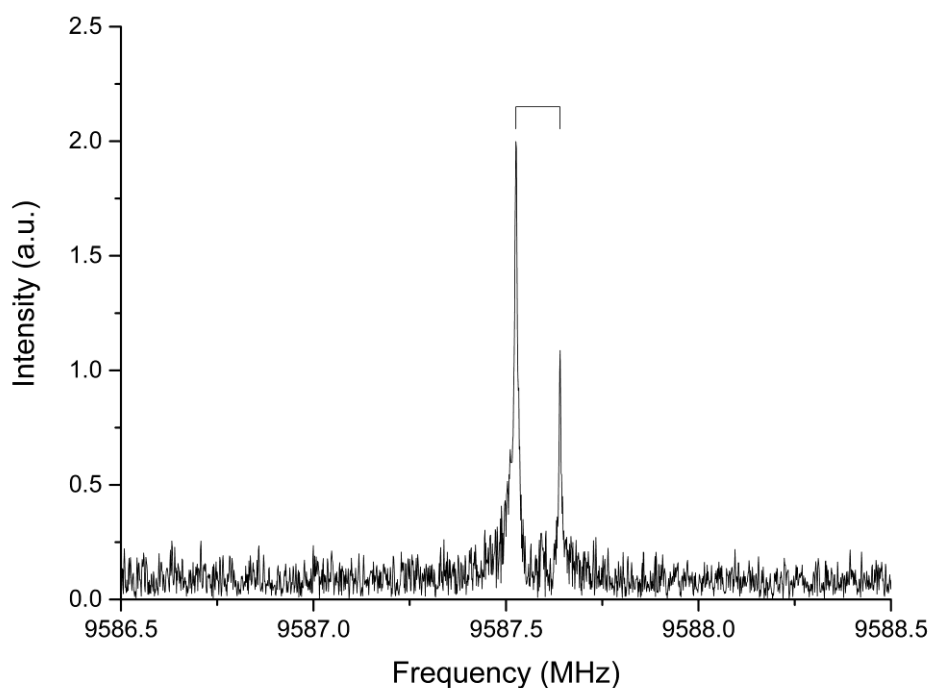


Figure 8.1. $6_{06} \leftarrow 5_{05}$ transitions of conformer *t*-1. The line appears as a doublet (indicated by square bracket) due to the instrumental Doppler effect.

In the case of DMSO-EtOH complex *t*-1 no A-E splitting pattern was observed in the rotational transitions in our frequency range ($J \leq 4$; 6-18 GHz). In order to understand this, the potential energy surface of the methyl torsion around the OC bond of DMSO in *t*-1 was calculated by changing the dihedral angle of $\tau = \text{HC-SC}$ on the regular grid of points with $\Delta\tau = 10^\circ$ and is shown in Figure 8.2b. Only one surface is needed as the two methyl groups are equivalent by symmetry in the *t*-1 conformer. The calculated data indicated by red bullets are well reproduced with the threefold function: $V(\tau) = \frac{1}{2}V_3[1 + \cos(3\tau)]$, which is shown as a blue line. The maximum value (12.9 kJ mol^{-1} for DMSO methyl rotors) represents the theoretical barrier hindering the methyl group internal rotation in the complex. It can be noted that this value is larger (about 5%) than the values obtained for DMSO monomer ($12.0 \sim 12.3 \text{ kJ mol}^{-1}$).⁶ Based on the calculated value of the barrier, no splitting is expected on the observed transitions of the complex in the observed range. According to the results in experiment of DMSO-water, also no triplet splitting pattern was observed. The increased barrier related to the methyl rotation in the complex compared to the isolated monomer, is related to the interactions between the hydroxyl oxygen and methylenic hydrogens of DMSO.

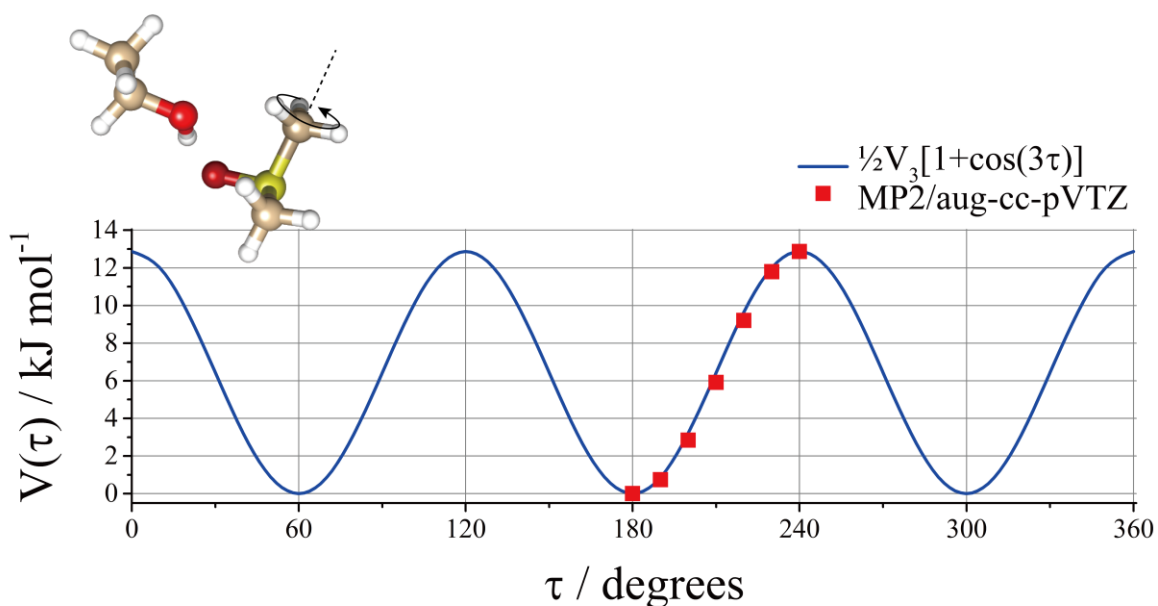


Figure 8.2. *Ab initio* methyl internal rotational potential energy surface for the methyl group of DMSO in *t*-1 conformer of DMSO-EtOH.

The rotational constants of the parent species of *t*-1 are reported in Table 8.2, while the observed transition frequencies are provided in the Appendix. As shown in Table 8.2, the value of the planar inertia moment P_{cc} of *t*-1 is $64.32 \text{ u } \text{\AA}^2$, which is consistent with the value of the planar inertia moment P_{aa} of DMSO ($60.5498(1) \text{ u } \text{\AA}^2$),⁵ confirming again that the *trans*-EtOH lies in the symmetry plane of DMSO (the *a*, *b* plane). The value of planar inertia moment P_{cc} of *t*-1 gradual increased along the growth of number of out-of-plane carbonyl hydrogens compared with the P_{bb} of DMSO-water ($60.74353(6) \text{ u } \text{\AA}^2$) and DMSO-methanol ($62.61943(5) \text{ u } \text{\AA}^2$).

Table 8.2. Experimental spectroscopic parameters of the observed conformers of the DMSO-EtOH complexes.

	<i>t</i> -1
<i>A</i> / MHz	3742.667(4)
<i>B</i> / MHz	803.0678(3)
<i>C</i> / MHz	794.9944(4)
<i>D_J</i> / kHz	-0.243(3)
<i>D_{JK}</i> / kHz	-2.67(5)
<i>P_{aa}</i> / u Å ²	564.9901(4)
<i>P_{bb}</i> / u Å ²	70.7113(4)
<i>P_{cc}</i> / u Å ²	64.3205(4)
<i>σ</i> /kHz	2.6
<i>N</i>	23

After measuring all possible transition of *t*-1, the recorded spectrum was extended to find the rotational transitions of *g*-1. In the studies reported in the literature, usually the *gauche* isomer is involved in the formation of the observed complexes of EtOH. The *g*-1 conformation has two equivalent forms with the EtOH moiety on two side of the DMSO plane so it has a double degeneracy with respect to the population distribution based on the Boltzmann equation. From its relative energy (calculated at MP2/aug-cc-pVTZ), the temperature prior to the expansion and taking into account the values of the dipole moment components, the most intense μ_a lines of *g*-1 were predicted to be three times more intense than that the most intense ones of *t*-1. The rotational transitions of *g*-1 were not observed in the spectrum although they should have been observable given the overall intensity of the spectrum. In order to understand this, the potential energy surface was calculated for the torsion of the EtOH around the S=O axis on a regular grid with a step of 10 degrees, as shown in Figure 8.3. The two global equivalent minima correspond to *g*-1 and *g'*-1, and the relative minima correspond to *t*-1. The missed conformation *g*-1 can be attributed to a possible relaxation of the population of this conformation onto *t*-1 conformer during adiabatic expansion. This is justified by the low barrier (around 3 kJ mol⁻¹) to interconversion between the two conformations, which has been calculated *ab initio* (MP2/aug-cc-pVTZ) and is depicted in Figure 8.3. A possible reason could be the low accuracy of the calculations of the system of DMSO-EtOH. In this case, calculations in different levels have been done and the result gives different global minima between two conformers *g*-1 and *t*-1, as shown in Table 8.3. The unconventional system DMSO-EtOH inspires us to study it further more in the future.

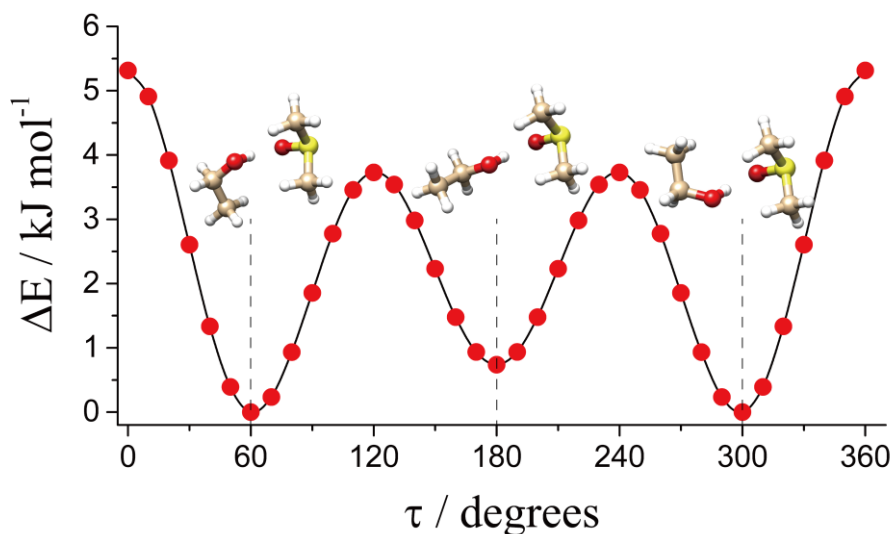


Figure 8.3. *Ab initio* (MP2/aug-cc-pVTZ) potential energy surface for the torsion of the EtOH's methyl group around the OH bond for the *g*-1. This motion interconverts *t*-1 conformer (relative minimum) with *g*'-1 (absolute equivalent minimum), and *g*-1 (absolute equivalent minimum).

Table 8.3. Comparison of the relative energies for the DMSO-EtOH conformers obtained at different levels of calculation.

		<i>g</i> -1	<i>t</i> -1
$\Delta E / \text{kJ mol}^{-1}$	B3LYP/def2tvzp	0.0	0.7
	B3LYP/6-311++G**	0.5	0
	MP2/def2tvzp	0.0	0.4
	MP2/6-311++G**	0.0	0.5
	MP2/aug-cc-pVTZ	0.0	0.7

In order to get a better visualization of the non-covalent interaction between the molecules, the analysis of the HBs in the three conformers was performed by Johnson's NCI method.²⁹ The NCI method considers the distribution of the electron density (ρ), its gradient (s) and its second derivatives matrix ($\lambda_1, \lambda_2, \lambda_3$). A comprehensive picture can be drawn using different plots of these quantities. According to the color code reported on the graphics, the gradient isosurfaces ($s=0.5$ a.u.) visible in the NCI plots, see Figure 8.4, represent the area for attractive and repulsive interactions. The comparison between *g*-1 and *t*-1 is shown in Figure 8.4(a-b). In the negative values of the

$\text{sign}(\lambda_2)\rho$ and small values of the RDG (<0.5 a.u.), the blue regions suggest a stronger OH \cdots O HB and the green regions suggest a weaker C–H \cdots O interaction. In the positive values of the $\text{sign}(\lambda_2)\rho$ and small values of the RDG (<0.5 a.u.), the orange regions suggest a weak repulsive interaction. A weaker C–H \cdots O–S interaction in the conformation *g*-1, as shown in Figure 8.4a. A stronger OH \cdots O HB and two weaker C–H \cdots O interactions were both observed in *g*-1 and *t*-1. The *gauche*- or *trans*-EtOH oxygen lone pairs participate in two C–H \cdots O interactions, involving two methylenic DMSO hydrogens.

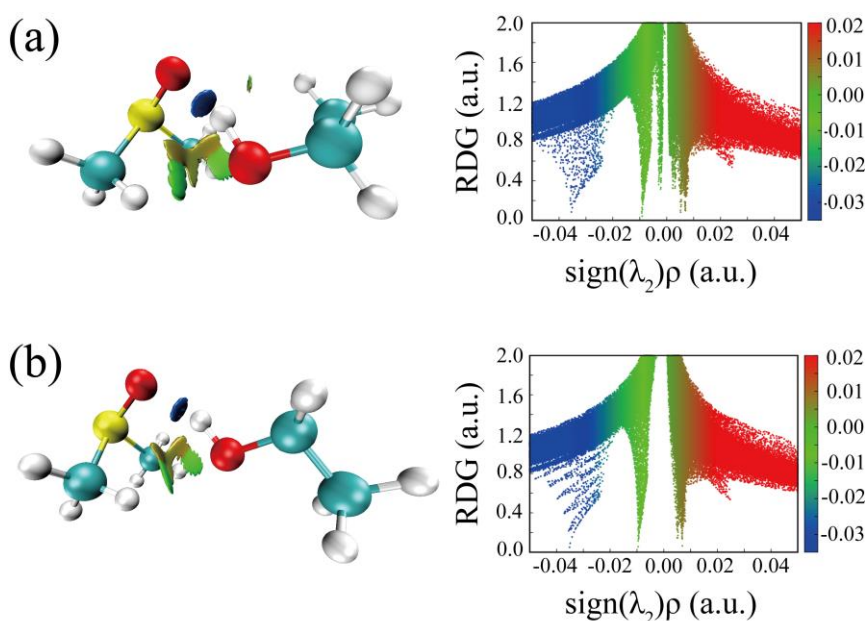


Figure 8.4. Gradient isosurfaces according to the values of electronic density $\text{sign}(\lambda_2)\rho$ ($-0.02\sim 0.02$ a.u.) were colored with blue (strong attractive interactions), green (weak attractive interactions), orange-red (repulsive interaction). The NCI plots of the RDG from the *ab initio* (MP2/aug-cc-pVTZ) outputs for the conformers: a) *g*-1 and b) *t*-1.

8.5. Conclusion

The rotational spectrum of the DMSO-EtOH complexes have been investigated by cavity based Fourier-transform microwave spectroscopy. In the only observed conformation the EtOH adopts the *trans* form and this is the different from the results presented in Chapter V for the complex of acrolein with EtOH where the complex formed with the *gauche* form of EtOH was measured). The observed conformation of DMSO-EtOH was determined with a similar structural pattern as the conformer DMSO-water in Chapter VI and DMSO-methanol in Chapter VII. The EtOH is located on the symmetry plane of DMSO (the *a,b* plane of the complex), and this is proved by the absence of the of the transitions involving μ_c (0.0) and the planar inertia moment P_{cc} ($64.32048(5) \text{ u } \text{Å}^2$). The value of P_{cc} (corresponding to the P_{bb} for DMSO-water ($60.74353(6) \text{ u } \text{Å}^2$) and DMSO-methanol ($62.61943(5) \text{ u } \text{Å}^2$)) slightly gradual increased along the growth of number of out-of-plane carbonyl hydrogens. The hydroxyl hydrogen of EtOH forms a $\text{OH}\cdots\text{O}$ HB with the DMSO oxygen atom where the EtOH works as the proton donor and the DMSO as proton acceptor. The oxygen lone pairs of EtOH participate in two $\text{C-H}\cdots\text{O}$ weak interactions, involving the EtOH oxygen with two methylenic DMSO hydrogens, which were characterized and visualized using NCI plots in observed conformation.

8.6. Reference

- 1 Ç. A. Akkök, K. Liseth, T. Hervig, A. Rynningen, Ø. Bruserud and E. Ersvær, *Cytotherapy*, 2009, **11**, 749–760.
- 2 H. Dreizler and G. Dendl, *Zeitschrift für Naturforsch. A*, 1964, **19**, 512–514.
- 3 W. Feder, H. Dreizler, H. D. Rudolph and V. Typke, *Zeitschrift für Naturforsch. A*, 1969, **24**, 266–278.
- 4 H. Dreizler and G. Dendl, *Zeitschrift für Naturforsch. A*, 1965, **20**, 30–37.
- 5 E. Fliege, H. Dreizler and V. Typke, *Zeitschrift für Naturforsch. A*, 1983, **38**, 668–675.
- 6 H. Dreizler and G. Dendl, *Zeitschrift für Naturforsch. A*, 1965, **20**, 1431–1440.
- 7 R. K. Kakar and C. R. Quade, *J. Chem. Phys.*, 1980, **72**, 4300–4307.
- 8 J. C. Pearson, K. Sastry, E. Herbst and F. C. De Lucia, *J. Mol. Spectrosc.*, 1996, **175**, 246–261.
- 9 J. P. I. Hearn, R. V Cobley and B. J. Howard, *J. Chem. Phys.*, 2005, **123**, 134324.
- 10 D. Loru, I. Peña and M. E. Sanz, *J. Mol. Spectrosc.*, 2017, **335**, 93–101.
- 11 A. Maris, W. Caminati, B. Velino, C. M. Andrews and B. J. Howard, *Chem. Phys. Lett.*, 2004, **399**, 39–46.
- 12 I. A. Finneran, P. B. Carroll, G. J. Mead and G. A. Blake, *Phys. Chem. Chem. Phys.*, 2016, **18**, 22565–22572.
- 13 I. A. Finneran, P. B. Carroll, M. A. Allodi and G. A. Blake, *Phys. Chem. Chem. Phys.*, 2015, **17**, 24210–24214.
- 14 L. Evangelisti, G. Feng, R. Rizzato and W. Caminati, *ChemPhysChem*, 2011, **12**, 1916–1920.
- 15 L. Evangelisti, G. Feng and W. Caminati, *Spectrochim. Acta Part A Mol. Biomol. Spectrosc.*, 2021, **261**, 120086.
- 16 K. Noack, J. Kiefer and A. Leipertz, *ChemPhysChem*, 2010, **11**, 630–637.
- 17 N. R. Dhumal, *Spectrochim. Acta Part A Mol. Biomol. Spectrosc.*, 2011, **79**, 654–660.
- 18 M. Becucci and S. Melandri, *Chem. Rev.*, 2016, **116**, 5014–5037.
- 19 S. Melandri, L. Evangelisti, A. Maris, W. Caminati, B. M. Giuliano, V. Feyer, K. C. Prince and M. Coreno, *J. Am. Chem. Soc.*, 2010, **132**, 10269–71.
- 20 L. B. Favero, B. M. Giuliano, A. Maris, S. Melandri, P. Ottaviani, B. Velino and W. Caminati, *Chemistry*, 2010, **16**, 1761–4.
- 21 J. U. Grabow, W. Stahl and H. Dreizler, *Rev. Sci. Instrum.*, 1996, **67**, 4072–4084.
- 22 T. J. Balle and W. H. Flygare, *Rev. Sci. Instrum.*, 1981, **52**, 33.

- 23 W. Caminati, A. Millemaggi, J. L. Alonso, A. Lesarri, J. C. López and S. Mata, *Chem. Phys. Lett.*, 2004, **392**, 1–6.
- 24 W. Caminati, L. Evangelisti, G. Feng, B. M. Giuliano, Q. Gou, S. Melandri and J.-U. Grabow, *Phys. Chem. Chem. Phys.*, 2016, **18**, 17851–17855.
- 25 H. M. Pickett, *J. Mol. Spectrosc.*, 1991, **148**, 371–377.
- 26 S. Grimme, *J. Chem. Theory Comput.*, 2019, **15**, 2847–2862.
- 27 P. Pracht, F. Bohle and S. Grimme, *Phys. Chem. Chem. Phys.*, 2020, **22**, 7169–7192.
- 28 M. J. Frisch, G. W. Trucks, H. B. Schlegel, G. E. Scuseria, M. A. Robb, J. R. Cheeseman, G. Scalmani, V. Barone, G. A. Petersson, H. Nakatsuji and others, *Gaussian Inc. Wallingford CT*.
- 29 E. R. Johnson, S. Keinan, P. Mori-Sánchez, J. Contreras-García, A. J. Cohen and W. Yang, *J. Am. Chem. Soc.*, 2010, **132**, 6498–6506.
- 30 H. E. Ayer and D. W. Yeager, *Am. J. Public Health*, 1982, **72**, 1283–1285.
- 31 H. Hartwig and H. Dreizler, *Zeitschrift für Naturforsch. A*, 1996, **51**, 923–932.
- 32 N. Hansen, H. Mäder and T. Bruhn, *Mol. Phys.*, 1999, **97**, 587–595.
- 33 Q. Gou, L. B. Favero, G. Feng, L. Evangelisti, C. Pérez and W. Caminati, *Chem. - A Eur. J.*, 2017, **23**, 11119–11125.

Appendix III

Table A3.1. Experimental (r_0 and r_s) and theoretical (r_e , MP2/aug-cc-pVTZ) principal axis system coordinates (Å) of C₆F₅Cl.

	r_0		$ r_s $		r_e	
	a_0	b_0	a_s	b_s	a_e	b_e
C ₁	1.116(7)	0	1.111 (6)	0.114*i (4) ^[a]	1.1222	0
C ₂ , C ₆	0.412(2)	±1.198(5)	0.391 (2)	1.1942 (4)	0.4145	±1.1999
C ₃ , C ₅	-0.973(4)	±1.204(2)	0.9682 (9)	1.1986 (4)	-0.9748	±1.2034
C ₄	-1.672(4)	0	1.6696 (5)	0.134*i (4)	-1.6704	0
F ₂ , F ₆	1.061(4)	±2.359(4)	-	-	1.0616	±2.3612
F ₃ , F ₅	-1.639(4)	±2.355(5)	-	-	-1.6416	±2.3539
F ₄	-3.002(4)	0	-	-	-2.9990	0
Cl	2.834(1)	0	2.83310(9)	0.027*i (4)	2.8323	0

[a] In a few cases the square of the coordinate has been determined to be small and negative leading to an imaginary value of the coordinate.

Table A3.2. Experimental (r_0 and r_s) and theoretical (r_e , MP2/aug-cc-pVTZ) principal axis system coordinates (Å) of C₆F₅Br.

	r_0		$ r_s $		r_e	
	a_0	b_0	a_s	b_s	a_e	b_e
C ₁	0.58(1)	0	-	-	0.5695	0
C ₂ , C ₆	-0.141(2)	±1.192(4)	0.09*i (2) ^[a]	1.192 (2)	-0.1381	±1.1987
C ₃ , C ₅	-1.529(2)	±1.203(6)	1.525(2)	1.199 (2)	-1.5273	±1.2033
C ₄	-2.229(2)	0	-	-	-2.2222	0
F ₂ , F ₆	0.489(4)	±2.363(9)	-	-	0.5044	±2.3628
F ₃ , F ₅	-2.192(8)	±2.356(6)	-	-	-2.1959	±2.3531
F ₄	-3.56(1)	0	-	-	-3.5510	0
Br	2.436(1)	0	2.43422 (2)	0	2.4271	0

[a] In a few cases the square of the coordinate has been determined to be small and negative leading to an imaginary value of the coordinate.

Table A3.3. Experimental (r_0 and r_s) and theoretical (r_e , MP2/aug-cc-pVTZ) principal axis system coordinates (Å) of C₆H₅Cl.

	r_0		$ r_s ^{[a]}$		r_e	
	a_0	b_0	a_s	b_s	a_e	b_e
C ₁	0.43(2)	0	0.43(5)	0	0.4295	0
C ₂ , C ₆	-0.250(8)	±1.215(5)	0.23(4)	±1.215(3)	-0.2514	±1.2137
C ₃ , C ₅	-1.645(3)	±1.209(4)	1.64(3)	±1.211(3)	-1.6450	±1.2057
C ₄	-2.346(3)	0	2.344(2)	0	-2.3445	0
H ₂ , H ₆	0.31(2)	±2.142(7)	-	-	0.3024	±2.1420
H ₃ , H ₅	-2.181(8)	±2.150(7)	-	-	-2.1815	±2.1453
H ₄	-3.436(3)	0	-	-	-3.4260	0
Cl	2.166(1)	0	2.165(3)	0	2.1658	0

^[a] Rotational constants taken from ref. [33]

Table A3.4. Experimental (r_0 and r_s) and theoretical (r_e , MP2/aug-cc-pVTZ) principal axis system coordinates (Å) of C₆H₅Br.

	r_0		$ r_s ^{[a]}$		r_e	
	a_0	b_0	a_s	b_s	a_e	b_e
C ₁	-0.25(3)	0	0.1888	0	-0.2545	0
C ₂ , C ₆	-0.943(9)	±1.215(7)	0.9332	±1.2144	-0.9362	±1.2140
C ₃ , C ₅	-2.336(4)	±1.209(6)	2.3340	±1.2064	-2.3299	±1.2055
C ₄	-3.036(3)	0	3.0341	0	-3.0290	0
H ₂ , H ₆	-0.40(3)	±2.15(1)	-	-	-0.3854	±2.1445
H ₃ , H ₅	-2.87(1)	±2.15(1)	-	-	-2.8663	±2.1453
H ₄	-4.126(3)	0	-	-	-4.1106	0
Br	1.632(1)	0	1.6326	0	1.6281	0

^[a] Rotational constants taken from ref. [34]

Table A3.5. Measured transition frequencies of four isotopologues of C₆F₅Cl, in MHz.

J'	K_a'	K_c'	J''	K_a''	K_c''	$F'_{+1/2}$	$F''_{+1/2}$	$\nu^{-35}\text{Cl}$	$\Delta\nu$	$\nu^{-37}\text{Cl}$	$\Delta\nu$	$\nu^{-13}\text{C1}$	$\Delta\nu$	$\nu^{-13}\text{C2}$	$\Delta\nu$	$\nu^{-13}\text{C3}$	$\Delta\nu$	$\nu^{-13}\text{C4}$	$\Delta\nu$
5	2	3	4	2	2	5	4	6614.971	-0.001										
5	2	3	4	2	2	6	5	6615.506	0.001										
5	2	3	4	2	2	4	3	6615.901	0.008										
5	2	3	4	2	2	7	6	6616.449	0.003										
5	2	3	4	2	2	5	5	6619.064	-0.002										
3	3	0	2	1	1	5	4	6696.764	-0.008										
5	3	2	4	3	1	6	5	6747.722	0.005										
5	3	2	4	3	1	5	4	6750.643	0.005										
5	3	2	4	3	1	7	6	6757.623	0.005										
5	3	2	4	3	1	4	3	6760.460	0.004										
6	3	4	5	3	3	7	6	7200.119	0.001	7073.336	-0.004	7190.133	-0.007	7193.791	0.000				
6	3	4	5	3	3	6	5	7200.927	0.002	7073.999	0.003	7190.945	-0.006	7194.588	-0.006	7188.214	0.000		
6	3	4	5	3	3	6	6	7201.701	-0.008										
6	3	4	5	3	3	8	7	7204.064	0.002	7076.557	0.005			7197.719	0.004	7191.342	0.003		
6	3	4	5	3	3	5	4	7204.849	0.000	7077.209	0.001			7198.494	-0.002	7192.113	-0.008		
6	3	4	5	3	3	5	5	7207.897	-0.001										
9	1	8	9	1	9	8	8	7325.275	-0.006										
9	2	8	9	0	9	8	8	7325.515	-0.004										
9	1	8	9	1	9	11	11	7325.789	0.003										
9	2	8	9	0	9	11	11	7326.029	0.004										
9	1	8	9	1	9	9	9	7328.500	0.005										
9	2	8	9	0	9	9	9	7328.726	-0.010										
9	1	8	9	1	9	10	10	7329.041	-0.002										
9	2	8	9	0	9	10	10	7329.282	-0.003										
7	2	6	6	2	5	8	8	7370.818	-0.001										
7	2	6	6	2	5	7	6							7371.809	0.005			7363.864	0.005
7	2	6	6	2	5	8	7							7371.957	-0.002			7364.002	-0.006
7	2	6	6	2	5	6	5	7382.359	0.002	7281.253	0.002			7372.537	-0.002				
7	2	6	6	2	5	9	8	7382.632	0.001	7281.529	0.001			7372.818	0.011	7367.724	0.004	7364.860	-0.005
7	1	6	6	1	5	8	8	7385.294	-0.005										
7	1	6	6	1	5	7	6	7396.423	0.002	7300.652	-0.001	7388.931	0.002	7386.035	0.000	7381.176	0.001		
7	1	6	6	1	5	8	7	7396.697	0.001			7389.204	-0.002	7386.299	-0.007	7381.443	-0.005		
7	1	6	6	1	5	6	5	7396.903	0.000			7389.413	0.007	7386.523	-0.002				
7	1	6	6	1	5	9	8	7397.189	0.002	7301.211	-0.001	7389.695	0.002	7386.808	0.002				
7	1	6	6	1	5	7	7	7399.097	-0.006										

7	1	6	6	1	5	6	6	7408.427	0.005										
6	4	3	5	4	2	6	6	7532.052	-0.004										
6	4	3	5	4	2	7	6	7532.223	0.001	7367.341	-0.005	7519.003	-0.005	7529.575	-0.002	7521.154	-0.004		
6	4	3	5	4	2	5	5	7534.453	0.000										
6	4	3	5	4	2	6	5	7534.870	-0.002	7369.453	0.005	7521.661	-0.002			7523.803	0.000	7505.258	0.003
6	5	2	5	5	1	7	6	7540.144	-0.006	7362.784	-0.004								
6	4	3	5	4	2	8	7	7541.470	-0.002	7374.683	0.001			7538.811	0.002	7530.395	0.003	7511.856	-0.005
6	4	3	5	4	2	5	4	7544.082	-0.002	7376.763	0.000	7530.886	-0.008			7532.999	-0.002		
6	5	2	5	5	1	6	5	7545.114	-0.006										
6	5	2	5	5	1	8	7	7555.654	-0.003	7374.903	-0.008								
6	5	2	5	5	1	5	4	7560.686	-0.006										
6	2	4	5	2	3	7	7	7567.182	-0.001										
6	2	4	5	2	3	5	4	7577.580	-0.001	7480.899	0.001	7570.232	-0.006	7566.378	-0.003	7561.650	-0.004	7560.947	-0.006
6	2	4	5	2	3	8	7	7578.468	0.000	7481.566	0.002	7571.127	0.005			7562.546	0.002	7561.837	0.004
6	2	4	5	2	3	6	5	7578.889	0.000	7481.722	-0.001	7571.525	-0.001	7567.713	-0.004	7562.980	-0.001	7562.211	-0.006
6	2	4	5	2	3	7	6	7579.786	0.001	7482.394	0.000	7572.419	0.000	7568.618	0.001	7563.879	-0.001	7563.104	-0.001
6	5	1	5	5	0	7	6	7580.980	-0.007	7393.638	-0.009								
6	2	4	5	2	3	6	6	7582.448	-0.001										
6	5	1	5	5	0	6	5	7586.078	-0.007	7397.627	-0.003								
6	2	4	5	2	3	5	5	7590.251	-0.002										
3	3	1	2	1	2	5	4	7591.418	-0.001										
6	5	1	5	5	0	8	7	7597.038	-0.007	7406.099	-0.001								
6	5	1	5	5	0	5	4	7602.195	-0.007	7410.102	-0.007								
3	3	1	2	1	2	3	2	7606.575	0.003										
3	3	1	2	1	2	4	3	7624.308	-0.005										
6	4	2	5	4	1	7	6	7918.864	-0.003	7695.576	0.004	7900.691	-0.001	7922.246	0.003	7910.692	0.002	7878.252	-0.002
6	4	2	5	4	1	6	6	7919.704	-0.004										
6	4	2	5	4	1	6	5	7922.031	-0.003	7698.108	0.002			7925.395	-0.009	7913.853	0.001	7881.429	0.003
6	4	2	5	4	1	5	5	7925.719	-0.001										
6	4	2	5	4	1	7	7	7926.811	-0.004										
6	4	2	5	4	1	8	7	7930.420	-0.001	7704.607	0.001	7912.257	0.003	7933.804	0.006	7922.245	0.004	7889.787	-0.002
6	4	2	5	4	1	5	4	7933.422	-0.001	7706.927	0.002	7915.259	0.000	7936.790	-0.010	7925.241	-0.002	7892.790	0.004
4	3	1	3	1	2	3	2	8034.221	-0.003	7991.376	-0.007								
4	3	1	3	1	2	6	5	8041.006	0.001	7996.995	-0.005								
4	3	1	3	1	2	5	5	8042.481	-0.003										
4	3	1	3	1	2	3	3	8047.808	0.002										
4	3	1	3	1	2	4	3	8049.097	-0.004	8003.793	-0.006								
4	3	1	3	1	2	4	4	8055.437	-0.004										

4	3	1	3	1	2	5	4	8055.995	-0.003	8009.481	-0.006								
11	2	9	11	2	10	11	11	8127.923	-0.006										
11	2	9	11	2	10	12	12	8128.220	-0.009										
11	3	9	11	1	10	11	11	8128.412	0.004										
6	3	3	5	3	2	7	6	8160.084	0.000	7978.161	0.005	8145.766	0.000	8157.172	0.004				
6	3	3	5	3	2	6	5	8160.588	0.000	7978.644	0.003	8146.285	0.005	8157.661	0.005				
6	3	3	5	3	2	6	6	8162.953	0.002										
6	3	3	5	3	2	8	7	8163.790	0.000	7981.407	0.004	8149.510	-0.003	8160.820	0.001			8131.721	-0.002
6	3	3	5	3	2	5	4	8164.255	0.000	7981.863	0.001	8149.995	0.006	8161.275	0.005	8152.207	-0.005		
6	3	3	5	3	2	5	5	8172.773	-0.006										
7	3	5	6	3	4	8	8	8180.139	0.000										
7	3	5	6	3	4	8	7			8059.011	0.002	8176.997	0.001	8177.837	-0.006	8171.444	0.008	8164.478	-0.001
7	3	5	6	3	4	7	6			8059.152	-0.004	8177.167	0.003	8178.012	0.006			8164.654	0.006
7	3	5	6	3	4	9	8			8060.578	-0.002			8179.714	-0.001	8173.323	0.010	8166.380	-0.006
7	3	5	6	3	4	6	5			8060.708	0.008							8166.530	-0.002
8	2	7	7	2	6	9	9	8242.347	0.003										
8	2	7	7	2	6	8	7	8253.961	-0.002	8142.746	-0.001			8242.810	-0.002	8237.192	-0.005	8234.360	-0.006
8	2	7	7	2	6	9	8	8254.156	-0.001	8142.903	-0.004			8243.009	0.003	8237.382	-0.009	8234.559	-0.003
8	2	7	7	2	6	7	6	8254.562	-0.002					8243.416	0.001	8237.800	0.002	8234.960	-0.005
8	2	7	7	2	6	10	9	8254.741	0.000	8143.347	-0.004			8243.593	0.002	8237.978	0.004	8235.151	0.008
8	2	7	7	2	6	8	8	8256.361	-0.002										
8	1	7	7	1	6	8	7	8257.678	0.000	8148.137	-0.008			8246.349	-0.006	8240.811	0.001	8238.359	0.010
8	1	7	7	1	6	9	8	8257.877	-0.001	8148.312	-0.002	8249.324	0.001	8246.557	0.004	8241.015	0.007	8238.551	0.000
8	1	7	7	1	6	7	6	8258.191	-0.003	8148.516	-0.001	8249.643	0.007	8246.870	-0.004	8241.321	-0.006	8238.854	-0.003
8	1	7	7	1	6	10	9	8258.402	-0.001	8148.690	-0.002	8249.834	-0.011	8247.083	0.002			8239.071	0.003
8	1	7	7	1	6	8	8	8260.083	-0.003										
8	2	7	7	2	6	7	7	8266.456	-0.002										
8	1	7	7	1	6	7	7	8270.193	-0.002										
7	2	5	6	2	4	8	8	8372.954	-0.003										
7	2	5	6	2	4	6	5	8382.640	-0.001	8291.670	-0.002	8375.599	-0.007	8368.768	-0.006	8364.184	0.002	8366.726	0.010
7	2	5	6	2	4	9	8	8383.217	-0.001	8292.160	-0.001	8376.195	0.008	8369.344	-0.001	8364.754	-0.001	8367.299	-0.001
7	2	5	6	2	4	7	6	8383.655	-0.001	8292.548	-0.002			8369.777	0.003	8365.193	0.002	8367.751	0.000
7	2	5	6	2	4	8	7	8384.241	0.000	8293.042	-0.003	8377.220	-0.001	8370.351	-0.002	8365.773	-0.001	8368.346	0.002
7	2	5	6	2	4	7	7	8386.319	-0.002										
7	2	5	6	2	4	6	6	8394.004	-0.001										
4	2	2	3	0	3	3	2	8426.260	-0.004										
4	2	2	3	0	3	5	4	8432.015	-0.004										
7	4	4	6	4	3	8	7	8721.670	-0.003	8547.240	0.000	8707.882	0.007	8716.448	-0.002	8707.650	-0.003	8690.681	-0.003

7	4	4	6	4	3	8	8	8722.226	-0.002										
7	4	4	6	4	3	7	6	8722.721	-0.003	8548.087	-0.002	8708.933	0.003	8717.508	0.012	8708.699	-0.001		
7	4	4	6	4	3	9	8	8726.694	-0.003	8551.312	0.001	8712.918	-0.001	8721.452	0.001	8712.662	0.003	8695.745	0.011
7	4	4	6	4	3	6	6	8727.298	-0.007										
7	4	4	6	4	3	6	5	8727.720	-0.004	8552.155	0.000					8713.681	-0.003	8696.763	-0.006
7	6	2	6	6	1	8	7	8794.215	-0.009	8585.193	-0.006								
7	6	2	6	6	1	7	6	8798.053	-0.010	8588.200	-0.009								
7	6	1	6	6	0	8	7	8806.731	-0.013	8594.001	-0.010								
7	6	2	6	6	1	9	8	8808.255	-0.010	8596.149	-0.007								
7	6	1	6	6	0	7	6	8810.600	-0.017	8597.047	0.004								
7	6	2	6	6	1	6	5	8812.150	-0.009	8599.192	-0.008								
7	6	1	6	6	0	9	8	8820.939	-0.011	8605.052	-0.009								
7	6	1	6	6	0	6	5	8824.865	-0.014	8608.111	-0.008								
7	5	3	6	5	2	7	7	8861.162	-0.011										
7	5	3	6	5	2	8	7	8861.989	-0.007	8654.882	-0.003			8860.502	0.005				
7	5	3	6	5	2	7	6	8864.384	-0.007	8656.772	-0.004			8862.879	-0.010				
7	5	3	6	5	2	9	8	8871.547	-0.004	8662.402	-0.006								
7	5	3	6	5	2	6	5	8873.919	-0.007	8664.285	-0.002								
7	5	2	6	5	1	8	7	9044.314	0.003	8797.006	-0.001								
7	5	2	6	5	1	7	6	9047.002	0.009	8799.077	-0.001								
7	5	2	6	5	1	9	8	9055.370	0.008	8805.467	-0.003								
7	5	2	6	5	1	6	5	9058.018	0.000	8807.523	-0.001								
9	2	8	8	2	7	9	8	9123.075	0.002										
9	2	8	8	2	7	10	9	9123.237	0.002										
9	2	8	8	2	7	8	7	9123.555	0.003										
9	2	8	8	2	7	11	10	9123.725	0.006										
9	1	8	8	1	7	9	8	9123.933	-0.002										
9	1	8	8	1	7	10	9	9124.100	0.002										
9	1	8	8	1	7	8	7	9124.391	-0.006										
9	1	8	8	1	7	11	10	9124.572	0.003										
8	2	6	7	2	5	7	6	9181.347	-0.011	9073.633	0.015								
8	2	6	7	2	5	8	7	9181.480	0.019										
8	2	6	7	2	5	10	9	9181.627	-0.005										
8	2	6	7	2	5	9	8	9181.753	0.018	9074.095	0.010								
7	3	4	6	3	3	7	6	9345.126	0.003										
7	3	4	6	3	3	6	5	9345.318	0.005	9185.778	0.008								
7	3	4	6	3	3	8	7	9345.488	0.008										
7	3	4	6	3	3	9	8	9345.685	0.007	9185.992	0.009								

7	4	3	6	4	2	8	7	9494.367	0.005	9239.097	0.007
7	4	3	6	4	2	7	6	9495.562	0.014	9240.088	-0.001
7	4	3	6	4	2	9	8	9500.754	0.009	9244.371	0.011
7	4	3	6	4	2	6	5	9501.925	0.009	9245.362	0.011
8	4	5	7	4	4	9	8	9810.078	0.006	9636.371	0.003
8	4	5	7	4	4	8	7	9810.448	0.009	9636.689	0.007
8	4	5	7	4	4	10	9	9812.701	0.003	9638.569	0.002
8	4	5	7	4	4	7	6	9813.052	0.008	9638.850	-0.008
5	3	2	4	1	3	4	3	9904.347	0.000		
5	3	2	4	1	3	7	6	9906.287	-0.005		
5	3	2	4	1	3	5	4	9908.177	-0.001		
5	3	2	4	1	3	6	5	9910.131	0.007		
8	7	2	7	7	1	10	9	10053.754	-0.005		
8	6	3	7	6	2	9	8	10139.693	-0.006		
8	6	3	7	6	2	8	7	10141.802	0.004		
8	5	4	7	5	3	9	8	10143.132	-0.001		
8	6	3	7	6	2	7	6	10151.217	-0.005		
8	6	2	7	6	1	9	8	10209.634	-0.013		
8	6	2	7	6	1	8	7	10211.863	0.007		
8	6	2	7	6	1	10	9	10219.733	0.011		
8	6	2	7	6	1	7	6	10221.927	0.005		
8	3	5	7	3	4	7	6	10267.883	0.009		
8	3	5	7	3	4	10	9	10268.422	-0.006		
8	3	5	7	3	4	8	7	10269.271	0.005	10146.542	0.009
8	3	5	7	3	4	9	8	10269.815	-0.010	10146.955	0.010
5	4	1	4	2	2	4	3	10448.027	0.007		
5	4	1	4	2	2	7	6	10454.284	-0.001		
5	4	1	4	2	2	5	4	10467.470	-0.006		
5	4	1	4	2	2	6	5	10473.886	-0.008		
8	5	3	7	5	2	8	7	10645.053	0.015		
8	5	3	7	5	2	10	9	10651.513	0.002		
8	5	3	7	5	2	7	6	10652.973	0.011		
8	4	4	7	4	3	9	8	10917.750	-0.003		
8	4	4	7	4	3	8	7	10917.969	0.020	10674.131	0.005
8	4	4	7	4	3	10	9	10920.196	0.002		
8	4	4	7	4	3	7	6	10920.386	0.013		
9	3	6	8	3	5	8	7	11039.503	-0.003		
9	3	6	8	3	5	11	10	11039.898	0.009	10927.575	-0.005

9	3	6	8	3	5	9	8	11040.586	0.007
9	3	6	8	3	5	10	9	11040.968	0.001
9	5	5	8	5	4	10	9	11341.146	-0.011
9	5	5	8	5	4	9	8	11341.697	0.019
9	5	5	8	5	4	11	10	11344.624	0.003
9	5	5	8	5	4	8	7	11345.137	0.015
9	7	3	8	7	2	10	9	11391.805	-0.018
9	7	3	8	7	2	11	10	11400.908	0.018
9	7	2	8	7	1	11	10	11424.596	-0.017
9	6	4	8	6	3	10	9	11479.539	-0.005
9	6	4	8	6	3	9	8	11480.707	-0.001
9	6	4	8	6	3	11	10	11485.964	0.007
9	6	4	8	6	3	8	7	11487.113	0.001
9	6	3	8	6	2	10	9	11731.823	0.011
9	6	3	8	6	2	11	10	11739.734	0.009
5	4	2	4	2	3	7	6	11758.968	0.016
6	4	2	5	2	3	5	4	11765.558	0.007
6	4	2	5	2	3	8	7	11768.274	0.015
6	4	2	5	2	3	6	5	11774.535	-0.001
6	4	2	5	2	3	7	6	11777.271	0.016
9	5	4	8	5	3	10	9	12256.240	0.004
9	5	4	8	5	3	9	8	12256.895	0.002
10	6	5	9	6	4	11	10	12771.618	-0.004
10	6	5	9	6	4	10	9	12772.243	-0.006
10	6	5	9	6	4	9	8	12776.462	0.014
10	4	6	9	4	5	9	8	12959.677	-0.002
10	4	6	9	4	5	12	11	12960.067	-0.008
10	4	6	9	4	5	10	9	12961.108	-0.007
10	4	6	9	4	5	11	10	12961.517	0.002
10	6	4	9	6	3	11	10	13387.732	-0.003
10	6	4	9	6	3	10	9	13388.601	-0.003
10	6	4	9	6	3	12	11	13393.878	0.009
11	4	7	10	4	6	10	9	13698.956	-0.005
11	4	7	10	4	6	13	12	13699.241	-0.002
11	4	7	10	4	6	12	11	13700.339	-0.004
11	6	6	10	6	5	12	11	13974.277	-0.014
11	6	6	10	6	5	13	12	13976.865	-0.001
12	4	8	11	4	7	14	13	14457.323	0.005

11	5	6	10	5	5	13	12	14812.237	-0.001
11	5	6	10	5	5	11	10	14812.492	-0.003
11	5	6	10	5	5	12	11	14812.710	-0.011

Table A3.6. Measured transition frequencies of four isotopologues of C₆F₅Br, in MHz.

J'	K_a'	K_c'	J''	K_a''	K_c''	$F'+1/2$	$F''+1/2$	ν - ⁷⁹ Br	$\Delta\nu$	ν - ⁸¹ Br	$\Delta\nu$	ν - ¹³ C2	$\Delta\nu$	ν - ¹³ C3	$\Delta\nu$
6	4	2	5	2	3	6	5	11754.946	0.011	11777.598	-0.010				
6	4	2	5	2	3	7	6	11723.677	0.012	11750.885	-0.006				
9	1	8	8	1	7	8	7			7025.211	0.003				
9	1	8	8	1	7	9	8			7024.177	0.006				
9	1	8	8	1	7	10	9			7021.957	0.008				
9	1	8	8	1	7	11	10			7023.191	0.004				
9	2	8	8	2	7	9	8	6991.226	0.007						
9	2	8	8	2	7	10	9	6989.267	0.008						
9	2	7	8	2	6	8	7			7808.907	0.005				
9	2	7	8	2	6	9	8			7807.756	0.009				
9	2	7	8	2	6	10	9			7805.242	0.007				
9	2	7	8	2	6	11	10			7806.911	0.008				
9	3	7	8	3	6	9	8	7478.613	0.009						
9	3	7	8	3	6	10	9	7477.675	0.010						
9	3	7	8	3	6	11	10	7468.702	0.008						
9	3	6	8	3	5	8	7	8164.867	0.011						
9	3	6	8	3	5	9	8	8176.853	0.012						
9	3	6	8	3	5	10	9	8174.984	0.013						
9	3	6	8	3	5	11	10	8165.671	0.012						
9	4	6	8	4	5	8	7	7656.742	0.004	7579.388	0.008				
9	4	6	8	4	5	9	8	7678.909	0.008	7597.822	0.004				
9	4	6	8	4	5	10	9	7680.147	0.008	7598.994	0.007				
9	4	6	8	4	5	11	10	7659.972	0.005	7581.972	0.008				
9	4	5	8	4	4	8	7			7787.334	0.009				
9	4	5	8	4	4	9	8			7809.308	0.009				
9	4	5	8	4	4	10	9			7811.013	0.005				
9	4	5	8	4	4	11	10			7790.379	0.013				
9	5	5	8	5	4	9	8	7676.318	0.005	7592.261	0.002				
9	5	5	8	5	4	10	9	7682.609	0.006	7597.392	0.003				
9	5	5	8	5	4	11	10	7647.448	0.004						
9	5	4	8	5	3	11	10	7672.531	0.002	7590.161	0.007				
9	6	3	8	6	2	8	7	7591.992	-0.007						
9	6	3	8	6	2	11	10	7601.890	-0.002	7524.163	0.000				
10	0	10	9	0	9	9	8	7018.764	0.008	6964.771	0.005				
10	0	10	9	0	9	10	9	7019.401	0.005	6965.273	0.007				
10	0	10	9	0	9	11	10	7017.505	0.005	6963.661	0.007				
10	0	10	9	0	9	12	11	7017.105	0.006	6963.327	0.006				
10	1	10	9	1	9	9	8	7017.138	0.007	6962.931	0.005				
10	1	10	9	1	9	10	9	7017.773	0.006	6963.448	0.007				
10	1	10	9	1	9	11	10	7015.955	0.007	6961.899	0.009				
10	1	10	9	1	9	12	11	7015.390	0.008	6961.425	0.007				
10	1	9	9	1	8	9	8	7720.312	0.007	7663.306	0.002	7712.448	-0.007		
10	1	9	9	1	8	10	9	7720.355	0.006	7663.211	0.006	7712.534	0.004		
10	1	9	9	1	8	11	10	7718.333	0.005	7661.506	0.006	7710.511	0.000	7699.056	-0.002
10	1	9	9	1	8	12	11	7718.616	0.007	7661.823	0.007	7710.765	0.000	7699.339	0.003

10	2	9	9	2	8	9	8	7673.325	0.008	7612.677	0.005	7666.530	0.007		
10	2	9	9	2	8	10	9	7675.463	0.006	7614.462	0.007			7656.513	-0.003
10	2	9	9	2	8	11	10	7673.859	0.006	7613.107	0.008				
10	2	9	9	2	8	12	11	7671.932	0.007	7611.487	0.007	7665.147	0.004	7652.989	0.003
10	2	8	9	2	7	9	8	8548.132	0.004	8484.798	0.001				
10	2	8	9	2	7	10	9	8544.731	0.004	8482.087	0.005				
10	2	8	9	2	7	11	10	8542.272	0.003	8480.012	0.005	8533.383	0.000		
10	2	8	9	2	7	12	11	8545.761	0.005	8482.805	0.002	8536.907	0.001	8524.389	-0.001
10	3	8	9	3	7	9	8	8223.031	0.005	8151.147	0.004				
10	3	8	9	3	7	10	9	8229.524	0.006	8156.594	0.006				
10	3	8	9	3	7	11	10	8228.347	0.008	8155.666	0.005				
10	3	8	9	3	7	12	11	8222.760	0.007	8150.857	0.008				
10	3	7	9	3	6	9	8	9071.037	0.008	8977.014	0.006				
10	3	7	9	3	6	10	9	9074.416	0.008	8980.404	0.008				
10	3	7	9	3	6	11	10	9074.728	0.008	8980.308	0.006				
10	3	7	9	3	6	12	11	9068.142	0.008	8974.883	0.008				
10	4	7	9	4	6	9	8	8503.875	0.004	8419.337	0.003				
10	4	7	9	4	6	10	9	8519.160	0.005	8432.101	0.004				
10	4	7	9	4	6	11	10	8519.370	0.007	8432.370	0.004				
10	4	7	9	4	6	12	11	8505.464	0.007	8420.584	0.007				
10	4	6	9	4	5	9	8	8899.012	0.004	8789.546	0.008				
10	4	6	9	4	5	10	9	8919.055	0.010	8806.200	0.011				
10	4	6	9	4	5	11	10	8919.807	0.011	8806.913	0.001				
10	4	6	9	4	5	12	11	8901.141	0.010	8791.233	0.011				
10	5	6	9	5	5	9	8	8530.049	0.000	8440.759	0.002				
10	5	6	9	5	5	10	9	8556.540	0.003	8462.812	-0.002				
10	5	6	9	5	5	11	10	8558.262	0.003	8464.288	0.001				
10	5	6	9	5	5	12	11	8534.293	0.004	8444.214	0.002				
10	5	5	9	5	4	9	8			8494.752	0.001				
10	5	5	9	5	4	10	9	8618.143	0.004	8517.679	-0.001				
10	5	5	9	5	4	11	10	8620.471	0.005	8519.755	0.002				
10	5	5	9	5	4	12	11	8594.592	0.002	8498.156	0.002				
10	6	5	9	6	4	9	8	8474.810	-0.010	8387.411	-0.005				
10	6	5	9	6	4	10	9	8511.920	-0.002	8418.179	-0.005				
10	6	5	9	6	4	11	10	8516.360	-0.002	8422.083	-0.004				
10	6	5	9	6	4	12	11	8481.384	-0.004	8392.718	-0.004				
10	6	4	9	6	3	10	9	8515.851	-0.002	8421.636	-0.007				
10	6	4	9	6	3	11	10	8520.499	-0.002	8425.250	-0.008				
10	6	4	9	6	3	12	11	8485.175	-0.006	8396.123	-0.004				
11	0	11	10	0	10	10	9	7686.165	0.004	7626.985	0.006				
11	0	11	10	0	10	11	10	7686.748	0.007	7627.439	0.006	7679.555	0.001		
11	0	11	10	0	10	12	11	7685.171	0.006	7626.106	0.007	7677.979	0.000		
11	0	11	10	0	10	13	12	7684.792	0.008	7625.788	0.007	7677.594	-0.001	7665.729	0.000
11	1	11	10	1	10	10	9	7685.495	0.005	7626.213	0.005				
11	1	11	10	1	10	11	10	7686.053	0.007	7626.660	0.006				
11	1	11	10	1	10	12	11	7684.528	0.007	7625.363	0.008			7665.025	0.003
11	1	11	10	1	10	13	12	7684.077	0.007	7624.985	0.007			7665.474	0.001
11	1	10	10	1	9	10	9	8373.573	0.006	8310.690	0.005				
11	1	10	10	1	9	11	10	8374.175	0.001	8311.098	0.005				
11	1	10	10	1	9	12	11	8372.606	0.004	8309.775	0.006				

11	1	10	10	1	9	13	12	8372.298	0.004	8309.572	0.005						
11	2	10	10	2	9	10	9	8350.349	0.005	8285.192	0.003	8342.746	0.000				
11	2	10	10	2	9	11	10	8351.839	0.005	8286.426	0.007	8344.237	-0.001				
11	2	10	10	2	9	12	11	8350.504	0.006	8285.291	0.007	8342.905	0.001				
11	2	10	10	2	9	13	12	8349.089	0.006	8284.115	0.005	8341.489	0.002				
11	2	9	10	2	8	10	9	9178.525	0.002	9113.925	-0.003						
11	2	9	10	2	8	11	10	9175.462	0.000	9111.765	0.000						
11	2	9	10	2	8	12	11	9173.482	0.001	9110.044	0.002						
11	2	9	10	2	8	13	12	9176.574	0.002	9112.663	0.000						
11	3	9	10	3	8	10	9	8951.668	0.003	8876.289	0.002						
11	3	9	10	3	8	12	11	8954.574	0.004	8878.781	0.005						
11	3	9	10	3	8	13	12	8951.092	0.004	8875.766	0.006						
11	3	8	10	3	7	11	10	9898.991	0.004	9807.133	0.001						
11	3	8	10	3	7	12	11	9897.111	0.002	9805.545	0.004						
11	3	8	10	3	7	13	12	9896.596	0.004	9804.819	0.004						
11	4	8	10	4	7	10	9	9326.981	0.000	9236.974	-0.001						
11	4	8	10	4	7	11	10	9337.513	0.005	9245.806	-0.001						
11	4	8	10	4	7	12	11	9337.174	0.002	9245.601	0.002						
11	4	8	10	4	7	13	12	9327.651	0.003	9237.472	0.001						
11	4	7	10	4	6	10	9			9801.580	0.004						
11	4	7	10	4	6	11	10			9813.599	0.005						
11	4	7	10	4	6	12	11			9813.587	0.003						
11	4	7	10	4	6	13	12			9802.416	0.006						
11	5	7	10	5	6	10	9	9414.325	-0.006	9315.398	-0.002						
11	5	7	10	5	6	11	10	9433.682	-0.001								
11	5	7	10	5	6	12	11	9434.651	0.002	9332.406	-0.002						
11	5	7	10	5	6	13	12	9416.751	0.000	9317.345	0.001						
11	5	6	10	5	5	10	9	9549.837	-0.003	9437.593	-0.002						
11	5	6	10	5	5	11	10	9572.059	0.001	9455.889	-0.002						
11	5	6	10	5	5	12	11	9573.430	0.004	9457.099	-0.001						
11	5	6	10	5	5	13	12	9552.597	-0.001	9439.793	0.000						
11	6	6	10	6	5	10	9	9363.660	-0.012								
11	6	6	10	6	5	11	10	9388.644	-0.007	9298.026	0.001						
11	6	6	10	6	5	12	11	9394.288	-0.004	9290.424	-0.010						
11	6	6	10	6	5	13	12	9366.092	-0.007	9265.044	-0.005						
11	6	5	10	6	4	10	9	9375.758	-0.014								
11	6	5	10	6	4	11	10	9404.258	-0.003	9299.079	-0.010						
11	6	5	10	6	4	12	11	9406.872	-0.007	9301.390	-0.007						
11	6	5	10	6	4	13	12	9380.049	-0.008	9278.938	-0.007						
12	0	12	11	0	11	11	10	8353.947	0.004	8289.599	0.003						
12	0	12	11	0	11	12	11	8354.453	0.004	8290.002	0.007						
12	0	12	11	0	11	13	12	8353.134	0.003	8288.882	0.004	8344.981	0.000	8332.078	0.002		
12	0	12	11	0	11	14	13	8352.792	0.007	8288.593	0.005						
12	1	12	11	1	11	11	10	8353.674	0.003	8289.280	0.003						
12	1	12	11	1	11	12	11	8354.168	0.004	8289.673	0.003						
12	1	12	11	1	11	13	12	8352.873	0.004	8288.574	0.004	8345.076	-0.001	8332.160	-0.003		
12	1	12	11	1	11	14	13	8352.499	0.005	8288.260	0.005	8344.701	0.001	8331.784	-0.004		
12	1	11	11	1	10	11	10	9033.483	0.001	8964.897	0.001						
12	1	11	11	1	10	12	11	9034.315	0.001	8965.521	0.004						
12	1	11	11	1	10	13	12	9033.020	0.001	8964.434	0.007						

12	1	11	11	1	10	14	13	9032.454	0.002	8963.993	0.003
12	2	11	11	2	10	11	10	9022.529	0.002	8952.654	0.000
12	2	11	11	2	10	12	11	9023.705	0.002	8953.614	0.004
12	2	11	11	2	10	13	12	9022.548	0.003	8952.636	0.005
12	2	11	11	2	10	14	13	9021.456	0.004	8951.731	0.004
12	2	10	11	2	9	11	10	9798.596	-0.001	9730.465	-0.001
12	2	10	11	2	9	12	11	9796.750	-0.003	9728.355	-0.001
12	2	10	11	2	9	13	12	9795.240	-0.003	9727.101	0.001
12	2	10	11	2	9	14	13	9797.159	-0.001	9728.816	-0.002
12	3	10	11	3	9	11	10	9658.718	-0.001		
12	3	10	11	3	9	12	11	9661.277	0.001	9582.125	-0.001
12	3	10	11	3	9	13	12	9660.237	-0.002	9581.259	0.002
12	3	10	11	3	9	14	13	9657.958	0.001	9579.304	0.000
12	4	9	11	4	8	11	10	10121.918	-0.004	10027.946	-0.002
12	4	9	11	4	8	12	11	10129.101	-0.001	10033.997	-0.002
12	4	9	11	4	8	13	12	10128.460	-0.003	10033.529	-0.001
12	4	9	11	4	8	14	13	10122.082	-0.001	10028.027	-0.001
12	5	8	11	5	7	11	10	10289.166	-0.007		
12	5	8	11	5	7	14	13	10290.570	-0.003		
12	6	7	11	6	6	12	11	10281.250	-0.009		
12	6	7	11	6	6	13	12	10280.656	-0.007		
13	0	13	12	0	12	12	11	9021.912	0.003	8952.410	0.002
13	0	13	12	0	12	13	12	9022.356	0.003	8952.761	0.001
13	0	13	12	0	12	14	13	9021.236	0.004	8951.813	0.005
13	0	13	12	0	12	15	14	9020.927	0.003	8951.554	0.004
13	1	13	12	1	12	12	11	9021.801	-0.001	8952.282	0.003
13	1	13	12	1	12	13	12	9022.239	0.000	8952.630	0.003
13	1	13	12	1	12	14	13	9021.127	0.000	8951.687	0.005
13	1	13	12	1	12	15	14	9020.810	0.003	8951.417	0.004
13	1	12	12	1	11	12	11	9697.220	0.001	9623.133	0.001
13	1	12	12	1	11	13	12	9698.100	-0.001	9623.814	0.002
13	1	12	12	1	11	14	13	9697.008	0.000	9622.896	0.002
13	1	12	12	1	11	15	14	9696.359	0.002	9622.373	0.001
13	2	12	12	2	11	12	11	9692.228	0.002	9617.458	0.000
13	2	12	12	2	11	13	12	9693.236	-0.001	9618.271	0.000
13	2	12	12	2	11	14	13	9692.217	0.002	9617.410	0.001
13	2	12	12	2	11	15	14	9691.324	0.000	9616.677	0.002
13	4	9	12	4	8	12	11	11831.098	-0.008	11718.969	0.002
13	4	9	12	4	8	13	12	11837.568	-0.005	11712.443	-0.008
13	4	9	12	4	8	14	13	11835.836	-0.007	11709.147	-0.005
13	4	9	12	4	8	15	14	11832.746	-0.006	11708.152	-0.005
13	5	8	12	5	7	12	11	11595.315	-0.005		
13	5	8	12	5	7	13	12	11610.380	-0.005	11042.675	-0.009
13	5	8	12	5	7	14	13	11610.762	-0.005	11042.695	-0.011
13	5	8	12	5	7	15	14	11596.471	-0.004		
13	6	8	12	6	7	12	11			11033.564	-0.018
13	6	8	12	6	7	15	14			11035.120	-0.013
13	6	7	12	6	6	12	11			11100.206	-0.016
13	6	7	12	6	6	13	12			11115.713	-0.019
13	6	7	12	6	6	14	13			11116.490	-0.016

13	6	7	12	6	6	15	14			11101.939	-0.016
14	0	14	13	0	13	13	12	9689.972	0.002	9615.319	0.000
14	0	14	13	0	13	14	13	9690.364	0.002	9615.633	0.002
14	0	14	13	0	13	15	14	9689.394	-0.001	9614.811	0.002
14	0	14	13	0	13	16	15	9689.121	0.001	9614.580	0.001
14	1	14	13	1	13	13	12	9689.928	0.001	9615.269	0.002
14	1	14	13	1	13	14	13	9690.320	0.003	9615.580	0.003
14	1	14	13	1	13	15	14	9689.355	0.002	9614.761	0.003
14	1	14	13	1	13	16	15	9689.075	0.002	9614.526	0.003
14	1	13	13	1	12	14	13			10284.218	-0.002
14	1	13	13	1	12	15	14			10283.429	-0.002
14	1	13	13	1	12	16	15			10282.897	-0.002
14	2	13	13	2	12	13	12			10280.986	-0.004
14	2	13	13	2	12	14	13			10281.711	-0.001
14	2	13	13	2	12	15	14			10280.948	-0.001
14	2	13	13	2	12	16	15			10280.324	0.000
14	2	12	13	2	11	13	12	11070.671	-0.009	10989.164	-0.009
14	2	12	13	2	11	14	13	11070.700	-0.008	10989.082	-0.006
14	2	12	13	2	11	15	14	11069.736	-0.005	10988.259	-0.006
14	2	12	13	2	11	16	15	11069.836	-0.007	10988.429	-0.008
14	3	12	13	3	11	13	12	11029.627	-0.002	10943.291	-0.010
14	3	12	13	3	11	14	13	11030.740	-0.005	10944.241	-0.004
14	3	12	13	3	11	15	14	11030.043	-0.006	10943.628	-0.006
14	3	12	13	3	11	16	15	11028.790	-0.006	10942.601	-0.004
14	3	11	13	3	10	14	13			11846.290	-0.014
14	3	11	13	3	10	15	14			11845.218	-0.013
14	4	11	13	4	10	13	12	11624.715	-0.012		
14	4	11	13	4	10	14	13	11627.932	-0.012		
14	4	11	13	4	10	15	14	11627.014	-0.015		
14	4	11	13	4	10	16	15	11624.481	-0.009		
14	8	7	13	8	6	13	12			11777.097	0.004
14	8	7	13	8	6	14	13			11796.934	0.002
14	8	7	13	8	6	15	14			11798.592	0.002
14	8	7	13	8	6	16	15			11779.450	0.004
14	8	6	13	8	5	13	12			11777.943	0.004
14	8	6	13	8	5	14	13			11797.792	0.002
14	8	6	13	8	5	15	14			11799.453	0.002
14	8	6	13	8	5	16	15			11780.274	0.004
14	9	6	13	9	5	13	12			11725.663	0.004
14	9	6	13	9	5	14	13			11750.318	0.001
14	9	6	13	9	5	15	14			11752.848	0.001
14	9	6	13	9	5	16	15			11728.740	0.004
14	9	5	13	9	4	13	12			11725.696	0.004
14	9	5	13	9	4	14	13			11750.351	0.001
14	9	5	13	9	4	15	14			11752.882	0.001
14	9	5	13	9	4	16	15			11728.773	0.004
15	0	15	14	0	14	14	13			10278.280	-0.002
15	0	15	14	0	14	15	14			10278.557	-0.003
15	1	15	14	1	14	14	13			10278.259	-0.003
15	1	15	14	1	14	15	14			10278.537	-0.002

15	1	14	14	1	13	14	13	11029.809	-0.004	10945.100	-0.007
15	1	14	14	1	13	15	14	11030.608	-0.008	10945.736	-0.005
15	1	14	14	1	13	16	15	11029.792	-0.001	10945.050	-0.002
15	1	14	14	1	13	17	16	11029.167	-0.002		
15	2	14	14	2	13	14	13	11028.841	-0.008	10943.974	-0.003
15	2	14	14	2	13	15	14	11029.667	-0.003	10944.626	-0.005
15	2	14	14	2	13	16	15	11028.858	-0.005	10943.950	-0.004
15	2	14	14	2	13	17	16	11028.190	-0.004	10943.400	-0.004
15	2	13	14	2	12	14	13	11723.507	0.006	11635.628	-0.012
15	2	13	14	2	12	15	14	11723.910	-0.012	11635.900	-0.012
15	2	13	14	2	12	16	15	11723.102	-0.012	11635.215	-0.011
15	2	13	14	2	12	17	16	11722.810	-0.010	11635.034	-0.007
15	3	13	14	3	12	14	13	11703.036	0.006	11612.346	-0.011
15	3	13	14	3	12	15	14	11703.929	-0.011		
15	3	13	14	3	12	16	15	11703.276	-0.012	11612.532	-0.011
15	3	13	14	3	12	17	16	11702.315	0.006	11611.736	-0.007
16	0	16	15	0	15	15	14	11026.217	-0.004	10941.274	-0.002
16	0	16	15	0	15	16	15	11026.533	-0.001	10941.525	-0.001
16	0	16	15	0	15	17	16	11025.787	-0.004	10940.888	-0.006
16	0	16	15	0	15	18	17	11025.571	0.000	10940.707	-0.002
16	1	16	15	1	15	15	14	11026.210	-0.005	10941.261	-0.008
16	1	16	15	1	15	16	15	11026.521	-0.006	10941.525	0.008
16	1	16	15	1	15	17	16	11025.777	-0.006	10940.881	-0.005
16	1	16	15	1	15	18	17	11025.561	-0.003	10940.697	-0.004
16	1	15	15	1	14	15	14	11697.133	-0.005	11607.268	-0.008
16	1	15	15	1	14	16	15	11697.920	-0.009	11607.844	-0.007
16	1	15	15	1	14	17	16	11697.183	-0.010		
16	1	15	15	1	14	18	17	11696.617	0.006	11606.763	0.002
16	2	15	15	2	14	15	14	11696.756	-0.009	11606.770	0.002
16	2	15	15	2	14	16	15	11697.507	-0.007	11607.356	-0.009
16	2	15	15	2	14	17	16	11696.800	0.005	11606.763	0.001
16	2	15	15	2	14	18	17	11696.185	-0.010	11606.260	-0.008
17	0	17	16	0	16	16	15	11694.373	-0.008	11604.281	-0.009
17	0	17	16	0	16	17	16	11694.655	-0.008	11604.505	-0.009
17	0	17	16	0	16	18	17	11693.995	-0.008	11603.945	-0.008
17	0	17	16	0	16	19	18	11693.797	-0.008	11603.778	-0.009
17	1	17	16	1	16	16	15	11694.373	-0.006	11604.281	-0.006
17	1	17	16	1	16	17	16	11694.655	-0.005	11604.505	-0.006
17	1	17	16	1	16	18	17	11693.995	-0.005	11603.945	-0.005
17	1	17	16	1	16	19	18	11693.797	-0.005	11603.778	-0.006

Table A3.7. Fitted structural parameters by STRFIT program^[55] for the C₆F₅Cl, C₆F₅Br, C₆H₅Cl, C₆H₅Br.

	C ₆ F ₅ Cl	C ₆ F ₅ Br	C ₆ H ₅ Cl	C ₆ H ₅ Br
C1X(Å)	1.718(6)	1.857(9)	1.74(2)	1.88(3)
C1C2(Å)	1.390(5)	1.393(7)	1.39(1)	1.40(2)
C2C3(Å)	1.386(5)	1.387(6)	1.40(1)	1.39(1)
C1C4(Å)	2.788(8)	[2.8079]	2.77(2)	2.79(3)
∠C2C1X(°)	120.5(2)	121.1(2)	119.1(9)	120(1)
∠C3C2C1(°)	120.7(4)	121.6(2)	119(1)	120(1)

Table A3.8. Orbital population and VPPA of the *p*-orbitals of the halogen atom in C₆H₅X and C₆F₅X (X= Cl, Br) calculated with the ETD model and the natural bond order NAO analysis.

ETD	p/s	<i>P</i> _{zz}	<i>P</i> _{yy}	<i>P</i> _{xx}	sum	<i>P</i> _{ave}	Δ <i>P</i> _{zz}	Δ <i>P</i> _{yy}	Δ <i>P</i> _{xx}
C ₆ F ₅ Cl	-	1.250	2	1.955	5.205	1.735	-0.485	0.265	0.220
C ₆ F ₅ Br	-	1.150	2	1.954	5.104	1.701	-0.551	0.299	0.253
C ₆ H ₅ Cl	-	1.335	2	1.965	5.300	1.767	-0.432	0.233	0.198
C ₆ H ₅ Br	-	1.265	2	1.975	5.240	1.747	-0.482	0.253	0.228
NAO (MP2/aug-cc-pVTZ)									
C ₆ F ₅ Cl	0.20	1.175	1.913	1.881	4.969	1.656	-0.481	0.257	0.225
C ₆ F ₅ Br	0.15	1.071	1.918	1.888	4.877	1.626	-0.555	0.293	0.262
C ₆ H ₅ Cl	0.21	1.234	1.923	1.89	5.047	1.682	-0.448	0.241	0.207
C ₆ H ₅ Br	0.17	1.134	1.924	1.892	4.95	1.65	-0.516	0.274	0.242

Appendix IV

Table A4.1 *Ab initio* spectroscopic parameters and relative energies of the ACR-MeOH complexes in the various methods.

	B3LYP/6-311++G**	MP2/6-311++G**	MP2/aug-cc-pVTZ
<i>t</i>-ACR-MeOH-1			
<i>A</i> / MHz	6287	6035	6233
<i>B</i> / MHz	1330	1369	1390
<i>C</i> / MHz	1106	1133	1145
μ_a/D	-2.5	2.3	-2.4
μ_b/D	-0.6	-0.4	-0.5
μ_c/D	-0.1	0.6	0.0
$\Delta E/kJ mol^{-1}$	0	0	0
<i>t</i>-ACR-MeOH-2			
<i>A</i> / MHz	13649	10706	11158
<i>B</i> / MHz	941	1020	1036
<i>C</i> / MHz	890	950	954
μ_a/D	3.5	-0.4	2.7
μ_b/D	0.3	-2.6	0.6
μ_c/D	-0.6	-1.3	0.0
$\Delta E/kJ mol^{-1}$	2.5	2.9	3.7
<i>c</i>-ACR-MeOH-1			
<i>A</i> / MHz	5871	5811	5974
<i>B</i> / MHz	1487	1494	1505
<i>C</i> / MHz	1199	1208	1211
μ_a/D	-2.3	1.8	-2.4
μ_b/D	-0.3	1.4	0.0
μ_c/D	0.4	0.7	0.0
$\Delta E/kJ mol^{-1}$	8.5	9.9	10.5
<i>c</i>-ACR-MeOH-2			
<i>A</i> / MHz	15443	14986	16485
<i>B</i> / MHz	959	1001	1007
<i>C</i> / MHz	914	959	955
μ_a/D	-3.6	2.4	-2.5
μ_b/D	-0.2	-1.5	0.2
μ_c/D	-0.7	0.9	0.0
$\Delta E/kJ mol^{-1}$	11.8	12.4	13.5

Table A4.2 Experimental transition frequencies (ν /MHz) and observed minus calculated values ($\Delta\nu$ /MHz) of *t*-ACR-MeOH-1.

J'	K_a'	K_c'	J''	K_a''	K_c''	ν_A	$\Delta\nu_A$	ν_E	$\Delta\nu_E$	$ \Delta_{A-E} $
3	1	3	2	1	2	7046.6260	0.0214	7068.3599	-0.0129	21.7339
1	1	1	0	0	0	7305.7175	-0.0352	7190.8750	0.02	114.8425
3	0	3	2	0	2	7368.6600	0.0002	7368.4800	-0.0076	0.18
3	2	2	2	2	1	7401.6220	0.0085	7417.7914	-0.0003	16.1694
3	2	1	2	2	0	7434.4795	0.0072	7418.2695	-0.0037	16.21
3	1	2	2	1	1	7746.1710	-0.0132	7724.2853	0.0007	21.8857
4	1	4	3	1	3	9386.2351	0.0253	9395.5371	-0.0176	9.302
2	1	2	1	0	1	9539.6625	-0.023	9480.9230	0.0151	58.7395
4	0	4	3	0	3	9786.8990	0.0075	9786.5630	-0.0047	0.336
4	2	3	3	2	2	9862.3325	0.0206	9899.3566	-0.0051	37.0241
4	2	2	3	2	1	9944.0027	-0.0039	9906.9896	-0.0101	37.0131
4	1	3	3	1	2	10318.0689	-0.0137	10308.5058	-0.0006	9.5631
3	1	3	2	0	2	11660.1396	-0.0005	11623.2166	0.0054	36.923
5	1	5	4	1	4	11718.4385	0.0321	11723.0429	-0.0253	4.6044
5	0	5	4	0	4	12174.0054	0.016	12173.4325	-0.0105	0.5729
5	1	4	4	1	3	12880.7055	-0.0129	12875.6853	0.0059	5.0202
4	1	4	3	0	3	13677.7065	0.0164	13650.2659	-0.0124	27.4406
6	1	6	5	1	5	14042.0113	0.0313	14044.4902	-0.0325	2.4789
6	0	6	5	0	5	14525.1437	0.0232	14524.2604	-0.0237	0.8833
6	1	5	5	1	4	15431.0750	-0.0062	15427.9723	0.0123	3.1027
5	1	5	4	0	4	15609.2463	0.0414	15586.7227	-0.0561	22.5236

Table A4.3 Experimental transition frequencies (ν /MHz) and observed minus calculated values ($\Delta\nu$ /MHz) of *t*-ACR-MeOH-2.

J'	K_a'	K_c'	J''	K_a''	K_c''	ν_A	$\Delta\nu_A$	ν_E	$\Delta\nu_E$	$ \Delta_{A-E} $
4	1	4	3	1	3	7618.1652	0.0004	7669.5224	-0.0693	51.3572
4	0	4	3	0	3	7766.8648	0.0169	7766.7462	-0.0272	0.1186
4	2	3	3	2	2	7771.9530	0.0289	7774.0058	-0.0243	2.0528
4	2	2	3	2	1	7776.1669	0.0265	7773.9603	-0.0014	2.2066
4	1	3	3	1	2	7922.9116	0.041	7871.4050	0.052	51.5066
5	1	5	4	1	4	9521.8170	0.0208	9557.8450	-0.0727	36.0280
5	0	5	4	0	4	9705.2723	0.0008	9705.1613	-0.0054	0.1110
5	2	4	4	2	3	9714.2845	0.0354	9718.3899	-0.074	4.1054
5	2	3	4	2	2	9722.7046	0.0258	9718.3356	-0.0462	4.3690
5	1	4	4	1	3	9902.6991	0.0403	9866.4500	0.0328	36.2491
6	1	6	5	1	5	11424.8810	0.0517	11448.9900	-0.039	24.1090
6	0	6	5	0	5	11641.5344	0.0258	11641.3295	-0.0361	0.2049
6	2	5	5	2	4	11656.1771	0.0402	11663.4286	-0.036	7.2515
6	2	4	5	2	3	11670.9086	0.0282	11663.4568	-0.01	7.4518
6	1	5	5	1	4	11881.8252	0.0058	11857.4600	-0.006	24.3652
1	1	1	0	0	0	12224.8994	0.0266	11878.5434	0.0008	346.3560
7	1	7	6	1	6	13327.2525	0.1002	13343.4699	0.0034	16.2174
7	0	7	6	0	6	13575.1642	0.0326	13574.8904	-0.0505	0.2738
7	1	6	6	1	5	13860.1917	-0.0273	13843.6488	-0.0633	16.5429
2	1	2	1	0	1	14091.6479	0.0134	13804.9290	0.0088	286.7189
3	1	3	2	0	2	15920.5022	-0.0034	15697.0406	-0.0453	223.4616

Table A4.4 Experimental transition frequencies (ν /MHz) and observed minus calculated values ($\Delta\nu$ /MHz) of *t*-ACR-MeOH-1-D.

J'	K_a'	K_c'	J''	K_a''	K_c''	ν_A	$\Delta\nu_A$	ν_E	$\Delta\nu_E$	$ \Delta_{A-E} $
3	1	3	2	1	2	7027.0586	0.0172	7043.4129	-0.0443	16.3543
1	1	1	0	0	0	7314.8287	0.0446	7223.9852	-0.0378	90.8435
3	0	3	2	0	2	7346.5420	0.0002	7346.3864	0.0086	0.1556
3	2	2	2	2	1	7378.8134	-0.0048	7394.5184	0.0012	15.7050
3	2	1	2	2	0	7411.0021	0.0057	7395.2325	-0.0026	15.7696
3	1	2	2	1	1	7720.3381	-0.024	7703.8324	0.0333	16.5057
4	1	4	3	1	3	9360.3391	0.026	9367.1896	-0.0253	6.8505
2	1	2	1	0	1	9543.2571	0.0512	9498.1757	-0.0414	45.0814
4	0	4	3	0	3	9758.1844	0.0035	9757.8938	0.0032	0.2906
4	2	3	3	2	2	9832.0584	0.0076	9867.5611	0.0026	35.5027
4	2	2	3	2	1	9912.0485	-0.0151	9876.5437	0.0156	35.5048
4	1	3	3	1	2	10283.8366	-0.0329	10276.7442	0.0188	7.0924
3	1	3	2	0	2	11659.2082	0.0807	11630.5405	-0.0973	28.6677
5	1	5	4	1	4	11686.3611	0.041	11689.7052	-0.0235	3.3441
5	0	5	4	0	4	12139.3056	0.0123	12138.8156	-0.0064	0.4900
5	1	4	4	1	3	12838.2829	-0.0345	12834.5547	0.0206	3.7282
6	1	6	5	1	5	14003.8979	0.0336	14005.6764	-0.0239	1.7785
6	1	5	5	1	4	15380.7339	-0.0347	15378.4092	0.0282	2.3247
7	1	7	6	1	6	16312.1489	0.033	16313.0716	-0.0451	0.9227
7	0	7	6	0	6	16793.8495	0.0316	16792.8117	-0.0343	1.0378
7	2	6	6	2	5	17153.7396	0.0532	17203.8502	-0.0512	50.1106
7	2	5	6	2	4	17575.4496	-0.0869	17525.6552	0.0834	49.7944
7	1	6	6	1	5	17907.8176	-0.0254	17906.0997	0.0373	1.7179

Table A4.5 Experimental transition frequencies (ν /MHz) and observed minus calculated values ($\Delta\nu$ /MHz) of *t*-ACR-MeOH-2-D.

J'	K_a'	K_c'	J''	K_a''	K_c''	ν_A	$\Delta\nu_A$	ν_E	$\Delta\nu_E$	$ \Delta_{A-E} $
4	1	4	3	1	3	7587.1949	0.0103	7629.6822	0.083	42.4873
4	0	4	3	0	3	7733.3951	-0.1417	7733.287	-0.0971	0.1081
4	1	3	3	1	2	7886.6855	0.0766	7844.0473	0.0691	42.6382
5	1	5	4	1	4	9483.1378	0.0067	9511.3792	0.0619	28.2414
5	0	5	4	0	4	9663.5796	-0.1213	9663.4362	-0.0669	0.1434
5	1	4	4	1	3	9857.4421	0.0506	9828.9955	0.066	28.4466
6	1	6	5	1	5	11378.5189	-0.0003	11396.7915	0.0254	18.2726
6	0	6	5	0	5	11591.6608	-0.0629	11591.4774	0.0013	0.1834
6	1	5	5	1	4	11827.5806	-0.0058	11809.0461	0.0461	18.5345
7	1	7	6	1	6	13273.2171	-0.0281	13285.2877	-0.0101	12.0706
7	0	7	6	0	6	13517.2298	0.0437	13516.9923	0.1091	0.2375
7	1	6	6	1	5	13796.9695	-0.098	13784.5897	-0.0179	12.3798

Table A4.6 MP2/aug-cc-pVTZ geometries of the two conformers of the ACR-MeOH complexes.

Bond lengths / Å		Valence angles/ °		Dihedral angles / °	
<i>t</i>-ACR-MeOH-1					
C2C1	1.340				
C2C2	1.465	C2C2C1	118.9		
O4C3	1.224	O4C3C2	124.7	O4C3C2C1	180.0
C5O4	3.787	C5O4C3	123.3	C5O4C3C2	0.0
O6C5	1.420	O6C5O4	39.9	O6C5O4C3	-0.1
H7C1	1.080	H7C1C2	121.9	H7C1C2C3	-180.0
H8C1	1.084	H8C1C2	120.5	H8C1C2C3	0.0
H9C2	1.083	H9C2C1	123.1	H9C2C1C3	180.0
H10C3	1.104	H10C3C2	115.3	H10C3C2C1	0.0
H11O6	0.970	H11O6C5	108.5	H11O6C5O4	0.0
H12C5	1.087	H12C5O4	147.1	H12C5O4C3	-0.2
H13C5	1.092	H13C5O4	89.9	H13C5O4C3	125.4
H14C5	1.092	H14C5O4	89.9	H14C5O4C3	-125.7
<i>t</i>-ACR-MeOH-2					
C2C1	1.339				
C2C2	1.464	C2C2C1	119.7		
O4C3	1.225	O4C3C2	123.8	O4C3C2C1	-180.0
O5O4	2.827	O5O4C3	90.7	O5O4C3C2	179.9
C6O5	1.419	C6O5O4	125.4	C6O5O4C3	180.0
H7C1	1.080	H7C1C2	122.0	H7C1C2C3	180.0
H8C1	1.083	H8C1C2	120.3	H8C1C2C3	0.0
H9C2	1.082	H9C2C1	122.7	H9C2C1C3	-180.0
H10C3	1.103	H10C3C2	115.9	H10C3C2C1	0.0
H11O5	0.970	H11O5O4	17.1	H11O5O4C3	180.0
H12C6	1.087	H12C6O5	107.2	H12C6O5O4	-179.9
H13C6	1.092	H13C6O5	111.9	H13C6O5O4	-61.1
H14C6	1.092	H14C6O5	111.9	H14C6O5O4	61.3

Table A4.7 The different splitting (Δ_{Split} / MHz) of A-E lines between parent species and deuterated species.

J'	K_a'	K_c'	J''	K_a''	K_c''	$ \Delta_{\text{A-E}} $		Δ_{Split}
						<i>t</i>-ACR-MeOH-1	<i>t</i>-ACR-MeOH-1-D	
3	1	3	2	1	2	21.7339	16.3543	-5.3796
1	1	1	0	0	0	114.8425	90.8435	-23.999
3	0	3	2	0	2	0.18	0.1556	-0.0244
3	2	2	2	2	1	16.1694	15.705	-0.4644
3	2	1	2	2	0	16.21	15.7696	-0.4404
3	1	2	2	1	1	21.8857	16.5057	-5.38
4	1	4	3	1	3	9.302	6.8505	-2.4515
2	1	2	1	0	1	58.7395	45.0814	-13.6581
4	0	4	3	0	3	0.336	0.2906	-0.0454
4	2	3	3	2	2	37.0241	35.5027	-1.5214
4	2	2	3	2	1	37.0131	35.5048	-1.5083
4	1	3	3	1	2	9.5631	7.0924	-2.4707
3	1	3	2	0	2	36.923	28.6677	-8.2553
5	1	5	4	1	4	4.6044	3.3441	-1.2603
5	0	5	4	0	4	0.5729	0.49	-0.0829
5	1	4	4	1	3	5.0202	3.7282	-1.292
						<i>t</i>-ACR-MeOH-2	<i>t</i>-ACR-MeOH-2-D	
4	1	4	3	1	3	51.3572	42.4873	-8.8699
4	0	4	3	0	3	0.1186	0.1081	-0.0105
4	1	3	3	1	2	51.5066	42.6382	-8.8684
5	1	5	4	1	4	36.028	28.2414	-7.7866
5	0	5	4	0	4	0.111	0.1434	0.0324
5	1	4	4	1	3	36.2491	28.4466	-7.8025
6	1	6	5	1	5	24.109	18.2726	-5.8364
6	0	6	5	0	5	0.2049	0.1834	-0.0215
6	1	5	5	1	4	24.3652	18.5345	-5.8307
7	1	7	6	1	6	16.2174	12.0706	-4.1468
7	0	7	6	0	6	0.2738	0.2375	-0.0363
7	1	6	6	1	5	16.5429	12.3798	-4.1631

Appendix V

Table A5.1. *Ab initio* spectroscopic parameters and relative energies of the acrolein-ethanol complexes in the various methods.

	TT1	TT2	TG1	TG'1	TG2/ TG'2	TG3	TG'3	CT1	CT2	CG1	CG'1	CG2	CG'2
MP2/aug-cc-pVTZ													
<i>A</i> / MHz	4841	7793	5024	3656	7474	4928	5365	5291	13080	3661	3850	6123	5964
<i>B</i> / MHz	890	689	937	1183	737	907	880	910	653	1269	1281	875	884
<i>C</i> / MHz	759	638	835	1074	700	862	854	784	627	1164	1099	835	840
μ_a / D	-2.2	-2.6	2.4	-2.6	-2.6	-2.9	3.5	-2.3	-2.5	-2.5	2.9	-2.7	3.2
μ_b / D	1.0	0.9	-0.3	-1.7	-0.7	2.2	-0.8	0.3	0.4	1.2	0.0	2.0	0.6
μ_c / D	0.0	0.0	-0.4	1.5	0.3	-0.3	2.1	0.0	0.0	1.9	2.3	0.5	2.0
ΔE / kJ mol ⁻¹	0.0	3.7	0.2	0.3	4.0	3.6	4.2	10.5	13.6	10.1	10.1	13.5	14.1
MP2/def2tzvp													
<i>A</i> / MHz	4429	6422	4217	3792	-	5077	6277	4317	10123	3762	3933	6246	6788
<i>B</i> / MHz	934	734	1105	1112	-	872	805	1089	688	1189	1227	851	811
<i>C</i> / MHz	801	684	980	1028	-	840	769	944	673	1103	1052	817	768
μ_a / D	2.5	-3.0	3.0	-2.5	-	2.9	3.3	2.5	2.9	2.4	-2.8	2.7	-3.1
μ_b / D	1.3	-1.6	0.7	-1.3	-	-2.0	-0.6	1.6	1.1	0.6	-0.1	-1.8	-0.3
μ_c / D	-1.3	-1.2	-2.0	1.6	-	-0.3	1.8	-1.8	1.3	-1.9	-2.2	0.7	1.8
ΔE / kJ mol ⁻¹	0.4	3.0	0.1	0	-	2.8	2.9	10.6	12.4	10.5	10.2	12.3	12.4

B3LYP/def2tzvp													
<i>A</i> / MHz	4345	6670	4954	3779	-	5064	7233	4702	10432	3757	4337	6203	7481
<i>B</i> / MHz	950	721	968	1111	-	874	752	1001	680	1201	1117	852	766
<i>C</i> / MHz	811	675	851	1021	-	832	715	867	665	1108	948	814	726
μ_a / D	2.7	3.3	-3.0	-2.6	-	-3.2	3.5	2.5	3.2	2.3	-2.7	3.1	-3.4
μ_b / D	1.6	1.7	-0.7	-1.5	-	2.2	-0.6	1.2	1.2	0.9	0.2	-2.0	-0.1
μ_c / D	-1.3	-1.1	-1.6	1.5	-	-0.2	1.6	-1.5	-1.4	-1.9	-1.8	0.5	1.6
ΔE / kJ mol ⁻¹	0.7	4.3	0.3	0	-	3.8	4.0	9.5	13.8	8.9	9.1	13.3	13.5

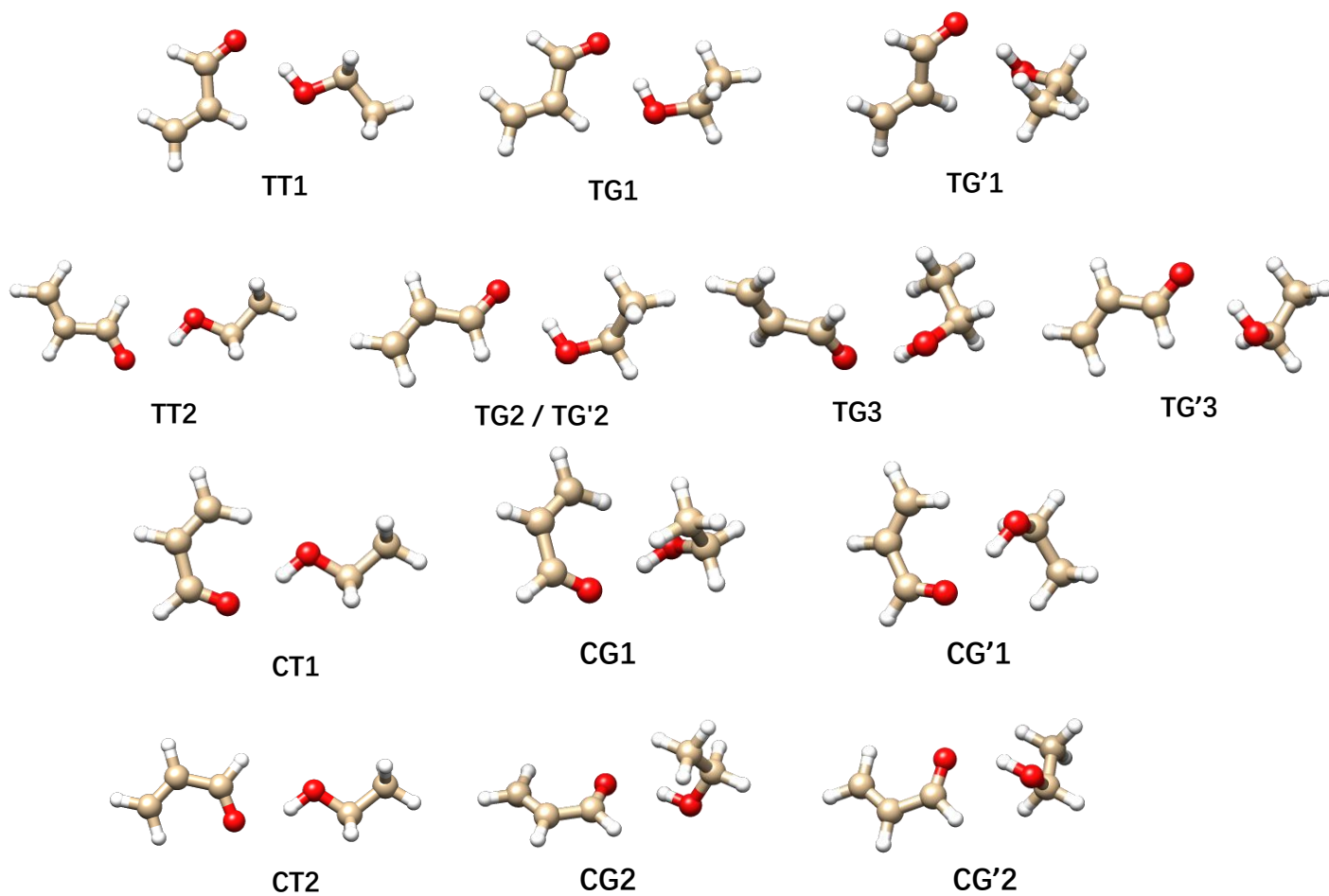


Figure A5.1. *Ab initio* (MP2/aug-cc-pVTZ) structures.

Table A5.2. Experimental transition frequencies (ν / MHz) and obs.-cal. values ($\Delta\nu$ / MHz) of TG1.

J'	K_a'	K_c'	J''	K_a''	K_c''	ν	$\Delta\nu$	J'	K_a'	K_c'	J''	K_a''	K_c''	ν	$\Delta\nu$
4	1	4	3	1	3	6686.532	0.0018	8	2	6	7	2	5	13878.32	-0.0003
4	0	4	3	0	3	6864.804	0.0003	8	1	7	7	1	6	14109.32	-0.0002
4	2	3	3	2	2	6880.764	0.0008	9	1	9	8	1	8	15004.68	0.0020
4	2	2	3	2	1	6897.484	0.0002	9	0	9	8	0	8	15288.54	-0.0019
4	1	3	3	1	2	7070.088	0.0014	9	2	8	8	2	7	15451.59	0.0011
5	1	5	4	1	4	8354.902	-0.0004	9	2	7	8	2	6	15643.39	-0.0013
5	0	5	4	0	4	8568.327	-0.0007	9	1	8	8	1	7	15859.92	0.0064
5	2	4	4	2	3	8598.635	0.0014	10	1	10	9	1	9	16659.98	0.0036
5	2	3	4	2	2	8631.982	0.0006	10	0	10	9	0	9	16941.53	-0.0040
5	1	4	4	1	3	8834.132	0.0021	10	1	9	9	1	8	17605.36	-0.0028
6	1	6	5	1	5	10021.2	-0.0014	2	1	2	1	0	1	7415.227	0.0001
6	0	6	5	0	5	10263.6	-0.0018	3	1	3	2	0	2	8992.462	-0.0010
6	2	5	5	2	4	10314.96	-0.0005	4	1	4	3	0	3	10524.44	0.0000
6	2	4	5	2	3	10373.03	0.0001	5	1	5	4	0	4	12014.54	-0.0017
6	1	5	5	1	4	10595.75	-0.0006	6	1	6	5	0	5	13467.42	0.0049
7	1	7	6	1	6	11685.1	-0.0013	7	0	7	6	1	6	8745.51	-0.0011
7	0	7	6	0	6	11949.31	-0.0032	9	0	9	8	1	8	12627.1	0.0029
7	2	6	6	2	5	12029.43	-0.0014	2	1	1	1	0	1	7702.951	0.0005
7	2	5	6	2	4	12121.59	-0.0013	3	1	2	2	0	2	9567.905	0.0004
7	1	6	6	1	5	12354.36	0.0009	4	1	3	3	0	3	11483.44	-0.0009
8	1	8	7	1	7	13346.33	-0.0005	5	1	4	4	0	4	13452.77	0.0027
8	0	8	7	0	7	13624.47	-0.0015	6	1	5	5	0	5	15480.19	-0.0030
8	2	7	7	2	6	13741.74	0.0001								

Table A5.3. Experimental transition frequencies (ν /MHz) and obs.-cal. values ($\Delta\nu$ /MHz) of TG1-D.

$J' K_a' K_c' J'' K_a'' K_c''$	ν	$\Delta\nu$	$J' K_a' K_c' J'' K_a'' K_c''$	ν	$\Delta\nu$
4 1 4 3 1 3	6696.837	0.0017	7 0 7 6 0 6	11966.39	-0.0036
4 0 4 3 0 3	6874.275	0.0008	7 2 6 6 2 5	12045.89	-0.0024
4 2 3 3 2 2	6890.153	0.0012	7 2 5 6 2 4	12137.2	-0.0034
4 2 2 3 2 1	6906.715	0.0000	7 1 6 6 1 5	12369.21	0.0000
4 1 3 3 1 2	7078.506	0.0019	8 1 8 7 1 7	13367.03	0.0068
5 1 5 4 1 4	8367.795	0.0007	8 0 8 7 0 7	13644.23	-0.0021
5 0 5 4 0 4	8580.272	0.0032	8 2 7 7 2 6	13760.57	-0.0014
5 2 4 4 2 3	8610.376	-0.0003	8 2 6 7 2 5	13895.91	-0.0037
5 2 3 4 2 2	8643.415	0.0032	9 1 9 8 1 8	15027.97	-0.0006
5 1 4 4 1 3	8844.673	0.0001	9 0 9 8 0 8	15311.03	-0.0016
6 1 6 5 1 5	10036.68	-0.0003	9 2 8 8 2 7	15472.8	0.0025
6 0 6 5 0 5	10278.08	-0.0028	9 2 7 8 2 6	15662.89	-0.0031
6 2 5 5 2 4	10329.06	0.0052	9 1 8 8 1 7	15879.16	-0.0013
6 2 4 5 2 3	10386.59	0.0009	10 1 10 9 1 9	16685.88	0.0038
6 1 5 5 1 4	10608.44	0.0007	10 0 10 9 0 9	16966.81	-0.0036
7 1 7 6 1 6	11703.18	-0.0048	10 1 9 9 1 8	17626.87	0.0058

Table A5.4. Experimental transition frequencies (ν /MHz) and obs.-cal. values ($\Delta\nu$ /MHz) of TG2.

J'	K_a'	K_c'	J''	K_a''	K_c''	ν	$\Delta\nu$	J'	K_a'	K_c'	J''	K_a''	K_c''	ν	$\Delta\nu$
5	0	5	4	0	4	7083.2811	0.0006	5	1	4	4	1	3	7157.0431	0.0005
6	0	6	5	0	5	8497.998	-0.0002	6	1	5	5	1	4	8587.4544	-0.0008
7	0	7	6	0	6	9911.6618	0.0022	7	1	6	6	1	5	10017.3217	0.0007
8	0	8	7	0	7	11324.0891	-0.0013	8	1	7	7	1	6	11446.5557	0.0008
9	0	9	8	0	8	12735.1171	-0.0005	9	1	8	8	1	7	12875.0723	-0.0013
11	0	11	10	0	10	15552.2867	0.0037	11	1	10	10	1	9	15729.6105	-0.0021
12	0	12	11	0	11	16958.0881	-0.0036	12	1	11	11	1	10	17155.4548	0.0024
5	1	5	4	1	4	7015.1979	0.0010	6	2	5	5	2	4	8507.6049	-0.0003
6	1	6	5	1	5	8416.8737	-0.0004	7	2	6	6	2	5	9924.0314	0.0037
7	1	7	6	1	6	9817.817	-0.0023	8	2	7	7	2	6	11339.7727	0.0025
8	1	8	7	1	7	11217.9194	-0.0002	9	2	8	8	2	7	12754.7411	-0.0001
9	1	9	8	1	8	12617.0676	0.0010	6	2	4	5	2	3	8510.7308	-0.0025
10	1	10	9	1	9	14015.1554	-0.0016	7	2	5	6	2	4	9929.0497	-0.0009
11	1	11	10	1	10	15412.0944	0.0015	8	2	6	7	2	5	11347.3373	-0.0040

Table A5.5. MP2/aug-cc-pVTZ geometries of the two conformers of the acrolein-ethanol complexes.

TG1				TG2			
Atom	x / Å	y / Å	z / Å	Atom	x / Å	y / Å	z / Å
C	-3.0095	1.3925	-0.0002	C	-3.6692	0.6829	-0.3337
H	-3.9814	0.9134	-0.0009	H	-3.2550	1.6662	-0.5198
H	-2.9838	2.4726	0.0002	H	-4.7399	0.5649	-0.4159
C	-1.8895	0.6573	0.0003	C	-2.8645	-0.3387	-0.0139
H	-0.8977	1.0914	0.0010	H	-3.2359	-1.3363	0.1800
C	-1.9999	-0.8038	-0.0003	C	-1.4199	-0.1209	0.0834
H	-3.0310	-1.1991	-0.0010	H	-1.0723	0.9063	-0.1197
O	-1.0480	-1.5735	-0.0001	O	-0.6165	-0.9998	0.3697
C	3.5268	0.7687	-0.0005	C	3.3699	-0.5752	-0.6195
H	4.5581	0.4171	-0.0009	H	4.4251	-0.7981	-0.4564
H	3.3676	1.3849	-0.8840	H	2.8027	-1.4958	-0.4783
H	3.3683	1.3851	0.8829	H	3.2365	-0.2441	-1.6481
C	2.5679	-0.3996	0.0000	C	2.8930	0.4956	0.3437
H	2.7327	-1.0225	0.8843	H	3.4552	1.4169	0.1971
H	2.7317	-1.0226	-0.8843	H	3.0543	0.1721	1.3770
O	1.2431	0.1222	0.0007	O	1.5278	0.8361	0.1367
H	0.6144	-0.6180	0.0007	H	0.9977	0.0349	0.2784

Appendix VI

Table A6.1. *Ab initio* spectroscopic parameters and relative energies of the DMSO-W complexes in the various methods.

	Conf. 1	Conf. 2	Conf. 3
MP2/aug-cc-pVTZ			
<i>A</i> / MHz	4261	6785	5172
<i>B</i> / MHz	2479	2072	2075
<i>C</i> / MHz	2459	1739	1904
μ_a / D	1.5	-3.2	4.1
μ_b / D	0.0	1.6	0.0
μ_c / D	2.3	-0.2	0.9
ΔE / kJ mol ⁻¹	0.0	6.9	25.1
B3LYP/def2tzvp			
<i>A</i> / MHz	4214	6760	4993
<i>B</i> / MHz	2473	2043	2072
<i>C</i> / MHz	2437	1715	1906
μ_a / D	-1.4	-3.2	-3.5
μ_b / D	0.0	-1.4	0.0
μ_c / D	-2.0	-0.7	-0.8
ΔE / kJ mol ⁻¹	0.0	8.0	26.1
MP2/def2tzvp			
<i>A</i> / MHz	4276	6871	5174
<i>B</i> / MHz	2473	2063	2061
<i>C</i> / MHz	2455	1731	1896
μ_a / D	-1.3	-3.0	-3.9
μ_b / D	0.0	-1.3	0.0
μ_c / D	-2.0	-0.5	-0.6
ΔE / kJ mol ⁻¹	0.0	7.2	24.1

Table A6.2. Experimental transition frequencies (ν /MHz) and obs-calc. values ($\Delta\nu$ /MHz) of conf. 1.

J'	K_a'	K_c'	J''	K_a''	K_c''	$C_2H_6OS-H_2O$		$C_2H_6O^{34}S-H_2O$		$^{13}CH_3OSCH_3-H_2O$		$C_2H_6OS-H_2^{18}O$	
						ν	$\Delta\nu$	ν	$\Delta\nu$	ν	$\Delta\nu$	ν	$\Delta\nu$
2	1	2	1	1	1	9502.1507	0.0016	9424.1848	-0.0010	9414.8785	-0.0017	9001.2722	0.0015
2	0	2	1	0	1	9540.8510	-0.0006	9460.3826	-0.0010	9470.2885	0.0003	9034.6371	-0.00038
2	1	1	1	1	0	9580.7044	-0.0024	9497.5736	-0.0018	9528.2573	-0.0073	9068.785	-0.00071
3	1	3	2	1	1	14252.6774	-0.0009					13501.4849	-0.0026
3	0	3	2	0	2	14309.5895	0.0027					13550.7418	-0.00094
3	2	2	2	2	1							13552.2444	0.00432
3	2	1	2	2	0							13553.9288	-0.00409
1	1	0	0	0	0	6687.9495	0.0001	6660.2927	0.0020	6590.6998	0.0012	13602.7587	0.002
2	1	1	1	0	1	11497.8908	-0.0013	11427.3769	-0.0011	11383.1282	0.0011	6553.412	0.00138
2	2	0	1	1	0	15215.0590	0.0006	15177.4460	0.0021	14924.1213	0.0038	11104.6338	-0.00101
2	2	1	1	1	1	15253.7250	-0.0025	15213.6082	-0.0021	14979.4863	-0.0038	15672.7544	0.00037
3	1	2	2	0	2	16327.5519	0.0026	16212.8654	0.0013	16204.2427	0.0023	15075.5084	0.00305
2	0	2	1	1	0	7623.6678	0.0015	7530.5832	0.0022	7615.4325	0.0069	15108.8365	-0.00305
3	0	3	2	1	1	12352.5475	0.0011	12222.1005	0.0003	12289.1360	-0.0023	6998.788	-0.00039
4	0	4	3	1	2	17058.3352	-0.0011	16892.2629	-0.0004	16927.2843	0.0001	11480.7465	0.00109
3	1	3	2	2	1	8501.0993	-0.0005						
3	1	2	2	2	0	8736.1557	-0.0015						

Table A6.3. Experimental transition frequencies (ν /MHz) and obs-calc. values ($\Delta\nu$ /MHz) of C₂H₆OS-DOH.

J'	K_a'	K_c'	J''	K_a''	K_c''	$F'+1/2$	$F''+1/2$	ν	$\Delta\nu$
2	1	2	1	1	1	1	0	9359.1684	0.0073
2	1	2	1	1	1	2	2	9359.1876	0.0068
2	1	2	1	1	1	3	2	9359.2073	-0.0066
2	0	2	1	0	1	3	2	9394.7940	0.0073
2	0	2	1	0	1	2	1	9394.7940	0.0069
2	1	1	1	1	0	1	2	9431.2871	-0.0059
2	1	1	1	1	0	3	2	9431.3212	0.0000
2	1	1	1	1	0	1	0	9431.3409	0.0017
2	1	1	1	1	0	2	1	9431.3409	-0.0002
3	1	3	2	1	2	2	1	14038.3347	-0.0064
3	0	3	2	0	2	3	2	14090.7686	0.0112
3	0	3	2	0	2	4	3	14090.7686	0.0106
3	0	3	2	0	2	2	1	14090.7686	0.0069
3	1	2	2	1	1	4	3	14146.5246	0.0138
3	1	2	2	1	1	3	2	14146.5246	0.0076
3	1	2	2	1	1	2	1	14146.5246	0.0056
1	1	0	0	0	0	2	1	6642.5303	-0.0004
1	1	0	0	0	0	1	1	6642.5612	-0.0004
2	1	1	1	0	1	1	0	11376.1715	-0.0012
2	1	1	1	0	1	3	2	11376.1715	-0.0046
2	1	1	1	0	1	2	1	11376.2058	-0.0045
3	1	2	2	0	2	2	3	16127.8931	0.0129
3	1	2	2	0	2	2	1	16127.8931	0.0035
3	1	2	2	0	2	4	3	16127.8931	-0.0071
3	1	2	2	0	2	3	2	16127.9341	-0.0062
2	2	0	1	1	0	2	2	15158.2368	0.0130
2	2	0	1	1	0	3	2	15158.2368	-0.0040
2	2	0	1	1	0	1	2	15158.2368	-0.0134
2	2	0	1	1	0	1	0	15158.3020	0.0056
2	2	1	1	1	1	3	2	15193.7761	-0.0022
2	2	1	1	1	1	1	2	15193.7761	-0.0121
2	2	1	1	1	1	2	1	15193.8102	0.0022
2	2	1	1	1	1	1	1	15193.8365	0.0009
2	0	2	1	1	0	2	2	7449.9448	-0.0039
3	0	3	2	1	1	4	3	12109.3596	-0.0090
3	0	3	2	1	1	3	3	12109.3906	0.0056
3	0	3	2	1	1	2	1	12109.3906	-0.0005
4	0	4	3	1	2	5	4	16747.8925	0.0095
4	0	4	3	1	2	4	4	16747.8925	-0.0056
4	0	4	3	1	2	3	2	16747.8925	-0.0066

Table A6.4. Experimental transition frequencies (ν /MHz) and obs-calc. values ($\Delta\nu$ /MHz) of C₂H₆OS-HOD.

J'	K_a'	K_c'	J''	K_a''	K_c''	$F'+1/2$	$F''+1/2$	ν	$\Delta\nu$
2	1	2	1	1	1	1	0	9053.9309	0.0245
2	1	2	1	1	1	2	2	9054.0392	-0.0014
2	1	2	1	1	1	3	2	9054.0020	-0.0095
2	1	2	1	1	1	1	2	9054.0020	0.0068
2	1	2	1	1	1	1	1	9054.0642	0.0097
2	0	2	1	0	1	3	2	9089.1657	-0.0021
2	0	2	1	0	1	2	1	9089.1657	-0.0080
2	1	1	1	1	0	1	1	9125.1904	0.0046
2	1	1	1	1	0	3	2	9125.1904	-0.0035
2	1	1	1	1	0	2	1	9125.2605	-0.0241
2	1	1	1	1	0	2	2	9125.2605	0.0031
3	1	3	2	1	2	2	1	13580.5915	0.0058
3	1	3	2	1	2	4	3	13580.5915	0.0031
3	1	3	2	1	2	2	3	13580.5730	0.0035
3	0	3	2	0	2	3	2	13632.4211	-0.0044
3	0	3	2	0	2	4	3	13632.4211	-0.0015
3	0	3	2	0	2	2	1	13632.4211	-0.0195
3	1	2	2	1	1	4	3	13687.3591	-0.0012
3	1	2	2	1	1	3	2	13687.3812	-0.0054
3	1	2	2	1	1	2	1	13687.3591	-0.0050
1	1	0	0	0	0	2	1	6570.3258	0.0008
1	1	0	0	0	0	1	1	6570.3000	0.0022
2	1	1	1	0	1	1	2	11150.6476	0.0037
2	1	1	1	0	1	3	2	11150.6742	-0.0050
2	1	1	1	0	1	2	1	11150.6476	-0.0086
3	1	2	2	0	2	2	3	15748.8595	0.0192
3	1	2	2	0	2	2	1	15748.8916	0.0000
3	1	2	2	0	2	4	3	15748.8697	-0.0020
3	1	2	2	0	2	3	2	15748.8595	-0.0096
2	2	0	1	1	0	3	2	15095.3266	-0.0015
2	2	0	1	1	0	1	0	15095.3266	-0.0120
2	2	1	1	1	1	1	0	15130.4100	0.0054
2	2	1	1	1	1	3	2	15130.4419	-0.0001
2	2	1	1	1	1	2	1	15130.4100	0.0014
2	0	2	1	1	0	1	1	7063.6600	0.0016
2	0	2	1	1	0	3	2	7063.6793	-0.0032
3	0	3	2	1	1	3	2	11570.9421	-0.0009
3	0	3	2	1	1	4	3	11570.9096	-0.0016
3	0	3	2	1	1	2	1	11570.9096	-0.0035
4	0	4	3	1	2	4	3	16057.6381	0.0031

4	0	4	3	1	2	5	4	16057.6381	0.0101
4	0	4	3	1	2	3	2	16057.6381	0.0035
4	1	4	3	1	3	5	4	18106.6089	-0.0204
4	0	4	3	0	3	5	4	18174.0849	0.0078
4	0	4	3	0	3	4	3	18174.0849	0.0063
4	0	4	3	0	3	3	2	18174.0849	-0.0007
4	1	3	3	1	2	5	4	18248.9933	0.0190
4	1	3	3	1	2	4	3	18248.9933	0.0073

Table A6.5. Experimental transition frequencies (ν /MHz) and obs-calc. values ($\Delta\nu$ /MHz) of C₂H₆OS-D₂O.

J'	K_a'	K_c'	J''	K_a''	K_c''	$F'+1/2$	$F''+1/2$	$(F'+1/2)$	$(F''+1/2)$	ν	$\Delta\nu$
2	1	2	1	1	1	3	2	3	2	8927.9521	0.0005
2	1	2	1	1	1	1	2	2	2	8927.9521	-0.0026
2	1	2	1	1	1	3	2	4	3	8927.9688	0.0119
2	1	2	1	1	1	2	2	2	1	8927.9688	0.0101
2	1	2	1	1	1	2	2	1	1	8927.9688	-0.0043
2	1	2	1	1	1	2	2	3	3	8927.9688	-0.0164
2	1	2	1	1	1	1	1	1	1	8927.9688	-0.0172
2	1	2	1	1	1	1	1	1	2	8928.0103	0.0163
2	1	2	1	1	1	1	1	2	1	8928.0103	0.0093
2	1	2	1	1	1	3	1	3	2	8928.0103	0.0044
2	1	2	1	1	1	1	1	2	2	8928.0103	0.0013
2	1	2	1	1	1	2	2	2	2	8928.0103	-0.0005
2	1	2	1	1	1	2	2	3	2	8928.0103	-0.0011
2	1	2	1	1	1	1	1	1	0	8928.0221	0.0019
2	1	2	1	1	1	3	1	2	1	8928.0221	-0.0066
2	1	2	1	1	1	1	1	0	1	8928.0555	0.0243
2	1	2	1	1	1	2	1	2	1	8928.0555	-0.0016
2	1	2	1	1	1	2	1	2	2	8928.0555	-0.0096
2	1	2	1	1	1	2	1	3	2	8928.0555	-0.0102
2	0	2	1	0	1	3	2	2	2	8960.3832	0.0168
2	0	2	1	0	1	2	1	1	0	8960.3832	0.0116
2	0	2	1	0	1	2	1	1	2	8960.3832	0.0000
2	0	2	1	0	1	3	2	4	3	8960.3832	-0.0006
2	0	2	1	0	1	3	2	2	1	8960.3832	-0.0031
2	0	2	1	0	1	3	2	3	2	8960.3832	-0.0035
2	0	2	1	0	1	2	1	3	2	8960.3832	-0.0040
2	0	2	1	0	1	2	1	1	1	8960.3832	-0.0060
2	0	2	1	0	1	2	1	2	2	8960.3832	-0.0130
2	0	2	1	0	1	3	2	3	3	8960.3832	-0.0151
2	0	2	1	0	1	2	1	2	1	8960.3832	-0.0190
2	0	2	1	0	1	1	0	0	1	8960.4320	-0.0201
2	1	1	1	1	0	1	0	1	1	8993.4460	0.0103
2	1	1	1	1	0	3	0	2	1	8993.4460	0.0087
2	1	1	1	1	0	1	2	2	2	8993.4460	-0.0049
2	1	1	1	1	0	1	2	1	2	8993.4751	0.0102
2	1	1	1	1	0	3	2	2	2	8993.4751	0.0086
2	1	1	1	1	0	1	2	2	1	8993.4751	-0.0024
2	1	1	1	1	0	1	2	2	3	8993.4751	-0.0030
2	1	1	1	1	0	3	2	2	1	8993.5085	0.0154
2	1	1	1	1	0	1	1	2	2	8993.5085	0.0064

2	1	1	1	1	0	1	1	0	1	8993.5085	0.0017
2	1	1	1	1	0	3	2	4	3	8993.5085	-0.0034
2	1	1	1	1	0	1	1	1	2	8993.5085	-0.0077
2	1	1	1	1	0	3	1	2	2	8993.5085	-0.0092
2	1	1	1	1	0	1	1	2	1	8993.5466	0.0102
2	1	1	1	1	0	3	2	3	3	8993.5466	-0.0025
2	1	1	1	1	0	1	1	1	1	8993.5589	0.0085
2	1	1	1	1	0	3	1	2	1	8993.5589	0.0069
2	1	1	1	1	0	2	2	1	2	8993.5589	0.0035
2	1	1	1	1	0	2	0	2	1	8993.5589	0.0004
2	1	1	1	1	0	2	2	3	2	8993.5672	0.0054
2	1	1	1	1	0	3	1	3	2	8993.5672	-0.0060
2	1	1	1	1	0	2	1	1	0	8993.5825	0.0030
2	1	1	1	1	0	2	2	2	2	8993.5825	-0.0052
2	1	1	1	1	0	2	2	3	3	8993.5825	-0.0065
3	1	3	2	1	2	2	1	2	1	13391.5705	0.0098
3	1	3	2	1	2	4	3	5	4	13391.5705	0.0067
3	1	3	2	1	2	4	3	4	3	13391.5705	0.0042
3	1	3	2	1	2	2	1	3	2	13391.5705	0.0018
3	1	3	2	1	2	4	3	3	2	13391.5705	0.0017
3	1	3	2	1	2	3	2	3	3	13391.5705	-0.0006
3	1	3	2	1	2	3	2	3	2	13391.5705	-0.0012
3	1	3	2	1	2	2	1	1	2	13391.5918	0.0083
3	1	3	2	1	2	3	2	2	1	13391.5918	0.0071
3	1	3	2	1	2	3	2	4	3	13391.5918	0.0021
3	1	3	2	1	2	4	1	3	2	13391.5918	-0.0047
3	1	3	2	1	2	2	1	1	1	13391.5918	-0.0067
3	1	3	2	1	2	3	2	2	2	13391.5918	-0.0073
3	1	3	2	1	2	3	3	3	4	13391.5918	-0.0076
3	1	3	2	1	2	4	3	3	3	13391.5918	-0.0078
3	1	3	2	1	2	3	3	3	2	13391.5918	-0.0083
3	0	3	2	0	2	4	3	5	4	13439.4541	0.0061
3	0	3	2	0	2	4	3	4	3	13439.4541	0.0056
3	0	3	2	0	2	4	3	3	2	13439.4541	0.0046
3	0	3	2	0	2	3	2	2	1	13439.4541	0.0041
3	0	3	2	0	2	3	2	4	3	13439.4541	0.0041
3	0	3	2	0	2	2	1	1	1	13439.4541	0.0030
3	0	3	2	0	2	3	2	3	2	13439.4541	0.0006
3	0	3	2	0	2	2	1	1	2	13439.4541	-0.0042
3	0	3	2	0	2	3	2	3	3	13439.4541	-0.0084
3	0	3	2	0	2	4	3	4	4	13439.4541	-0.0090
3	0	3	2	0	2	2	1	3	2	13439.4541	-0.0110
3	1	2	2	1	1	2	1	1	2	13489.8981	0.0150
3	1	2	2	1	1	3	2	2	2	13489.8981	0.0134
3	1	2	2	1	1	2	3	3	2	13489.8981	0.0085

3	1	2	2	1	1	4	3	5	4	13489.8981	-0.0026
3	1	2	2	1	1	4	3	3	2	13489.8981	-0.0054
3	1	2	2	1	1	2	1	3	2	13489.8981	-0.0071
3	1	2	2	1	1	3	2	2	3	13489.8981	-0.0124
3	1	2	2	1	1	2	1	1	0	13489.8981	-0.0146
4	1	4	3	1	3	4	3	4	4	17854.7029	0.0146
4	1	4	3	1	3	3	2	2	1	17854.7029	0.0036
4	1	4	3	1	3	5	4	6	5	17854.7029	0.0029
4	1	4	3	1	3	5	4	4	3	17854.7029	0.0027
4	1	4	3	1	3	5	4	5	4	17854.7029	0.0025
4	1	4	3	1	3	3	2	3	2	17854.7029	0.0011
4	1	4	3	1	3	3	2	4	3	17854.7029	-0.0013
4	1	4	3	1	3	4	3	4	3	17854.7029	-0.0040
4	1	4	3	1	3	4	3	3	2	17854.7029	-0.0066
4	1	4	3	1	3	4	3	5	4	17854.7029	-0.0086
4	0	4	3	0	3	5	4	4	4	17917.1494	0.0168
4	0	4	3	0	3	4	3	3	3	17917.1494	0.0132
4	0	4	3	0	3	3	2	2	2	17917.1494	0.0074
4	0	4	3	0	3	5	4	5	4	17917.1494	-0.0009
4	0	4	3	0	3	5	4	6	5	17917.1494	-0.0014
4	0	4	3	0	3	4	3	5	4	17917.1494	-0.0026
4	0	4	3	0	3	5	4	4	3	17917.1494	-0.0025
4	0	4	3	0	3	4	3	4	3	17917.1494	-0.0032
4	0	4	3	0	3	4	3	3	2	17917.1494	-0.0034
4	0	4	3	0	3	3	2	4	3	17917.1494	-0.0095
4	0	4	3	0	3	3	2	3	2	17917.1494	-0.0104
4	0	4	3	0	3	3	2	2	1	17917.1494	-0.0118
4	1	3	3	1	2	5	4	6	5	17985.8070	0.0021
4	1	3	3	1	2	5	4	4	3	17985.8111	0.0035
4	1	3	3	1	2	3	2	4	3	17985.8111	0.0014
4	1	3	3	1	2	5	4	5	4	17985.8111	0.0007
4	1	3	3	1	2	4	3	3	2	17985.8111	-0.0029
4	1	3	3	1	2	4	3	5	4	17985.8111	-0.0030
4	1	3	3	1	2	3	2	2	1	17985.8111	-0.0037
4	1	3	3	1	2	3	2	3	2	17985.8111	-0.0092
4	1	3	3	1	2	5	2	4	3	17985.8111	-0.0104
4	1	3	3	1	2	4	3	4	3	17985.8111	-0.0109
1	1	0	0	0	0	1	1	1	1	6529.3689	0.0062
1	1	0	0	0	0	1	1	1	2	6529.3689	0.0062
1	1	0	0	0	0	1	1	2	1	6529.4019	0.0049
1	1	0	0	0	0	1	1	2	2	6529.4019	0.0049
1	1	0	0	0	0	2	1	3	2	6529.4230	0.0019
1	1	0	0	0	0	2	1	1	0	6529.4230	0.0014
1	1	0	0	0	0	1	1	0	1	6529.4230	-0.0012
1	1	0	0	0	0	2	1	2	1	6529.4500	0.0017

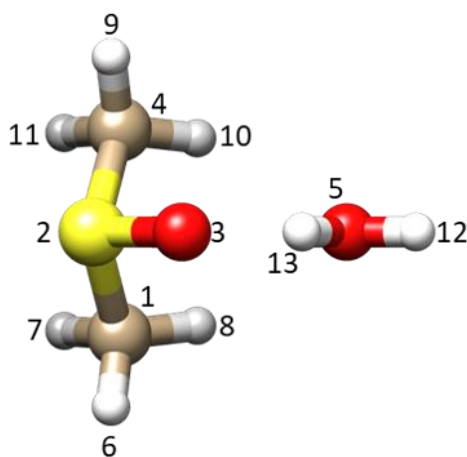
1	1	0	0	0	0	2	1	2	2	6529.4500	0.0017
1	1	0	0	0	0	0	1	1	1	6529.4779	0.0005
1	1	0	0	0	0	0	1	1	2	6529.4779	0.0005
2	1	1	1	0	1	1	2	2	3	11042.4993	0.0054
2	1	1	1	0	1	2	1	1	0	11042.4993	0.0045
2	1	1	1	0	1	1	2	1	2	11042.4993	0.0030
2	1	1	1	0	1	3	2	2	2	11042.4993	0.0014
2	1	1	1	0	1	1	2	2	1	11042.4993	-0.0029
2	1	1	1	0	1	2	1	1	1	11042.5143	0.0018
2	1	1	1	0	1	2	1	3	2	11042.5143	0.0014
2	1	1	1	0	1	3	2	2	1	11042.5143	-0.0035
2	1	1	1	0	1	3	2	4	3	11042.5269	-0.0009
2	1	1	1	0	1	2	1	2	2	11042.5493	0.0106
2	1	1	1	0	1	2	1	2	1	11042.5493	0.0045
2	1	1	1	0	1	3	2	3	2	11042.5493	-0.0041
2	1	1	1	0	1	2	2	1	2	11042.5861	-0.0007
2	1	1	1	0	1	2	2	3	2	11042.5861	-0.0072
2	1	1	1	0	1	1	0	0	1	11042.5861	-0.0077
2	1	1	1	0	1	2	2	3	3	11042.6002	-0.0047
2	1	1	1	0	1	2	2	1	1	11042.6002	-0.0065
3	1	2	2	1	1	3	2	2	2	13489.8981	0.0134
3	1	2	2	1	1	2	3	3	2	13489.8981	0.0085
3	1	2	2	1	1	4	3	5	4	13489.8981	-0.0026
3	1	2	2	1	1	4	3	3	2	13489.8981	-0.0054
3	1	2	2	1	1	2	1	3	2	13489.8981	-0.0071
2	2	0	1	1	0	2	1	2	2	15042.5608	0.0043
2	2	0	1	1	0	2	1	3	2	15042.5608	-0.0047
2	2	0	1	1	0	3	0	2	1	15042.5928	0.0066
2	2	0	1	1	0	2	1	2	1	15042.5928	0.0020
2	2	0	1	1	0	3	2	3	2	15042.5928	-0.0023
2	2	0	1	1	0	2	1	1	1	15042.6045	0.0007
2	2	0	1	1	0	3	2	2	2	15042.6045	-0.0109
2	2	0	1	1	0	3	2	3	3	15042.6421	0.0198
2	2	0	1	1	0	1	0	1	1	15042.6421	0.0191
2	2	0	1	1	0	1	0	2	1	15042.6421	0.0118
2	2	0	1	1	0	3	2	4	3	15042.6421	0.0053
2	2	0	1	1	0	1	0	0	1	15042.6421	0.0005
2	2	0	1	1	0	3	2	2	1	15042.6421	0.0000
2	2	0	1	1	0	3	1	3	2	15042.6421	-0.0043
2	2	0	1	1	0	1	2	1	2	15042.6421	-0.0101
2	2	0	1	1	0	1	1	1	0	15042.6826	0.0063
2	2	0	1	1	0	1	2	2	1	15042.6826	-0.0035
2	2	0	1	1	0	1	2	2	3	15042.6829	-0.0037
2	2	0	1	1	0	3	1	2	1	15042.7004	-0.0005
2	2	0	1	1	0	1	1	1	2	15042.7004	-0.0031

2	2	0	1	1	0	1	1	2	2	15042.7102	-0.0005
2	2	1	1	1	1	2	2	2	2	15074.9281	0.0034
2	2	1	1	1	1	2	2	3	2	15074.9281	-0.0059
2	2	1	1	1	1	2	2	1	2	15074.9496	0.0114
2	2	1	1	1	1	1	0	1	1	15074.9496	0.0035
2	2	1	1	1	1	1	0	2	1	15074.9496	-0.0040
2	2	1	1	1	1	2	1	2	1	15074.9827	0.0117
2	2	1	1	1	1	2	1	2	2	15074.9827	0.0037
2	2	1	1	1	1	3	2	2	1	15074.9827	-0.0011
2	2	1	1	1	1	2	1	1	1	15074.9827	-0.0018
2	2	1	1	1	1	2	1	3	2	15074.9827	-0.0056
2	2	1	1	1	1	3	2	3	3	15074.9827	-0.0058
2	2	1	1	1	1	2	1	1	2	15075.0038	0.0113
2	2	1	1	1	1	3	2	4	3	15075.0038	0.0001
2	2	1	1	1	1	3	2	3	2	15075.0177	0.0030
2	2	1	1	1	1	2	1	1	0	15075.0177	-0.0010
2	2	1	1	1	1	1	2	1	1	15075.0177	-0.0025
2	2	1	1	1	1	1	2	2	1	15075.0177	-0.0100
2	2	1	1	1	1	3	1	3	2	15075.0738	0.0048
2	2	1	1	1	1	1	2	2	2	15075.0738	-0.0059
2	2	1	1	1	1	3	1	2	1	15075.0738	-0.0083
2	0	2	1	1	0	3	2	2	1	6911.3736	0.0120
2	0	2	1	1	0	3	2	4	3	6911.3736	0.0057
2	0	2	1	1	0	3	2	3	3	6911.3736	-0.0088
3	0	3	2	1	1	4	3	3	3	11357.2806	0.0180
3	0	3	2	1	1	2	3	3	4	11357.2806	0.0093
3	0	3	2	1	1	4	3	4	3	11357.2806	-0.0013
3	0	3	2	1	1	2	1	1	1	11357.2806	-0.0038
3	0	3	2	1	1	2	3	3	2	11357.2806	-0.0090
3	0	3	2	1	1	3	2	2	2	11357.3039	0.0095
3	0	3	2	1	1	2	1	2	1	11357.3039	0.0003
3	0	3	2	1	1	4	3	5	4	11357.3039	0.0000
3	0	3	2	1	1	2	1	3	2	11357.3039	-0.0013
3	0	3	2	1	1	3	2	3	2	11357.3233	0.0123
3	0	3	2	1	1	2	1	2	2	11357.3233	0.0057
3	0	3	2	1	1	4	3	3	2	11357.3233	0.0053
3	0	3	2	1	1	4	3	4	4	11357.3233	0.0042
3	0	3	2	1	1	3	2	4	3	11357.3233	-0.0010
3	0	3	2	1	1	3	2	2	1	11357.3233	-0.0034
3	0	3	2	1	1	2	1	1	0	11357.3233	-0.0047
3	0	3	2	1	1	4	1	3	2	11357.3233	-0.0103
3	0	3	2	1	1	3	2	3	3	11357.3233	-0.0135
4	0	4	3	1	2	5	4	4	4	15784.5207	0.0189
4	0	4	3	1	2	4	3	3	3	15784.5207	0.0116
4	0	4	3	1	2	3	2	2	2	15784.5207	0.0043

4	0	4	3	1	2	5	4	5	4	15784.5207	0.0012
4	0	4	3	1	2	4	3	4	3	15784.5207	-0.0048
4	0	4	3	1	2	3	2	3	2	15784.5207	-0.0135
4	0	4	3	1	2	3	4	4	3	15784.5593	0.0143
4	0	4	3	1	2	5	4	6	5	15784.5593	0.0052
4	0	4	3	1	2	4	3	5	4	15784.5593	0.0045
4	0	4	3	1	2	3	2	4	3	15784.5593	0.0004
4	0	4	3	1	2	4	3	3	2	15784.5593	-0.0032
4	0	4	3	1	2	5	4	4	3	15784.5593	-0.0071
4	0	4	3	1	2	4	3	4	4	15784.5593	-0.0086
4	0	4	3	1	2	5	4	5	5	15784.5593	-0.0093
4	0	4	3	1	2	3	2	3	3	15784.5593	-0.0128

Table A6.6. MP2/aug-cc-pVTZ geometries of the Conf. 1.

Bond lengths / Å		Valence angles / °		Dihedral angles / °	
S2C1	1.795282				
O3S2	1.501815	O3S2C3	106.667		
C4S2	1.795279	C4S2O3	106.691	C4S2O3C1	-102.142
O5O3	2.762038	O5O3S2	100.547	O5O3S2C1	51.132
H6C1	1.089631	H6C1S2	106.778	H6C1S2C4	176.658
H7C1	1.090991	H7C1S2	109.158	H7C1S2C4	-64.739
H8C1	1.090824	H8C1S2	109.048	H8C1S2C4	57.483
H9C4	1.089645	H9C1S2	106.777	H9C1S2C1	-176.617
H10C4	1.090811	H10C4S2	109.078	H10C4S2C1	-57.429
H11C4	1.090995	H11C4S2	109.136	H11C4S2C1	64.798
H12O5	0.961678	H12O5O3	120.762	H12O5O3S2	-179.753
H13O5	0.978894	H13O5O3	15.040	H13O5O3S2	179.891

**Figure A6.1.** Sketch, principal axis, and atom numbering adopted for the Conf. 1.

Appendix VII

Table A7.1. Experimental transition frequencies (ν /MHz) and observed minus calculated values ($\Delta\nu$ /MHz) of DMSO-MeOH.

J'	K_a'	K_c'	J''	K_a''	K_c''	ν_A	$\Delta\nu_A$	ν_E	$\Delta\nu_E$
3	0	3	2	0	2	7706.8460	0.0025	7706.5710	-0.0007
3	1	3	2	1	2	7689.5280	-0.0024	7702.7510	0.0067
3	1	2	2	1	1	7724.3300	0.0062	7710.8310	0.0002
4	0	4	3	0	3	10275.5590	0.0023	10275.1880	-0.0019
4	1	4	3	1	3	10252.5930	-0.0022	10266.5530	0.0080
4	1	3	3	1	2	10298.9920	0.0065	10284.6640	-0.0002
4	2	3	3	2	2	10275.7010	0.0087	10275.6760	0.0108
4	2	2	3	2	1	10276.0430	-0.0002	10275.6140	-0.0155
5	0	5	4	0	4	12844.0700	0.0036	12843.6010	-0.0014
5	1	5	4	1	4	12815.5590	-0.0040	12828.3230	0.0010
5	1	4	4	1	3	12873.5580	0.0071	12860.3350	0.0036
5	2	4	4	2	3	12844.4500	-0.0061	12844.5710	0.0158
5	2	3	4	2	2	12845.1580	-0.0009	12844.4920	-0.0163
6	0	6	5	0	5	15412.3270	0.0023	15411.7540	-0.0036
6	1	6	5	1	5	15378.4020	-0.0089	15388.9340	-0.0028
6	1	5	5	1	4	15448.0010	0.0070	15436.9250	0.0034
6	2	5	5	2	4	15413.1100	-0.0037	15413.4550	0.0267
6	2	4	5	2	3	15414.3390	-0.0037	15413.3500	-0.0187
2	1	1	1	0	1	8027.5220	-0.0114	8115.0850	-0.0126
3	1	2	2	0	2	10613.8680	-0.0092	10688.1200	-0.0076
4	1	3	3	0	3	13206.0130	-0.0058	13266.2190	-0.0019
5	1	4	4	0	4	15804.0090	-0.0043	15851.3640	0.0010
2	2	0	1	1	0	13748.5870	0.0049	13847.6840	0.0102
2	2	1	1	1	1	13760.1480	0.0028	13631.5800	-0.0077
3	2	1	2	1	1	16305.9770	0.0006	16415.2910	0.0031
3	2	2	2	1	2	16340.5980	0.0028	16201.6750	0.0006

Appendix VIII

Table A8.1. Experimental transition frequencies (ν /MHz) and observed minus calculated values ($\Delta\nu$ /MHz) of conformer *t*-1.

J'	K_a'	K_c'	J''	K_a''	K_c''	ν	$\Delta\nu$
4	1	3	3	1	2	6408.2824	0.00327
5	1	5	4	1	4	7969.9048	-0.00259
5	0	5	4	0	4	7989.8571	-0.0008
5	2	3	4	2	2	7990.3768	-0.00163
5	1	4	4	1	3	8010.2746	0.00065
6	1	6	5	1	5	9563.7757	-0.00376
6	0	6	5	0	5	9587.5819	-0.00088
6	2	5	5	2	4	9587.9585	-0.00255
6	2	4	5	2	3	9588.5438	0.00156
6	1	5	5	1	4	9612.2208	0.00213
7	1	7	6	1	6	11157.5938	0.00176
7	0	7	6	0	6	11185.1727	-0.00045
7	2	6	6	2	5	11185.822	-0.00224
7	2	5	6	2	4	11186.7574	0.00334
7	1	6	6	1	5	11214.1015	-0.00166
8	1	8	7	1	7	12751.3378	0.00242
8	0	8	7	0	7	12782.6083	0.00162
8	2	6	7	2	5	12785.0224	0.0006
8	1	7	7	1	6	12815.9152	-0.00201
3	1	3	2	0	2	7713.5542	0.00337
4	1	4	3	0	3	9295.44	-0.0023
7	0	7	6	1	6	8325.5115	0.00591
8	0	8	7	1	7	9950.5154	-0.00483

Conclusion

Rotational spectroscopy is an extremely valuable tool to determine the structure of molecules and their different conformations, and to characterize the non-covalent interactions in weakly bound molecular complexes. Through rotational spectroscopy it is also possible to study internal motion taking place in the molecules or in the complexes and to attain information on the electronic structure through the study of nuclear hyperfine coupling effects.

This thesis presents results of rotational spectra and theoretical modelling on different selected molecular systems in order to deepen the contribution of electronic effects and non-covalent interactions on their conformational landscape.

Firstly, we discuss the effects of perfluorination on the structural and the electronic properties of C_6F_5Cl and C_6F_5Br . Enhancement of the σ -hole on the halogen atom of aryl halides due to perfluorination of the ring is demonstrated by use of the Extended Townes–Dailey (ETD) model coupled to a Natural Atomic Orbital Bond analysis on two perfluorinated aryl halides (C_6F_5Cl and C_6F_5Br) and their hydrogenated counterparts. The experimentally determined rotational constants combined with theoretical data at the MP2/aug-cc-pVTZ level provide precise structural information from which an elongation of the ring along its symmetry axis due to perfluorination is proved.

Secondly, the rotational spectrum of two conformations for *s-trans*-acrolein...methanol and two conformations for *s-trans*-acrolein...*gauche*-ethanol complexes and their deuterated isotopologues have been observed and analysed. Two HBs, a strong OH...O HB and a weak C–H...O HB, were observed in all four conformations. The three-fold barriers to internal rotation of the methyl group, V_3 , in *s-trans*-acrolein...methanol-1 (2.629(5) kJ mol⁻¹) and *s-trans*-acrolein...methanol-2 (2.722(5) kJ mol⁻¹) were determined. They are smaller than the value determined in the methanol monomer (4.462 kJ mol⁻¹). The apparent barrier reductions is partly predicted by the quantum chemical calculations but the larger effect could be related to the coupling effect of the large-amplitude librational motion of the MeOH unit.

Finally, rotational spectroscopy is used to study the conformational equilibria and isotopologues species of DMSO-W, DMSO-MeOH and DMSO-EtOH. The combination of rotational spectroscopy and theoretical methods provides a synergistic method for studying the structure and

HB in the complexes. A strong OH...O HB accompanied by two weak C-H...O HBs were observed in all three complexes. The three conformers were determined with a similar symmetrical structural pattern where the second moiety (water, methanol or ethanol) is located on the symmetry plane of DMSO. This is proved by the null value of the dipole moment component perpendicular to the symmetry plane of DMSO and the value of the planar inertia moment along the same axis which is very similar to that of DMSO alone.

Acknowledgements

I would like to express my heartfelt thanks to my supervisor, Prof. Sonia Melandri, for her patient teaching, her immense knowledge and her academic attitude. Thanks for her help in my work and life during my Ph.D. Thanks for her guiding help with my thesis. Thanks for sharing the story of the laboratory, for the Pasta she cooked which is really delicious and I will miss it. Many thanks to my co-supervisor Dr. Luca Evangelisti for training me to use the instrument and teaching me to analysis the data, for the help in my work and life especially the first year when was really hard for me, for his plant which is lucky half alive.

Special thanks to Dr. Assimo Maris who have always been there to help me in the lab, coming up with solutions whenever things went wrong and for all our insightful discussions. Many thanks to Laura B. Favero for helping me to analysis the really difficult spectra and for the kindly help in my life. I would also like to thank other members of the group: Wentao Song, Ningjing Jiang and Giovanna Salvitti. They make me to live in a foreign country much easier and bring me a lot good memory.

I gratefully acknowledge China scholarship council (CSC) funding me for the Ph. D research.

I would like to thank my family for all their love and encouragement. Special thanks to my wife Yunxue Li for her support and company. Lastly, I would like to thank my baby who will be born in the next June. Thanks for his or her coming which making all this more meaningful.